Model-Based Enhanced Operation of Building Convective Heating Systems & Active Thermal Storage

Jennifer Date

A Thesis

In the Department

of

Building, Civil and Environmental Engineering

Presented in Partial Fulfillment of the Requirements

for the Degree of Doctor of Philosophy (Building Engineering) at

Concordia University

Montréal, Québec, Canada

October 2021

CONCORDIA UNIVERSITY

School of Graduate Studies

This is to certify that this thesis is prepared

By: **Jennifer Date**

Entitled: **Model-Based Enhanced Operation of Building Convective Heating Systems & Active Thermal Storage**

and submitted in partial fulfillment of the requirements for the degree of

Doctor of Philosophy (Building Engineering)

complies with the regulations of the University and meets the accepted standards
with respect to originality and quality.

Signed by the final examining committee:

Dr. Pouya Valizadeh	Chair
Dr. I. Beausoleil-Morrison	External Examiner
Dr. G. Vatistas	External to Program
Dr. L. Wang	Examiner
Dr. R. Zmeureanu	Examiner
Dr. A. Athienitis	Thesis Co-Supervisor
Dr. J. Candanedo Ibarra	Thesis Co-Supervisor

Approved by

Dr. Mazdak Nik-Bakht, Graduate Program Director

Dr. Mourad Debbabi, Dean
Gina Cody School of Engineering and Computer Science

Date October 5th, 2021

Abstract

Model-Based Enhanced Operation of Building Convective Heating Systems & Active Thermal Storage

Jennifer Date, Ph.D.

Concordia University, 2021

This thesis presents an experimental and theoretical study of a reduced-order modelling methodology and dynamic response of convectively heated buildings and active thermal storage. A methodology was developed for the generation of control-oriented building models which can be used within model predictive control (MPC) or other model-based control strategies to satisfy occupant comfort and improve building-grid interaction. A methodology to identify and evaluate MPC strategies is presented to improve a building's energy flexibility. There is an emphasis on modelling building thermal mass and a dedicated thermal storage device. The two applications for reduced-order thermal modelling (buildings and dedicated active thermal energy storage devices) require different modelling approaches for control applications. Several case studies are introduced and are typical Québec construction with convective-based heating systems: a detached low-mass house, a low-mass retail building, and a warehouse (with active thermal storage device).

The residential building study outlined a methodology for multi-level control-oriented modelling with several zones and multiple floors. This multi-level approach allows the user to "zoom in and out" so that models at each control level remain manageable. In the second case study, implementation of MPC was presented for a conventional bank building to reduce the yearly utility bill and avoid the summer peak load penalty. A cost savings of 25% on the yearly electric utility bill and a peak power reduction of 38% were achieved. With the new optimized operation, the cost per square meter for the bank would decrease from \$30.19/m^2 to \$22.57/m^2, or a yearly savings of \$7.62/m^2.

The last case study comprises a 1650 m^2 warehouse equipped with a dedicated active high-temperature thermal energy storage device. A methodology was presented for the development and analysis of control-oriented models for enhanced operation of the electric thermal storage device. The goal was to maximize the building energy flexibility the building could provide to the grid by evaluating the Building Energy Flexibility Index ($BEFI$). A $BEFI$ of 55% to 100% was achieved. The average demand during the critical times was reduced between 36 kW and 65 kW and the utility cost to the customer can be reduced by 12-30%.

Acknowledgements

I would like to express my gratitude to my two thesis supervisors, Professor Andreas K. Athienitis and Professor José Candanedo. Their knowledge and experience within the research field of building physics and controls were vital resources for my progress and growth and their guidance was critical for the completion of this work. It has been a great opportunity to have such access to the resources made available by my supervisors throughout my studies, including knowledge on the fundamentals, access to case studies, measurement data, facilities, and equipment, to name a few. The dedication shown by my supervisors for the progress of research and development in the field of building engineering, particularly in Canada, has been inspiring and motivating.

My participation in *The NSERC/Hydro-Québec Industrial Research Chair in Optimized Operation and Energy Efficiency: Towards High Performance Buildings* was an invaluable experience. I was also fortunate to have the opportunity to work at CanmetENERGY-Varennes with bright colleagues within the Intelligent Buildings group and contribute to and learn from their interesting research projects. I would like to thank all the staff at Hydro-Québec LTE for their valuable collaboration and insights, and particularly to Karine Lavigne for facilitating access to useful data, her guidance, and her contribution to this work.

Financial support from various sources helped ease these past years, including the doctoral scholarship from FRQNT, ASHRAE Grant-in-Aid, and scholarships given through Concordia University. This support helped me push through the years and reinforced why I decided to pursue this rewarding and challenging research work.

My biggest thanks are given to the numerous colleagues I met at Concordia throughout my graduate studies journey since 2013. I met countless bright, ambitious, and kind people who each had a unique and positive impact on me and my experience.

I cannot express enough my appreciation for my family who encouraged me throughout my many academic years. To my parents and my sister, thank you for all your unwavering support. My husband Boris and daughter Elodie, I love you both and I am so glad we are on this journey together. I am excited to see what life has in store for us next.

Table of Contents

List of Figures

List of Tables

Nomenclature

Symbols

A	Area	m^2
A_i	Area of surface(s) represented by node i	m^2
A_w	window area	m^2
Bi	Biot number	
C	Capacitance	J/K
cfm	cubic feet per minute	ft^3/min
C_{bricks}	Thermal capacitance of brick storage medium	J/K
C_i	thermal capacitance at node i	J/K
c_p	specific heat	J/K
D	diameter of the globe	m
DH	Hydraulic Diameter	m
e_i	error between setpoint and air temperature	°C
	at time step i	°C
f_{eff}	ratio of radiating surface of the human body	
	to its total DuBois surface area	
G	solar radiation	W/m^2
GT	globe temperature	°C
h_c	convective heat transfer coefficient	W/(m^2K)
h_i	interior film coefficient	W/(m^2K)
h_r	radiative heat transfer coefficient	W/(m^2K)
h_o	exterior film coefficient	W/(m^2K)
i, k	nodes	
J	Objective function	
k	thermal conductivity	W/mK
K_i	integral control constant	W/(°Cs)
K_p	proportional control constant	W/°C
L	thickness of a surface	m
M	Volumetric flow rate	m^2/s
$\dot{m}$	Mass flow rate	kg/s
N	Number of time steps	
Nu	Nusselt number	
p	time step	
P	power	W (Js^{-1})
PH	Prediction Horizon	
P_{ETS}	Electrical heat input to storage medium	%
P_{max}	Maximum input of ETS	kW
P_{ref}	Reference power demand	kW

q	heating load	W (Js^{-1})
q_{aux}	auxiliary heating source	W (Js^{-1})
q_i	Source entering node i	W (Js^{-1})
q_{conv}	Convective heat flux	W/m^2
q_{rad}	Radiative heat flux	W/m^2
Q	Power	W
Q_{source}	Electrical heat input to storage medium	W
Q_{conv}	Heat extracted from storage medium to air in channel	W
Q_s	Solar gains	W (Js^{-1})
R_i	thermal resistance at node i	K/W
R_{bricks}	Thermal resistance of brick storage medium	K/W
R_{ins}	Thermal resistance of ETS insulation layer	K/W
R_{int}	Thermal resistance from ETS surface to room air	K/W
T	Temperature	°C
T_a	air temperature	°C
T_{db}	air (dry bulb) temperature	°C
T_{eo}	sol-air temperature	°C
T_i	temperature at node i	°C
T_o	operative temperature	°C
T_{mr}	Mean Radiant Temperature	°C
T_{room}	Room air temperature	°C
t	Time	seconds
t_{notice}	Time of notification of DR event	
UA	Conductance	W/K
U_i	thermal conductance at node i	W/K
U_{inf}	Infiltration conductance	W/K
V_a	air velocity at the level of the globe	m/s
W	Width of air channel	m
Z	Length of vertical axis	m
$\|\|f\|\|_\infty$	Infinity Norm	

Greek letters

α	Thermal diffusivity, k/ρc$_p$	m^2/s
α_s	solar absorptance of the wall	
ε	emissivity of the globe	
ρ	density	Kg/m^3
σ	Stefan-Boltzmann constant 5.67×10^{-8}	$W/(m^2K^4)$
Δt	simulation time step	s

Abbreviations

1R1C	1-Capacitance, 1-Resistance
ach	air change per hour
AI	Artificial Intelligence
ASHRAE	American Society of Heating, Refrigerating, and Air-Conditioning Engineers
BAS	Building Automation System

BAU	Business As Usual
BEFI	Building Energy Flexibility Index
BEMS	Building Energy Management System
BOPTEST	Building Optimization Performance Test
CAISO	California Independent System Operator
CEMS	Centralized Energy Management System
CFD	computational fluid dynamics
C & I	Commercial and Institutional
CO_2	Carbon Dioxide
CTF	Conduction Transfer Function
CVFD	Control Volume Finite Difference
CV-RMSE	coefficient of variation of the root mean squared error
DOE	(US) Department of Energy
DR	Demand Response
DSM	Demand Side Management
EKF	Extended Kalman Filter
ETS	Electric Thermal Storage
EUI	Energy Use Intensity
FMU	Functional Mock-up Unit
GHG	Green House Gas
GUI	Graphical User Interface
HVAC	Heating, Ventilation and Air Conditioning
IEA EBC	International Energy Agency in Buildings and Communities
KCl	Potassium chloride
MAE	Mean Absolute Error
$MgCO_3$	Magnesite
MHE	Moving Horizon Estimation
MILP	Mixed-Integer Linear Program
MIMO	Multiple Input Multiple Output
MOR	Model Order Reduction
MPC	Model Predictive Control
NaCl	Sodium chloride
NMBE	mean biased error
P2P	Peer-to-peer
PCM	Phase change material
PID	Proportional-Integral-Derivative
PLC	Programmable Logic Controller
PSO	Particle Swarm Optimization
RBC	Rule Based Control
RC model	Resistance-Capacitance model
RL	Reinforcement Learning
ROM	Reduced Order Model
RSME	root mean squared error
SLSQP	Sequential Least Squares Quadratic Programming
SVM	Support Machine Vector
TF	Transfer-Function
TOU	Time-of-use
UKF	Unscented Kalman Filter

Chapter 1

Introduction

Construction and operation of buildings are among the largest energy consumers in the world, as they represent 36% of global final energy use and 39% of energy-related carbon dioxide (CO_2) emissions in 2017 (IEA, 2018). The operation of a building is directly affected by the fluctuations in weather and occupancy that are then reflected in variations in the space conditioning loads that buildings impose on the utility grid during daytime and nighttime. To deal with these fluctuations in an optimal manner, a good understanding of the thermodynamic behaviour of buildings and a focus on energy management is necessary.

One of the critical challenges associated with buildings and renewable energy is that the peak consumption periods seldom coincide with the availability of power generation from renewable sources. In the case of the utility grid in California, this supply-demand mismatch has been illustrated in Figure 1.1 by the concept of the California Independent System Operator (CAISO) "duck curve" (Denholm et al., 2015): peak consumption periods (morning and evening) do not coincide with the period of maximum generation which occurs in the middle of the day. Furthermore, the price and the available power supplied by the electric grid are usually significantly variable.

On the other hand, the province of Québec faces a different problem with electricity supply and demand mismatch during the winter due to space heating, rather than summer space cooling. In Québec, where more than 99.8% of the electric power is generated through hydroelectric plants of roughly 37 MW (Hydro-Québec, 2016), it is not unusual to find commercial buildings using electricity as their only energy source.

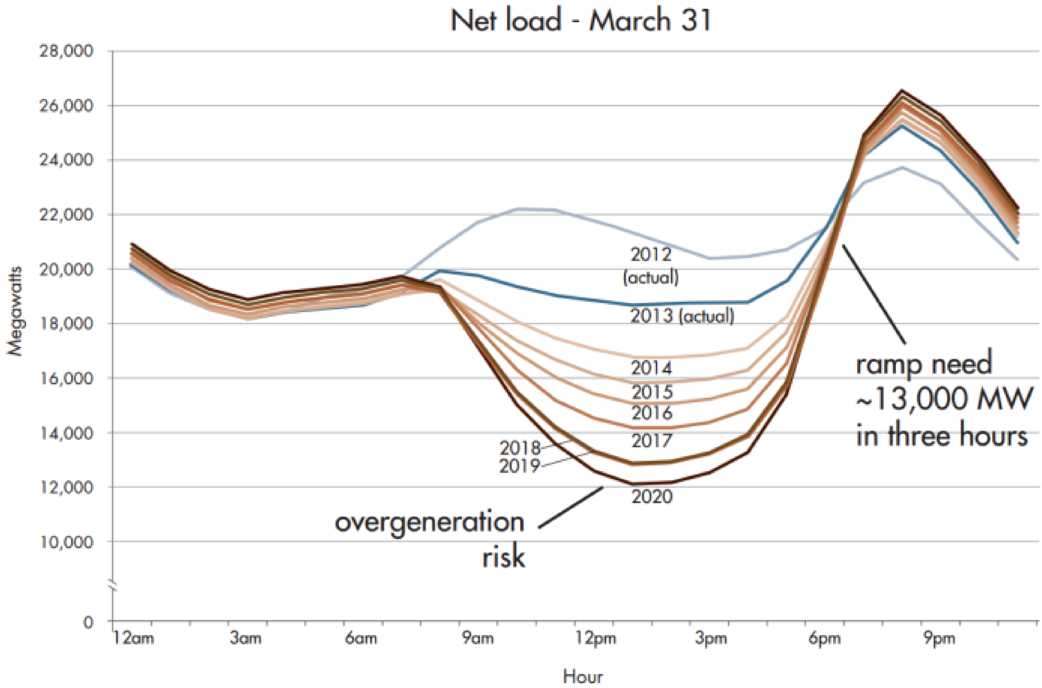

Figure 1.1: The CAISO duck chart: net load of California electric grid, *reprinted with permission from The California Independent System Operator Corporation* (as viewed at Figure 1, Denholm et al. (2015))

This is a result of low electricity rates, high fuel prices and limited distribution of gas in certain regions. It is estimated that heating in the Commercial and Institutional (C&I) building sector accounts for 9% of the province's winter peak demand (Hydro-Quebec Distribution, 2012). These buildings represent a significant portion of the electric load in the province. It is reported that 85% of Québec residential sector has electric based heating systems (Canada, 2011), while in Canada 27% of the Commercial & Institutional sector is electrically heated (Canada, 2012). During winter, peak loads associated with space heating impose a heavy burden on the grid, as shown in Figure 1.2. It should be noted that Figure 1.2 is an example representation of the problem and does not depict true values, as these numbers are not publicly available, although, generally the maximum peak value is disclosed as well as the general hours of the two observed daily peaks. Thus, there is increasing interest in demand response strategies, especially on cold winter days, and enabling energy flexibility and better building-grid interaction.

A report published in 2021 outlines the portion of energy consumption associated with different sectors in specifically in Québec. (Whitmore & Pineau, 2021). It was reported that in the province of Québec, 31% of energy consumption is done by buildings, with 18% associated with residential buildings and 14% associated with Commercial and Institutional (C&I)

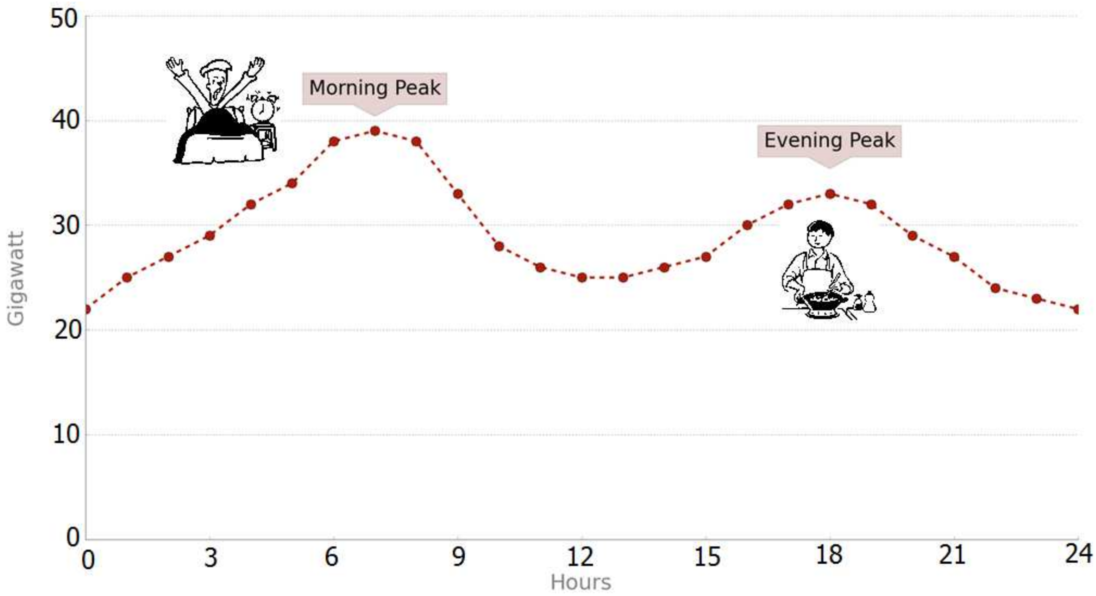

Figure 1.2: Peak electricity demand in Québec (example representation)

buildings (Figure 1.3).

Building load flexibility could be described as the ability to reduce the building energy demand and/or peak load, during a certain period of a day, through shifting or postponing consumption compared to a reference scenario. Building load flexibility – which may be enhanced by the incorporation of energy storage devices (Jensen et al., 2017, Reynders et al., 2018) – coupled with model-based control strategies is a key factor to optimize energy consumption to match the availability of renewable energy or available supply from the grid. The implementation of model-based control is an essential strategy for the optimization of energy consumption while preserving occupant comfort. Effective control strategies should be able to manage the various systems of a building, including thermal and/or electrical storage devices, and should take advantage of the thermal inertia of the building structure (Junker et al., 2018, Liu & Heiselberg, 2019, Reynders et al., 2018, 2017).

This work focuses on the development of control-oriented thermal models for buildings with convective heating systems, and convective active thermal energy storage devices, as well as the development of improved control strategies. These models are intended to be used within a model-based control strategy methodology for energy and load management in typical Quebec buildings during the heating season. While most research efforts have focused on improvements to the building envelope and energy-efficient HVAC systems, model-based control strategies

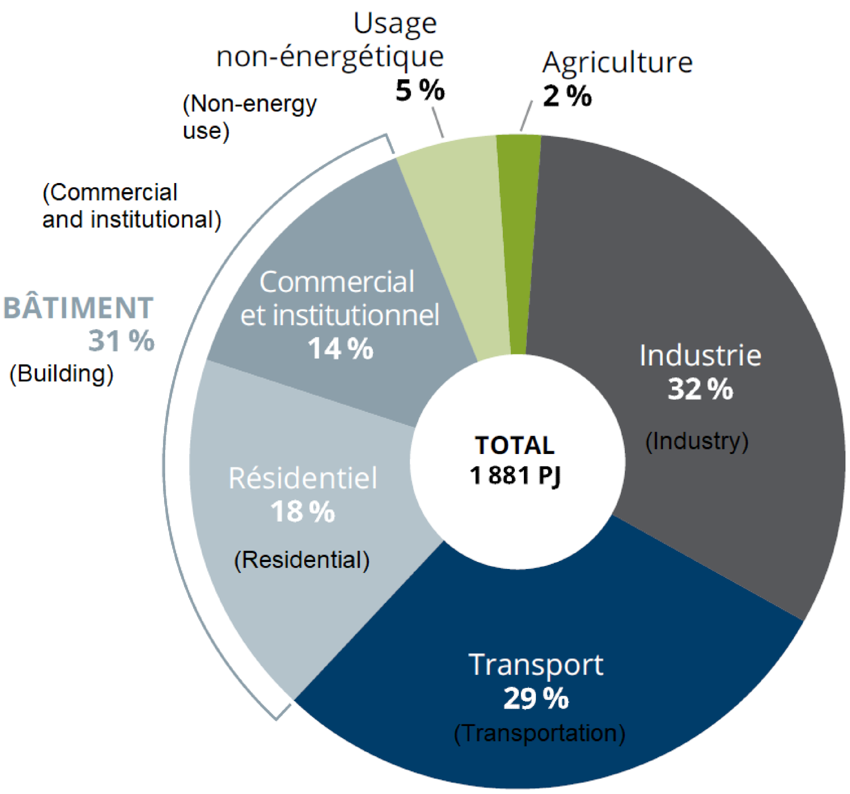

Figure 1.3: Energy consumption by sector, Québec, Canada, *reprinted and adapted with permission from Chair In Energy Sector Management, HEC Montréal* (Whitmore & Pineau, 2021)

have a largely unexploited potential in industry for saving energy, improved load regulation and optimizing thermal comfort.

The focus of this work is on typical buildings found in Quebec, where the methodologies developed could then be extrapolated to many similar style buildings in similar climate regions. Control strategies will target both energy savings and load management while considering the interaction between HVAC systems and the energy storage capacity in the thermal capacitance of the building structure and in dedicated thermal and/or electrical energy storage devices when present.

One major challenge for the implementation of model-based operation or model predictive control (MPC) in buildings is the effort needed to develop the thermal building model. This model must be accurate yet simple; however, obtaining such a well-performing model is often a difficult and time-consuming task. Modelling techniques suitable for the thermal dynamics of a building and its systems, such as grey-box linear modelling approaches (resistance-capacitance (RC) thermal networks, state-space representation, etc.) will be used. Model parameters will be identified based on knowledge of the geometry and materials of the building and through real-time calibration with measured data. Key model parameters may also be estimated using optimization algorithms.

1.1 Motivation and objectives

1.1.1 Problem statement

Theoretical background and research in MPC and model-based operations for buildings is well developed, with many strong and active research teams working in this area. However, examples of practical and robust model-based control strategies and methodologies that have been implemented in the building industry are still very limited.

The general objective of this study is to develop a robust and applicable model-based control methodology, with a foundation on state-of-the-art model-based control research findings and translate this foundation to operational rules that can be implemented in the existing building stock with convective heating systems. Linearized building thermal models are used, rules are developed for typical Quebec buildings, and the generalization scope for these strategies is discussed. While machine learning techniques are increasingly used to create control-oriented models and are expected to play a key role in the foreseeable future, purely data-driven modelling approaches are outside the scope of this thesis and reduced-order physics-based models (grey-box models) are employed in this work.

The phenomena and processes that occur in buildings typically are non-linear and discontinuous and require complex physical models ("white-box") or advanced data-driven models ("black-box") to accurately represent such detailed processes. However, the computational demand is increased in MPC when more complex models are employed, through increased simulation time as well as not being suitable for efficient optimization algorithms, which could be replaced with gradient-free algorithms (Drgoňa et al., 2020). Also, developing a detailed physics-based model of a building can be much more time-consuming and may require even more expert knowledge in the heat transfer and/or building performance simulation tools. It is therefore important that an acceptable compromise between model accuracy and simplicity is achieved.

Black-box models learn the building dynamics from measured data and make no prior assumptions of the physical relationships. The main advantages of the black-box modelling approach are that there is usually a lower associated development cost and that any signal can be an input or output, as there is no direct modelling of physical phenomena involved. One disadvantage of black-box models, however, is that they require extensive high-quality training data (Afroz et al., 2018) and are not reliable in operational situations outside of the training range (Afram & Janabi-Sharifi, 2014).

Special attention is required with data sets intended for training data-driven models, as poor or incomplete data may not capture all important system dynamics. Training data can be obtained from a detailed model (usually for research purposes) or from actual measurements (implementation purposes). With the first approach, different excitation signals can be introduced at no additional cost, however, an initial reliable and detailed model is required. In the second approach, when employing real measurements, the input excitations for obtaining sufficient training data are limited by the constraints of the current HVAC system operation.

When the main objective is designing building models suitable for control, the generated inputs must cover the control-relevant options of operating situations. Many system identification studies have used data from normal building and system operation; however, this data is routinely inadequate for a model to learn from and reliably estimate the building's behaviour and operational potential (Prívara et al., 2013). This is due to only a small portion of the possible HVAC operating range being used during normal operation. Consequently, the other underutilized operating conditions remain unexplored in the data by the model and thus cannot be learned. This is an important consideration for MPC, as often the identified optimized operating strategy is new and/or has never been implemented before in the building.

Modelling is one of the main barriers to implementing MPC in real buildings. The choice of a particular modelling approach (white-, grey-, or black-box) mainly depends on the available resources and information about the building and/or system. If detailed technical documentation of the building and expert physics-based modelling knowledge is available, then a white-box modelling approach may be desirable, as it leads to reliable and interpretable models which are based on physics, and with minimal requirements on sensor data quality/quantity (Afroz et al., 2018). While, if reliable and abundant sensor data are available, modelling using a black-box approach provides predictions with better accuracy and the model structure can be compatible with different buildings and systems (Afroz et al., 2018). In industry, there is a trend towards data-driven modelling approaches as they can be more easily automated and do not need an expert level of knowledge of the underlying heat transfer phenomena. Lastly, if adequate information about the building and HVAC system is available, along with useful historical measurements, the grey-box modelling approach may be more advantageous, as it comprises useful attributes from both white- and black-box approaches (Afroz et al., 2018).

Incorporating the principles of building energy flexibility together with on-site energy storage devices and advanced or optimized control strategies is essential for optimizing energy consumption and matching demand with the availability of energy from the grid at critical times, and the development of a suitable control-oriented thermal model is crucial for improving building energy flexibility and building-grid interaction. In this work, the focus was put on the grey-box type of modelling approach for building thermal modelling of buildings with convective heating systems and modelling for thermal energy storage devices. The two applications for reduced-order thermal modelling (buildings and thermal energy storage devices) require different modelling approaches for control applications. It was observed that many available case studies – which are representative of typical Quebec buildings – have adequate sensor points and data for creating a low-order model suitable for control, and grey-box modelling has strengths from both physics-based modelling, while also incorporating machine learning or optimization in the model development and calibration. However, further work could include investigating how purely data-driven models perform with the typically available data in representative Quebec buildings. Also, as buildings change, in terms of operation, physical elements, or occupancy schedules, a grey-box model can be easily modified to account for these changes. It is also expected that in the future, measured real-time data from the BAS will play an important role in the continuous calibration of the low order models that have been developed.

1.1.2 Objectives

The goal of this research work is to develop a methodology for the generation of control-oriented building models which can then be used within MPC or other model-based control strategies for eventual implementation into the building HVAC industry that can satisfy occupant comfort and improve grid interaction. A focus on developing a methodology to identify and evaluate MPC strategies that improve a building's energy flexibility or building-grid interaction capabilities. The focus of this research is on the winter operation of archetypal buildings found in Quebec, mainly low-mass and low-rise buildings. Radiant floor heating and other types of heating systems are applicable to these buildings; however, only convective heating systems will be considered in this work and in the case studies. Also, there is an emphasis on modelling thermal mass and thermal storage devices, while devices containing advanced materials such as phase change materials (PCM) are not considered.

Specific objectives of this study are:

- To develop and apply reduced-order models for model-based control of convective heating systems.
- To develop model-based predictive control strategies to optimize comfort and load management in typical Quebec buildings with active and passive thermal storage and convective heating systems.
- To apply the developed model-based control algorithms in typical case study buildings and study the benefits of MPC (and other model-based control approaches) applied to these building types.

Case studies Several case studies, shown in Figure 1.4, where measured operational data from the buildings can be used for model development and calibration, are used in this research. The chosen buildings are typical construction with convective-based heating systems widely seen throughout Quebec: a detached low-mass house, a low mass retail building, and a warehouse (with incorporated active thermal storage device).

Figure 1.4: Case studies: house (left), bank building (middle), Thermelect, *reprinted with permission from Karine Lavigne* (Lavigne, 2006) (right)

By looking at a wide array of archetypal buildings, a generalized methodology for the generation of robust reduced-order thermal building models was developed, tested, and used for different scenarios. It is typical for a detailed model of a single zone to have 20 to 50 capacitance nodes, while a reduced-order control-oriented model will typically have one to five nodes for a single zone. Models ranging from first-order (reduced-order model) up to 32^{nd} order (detailed benchmark model) have been developed for different purposes. Another goal of this research was to develop suitable control-oriented models for a thermal storage device; these models could be incorporated within advanced control strategies, such as model-based predictive control (MPC). Control-oriented models, along with a robust methodology, should facilitate the widespread adoption of advanced control by the building HVAC industry, leading to significant improvements in terms of load management, building energy flexibility and building-grid interaction, occupant comfort and an overall smoother operation.

1.2 Thesis overview

This thesis is organized in the following manner:

- **Chapter 1** presents the problem under study and the objectives of the investigation.
- **Chapter 2** presents a literature review describing the current state of theoretical and experimental tools available for building control, building control-based modelling techniques, real case studies of MPC implementation, building energy flexibility, and modelling of a high-temperature thermal storage device.

- **Chapter 3** provides the theoretical background for this research regarding thermal modelling methods such as finite difference methods, thermal networks, optimization and MPC.
- **Chapter 4** describes the general methodology employed in the development of the control algorithm and models useful for controls for convectively heated houses. This chapter also presents a residential building application and small commercial building application as demonstration projects. The results and contributions from this work are discussed.
- **Chapter 5** presents a methodology for reduced-order thermal dynamic model development of an electrically-heated high-temperature thermal storage device with heuristic control scenarios to improve peak demand of the building.
- **Chapter 6** introduces the Building Energy Flexibility Index ($BEFI$) and a methodology for MPC and Contingency studies with an active thermal storage device and associated warehouse building.
- **Chapter 7** presents the conclusion of the thesis, contributions, and suggestions for future work.

Chapter 2

Literature Review

Today, there is a growing trend to use Building Energy Management System (BEMS) in buildings to make the indoor built environment more comfortable and to use energy in a more efficient way. Currently, BEM's lack a building heating model and the control is often reactive and based on the current temperature of zones. The integration of a robust building heating model, along with future weather and occupancy forecasts into BEMS may assist in monitoring and planning the heating of buildings in an optimal way.

This chapter discusses existing literature on the topics of building thermal modelling, model-based predictive control, model parameter identification, building energy flexibility, and previous work on thermal energy storage, with specific interest on electrically-heated high-temperature energy storage (an economical alternative to batteries and a suitable storage device for buildings in Canada or other cold climates). In section 2.1, an overview of building thermal modelling approaches is presented. In section 2.2, reduced-order models (ROM) for building thermal modelling and modelling for building controls are presented. In section 2.3.1, work on MPC for buildings is presented. Section 2.4 introduces research work done on building-grid interaction and the concept of building energy flexibility, and section 2.5.1 outlines previous work on thermal energy storage devices suitable for applications in buildings. The following literature review outlines meaningful research work that has been developed for the areas of building thermal modelling and modelling for thermal energy storage devices – the first being considered as a *passive* storage medium, while the latter is an *active* storage medium – where the two (passive and active) require differing modelling approaches for control applications. The literature review includes work on non-convective heating and/or cooling studies to give a general overview to the topic, however, the scope of this thesis is solely on zones with convective heating systems and an air-based (convective) electrically-heated high-temperature thermal storage device.

2.1 Building thermal modeling approaches

The research field related to building modelling and energy performance prediction is very productive, involving various research domains (Foucquier et al., 2013). Among them one can distinguish physics-related fields, focusing on the resolution of equations simulating building thermal behaviour and mathematical-related ones, consisting in the implementation of a prediction model with the use of machine learning techniques. There is a third area where physics-based and mathematical-based techniques are combined, commonly referred to as grey-box models.

Obtaining a model that provides reliable predictions and can be implemented in real controllers is crucial for achieving optimal building performance. It is rather difficult to directly use sophisticated building models (EnergyPlus) for predictive control strategies as they are far too complex, their execution times become intolerable, and many inputs are required which are often not known. Models for control purposes must be sufficiently simple, but also robust and accurate enough for the desired application. Much research has focused on resistance-capacitance (RC) thermal networks for control applications where the parameters of the models have physical meaning, but mathematical techniques can also be implemented for parameter value identification and model order reduction.

2.1.1 Physics based modeling ("white-box")

The physical-based techniques of building thermal modelling are based on solving equations describing the physical behaviour of heat transfer. The principal in-coming and out-coming fluxes taking place in the heat transfer are conduction through the walls, convection, long wave and short-wave radiation and ventilation. The corresponding and relevant heat exchanges on a wall are shown in Figures 2.1 and 2.2 (DOE, 2013).

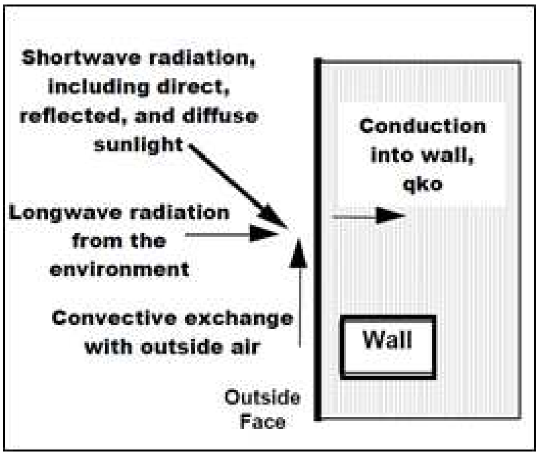

Figure 2.1: Outside heat balance control volume diagram, *reprinted with permission from Dr. Amir Roth* (DOE, 2013)

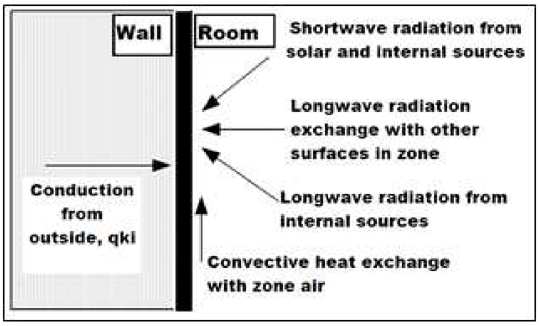

Figure 2.2: Inside heat balance control volume diagram, *reprinted with permission from Dr. Amir Roth* (DOE, 2013)

Commercial software for building thermal modelling and building performance simulation include TRNSYS (TRNSYS, 2020), EnergyPlus (EnergyPlus, 2020), IDA-ICE (IDA, 2020), ESP-r (ESP-r, 2020), Clim2000 (Bonneau et al., 1993), BSim (Rode & Grau, 2011) and BUILDOPT-VIE (BuildOpt-VIE, 2020), which all employ the lumped parameter method or conduction transfer functions. In the lumped parameter method, one zone is approximated to a node that is described by a unique temperature, pressure, etc. A node generally represents a room, a wall or the exterior of the building and can also represent more specific loads such as internal gains from occupants or equipment. The finite difference method is notably employed using a description of the heat transfers from an electrical analogy. It is very useful since it simplifies the physical problem through linearization of the equations and thus reduces the computation time. The principle of the electrical analogy is to associate a thermal resistance R and a thermal capacity C to a wall. The analogy gives the following equivalence with Ohm's law: $U_1 - U_2 = RI \Leftrightarrow \theta_1 - \theta_2 = \frac{e}{\lambda S}\Phi_L$. The temperature θ is equivalent to voltage U, the heat flux Φ_L to current I and the thermal resistance $e/\lambda S$ (L/kA) to electrical resistance R.

The great advantage of this technique is its ability to describe the behaviour of a multiple zone building on a large scale with a small computation time. It is well suited for the estimation of the energy consumption and the evolution of the space-averaged temperature in a room. One disadvantage is it difficult to study thermal comfort and air quality inside, due to simplifications used in the technique.

An alternative approach in dynamic thermal modelling involves using frequency-domain techniques. The frequency-domain approach has been shown to be efficient in building energy analysis in combination with thermal network theory (Athienitis et al., 1990a). This method can facilitate the integration of design and control (Chen et al., 2013). Shou (1991) stated some potential advantages of frequency-domain techniques over time-domain techniques: 1) More efficient and less expensive solutions than time domain since there is no time step involved in calculations in the frequency-domain, and 2) Discretization of elements with thermal mass is not needed. Rather, the exact solution is obtained from solving the equation for 1-D conduction heat transfer in the Laplace domain. The main disadvantage of frequency domain modelling is the challenge of incorporating non-linearities, such as temperature-dependent heat transfer coefficients. However, it is often acceptable to linearize equations for heat transfer phenomena (Shou, 1991). Athienitis et al. (1986) presented an analytical method to determine swings in room temperature in rooms with direct gain. Also, Athienitis et al. (1987) used discrete frequency domain methodology to determine auxiliary energy load in buildings. Haghighat & Athienitis (1988) compared two computer programs; one in a frequency-domain and the other in time-domain and compared their result with the experimental data.

Generally, a main disadvantage of the physical formulation is the fact that it suggests a detailed description of the physical behaviour. Therefore, it requires extensive knowledge on the physical system, especially on the mechanisms occurring inside and outside the building geometry. Unfortunately, this information is not always available. In contrast, statistical tools (black-box models) can produce models from measurements only using techniques such as machine learning or system identification.

2.1.2 Purely data-driven models ("black-box")

Black-box models learn the building dynamics from measured data and make no prior assumptions of the physical relationships. The main advantages are that there is usually a lower associated development cost and that any signal can be an input or output, as there is no direct modelling of physical phenomena involved. One disadvantage of black-box models, however, is that they require extensive high-quality training data (Afroz et al., 2018) and are not reliable in operational situations outside of the training range (Afram & Janabi-Sharifi, 2014).

The simplest black-box models are the parametric *linear models*. The forecasts of these models are linear in the observations, the uncertainty increases with the prediction horizon, and are commonly written in state-space formulation. The parametric *nonlinear models* provide a nonlinear relation between the inputs and outputs of the model and have a varying increase of their uncertainty over the prediction period. Artificial Neural Networks (ANN) may be the most well-known type of linear black-box models (Billings & Chen, 1992, Hagan et al., 1997, Siegelmann & Sontag, 1995). Huang et al. (2014) state that the application of ANN for MPC on real commercial buildings is challenging because of the complicated structure, which results in non-convex optimization problems that can be hard to solve, however, Chen et al. (2019) found the use of convex ANN in optimal control of the building HVAC system performed better than classical linear models. The *nonparametric models*, like k-Nearest Neighbors (kNN), Support Vector Machines (SVM), Decision trees (DT), and Random Forest (RF), do not make firm assumptions about the model structure. Therefore, these models can learn generic function mapping between inputs and outputs. The main drawbacks of these modelling approaches are the larger data requirements and the higher risk of over-fitting. Jain et al. (2017a,b), Smarra et al. (2018) present control-oriented building models based on regression trees and random forests. One last powerful nonparametric stochastic model type is the Gaussian Processes (GP). GP can account for the model uncertainty directly and provide a distribution of the predictions of the model, while also using prior knowledge in the system identification process. A study by (Zhang et al., 2015) found that GP used for building energy prediction are accurate and flexible.

2.1.3 Grey-box (hybrid) models

It is possible to overcome limitations of physics-based and statistical-based modelling methods by coupling them through a technique which is commonly referred to as Grey-box modelling. By retaining a part of physical meaning, the interpretability of the problem is not lost. Building characteristics can be determined by optimization techniques such as genetic algorithms gradient descent-based algorithms. Thus, it is not a requirement to have all physical and geometrical input parameters.

The principle of grey-box (or hybrid) models is based on the coupling of statistical and physical models. Grey-box modelling is well proven as a comprehensive and accurate method to model dynamical systems and obtain knowledge of the thermal properties of a building (Bacher & Madsen, 2011). One strategy consists of using statistical methods in fields where physical models are not effective or accurate enough. Another application would be to determine the heat behaviour in multiple zone buildings where the thermal properties of some zones are unknown. Some zones would be physically studied while others would need to be described statistically via measurements collected in these zones. One strategy consists in using machine learning as physical parameters estimator. Another strategy is to use statistics to implement a learning model describing the building behaviour.

The main advantage of the grey-box method is that it allows one to consider only a limited amount of data. Furthermore, the input parameters do not need to be fixed at the initial time of the simulation. Specified bounds on physical parameters can be used, and thus a rough characterization of the building geometry and thermal parameters is sufficient. Also, the hybrid methods allow one to retain a physical interpretation. The major pitfall to this approach is the potential difficulty in determining the value of the model parameters. They vary for every individual building and in many cases are time-variant. Thus, the choice of parameter estimation technique for inverse modelling is crucial; so that models of low complexity can be trained with minimal computational effort to yield reliable parameter estimates.

2.2 Reduced order building thermal models

Reduced-order models (ROM) offer distinct advantages for district modelling (Baetens et al., 2015, Lauster et al., 2014) and advanced control strategies (Bacher & Madsen, 2011, Lin et al., 2012, Wang & Xu, 2006). Simplified models allow for rapid simulation of complex and/or large systems with acceptable accuracy and benefit from quicker calibration procedures (Kummert et al., 2006). Research has focused on single-zone modelling and simplified modelling of multi-zone buildings (Deng et al., 2014, Hu & Karava, 2014, Kim & Braun, 2015). One common approach for simplified building modelling is grey-box RC thermal networks (Inderfurth et al., 2015), where system identification techniques are used to determine effective resistance and capacitance values for the model. Besides energy conservation measures, there is interest in

Table 2.1: Control-oriented modeling in buildings

References	HVAC System Type	Study type	Location	Simulation Software	Testing period
Bacher & Madsen (2011)	Electric heaters single zone	Iterative method to find RC models (Simulation and experiment)	Denmark	CTSM	Several months
Lin et al. (2012)	Single duct multi-zone	Varying model complexity (Simulation and experiment)	Florida	Not specified	1 summer day and 1 winter day
Goyal & Barooah (2012)	Single duct multi-zone	Model reduction method (Simulation)	Florida	MATLAB	1 day
Inderfurth et al. (2015)	Single duct multi-zone	Parameter identification (Simulation)	Germany	Modelica and GenOpt	1 year
Reynders et al. (2014c)	Heat pump with radiators	Parameter identification of reduced order models (Simulation)	Belgium	Modelica	5 data sets (February – June)
Wang & Xu (2006)	Multi-zone high rise	Identification of RC networks (Simulation and experiment)	Hong Kong	Not specified	Cooling season (14 days)
Kim & Braun (2018)	Single duct single zone	Field test	Florida	Not specified	Spring/summer (120 days)

ways to reduce peak power demand (due to space heating or cooling) at critical times (Fournier & Leduc, 2014, Leduc et al., 2011) and improve building-grid interaction.

There exist several specific studies on reduced-order thermal modelling of buildings, with noteworthy studies highlighted in Table 2.1. Hu & Karava (2014) presented a control-oriented modelling approach for multi-zone buildings with mixed-mode cooling, based on the linear state-space representation with varying coefficient matrices. Key features are the time-variant thermal resistances, associated with the heat extraction due to airflow, calculated using an airflow network model. A 53rd order LTV-SS mode was developed (Fig 2.3). Simulation results obtained with the LTV-SS model were compared with predictions using a non-linear finite different model to investigate the impact of the use of radiative and convective coefficients from the previous time step on dynamic system behaviour. The 53rd order LTV-SS model was considered as a true representation of the mixed-mode test-building and was used to identify the parameters of 4th order model (Fig 2.4) so that the difference of their outputs is minimized. Different prediction errors were found for the south and north zone. The reason is that the two zones have different system inputs, and each zone could be viewed as a thermal dynamic system. The inputs for the south zone include solar gain, outdoor temperature, natural and mechanical cooling. The north zone temperature dynamics mainly depend on the outdoor temperature, which is a continuous excitation with a smaller fluctuation magnitude.

Lin et al. (2012) raised two important questions related to control-oriented thermal models. (i) Q1: What is the minimum model complexity that is required to predict the temperature dynamics of a single zone with an acceptable degree of accuracy so that it can be used in MPC? (ii) Q2: How to identify the values of the uncertain parameters from measured data, and what

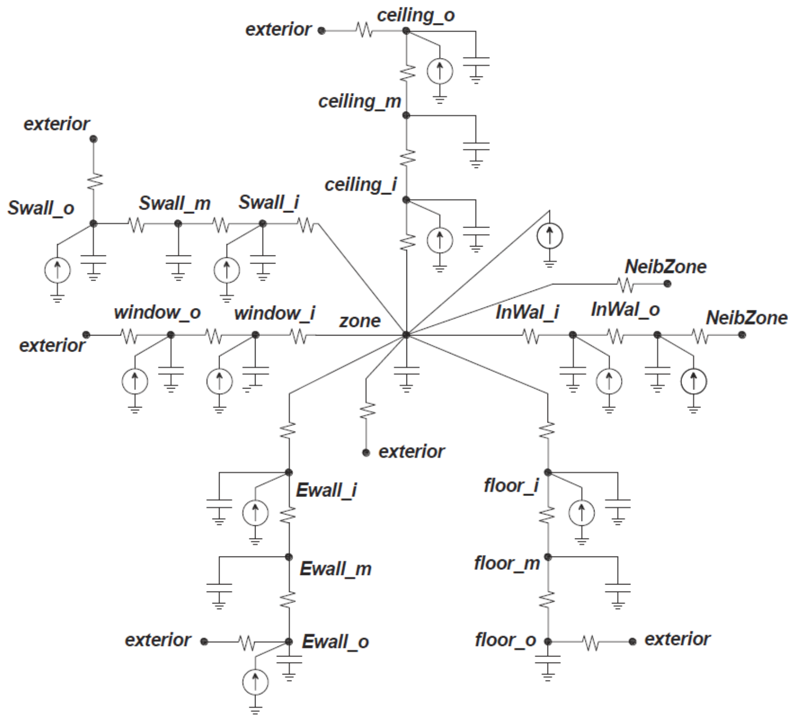

Figure 2.3: Thermal network of the test-building (south zone) - detailed model, *reprinted with permission from Dr. Panagiota Karava* (Hu & Karava, 2014).

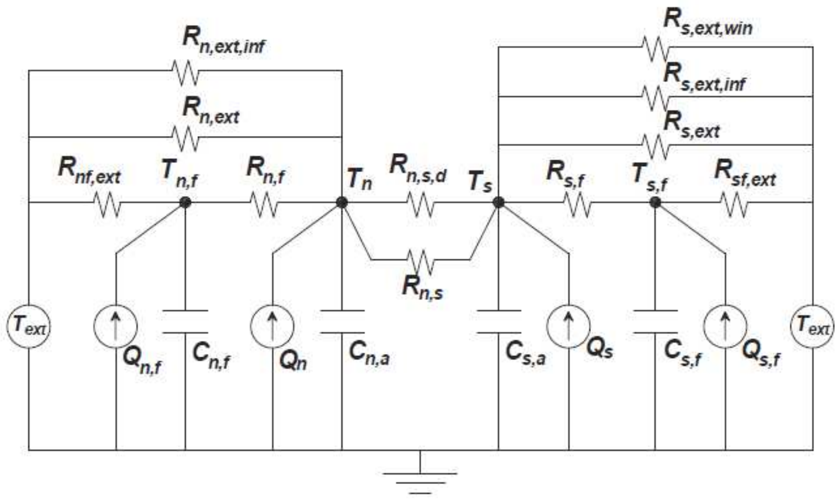

Figure 2.4: Thermal network for the test-building (two zones) - low-order model, *reprinted with permission from Dr. Panagiota Karava* (Hu & Karava, 2014).

kind of measured data is required, to achieve this level of accuracy? They compared a detailed model of a zone that employs the 3R-2C wall configuration that is commonly used to two low-order models (a first-order model and a second-order model). For calibration, two methods for parameter estimation, with different cost functions are studied: 1) Least-squares and 2) Maximum likelihood method. In minimizing the cost functions, the direct search method is used. The cost functions are non-convex, and optimization algorithms like gradient descent often get stuck in a local minimum. By using the direct search method, this problem is avoided.

Lin et al. (2012)'s analysis showed that for almost all closed-loop data, such comparison is meaningless; grossly "wrong" models can reproduce such data quite accurately. That the model is wrong becomes evident only when it is asked to predict measurements with very specific features, namely when there are large differences between the temperature of the room and the temperatures of the surroundings. This is in fact the situation that the model needs to be able to predict if it is going to be useful for control algorithms that seek to reduce energy, because the controller may let the temperature float up or down when the zone is unoccupied. Thus, they conclude, that unless specific forced response tests are conducted to gather certain types of data, one is better to use ASHRAE suggested R and C values of parameter rather than to estimate parameters from closed-loop data.

Foucquier et al. (2013) presented a comparison and a validation of a simplified model with the numerical software EnergyPlus on both low and high insulation mono-zone buildings. They study the effect of merging walls on the accuracy and the computation time. Contrary to expectations, increasing (or decreasing) the number of elements does not necessarily lead to minimizing (or increasing) the error, showing that the choice of the merged walls is essential. In a calibrating phase, it is quite difficult to find constant parameters for the entire year considering the season variation. Shamsi et al. (2019) devised a general reduced-order grey-box modelling approach to predict the thermal behaviour of commercial buildings. Based on easily identifiable building metrics, then a general structure to obtain the reduced-order models is produced, which reduces modelling complexities of dynamic simulation. Further development is needed on the identification of the walls between two zones. The thermal coupling between the zones obtained by the virtual experiments that were carried out resulted in a significant correlation between the temperatures in both zones. As a result, identifiability problems occur for the walls between the zones as well as for the integrated models for which both zones are identified at the same time.

Reynders et al. (2014b) studied 5 model types ranging from first to 5th order models (Figure 2.5). In general, two approaches are found to derive reduced-order models. The first group of reduced-order models is represented by physical white-box models that simulate the heating demand by simplified physical equations. In Reynders et al. (2014b)'s work, the influence of the used realistic measurements for the input signals is compared against a reference scenario where ideal data is used to identify suitable grey-box models. The identification process is carried out for both a well-insulated and a non-insulated single-family house.

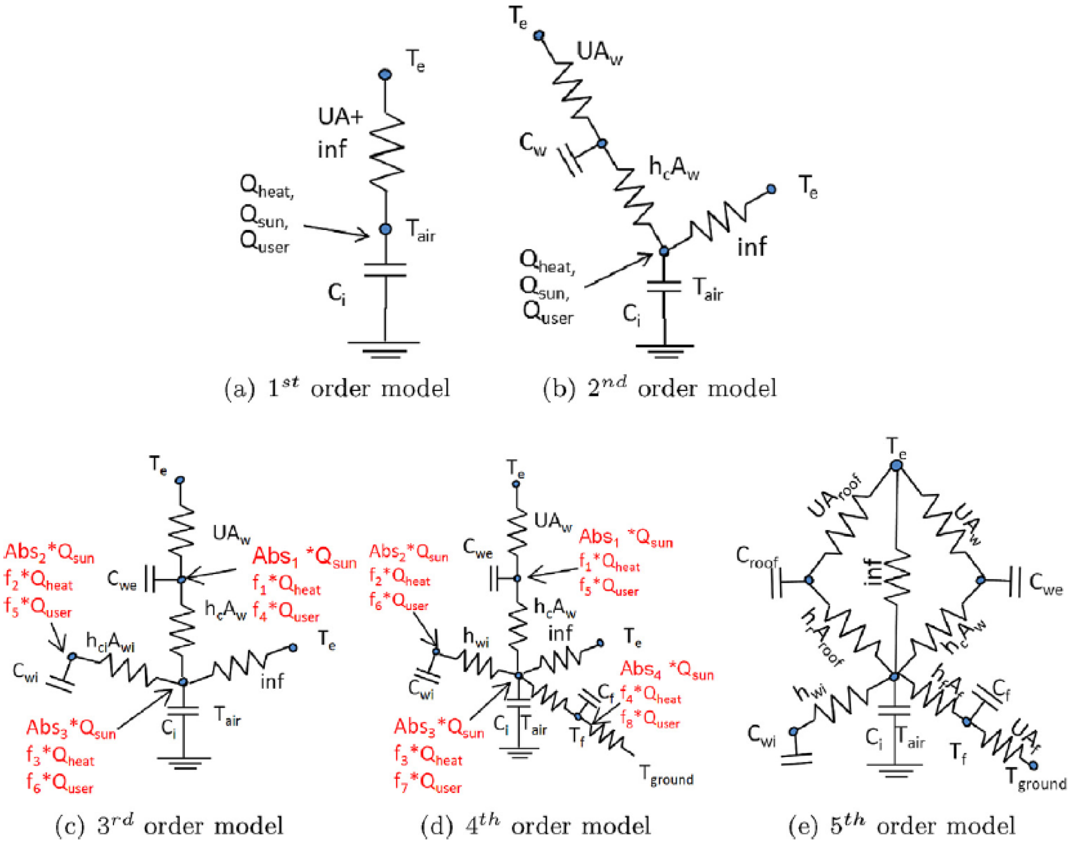

(a) 1^{st} order model (b) 2^{nd} order model

(c) 3^{rd} order model (d) 4^{th} order model (e) 5^{th} order model

Figure 2.5: RC-analogy of reduced order building models, *reprinted with permission from Dr. Dirk Saelens* (Reynders et al., 2014b)

In the first phase by Reynders et al. (2014b), the optimal model order for both building types is identified. For the non-insulated building, a 4th order model was selected since over-fitting problems occurred for the 5th order model. Although the improvement is small, the 5th order model results in a lower level of residuals for the insulated building. They conclude that their observed small differences in model structure between a well-insulated and an uninsulated building indicate that only a few model orders are adequate to represent the majority of buildings. In the second phase, a comparison of alternative, more feasible, measurements for the effective solar and internal gains, shows that the use of respectively the total irradiation on the vertical planes along the cardinal directions and the domestic electricity demand are suitable alternatives as inputs. Especially in winter, the dynamic indoor temperature and the instantaneous heat demand are well predicted, making the models suitable for application in the context of demand-side management using the structural thermal mass as a storage capacity in Smart Grids.

Ramallo-González et al. (2013) developed a new, more accurate, analytic method, named the Dominant Layer Method, for creating parameters of a second-order lumped parameter model, which can be used to represent multi-layered constructions. This new method does not require complex numerical operations but is obtained using a simple analysis of the relative influence of the different layers within a construction type on its overall dynamic behaviour.

2.3 Modeling for building thermal controls

Modelling for the purpose of developing building control strategies is different than the simulation of a building for analyzing its overall performance or for design. Suitable simplified multi-zone thermal models enable a rapid assessment of control strategies targeting such things as energy reduction, building-grid interaction, or occupant thermal comfort (Bacher & Madsen, 2011, Candanedo et al., 2011, Lin et al., 2012, Wang & Xu, 2006) and advanced control strategies could greatly benefit from adequate, simple models (Sturzenegger et al., 2016).

Models that are developed using special building performance software (e.g., EnergyPlus, TRNSYS, etc.) may produce highly accurate building heating models. Even though they are usually highly accurate, they may have a high computational burden with a delayed response that makes them unsuitable for control applications. More importantly, they also take more time to create and are more difficult to calibrate since they involve many parameters. Therefore, the selection of a physics-based building heating model for online control should consider the model complexity, desired accuracy, and ease of calibration.

Classical control techniques such as bang-bang or "thermostat control" (On/Off control with predefined setpoints) or proportional-integral closed-loop feedback control are popular control algorithms used in BEMS. However, the behaviour of the thermal dynamics of a building is variable, owing to the thermal interactions among the different zones and HVAC (Heating, Ventilation, and Air Conditioning) system, and the variable boundary conditions from weather conditions. Therefore, the use of classical control algorithms in such variable building systems may fall short to deliver the expected (desired or maximum potential) performance levels.

Presented in the following paragraphs are relevant works in the area of model-based control in buildings. Nguyen-Hong et al. (2017) presents an approach which is called meta-optimization combining with scattering analysis used to enhance on-site real-time temperature anticipation for energy management. The aim of this approach is to analyze the sensitivity of the parameters to simplify, and then attain, the best reduced model able to match with measurements regularly in a robust manner. The main idea of scattering parameters analysis initially introduced by (Le Mounier et al., 2014) is to find which parameters are the most scattering and hard to converge through optimization. After that, they are fixed to their physical value, hence decreasing the number of dependent parameters and hopefully, the optimization process could converge easier. The methodology integrating meta-optimization and scattering analysis improves the model identification process. It also decreases the calculation time by providing a logical way to simplify the model. Some aspects could be improved, such as the numbers and procedures of meta-optimization progress per cycle, which are still the most consuming processes. Improving initial values of parameters sets the distribution in the searching range could also enhance optimization performances.

Donghun & Braun (2012) presents methods and results for representing the complex thermal network of a building envelope and interior in the form of reduced-order state-space equations that can more easily be applied in model-based predictive and other advanced control approaches. The complexities of heat transfer phenomena through glazings and long-wavelength exchanges among walls make the representation difficult. The model employs the net radiosity method for long-wave interaction, one-dimensional transient conduction through walls, conductive and convective coupling between zones, etc. Model order reduction is applied to simplify the state-space representation.

Perera et al. (2016) studied modelling strategies that are suitable for online control with acceptable performance and accuracy. They studied physics-based multi-floor building heating models developed in MATLAB and Modelica environments (Figure 2.6). The model should be application-independent and can thus apply to different building configurations. It is essential that the model can perform in BEMS to improve the energy efficiency of buildings. Models for multi-zone buildings often appear with building-specific software tools such as EnergyPlus, Fluent and TRNSYS, but there are still challenges in modelling the inter-flow air exchanges and conduction heat transfers through intermediate walls and floors. In their review, Perera et al. (2016) found no published articles on the simplified physical modelling of multi-floor buildings. Convection heat transfer is one of the primary modes of heat transfer in buildings. They reported a lack of building heating models developed for multi-floor buildings, where inter-floor air/heat circulations contribute significantly to the differing energy consumption of the different zones. The determination of the vertical air exchange rate between two floors is not straightforward. This mass flow rate depends on the density difference and pressure difference between the two spaces. The measurement of the pressure difference between the two floors is a challenge because it is small, and the accuracy of pressure sensors is typically similar to the real pressure difference. Though previously developed models do achieve good results in modelling applications, they are, for the most part, building type specific and limited to a few heat-transfer processes. Models that are simple, flexible, robust, and suitable for control applications are still lacking. The significance of the model developed by Perera et al. (2016) is that it addresses ventilation heat losses in between inside-outside and inside-inside. Inside-inside heat losses between different floors are modelled using a non-linear algebraic equation. Walls, floors, roofs, and intermediate floors normally consist of several layers of dissimilar materials such as wood, concrete, and insulation.

Figure 2.6: Modeling of multi-floor buildings, *reprinted with permission from Wathsala Perera* (Perera et al., 2016)

Srivastava et al. (2019) conducted a nationwide survey of 448 building energy management professionals in the United States to help answer the following questions: 1) what impacts the adoption of data analytics and simulation among building energy management professionals; 2) in what phases of the building energy management decision-making process are data analytics and simulation currently used, and 3) what are the barriers of use for data analytics and simulation and how can they be improved to better support building energy management decision-making.

Overall, their key insights include:

- Professional domain plays a large role in driving the uses, barriers and expectations for data analytics and simulation tools.
- Data analytics and simulation are most used in similar phases of the decision-making process and can be coupled to leverage their functions.
- The accuracy of results needs to be improved for both data analytics and simulation tools.
- Professionals need more and improved training, especially for simulation tools.

Model order reduction (MOR) methods are attractive and much more reliable than identification approaches since they directly extract a lower-dimensional model from a detailed physics-based model without any pre-simulations. However, because of computational and data storage requirements, there are challenges of applying these methods to a large-scale building. To overcome the problem, Kim et al. (2020) introduced the Krylov subspace method to the building science field. Technical issues in applying the method to building applications are addressed and a suitable algorithm that overcomes those challenges is presented. To demonstrate the reliability of the algorithm, comparisons between the resulted reduced-order model (ROM) and a high-fidelity model from a commercial BES software for a 60-zone case study building are provided. The ROM was a factor of 100 faster than the high-fidelity model but with high accuracy.

Ye et al. (2020) aimed to develop new baseline models for the U.S. medium office buildings. The methodology they introduced consists of three phases: (1) identification of model inputs, (2) model calibration, and (3) model validation with uncertainty analysis. The evaluation index is the coefficient of variation of the root-mean-square deviation (CV(RMSD)) of site energy use intensities (EUIs) between the modelled baseline and empirical baseline. Thirty baseline models for two vintages (pre- and post-1980) and 15 climate zones were then created and evaluation showed that the CV(RMSD) is lower than 0.05 for the modelled baselines produced by the new baseline models. As a comparison, the CV(RMSD) is higher than 0.1 for the existing modelled baselines generated by DOE Commercial Reference Building Models. Further analysis showed that the newly developed baseline models were able to capture the uncertainties of representative features of existing buildings.

Arroyo et al. (2020) proposed a methodology to facilitate the identification of higher-order grey-box models for multi-zone buildings following a centralized approach. The methodology is implemented for an emulator building of the Building Optimization Performance Test (BOPTEST) framework (Blum et al., 2019) and compared against a decentralized and a single-zone model in both simulation and control performance. The results show a relevant impact of the used training data length. One week of data is enough to identify the multi-zone building model. When comparing the models in simulation performance, the centralized model slightly outperforms the decentralized model and shows similar accuracy as the single-zone model. In control performance, the differences are more significant: the decentralized model is the one exhibiting the worst comfort whereas the centralized model does not overestimate the temperature in any zone which leads to the minimum possible comfort violations. The multi-zone centralized model also outperforms the single-zone model by achieving lower discomfort that is more heavily penalized than the cost in the objective function. However, the single-zone model shows a surprisingly good performance, although a perfect hydraulic balance is assumed. These results suggest that the thermal interactions among zones should be modelled for multi-zone buildings and that single-zone models are suitable as well if the heat distribution to the zones is properly balanced.

Assessing the system-wide DR potential from heat pumps requires adequate models to account for the thermal response of the building stock to flexible operating strategies. Sperber et al. (2020) looked at reduced-order thermal response models of twelve representative German building types in three insulation states based on a grey-box modelling approach. The identified models reveal a good compromise between the accuracy of the simulated indoor temperature (RMSE of on average 0.6 °C) and computational cost (acceleration by factor 250) compared to the complex building simulation software TRNSYS. Furthermore, these reduced-order models are employed in a case study to estimate the technical DR potential of heat pumps by passive storage at specified ambient conditions.

Modelling techniques suitable for the thermal dynamics of a building and its systems, such as grey-box linear modelling approaches (RC thermal networks, state-space representations, etc.) can be used for control purposes (Candanedo et al., 2013, Inderfurth et al., 2015). Model parameters can be identified based on knowledge of the geometry and materials of the building and through real-time calibration with measured data. System identification techniques can also be used to determine effective resistance and capacitance values for the model (Deng et al., 2014, Fux et al., 2014, Kim & Braun, 2015).

Low-order models allow for fast and easy simulations to help choose proper operation and control strategies in order to improve energy consumption, occupancy comfort or peak demand reduction; these types of models can also be useful for such anticipatory or MPC applications (Cigler et al., 2013b, Donghun & Braun, 2012, Kummert et al., 2001, Moroşan et al., 2010, Oldewurtel et al., 2012, Picard et al., 2016, Touretzky & Baldea, 2014).

The goal of this research is to develop suitable control-oriented models for buildings and thermal storage devices with the purpose of using these models within advanced control strategies schemes, such as model-based predictive control (MPC). Reduced-order models suitable for control applications, along with a comprehensive methodology, will help facilitate the widespread adoption of advanced control by the building HVAC industry, leading to significant improvements in terms of load management, building energy flexibility and building grid-interaction, and occupant comfort.

2.3.1 Model-based predictive control for buildings

Model Predictive Control (MPC) is a multivariable control algorithm that uses an internal dynamic model of the system, a history of past control moves, forecasts of future disturbances (i.e., weather forecast) and an optimization cost function that is minimized over the receding prediction horizon (i.e., the period for which future information is available, ranging from a few hours to a few days). The potential of MPC to improve energy management in buildings has been amply demonstrated over the last decade (Cigler et al., 2013b, Kummert et al., 2001, Oldewurtel et al., 2012, Touretzky & Baldea, 2014). The basic principle of MPC in buildings is that knowledge of forecast weather and anticipated occupancy schedules enables better control of the building energy systems, for example, by better managing thermal storage capabilities. Because of the number of variables and constraints that must be considered, optimization of the problem can become quite complex. Once the optimization algorithm determines the optimal sequence of control moves, these moves are applied to a “control horizon”, a period that is often shorter than the prediction horizon.

Setting up a suitable control-oriented model for the building is crucial for MPC. The degree of modelling effort is difficult to assess in advance as each model is typically tailored for one specific building. MPC design requires a certain degree of knowledge on building modelling, such as a good understanding of what details are appropriate to include or exclude in the control model. One modelling approach is to develop a low-order grey-box resistance-capacitance (RC) thermal network to represent the building. The parameters of this grey-box model should be calibrated by using real measurement data from the existing building. Purely data-driven models are reliable and robust, but they cannot be easily applied in other buildings, and cannot identify (potentially optimal) control moves that were not present in the training data set.

Simulation studies often use two building models: a simulation model, meant to represent the building as accurately as possible, and a control-oriented model, a simpler representation that facilitates the solution of the optimization problem (Hu & Karava, 2014, Moroşan et al., 2010, Oldewurtel et al., 2012). In field studies or experiments, only the control-oriented model is necessary (De Coninck & Helsen, 2016).

An alternative to a formal MPC approach for identifying optimal temperature setpoints consists of implementing simple linear ramping profiles in place of abrupt setup or setback profiles. Gradual ramps over a given period of time can result in a significant reduction in the peak power demand required to change from one setpoint value to another, as demonstrated in Date et al. (2016b,c), Morris et al. (1994). Ramp setpoint profiles with different start times can be used in different zones of a building to stagger when heating the zones begin. By staggering the start times, the building heating demand is smoothed over a certain period. Preheating by a few degrees can also be used when transitioning from a night setback to a comfortable temperature. By preheating during an off-peak time and to a temperature that is still satisfactory to occupants, the peak demand during critical times can be further reduced. Pre-determined rules of operation based on the building dynamics and short-term dynamics offer a pathway to optimize the operation of the building. For example, Candanedo et al. (2015) proposed near-optimal profiles for transitioning between a night setback and a daytime temperature profile. This optimal transition curve, which significantly reduces the peak load in this period, depends only on the time constant of the space and the "transition time" established by the building operator.

MPC for buildings has been a popular research topic in the past years. Several studies and experimental setups have shown the energy savings potential of MPC up to 30% compared to the conventional control strategies. Besides modelling of the buildings, the bottleneck of MPC wide spreading is the understanding of the concept of MPC by HVAC engineers and managers. Therefore, the objective of Cigler et al. (2013b) was to develop a tool that would make MPC strategy for buildings more understandable for the wide public. The application BuildingLAB enables users to explore the controller's behaviour, tune controllers with aid of displaying and comparing simulation results, validate mathematical models of the particular building, etc.

Most current building control systems rely on a combination of bang-bang or PID feedback control and schedule-based setpoint, without considering all the necessary information to decide an optimal performance trajectory for a given objective (weather forecasts, energy prices, occupancy). In addition, the current control systems do not provide meaningful feedback to operators about the impact of certain control actions on system performance, which would help operators better manage systems according to their objectives.

MPC is an established control technique in other fields, such as chemical processing and electrical engineering (Qin & Badgwell, 2003); it is also a promising strategy for improved controls in buildings. MPC has received increasing attention in building operations research but has yet to become a mainstream practice in the industry. Due to the number of variables and constraints that must be considered, optimization can quickly become quite complex. Establishing suitable control-oriented models for buildings is essential for well-functioning MPC. The degree of modelling effort is difficult to assess in advance as each model is typically tailored for one specific building. Today, MPC design and implementation requires expert knowledge on building modelling and systems, namely, a good understanding of what details are appropriate to include or exclude in the building control model. The time lags introduced by the building, its HVAC system and the sensor-control system are one of the major causes of complexity in controlling indoor environments (Athienitis et al., 1990b). Decisions must be taken with anticipation, considering the inertia of the system. Storage and control are some of the key problems of solar energy engineering. Predictive control can help in dealing with solar energy variability. MPC techniques have been mostly applied to commercial building applications. Simplified models obtained from more detailed models, can be used to implement MPC strategies. With both grey-box and white-box modelling approaches, determining the required level of model complexity to develop an adequate MPC strategy remains a challenge, and no systematic method to determine this optimal model complexity is yet available (or standardized) (Houda et al., 2015, Kircher & Zhang, 2015, Lin et al., 2012, Reynders et al., 2014c).

Conventional control in buildings is often reactive: the operation of the system is based on basic feedback loops (ON/OFF, PID) and heuristic rules. Model-based Predictive Control (MPC), depicted in Figure 2.7, uses a model of the system (building and HVAC) and predictions of future disturbances (weather, occupancy) to select an optimal set of control operations. Model-based control strategies have largely unexploited potential for reducing the building energy demand and the peak load, while subject to operating constraints such as occupant thermal comfort. To deal with load fluctuations, a good understanding of the dynamic behaviour and a focus on energy management is necessary. Selecting the complexity level of the building model remains a fundamental problem. More research is needed on the selection of adequate model resolution in building simulation. The difficulty of this task lies in deciding which details can be neglected without jeopardizing the validity of the conclusions.

In the following paragraphs, past research on MPC model development is presented and a list of projects successfully implementing MPC in a real building is shown in Table 2.2. Jorissen & Helsen (2016) present a Linear Automated Toolchain for MPC (LAT-MPC) that allows highly automating the process of setting up a controller model and running a linear MPC. From this process automation, new research comes into the picture such as integrated optimal control and design of buildings.

Hou et al. (2016) investigated a distributed MPC approach based on a variant of the Alternating Direction Method of Multipliers (ADMM). The proposed method is highly scalable and facilitates a device-level plug-and-play implementation. A case study was carried out in an open office space of multiple thermal zones with individual thermostat controls. There are significant thermal couplings due to direct air exchange and noticeable load gradient between zones, thus a multiple thermal zones coordination problem is formulated with the objective of optimally scheduling the different thermostat setpoints for energy minimization and comfort

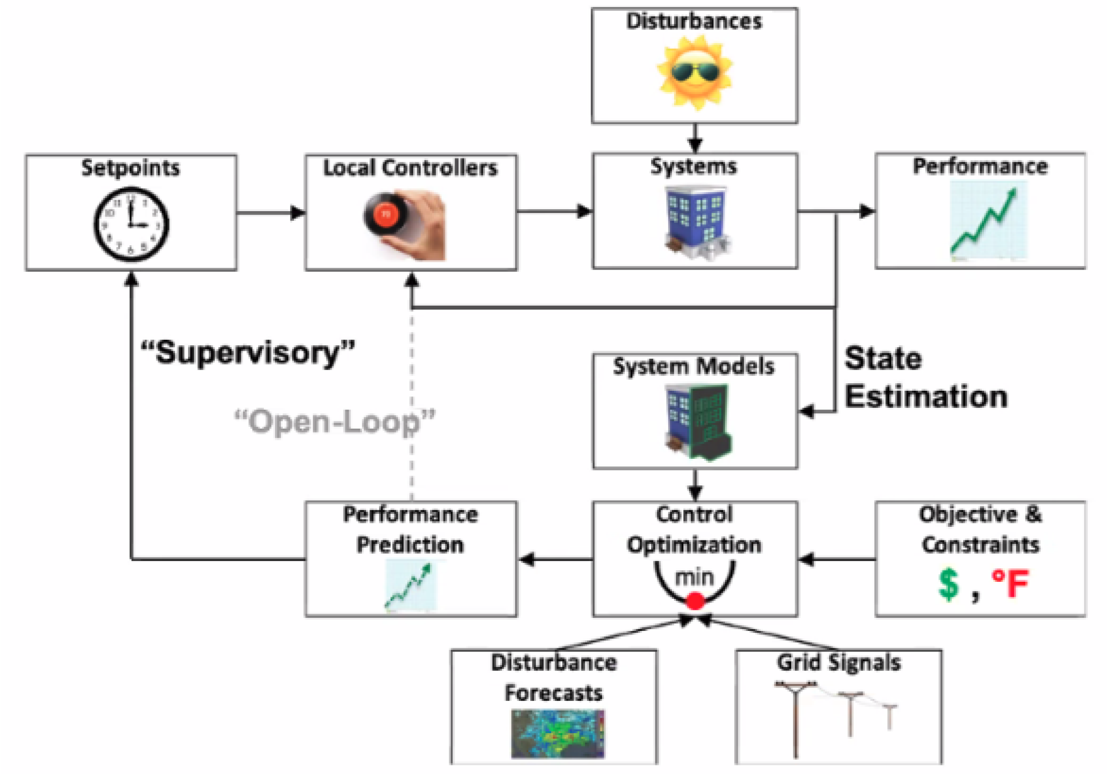

Figure 2.7: Model Predictive Control (MPC) concept, *reprinted with permission from Dr. David Blum* (Blum, 2019)

Table 2.2: Model-based control implemented in real buildings

References	HVAC System & Building Type	Model type	Location	Testing Period	Results
Sturzenegger et al. (2016)	Office building, radiant heating/cooling	RC network approach	Switzerland	Seven months	- 17% energy savings, - compared with EnergyPlus model
Váňa et al. (2014)	Office building, radiant heating/cooling	Grey-box RC network with identified parameters	Belgium	25 days	- 17% energy savings, - Compared with similar periods under RBC
De Coninck & Helsen (2016)	Office building, heat pumps and gas boiler	4th-order grey-box RC network (single zone)	Belgium	Heating season (60 days)	- 30% energy savings - Compared with similar periods under RBC
West et al. (2014)	Two office buildings, air system	Grey-box RC network	Australia	Heating season (60 days)	- 19% & 32% energy savings -
Prívara et al. (2011)	Large university building, ceiling radiant heating/cooling	Black-box, state-space	Czech Republic	Heating season (1.5 months)	- 17% to 24% energy savings
Široký et al. (2011)	Large university building, ceiling radiant heating/cooling	Grey-box RC network	Czech Republic	Two months	- 15% to 28% energy savings
Hilliard et al. (2017)	Academic building (LEED), campus loop, heat pumps, air system	EnergyPlus + black-box	Nova Scotia	Four Months	- 29% HVAC electrical reduction, - 63% thermal energy reduction
Afram et al. (2017)	Residential house, radiant floor with GSHP, AHU, TOU rates	White-box model	Toronto	Cooling season (22 days),	- Focus on load shifting in summer: - 16% - 50% cost savings

delivery while satisfying actuation constraints. Moroşan et al. (2010) performed a distributed MPC study. One information exchange per time step is proposed in this distributed MPC algorithm and good control performances and low computational requirements were observed. The distributed MPC takes advantages of both the decentralized control structure, as well as the centralized control structure. Blum & Wetter (2017) introduced the development of an open-source software platform for MPC in buildings, *MPCPy*. A number of specific features are expected to contribute to the solution:

- An emphasis is put on the use of adaptive models, which use measurements of the building performance to continually update and remain accurate enough for control optimization. Such models are expected to drastically reduce model setup and maintenance costs.
- Automatic model parameter estimation and optimization problem formulation together with flexible data input modules reduce the required MPC and programming expertise of users.
- The use of open software standards enables contributions from other researchers and adoption by industry while maintaining code maintenance and longevity due to the use of standards that have support in many industrial sectors.
- An extensible architecture enables rapid development and distribution of new MPC methods.

A newer iteration of a more general framework for testing any advanced control strategies in buildings was presented in 2019 (**?**). External components are currently based on the Modelica and Functional Mock-up Interface open standards, with system emulation models and MPC models able to be defined as native Modelica files or as Functional Mock-up Units (FMU).

The paper by Cai et al. (2016b) presented a general multi-agent control methodology that can be applied to building energy system optimization in a "plug-and-and-play" manner. A multi-agent framework is developed to automate the controller design process and reduce the building-specific engineering efforts. To support distributed decision-making, two alternative consensus-based optimized algorithms are adapted and implemented within the framework. Cai et al. (2016a) presented a general approach for determining maximum monthly energy cost savings associated with optimal supervisory control for cooling in commercial buildings in the presence of utility rates that include both demand and time-of-use energy charges. The developed tool incorporates a month-long time horizon due to the nature of demand charges and is only useful for bench-marking the performance of simpler and shorter-term demand response and optimal control approaches. The bench-marking problem was formulated as a dynamic optimization problem within a multi-agent control framework so that the monthly optimization problem is segmented into several sub-problems where each sub-problem involves system optimization for a shorter period of time, for example, a 1-day period.

De Coninck & Helsen (2016) implemented MPC in a medium-sized office building in Brussels and found an energy cost reduction of more than 30% for this particular building. In their paper, they outline monitoring techniques, model identification, forecasting of disturbances, state estimation, formulation and solving of the optimization problem and transmission of control signals. They note that an important step for wider implementation of MPC in buildings is to evaluate the performance with real operating conditions including measurement errors, limitations of the installed control system, communication issues, etc. The main differences between the MPC and original rule-based control (RBC) strategies are that the MPC uses the heat pumps much more, starts up earlier to pre-heat the building and strongly reduces the supply water temperature once the comfort setpoint has been reached. They also acknowledge that if the original RBC was different (or improved) and used the heat pumps more often the energy savings with MPC would have been smaller. However, the results of this single experiment with MPC containing many simplifications are encouraging for MPC use for controlling thermal systems in buildings.

Rehrl & Horn (2011) performed MPC on a real-world HVAC system consisting of standard industrial components. The core components of the system are water-to-air heat exchangers, both for heating and for cooling purposes as well as a steam humidifier. The following properties of HVAC systems make MPC a well-suited control methodology: the plant is a multiple input, multiple output system and its inputs are constrained – both in their value and in their rate of change. Also, several disturbances acting on the plant like varying outdoor air temperature or outdoor humidity can be measured. Furthermore, time constants are relatively large which makes it easy to perform the required optimization of the MPC strategy in time. The proposed control strategy in this study, namely the exact feedback linearization in combination with MPC proved to be a powerful approach to control HVAC systems.

Prívara et al. (2011) presented a model predictive controller (MPC) applied to the temperature control of a real building. The controller utilizes information on the thermal capacity of a building with the objective to minimize energy consumption, while the inside temperature is maintained at the desired level. Subspace methods are used to identify multiple input multiple output (MIMO) models. The controller was tested on a large university building during a heating season and achieved savings of 17–24% compared to the original controller.

Drgoňa et al. (2018) proposed a compact methodology for the construction of simple sub-optimal MPC-like control strategies for building control applications by using advanced machine learning algorithms. The focus is on the creation of a systematic and universal framework applicable to a variety of large-scale building control problems while providing valuable insights into the selection of the most relevant features and an appropriate type of approximation model. Although some approaches for a fast and simple online implementation of MPC for building control applications have been suggested previously (Ma et al., 2011, 2012), the task remains challenging, especially when using existing control hardware, such as programmable logic controllers (PLC). There are two main difficulties. First, such simple hardware provides only limited computational capabilities with a limited amount of memory storage (typically in the range of kilobytes). Second, most PLCs do not allow the control algorithm to be implemented in high-level languages. As a result, implementation of the complex, optimization-based control algorithms on simple hardware is cumbersome (Huyck et al., 2012). Though these hardware issues are one of the main barriers to the adoption of MPC, this work does not delve into looking into possible solutions to this particular problem.

Jorissen et al. (2019) developed TACO (Toolchain for Automated Control and Optimization), which is a Modelica-based automated toolchain for MPC of building systems. Its goal is to significantly reduce the engineering expertise and the time investment required for applying MPC to buildings. The implementation is verified using two example models and is benchmarked concerning accuracy and computation time. These results show that the computation time can be reduced significantly using the tool-chain options, while only slightly reducing the controller optimality. The numerous advantages of MPC for the control of building energy systems have been well documented. A key requirement for the successful implementation of such approaches is that strategies can be easily adapted to accommodate a range of building types with minimal commissioning effort. O'Dwyer et al. (2017) introduced an MPC-based building heating strategy, where the objectives of energy and thermal comfort are optimized in order of priority, where balancing the weights in the objective function is eliminated and thus the design of the strategy is simplified.

Bursill et al. (2020) proposed and tests an approach to MPC using rule extraction (RE) that can be easily implemented in building controllers to override sub-optimal control. The resulting decision trees could be implemented by building control programmers to save energy when ambient conditions are predicted to satisfy the thermal requirements of the spaces. A detailed MPC algorithm using inverse models was implemented in 27 rooms of an institutional building to provide data for a classification learning approach. Cooling and heating season decision trees were generated based on the inputs and outputs of the detailed MPC algorithm. An ensemble and sample randomization were used to generalize the trees across rooms and prevent over-fitting to individual rooms. A study by Ma et al. (2009) presented an MPC approach to building cooling systems with thermal energy storage. They focused on buildings equipped with a water tank to actively store cold water produced by a series of chillers. Using a simplified hybrid model of the system, a periodic robust invariant set as terminal constraints, and a moving window blocking strategy, through experiments they showed a reduction in the central plant electricity cost and an improvement in efficiency.

In 2016, Hilliard et al. (2016) performed a survey on the current MPC trends and opportunities highlights areas for further research and improvement. These areas included the optimization strategy, the effects of forecast disturbance assessment, and desirable traits of existing buildings under consideration for MPC implementation. The ability to integrate artificial intelligence into building models is another area of advancement, where the plant model can be updated based on recorded measurements from the building, leading to more accurate models that can adapt to equipment or operational changes over time. From their review, four studies analyzed single-zone systems, with two of the works derived from OptiControl (OptiControl, 2019). A key factor in zone-level studies is that more than one piece of equipment is operating to maintain thermal comfort, and the MPC takes a coordinated approach. Multi-zonal optimization for systems with both heating and cooling (Bengea et al., 2014, May-Ostendorp et al., 2013, West et al., 2014, Zhao et al., 2013) represents the most advanced systems and challenging control scenario in buildings. Such scope is advantageous because inter-zonal transfers of energy may be predicted.

The first noticeable trend of the research reviewed is the use of simplified models to represent the thermal dynamics of the building, whether it be RC models, linearized state-space models, or black-/grey-box models. Most of the reviewed papers used linear or quadratic optimization techniques, due to their simplicity and ability to guarantee to find the global minimum. The MPC optimization method will influence results. Linear and quadratic optimization techniques constitute over two-thirds of the optimizers reviewed. Nonlinear and particle swarm solving techniques are advantageous in that they allow for unique cost function structures, as they do not require derivatives and/or continuity. The trade-off to using these techniques is that they can be slow, computationally expensive, and may not find the optimal solution if the problem is too complex. Approximately one-third of reviewed articles by Hilliard et al. (2016) were experimentally verified. Ideally, all the studies should have experimental verification, and a greater emphasis should be placed on the results containing experimental verification.

A large body of work has shown that MPC can help enable buildings to meet these new requirements (Rockett & Hathway, 2017). However, despite its widespread adoption in other industries and its success in research, MPC has not been widely adopted in the building industry, except for a few companies offering MPC as a software service (BuildingIQ, 2019, QCoefficient, Inc, 2019) for commercial buildings and campus central plants (Johnson Controls, 2015). Several factors contribute to the lack of penetration of MPC into industry, as outlined by Rockett & Hathway (2017), with the foremost being 1) the lack of long-term trials showing the effectiveness of MPC and 2) the expense and skill required for installation and maintenance. This is particularly true for initial model configuration and maintaining model accuracy as building operation changes over time. Also, penetration of advanced building control techniques into the market has been slow since buildings are unique and site-specific controller design can be costly. Often, in medium- to large-sized commercial buildings, HVAC system configurations are very complex, which makes centralized control infeasible.

The development of self-learning models for both building response and optimization represents an area of research that has yet to be fully explored in relation to buildings. Further research should focus on evidence that directly compares the performance of specific optimization algorithms, parameters (time-step, horizon), and climate forecast accuracy for the same scenario. It is suggested that the sensitivity analysis of time-step and horizon, and climate forecast accuracy be further explored to fully understand the effects they have on performance. This will enable better methods to minimize and deal with these uncertainties in using MPC for building control.

Huang et al. (2016) investigated robust MPC which integrates uncertainty to improve the stability of MPC but found that the additional computational burden impeded performance and practicality. Jorissen & Helsen (2016) recognized the challenges of developing the required model of each building for an MPC controller, and that significant expert knowledge is often required for proper building thermal model development. Sturzenegger et al. (2016) showed a successful case of implementing MPC for 3 months in a real office building located in Switzerland. Data showed that adequate comfort levels for occupants were maintained, and it suggested that the MPC performance was greater compared to the original strategy.

Reinforcement Learning (RL), as another emerging technique that could be suitable for controls in buildings. RL has attracted growing research interest and demonstrated its potential to enhance building performance while touching some disadvantages of other advanced control techniques, such as MPC. Wang & Hong (2020) conducted a review of existing research on applied RL for building controls and found that RL is still in the research stage with limited applications in real buildings. Three noteworthy implementation barriers of RL controllers in actual building controls include: (1) a time-consuming and data-demanding training process, (2) lack of adequate control security and robustness, and (3) the generalization of RL controllers should be improved using approaches such as transfer learning.

2.3.2 Model parameter value identification

In most cases, simplified models for control applications must be calibrated and/or their model parameter values must be identified through either manual or automated mathematical techniques. There are many mathematical techniques for parameter value identification that have been explored in the context of building thermal modelling.

Since the real building parameters are often unknown in existing buildings and tend to deviate from the values used during the design of the control system, the use of statistical black-box models that have self-learning capabilities is an interesting topic (Chen et al., 2006, Cigler & Prívara, 2010, Liu & Henze, 2006). However, a substantial amount of data might be required to achieve the model accuracy needed for MPC. Moreover, the resulting parameters do not necessarily have a direct relation to the physical properties and can therefore not be extrapolated. To overcome this problem, grey-box models are introduced. Grey-box models rely on physical knowledge about the system dynamics to define the model structure. Statistical methods are then used to estimate the unknown parameters. If the model structure represents the physical behaviour of the system, these parameters could be linked directly to the physical properties of the building (Bacher & Madsen, 2011, Xu & Wang, 2008).

Vande Cavey et al. (2015) compared three different state estimation techniques and showed how they can improve the ability of the building model to correctly predict the behaviour of the real building. The methods studied in (Vande Cavey et al., 2015) are the unscented Kalman filter, the deterministic approach, and a moving horizon estimation scheme.

Houda et al. (2015) studied three optimization techniques to enable for the reliable calculation of as-built envelope thermal parameters (resistance and capacitance) based on measurements collected over a limited time period. The tool developed by Houda et al. (2015) is based on a combination of a basic physical model and optimization algorithms that automatically calibrate the model from measurements. The first method studied was based on a simple greedy resolution (Particle Swarm Optimization) and the other two methods were based on substitution model (Support Vector Regression and Meta-models). They found that meta-models coupled with a cross-validation method (kriging) lead to the best results. Based on a simple mono-zone building use case, the results show that convergence is faster in the case of PSO-SVM and kriging. PSO alone tends to get attracted by local minima and does not perform as well. The convergence patterns also suggest that kriging will be more robust and probably, the best candidate.

Inderfurth et al. (2015) proposed an approach to identify parameter sets for existing buildings based on low-order building models and optimization strategies using the Jeeves-Hooke general pattern search algorithm, as described in the GenOpt manual, for parameter identification. In numerous iterations, the algorithm minimizes a cost function. One noteworthy finding was that the identified parameter sets vary greatly from year to year. Especially parameters for thermal capacities are subject to huge variations. In lesser manner air change rates, window-wall ratios and thermal transmittance also differ from the derived values. This suggests that more than one combination of parameters can reflect the thermal behaviour of a given building reference. It was observed that considerably different combinations of parameters can reproduce the thermal behaviour of a given reference building model with reasonable accuracy for different years.

Reynders et al. (2014a) studied a bottom-up multi-zone modelling approach of Belgium residential building stock and one major finding was that the coupling between two adjacent rooms was found to reduce the identifiability of the model parameters, resulting in unreliable estimates of the inter-zonal heat flows. Reynders et al. (2014a) used two approaches to calculate the model parameters: (1) a theoretical calculation of the building parameters based on the building stock data completed by assumptions and rules-of-thumb, and (2) parameter identification using grey-box modelling, where a forward selection procedure was implemented. The model is systematically increased until the identified model captures all dynamics that are available in the dataset. It was found that the thermal dynamics can be described by 4 thermal capacities for the day-zone, 3 thermal capacities for the night-zone and 2 thermal capacities for the floor between day- and night-zone.

Various other researchers employed differing statistical approaches to solve the problem of parameter value identification. These attempts include recursive least-square methods (Chen & Athienitis, 2003), (Loveday et al., 1992), the extended Kalman filter (EKF) (Fux et al., 2014) and the unscented Kalman filter (UKF) (Radecki & Hencey, 2012). These techniques still have their shortcomings including local minimization (i.e., finding the minimal value in a certain range and not the overall minimum of the function) and the need for accurate starting values; both of which are problematic in a system designed to reduce the intervention by a technician or other knowledgeable individual.

2.4 Building energy flexibility: building-grid interaction

Building load flexibility can be described as the capability to alter the energy demand of a building at a specific time of day by postponing or shifting consumption when compared to a reference scenario (Business as Usual). Incorporating principles of building energy flexibility together with on-site energy storage devices and advanced or optimized control strategies is essential for optimizing energy consumption and matching demand with the availability of energy from the grid at critical times (Jensen et al., 2017, Reynders et al., 2018). In recent years, studies on the quantification and utilization of building energy flexibility have been conducted by various international research groups and there is now a comprehensive list of publications in this relatively new research area (International Energy Agency, 2020). Many studies have focused on the adjustability or flexibility of a building's space conditioning systems. In general, these studies study the impact of Demand Side Management (DSM) strategies at the building and/or energy infrastructure level.

Flexibility in individual buildings There exists several studies where they looked at a single building to determine its' energy flexibility potential. Le Dréau & Heiselberg (2016) assessed the potential of residential buildings to regulate heating power and identify strategies to capitalize on flexibility potential. Hurtado et al. (2017) proposed a method to quantify the demand flexibility potential of individual buildings, where they assessed the effects on demand flexibility due to weather fluctuations, construction variations, and occupant comfort consideration. Other researchers found that specific technologies and parametric optimizations are necessary for energy flexibility maximization in residential buildings, such as Weiß et al. (2019) who found that for buildings in Austria built after 1980, peak loads from space heating can be shifted to off-peak times by up to 50%.

Flexibility in building clusters Groups of buildings in operation together have also been considered in order to evaluate the potential of aggregated energy flexibility. Vigna et al. (2018) studied a cluster of buildings, where it is possible to take advantage of the disparities in energy consumption patterns between different building types. Foteinaki et al. (2018) investigated the potential for flexibility of low-energy buildings and analyzed the thermal storage capacity present in the structural mass. The study showed that low-energy buildings can remain autonomous for several hours and that when many buildings are aggregated together - rather than a stand-alone building - the flexibility becomes significant.

Energy flexible buildings, through smart DSM, smart DR, and incorporating efficient energy storage, are one of the most encouraging prospects to roll out storage and renewable technologies on a large scale in existing electricity networks.

From field study data, Aduda et al. (2016) demonstrated that office buildings can provide energy flexibility to the grid. However, they concluded that accurate flexibility potential estimation may be challenging due to variations in indoor air quality and thermal comfort in different zones within a building. In a study by Sánchez Ramos et al. (2019), demand management measures were analyzed by using the buildings' thermal mass as thermal storage. Cost savings of 3.2% for heating and 8.5% for cooling were observed after the implementation of the improved demand management control strategies. Previously refurbished buildings observed twice the amount of savings. They concluded that low installation costs of these measures make them feasible, given that regional electric pricing and user behaviour allow for acceptable flexibility. Perez et al. (2016) looked at the ability of individual residential customers to lower community-level peak demand. By harnessing individual preferences and physical differences between houses (i.e. insulation values, window type, how many floors, orientation etc), through control and scheduling, the peak demand was minimized for the neighbourhood. A reduction of one-quarter of the daily peak load was achieved for a group of houses when compared with the reference case of individually controlled thermostats and appliances. Sharma et al. (2016) proposed a centralized energy management system (CEMS) where optimized decisions were determined by considering realistic model parameter settings and customer preferences. Over a course of a day, it was shown to reduce both the energy cost and energy consumption of the customers. Patteeuw et al. (2016) investigated how the participation of residential heat pumps in load shifting could reduce operational costs and CO_2 emissions and potential ways to motivate homeowners with heat pumps to enable flexibility measures to see their benefits. From this study, it was seen that Operation during dynamic time-of-use (TOU) pricing performed well, however, dynamic TOU showed poorer outcomes at high levels of residential heat pump penetration. The *Smart Grid Application Guide: Integrating Facilities with the Electric Grid* by ASHRAE (2020) provides building owners, managers, and designers with guidance on the smart grid, applicable smart grid standards and regulations, and the design and operation of systems in this emerging industry. The guide details the concrete steps needed to prepare a building – whether new construction or renovation – for integration with the smart grid. Energy flexible buildings through smart demand-side management (DSM) or smart demand response (DR) using efficient energy storage, are currently one of the most promising options to deploy low-carbon technologies in the electricity networks without the need of reinforcing existing networks.

Zhu et al. (2016) propose a Cost-for-Deviation (CfD) retail-pricing scheme, which is designed to minimize the demand uncertainty of individual customers or communities. Day-ahead planning and real-time tracking optimization problems for individual buildings was developed. CfD pricing scheme for a community of two buildings was formulated and a collaboration scheme by which the two buildings negotiate was devised. A series of experiments demonstrate that CfD pricing was able to reduce demand uncertainty in a building or a community. By the virtue of end-users being able to closely monitor their daily loads and by paying fines for not adhering to their plans would ultimately benefit energy efficiency and will reduce infrastructure costs. Kolokotsa (2016) addresses critical issues on smart grid technologies and the integration of buildings in this new power grid framework. The main objective of this paper is to provide a contemporary look at the current state of the art in the potential of buildings and communities to be integrated into smart grids as well as to discuss the still-open research issues in this field. The challenges for the building sector are discussed and future research prospects are analyzed.

Talebi et al. (2017) report the development of a simplified model for predicting the thermal demand profile of a district heating system. The paper describes the method used to develop two types of simplified models to predict the thermal load of a variety of buildings (residential, office, attached, detached, etc.). The predictions were also compared with those made by the detailed simulation models. The simplified model was then utilized to predict the energy demand of a variety of district types (residential, commercial or mix), and its prediction accuracy was compared with those made by a detailed model: a good agreement was observed between the results.

A bottom-up method to generate synthetic residential loads realistically, but with minimal computational resources, is presented by Mammoli et al. (2019). Distributions for the number of events, start time and duration are proposed for four demographic categories: singles, couples, families, and retired people. The distributions are augmented by elasticity parameters that allow load control and shaping. The distributions are based on information from focus groups and online surveys. In principle, the method can produce data at arbitrary temporal and topological resolution and is thus suitable for a range of applications from machine learning of energy consumption patterns to detailed transient power flow analysis. It is shown that aggregated loads can be shaped to follow a desired signal, for example, to balance intermittent solar generation.

Significant load reduction achieved by residents' behavioural response is also demonstrated. Such load reductions could be invoked in the case of low-probability, high-consequence events, and could contribute to increased energy resilience at the community level.

In a paper by Zepter et al. (2019), they propose a framework to integrate prosumer communities into the existing day-ahead and intraday markets. Using a two-stage stochastic programming approach, we incorporate the sequenced decision-making in the wholesale system under uncertainty of renewable generation and spot prices. We focus on the value of peer-to-peer (P2P) trading in the integration of prosumers in the day-ahead and intra-day markets and investigate how residential battery storage contributes to local demand-side flexibility in an integrated market setting. To this end, they introduced the Smart elecTricity Exchange Platform (STEP) that represents the interface between the wholesale electricity markets and the prosumer communities and coordinates the community's operational supply-demand decisions. A study on residential buildings in London shows that both P2P trade and battery storage by themselves each induce a reduction of electricity bills by 20%–30%. Combined, P2P trade and battery storage may lead to savings of almost 60%. In other words, we find that peer-to-peer trade and flexibility options such as local storage generate higher levels of the community's self-sufficiency.

Badiei et al. (2019) described a new method to swiftly model the dynamics of heating energy demand and indoor air temperatures of houses and housing stocks. The Reduced data Energy Model (RdDEM) provides a cost-effective alternative to steady-state modelling by enhancing the input dataset from the Reduced data Standard Assessment Procedure (RdSAP) – the method used to calculate Energy Performance Certificates (EPC) in the UK. The new inferences and methodological enhancements were first tested and then implemented at scale using a sample of 83 semi-detached houses. Most energy results from RdDEM were within 10% of those from RdSAP. The differences are explained by the different ways that indoor air temperature is calculated.

Iria & Soares (2019) proposes a cluster-based optimization approach to support an aggregator in the definition of demand and supply bids for the day-ahead energy market. This approach consists of two steps. In the first step, the aggregated flexibility of the entire portfolio is computed by a centroid-based clustering algorithm. In the second step, the supply and demand bids are defined by an optimization model that can assume the form of a deterministic or a two-stage stochastic problem. A case study of 10,000 prosumers from the Iberian market is used to evaluate and compare the performance of the bidding optimization models with and without pre-clustering. The numerical results show that the optimized bidding strategies outperform an inflexible strategy by more than 20% of cost savings. The centroid-based clustering algorithm effectively reduces the execution times of the bidding optimization problems, without affecting the quality of the energy bids.

A stochastic bottom-up model for the generation of electric load profiles is introduced in a paper by Fischer et al. (2015). The model is designed for investigating the effects of occupant behaviour, appliance stock and efficiency on the electric load profile of an individual household. Probability distributions are incorporated for when and how often an appliance is operated. Duration of operation is given as probability density conditional on the start time. The results showed an accuracy of 91% and a correlation of up to 0.98. In the paper by Mikkola & Lund (2014), they present a new model for generating spatio-temporal power demand data for urban areas of the form P(x,y,t). The model is flexible and can be adjusted to different cases and local conditions. The dimensions of the model are not restricted, but a typical case would comprise an hour-by-hour simulation over a whole year with a spatial resolution from a few hundred meters up to several kilometres, depending on the area to be covered. These kinds of load profiles are useful when analyzing, e.g., smart grids, demand-side management, and renewable energy in the urban context.

Work by Kotzur et al. (2020) proposes a novel bottom-up model that consists of an aggregation algorithm to create a spatially distributed set of typical residential buildings from census data. Each typical building is then optimized with a Mixed-Integer Linear Program to derive its cost-optimal technology adoption and operation, determining its changing grid load in future scenarios. In a future scenario for 2050, photovoltaic and heat pumps are predicted to be the most economically and ecologically robust supply solutions for the different building types. Nevertheless, their electricity generation and demand temporally do not match, resulting in a doubling of the peak electricity grid load in the rural areas during the winter. The urban areas can compensate for this with efficient co-generation units, which are not cost-efficient in the rural areas.

Mata et al. (2014) presented a methodology by which national building stocks may be aggregated through archetype buildings. The accuracy of the description is validated by simulating energy demand using the ECCABS Building Stock Model and comparing the final energy demand modelled with corresponding statistical data. The total final energy demand calculated for these countries differs from available statistics by between 6% and 12%, which is considered satisfactory. Fernandes et al. (2014) proposed an innovative method to manage the appliances on a house during a demand response event. A dynamic load priority (DLP) method is proposed to change the load priority during a demand response event. A case study with two scenarios is presented considering a demand response with 30 min duration, and another with 240 min (4 h).

Di Giorgio & Liberati (2014) presented an event-driven MPC approach for a local energy management system, enabling residential consumers to automated participation in demand-side management (DSM) programs. Resources are coordinated according to the needs of maximizing self-consumption and minimizing the cost of energy consumption, in a contractual scenario characterized by designed or market indexed pricing models, with DSM options. The control action (appliances' start times, the storage charging profile and the IEC 61851 compliant charging profile of the electric vehicles) is updated every time an event triggers the controller, such as a user request, a price/volume signal, or the notification of a new forecast of micro-generation from the photovoltaic unit. Using a regression-based baseline model, Mathieu et al. (2011) presented a method to compute the error associated with estimates of several DR parameters. A metric was also developed to determine the amount of observed DR variability resulted from baseline model error rather than real variability in response. It was seen that most observed variability in the results was due to baseline model error.

The paper by Missaoui et al. (2014) deals with the performance analysis of a Global Model-Based Anticipative Building Energy Management System (GMBA-BEMS) managing household energy. This GMBA-BEMS can optimize a compromise between user comfort and energy cost considering occupant expectations and physical constraints like energy price and power limitations. To validate the GMBA-BEMS, the model of a building has been developed in MATLAB/Simulink. This work analyzes GMBA-BEMS application that manages appliances such as heating, washing machine and dishwasher from a grid point of view. Yoon et al. (2014) presented a controller that reduces peak load as well as saves electricity cost while maintaining reasonable thermal comfort. The controller changes the setpoint temperature when the electricity retail price is higher than a customer's pre-set price. Through simulation, they show that the controller could provide up to 10.8% of energy cost savings when dynamic pricing is present. Also, the results present the potential for peak load savings of 24.7% and 4.3% of total annual electrical energy savings for HVAC in homes.

The study by Yalcintas et al. (2015) investigates potential cost conservation measures that focus on reducing energy at times of higher energy costs to maximize energy savings. It is shown that shifting work schedules of office buildings with one shift 1 h early can slightly reduce monthly electricity rates by 1–3% and that thermal energy storage systems can be cost-effective for retrofits with dynamic pricing schedules and areas that need full replacement of air conditioning. The paper by Pallonetto et al. (2016) is concerned with the development and evaluation of control algorithms for the implementation of demand response strategies in a smart grid enabled all-electric residential building. An EnergyPlus model of a highly instrumented building is used to assess the effectiveness of demand response strategies using different time-of-use electricity tariffs in conjunction with zone thermal control. The analysis identified an annual reduction of consumer electricity consumption of up to 15.9%, lower carbon emissions of 27% and facilitated greater utilization of electricity generated by grid-scale renewable resources, resulting in a reduction of generation costs for the utility of up to 45.3%.

The study by Shen et al. (2016) evaluated the performance of conventional demand response at the building-group-level under common electricity prices. The evaluation results disclose major limitations of conventional demand response due to lack of coordination. Under time of use pricing, conventional HVAC demand response cannot effectively and efficiently reduce peak demand at the building-group-level. Under dynamic pricing, conventional HVAC demand response can cause a new undesirable peak demand at the building-group-level which could be much larger than the original one and impose stress on the grid. Coordinating demand response of individual buildings can solve these limitations. With improved performance at the building-group-level, simple coordinated examples have been given to demonstrate the need for coordination in conventional demand response. The study results show the significance of coordination in demand response and the grid pressures imposed by building peak demands can be better released if coordinated demand response is implemented.

2.5 Thermal energy storage in the context of buildings

The structural components of a building can themselves be treated as a thermal storage system in which the thermal energy is stored within the building materials, i.e., floor, walls ceilings and furnishings. As emphasized by Braun (Braun, 1990), both energy costs and peak electrical use can be significantly reduced through optimal strategies while considering the use of intrinsic thermal storage within the building structure. Some simulated-based and experimental results also show that MPC strategies which take into account both the structural storage capacity of the building, i.e., the thermal mass embedded in the building structure, and the non-structural storage capacity, i.e. the storage capacity embedded in the thermal systems, may result in substantial energy cost saving.

Adding dedicated active thermal storage to a building system will add additional storage capabilities and opportunities for greater building energy flexibility and improved building-grid interaction. An active thermal storage device can be controlled more precisely than passive building thermal mass during both thermal charging and discharging phases, thus making active thermal storage an attractive technology to incorporate into building design.

Usually, control strategies applied to energy storage devices are far from optimal. These strategies typically consist of heuristic rules (e.g., “charge whenever possible”, or “charge the device in the nighttime”). While these approaches may address peak load issues, they usually entail other problems, such as significant heat losses when the device is unnecessarily charged at high temperatures, for example, during the shoulder seasons. In this context, model-based predictive control provides the opportunity to plan the charging and discharging cycles of the storage device as a function of the expected heating load over a specified prediction horizon; depending on the application, the prediction horizon may range from a few minutes to a couple of days.

2.5.1 Electrically-heated high temperature thermal energy storage

Active technologies such as Electric Thermal Storage (ETS) can assist in building heating load management and can complement the building’s passive thermal storage capacity.

ETS systems can convert electricity to stored heat during a low electricity price period (or when demand on the grid is low) in a high-temperature storage medium (normally bricks heated up to 800-900°C), thus requiring smaller storage space and provide heat to the building during peak demand periods (Moffet et al., 2012). The purpose of the device is not to reduce the total energy consumption of the building, but rather to provide a considerable reduction of the electricity bill in the presence of a demand charge within the utility pricing structure (Bedouani et al., 2001, Syed, 2011). With a mix of electric heating during both on-peak and off-peak times, the load can be smoothed and installing new generating capacity can be delayed (Cooke et al., 1980). During low price periods or off-peak times, the ETS system uses bricks to store heat for later use. In peak periods, the stored heat is released from the bricks to the building with the help of a thermostat-controlled fan.

A detailed thermal model of the energy storage device considered was developed in a previous Master's thesis (Lavigne, 2006). This model, intended primarily for design purposes, focused on the assessment of different design alternatives –including the use of phase change materials (NaCl and KCl)– to increase the storage capacity of the device. The model yielded results that predicted satisfactorily the experimentally obtained results. It was found that adding these salts increased the storage capacity of the device, although the introduction to these materials had several important practical complications. Lavigne (2006) carried out a highly refined discretization of the energy storage medium (with hundreds of control volumes) and the air in the channels. This approach –which emphasized the comparison of design options- also considered a detailed analysis of convective heat transfer from the solid to the fluid circulating in the channels, and radiative heat transfer between the surfaces of the control volumes for the energy storage medium. Moreau & Steffes (2009) presented an application of the ETS technology in a 4,000-m2 building in Québec City. It was shown that two energy storage devices managed to keep the load of the building within a maximum value of 160 kW, versus 400 kW before their installation. Other researchers have looked at the ETS coupled with smart grid features and have examined how the ETS can be used with hydroelectric and abundant wind resources to meet load growth in isolated electric grids (Wong et al., 2017, Wong & Pinard, 2017). They found that the ETS, especially when controlled dynamically through Smart Grid signals, is effective in reducing diesel consumption by capturing the wind and hydro potential that would otherwise be lost. The operation of an ETS device sized for residential applications (22 kW) was also investigated (Cooke et al., 1980). The models used for the design of the device were based on one-dimensional lumped parameter equations for heat conduction and energy conservation. The authors chose to neglect many of the dynamic terms, hence they dealt with quasi steady-state models. The models calculated the average brick temperature in the average air passage, thus they assumed uniform heat and air distribution. These very simple models may be good for devices with steady input and output, but are not suitable for more transient operating modes, thus further need for studies on control-oriented modelling was identified.

Effective advanced control strategies utilize the thermal inertia that is present in the building structural components and coordinate the operation of different systems such as thermal storage, electrical storage, on-site renewables, and heat pumps (Junker et al., 2018, Liu & Heiselberg, 2019, Reynders et al., 2017). The fluctuations in weather and occupancy directly affect the operation of a building, which can result in significant load variations between daytime and nighttime and thus large demand variations. To manage these fluctuations, proper energy management and solid knowledge of the dynamic behaviour of buildings are crucial.

2.6 Research needs in control-oriented modeling & enhanced operation of buildings

Despite the intensive research outlined in this chapter, the transfer of MPC or other enhanced building operation strategies is still largely in its early stages. There are four main reasons for this outlined by Cigler et al. (2013a):

1. An accurate yet simple building model is required, however, obtaining such a well-performing model is often a difficult and time-consuming task.
2. The design and tuning of MPC controllers are challenging. Commission engineers are often not trained or familiar with complex control systems based on numerical optimization. Also, contrary to the prevalent application of MPC in the industrial sector, buildings are not operated with on-site engineers monitoring and supervising the control system.

3. There is also a strong need for data availability and processing power as the computation of MPC control actions for complex systems can be easily based on hundreds or even thousands of parameters/states.

4. The online solution of the corresponding optimization problem and the extensive data processing imposes considerable challenges on hardware and software infrastructure, which is not a standard in today's buildings.

Further studies were conducted that use models to test different operating approaches and control strategies. Control-oriented models will be used, along with knowledge of future conditions (such as electricity pricing, occupancy, weather forecasts etc.) to plan the operation strategies to better regulate electrical heating loads at hours that are critical for the electric grid (for example in the morning between 6am and 9am).

Though MPC is an established control technique in other fields and has received increasing attention in buildings research, it has yet to become common in buildings operations. Due to the majority of buildings having unique designs, and different types of heating systems (e.g., convective considered in this study vs radiant), differing construction qualities and other factors, it is difficult to automate the model development step in the MPC and model-based energy management process in buildings.

There is still a need to further develop rapid deployment of thermal models of buildings that are accurate, simple, and robust, which can be used to predict operational processes, power demand, energy consumption and comfort, in such a way that an energy modelling *expert* is not needed for every building. Future research should focus on evidence that directly compares the performance of specific optimization algorithms, parameters such as time-step and prediction horizon, and climate forecast accuracy.

In this work, specific research needs were touched upon, though there is still left further opportunities for advancements in this area. This work focused on the development of control-oriented thermal models for buildings with convective heating systems, and convective active thermal energy storage devices, as well as the development of improved control strategies, mainly in the form of set point modulation. These models are intended to be used within a model-based control strategy methodology for energy and load management in typical Québec buildings during the heating season. Appropriate grey-box thermal network models for typical buildings and a dedicated thermal storage device were identified and compared, with some auto-generation of a model in the methodology, though a fully automated model development methodology is still needed. Some important features of the developed methodology are calibration of models with existing measured data and periodic checking of the model against real-time operation, though it is expected that measured real-time data from the BAS will eventually play a key role in *continuous calibration* of the reduced-order models developed, but research is still needed on how to make this feasible.

Chapter 3

Methodology: Control-Oriented Modelling and Analysis of Buildings with Convective Heating Systems & Thermal Storage

In this chapter, the thermal modelling approach used for the studies is presented as part of an overall modelling methodology that can be applied to buildings equipped with convective heating systems and an active thermal storage device. This modelling approach may be applied for model-based control and building energy flexibility quantification, utilizing simulation and model predictive control (MPC). The focus of this research is on the winter operation of archetypal buildings found in Québec, mainly low-mass and low-rise buildings. Radiant floor heating and other types of heating systems apply to these buildings; however, only convective heating systems will be considered in this work and in the case studies. Also, there is an emphasis on modelling thermal mass and thermal storage devices, while devices containing advanced materials such as phase change materials (PCM) are not considered.

The main approach for modelling heat transfer in the enclosure (building or zone) is a low-order lumped parameter explicit finite difference method that can incorporate parameter calibration and/or parameter identification techniques, such as optimization. The control-oriented models for building zones and thermal storage devices are based on one- or two-dimensional lumped parameter equations for heat conduction and energy conservation. These models use a grey-box modelling approach, in which physically-meaningful parameters can be calibrated with measured data or identified using optimization techniques. A model-based approach has the important following advantages:

- A physics-based grey-box model does not require training data to run with predictions, while a black-box model always needs training data. However, a training period does help with improving calibration/prediction results.
- A physics-based model provides insight into the understanding of the basic phenomena.
- It is easier to infer general conclusions from particular models.
- Sensitivity analysis is easily facilitated.

Therefore, a physics-based mathematical model grey-box approach has been selected for this work. The often-unavoidable inaccuracies of modelling a physical system, due to the required assumptions, uncertainties, and sometimes simplifications, can be handled in part with some form of calibration or automated model parameter estimation.

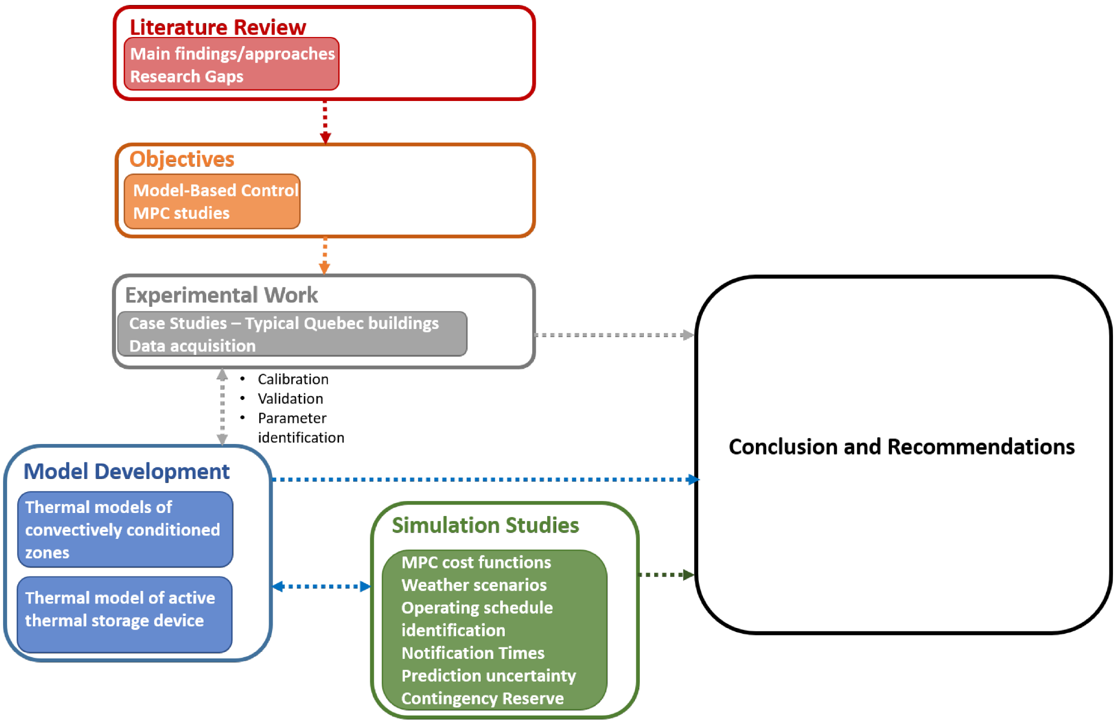

Figure 3.1: Flow of methodology

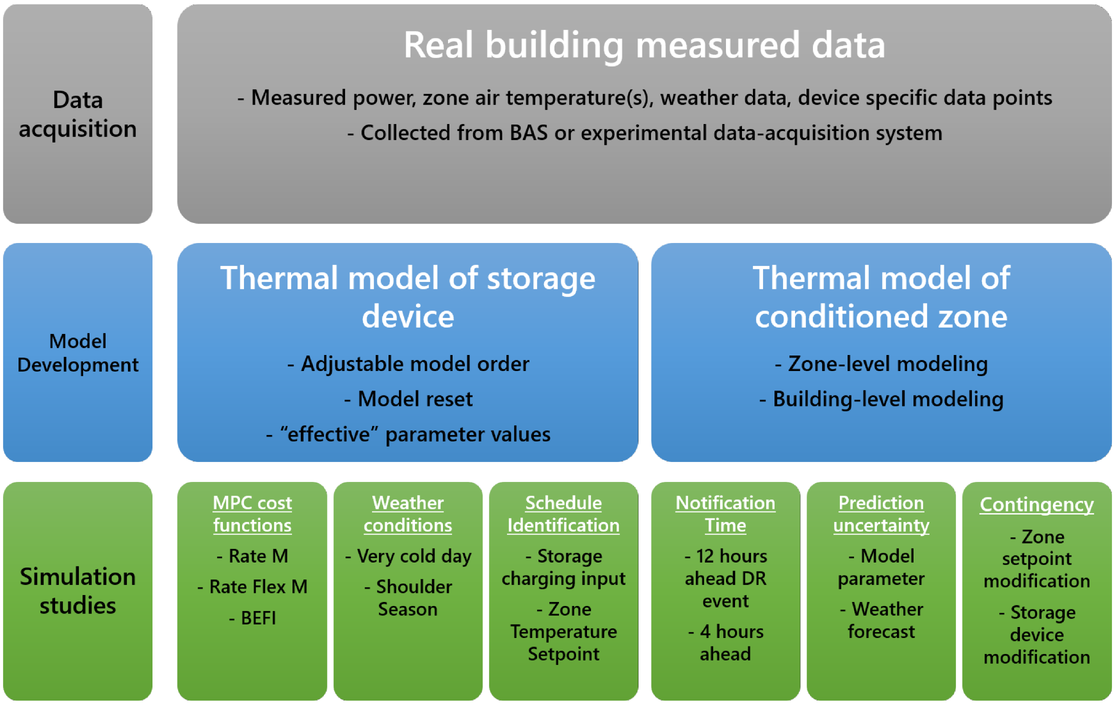

Figure 3.2: Outline of methodology

The developed methodology is outlined in Figures 3.1 and 3.2 and the following list, which will also be elaborated on further in the coming sections and chapters:

1. Real building (case study) measurement data were collected from the BAS. Data includes variables such as building power demand [kW], zone air temperatures, on-site weather data if available, and specific data related to systems, such as the thermal energy storage device.
2. The building envelope elements of the building (walls, floor, ceiling) are represented as a thermal network of resistances and capacitances. Internal partitions should also be included if they have considerable thermal mass. The level of model complexity of the network will depend on each case.
3. Physics-based models of important HVAC elements (convective systems in this case) were developed. These models are physics-based ROM grey-box RC thermal networks.
4. Calibration of model parameters is carried out either manually or effective parameters are identified using an optimization routine. Calibration of these models was carried out

using the collected data from the first step. The gradient descent-based optimization function *fmincon* in MATLAB or SLSQP in Python was used to identify important parameter values.

5. Model-based operational strategies were tested and developed using the developed thermal models for better load management and/or improved occupant comfort. Heuristic approaches were compared to optimized control MPC using *fmincon* in MATLAB for some of the case studies (Figure 3.3).
6. Model prediction uncertainty due to identified model parameters and the weather forecast was accounted for by evaluating various uncertainty scenarios and plotting the uncertainty bounds for the duration of the identified operation schedule. This was carried out with one of the case studies.
7. Contingency strategies were evaluated (on one case study) to quantify the energy flexibility available from the building to the grid at specific times.

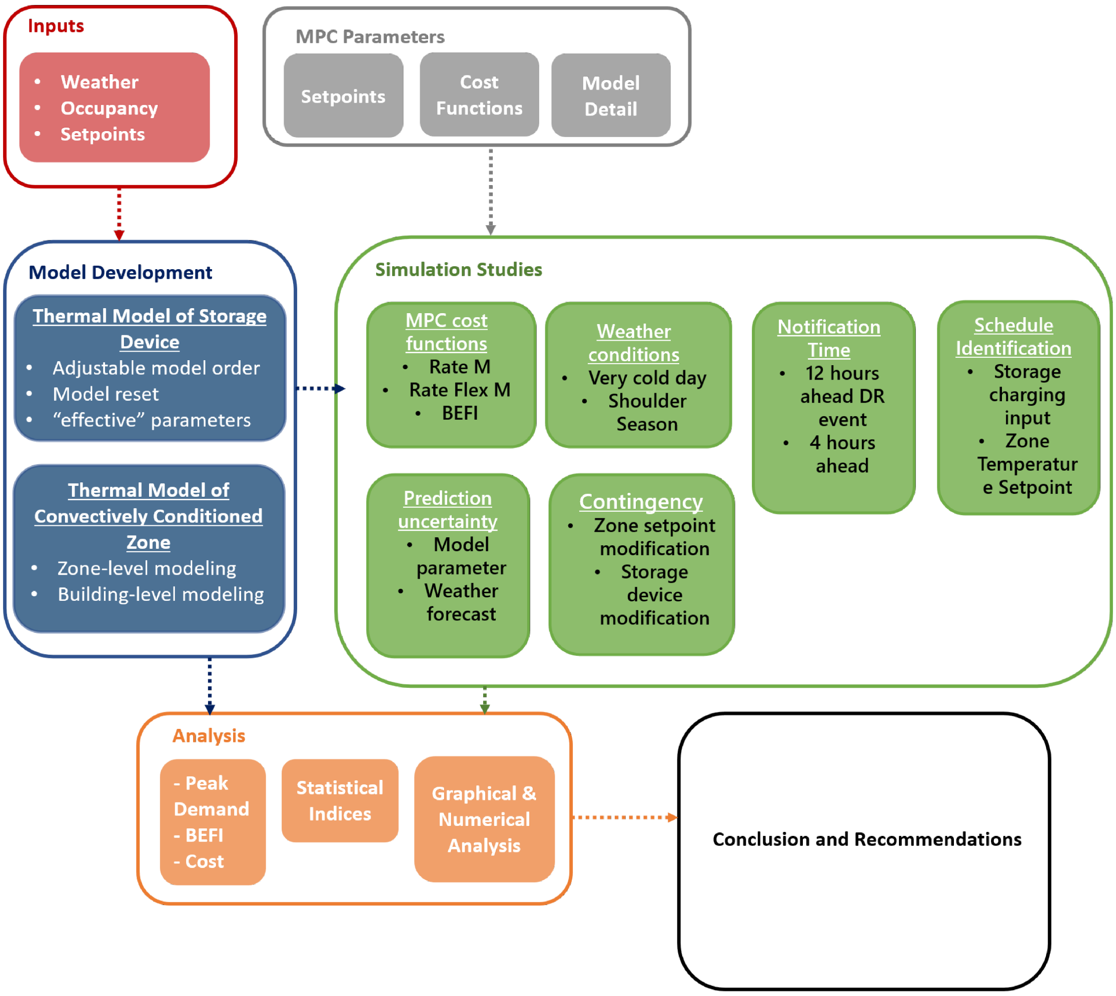

Figure 3.3: Simulation flowchart

3.1 Background: thermal modeling approaches for model-based control in buildings

Thermal networks, in which thermal phenomena are modelled based on electric network analogies, are commonly used for building energy modelling. Conduction heat transfer through opaque building surfaces is modelled by two common approaches: (1) conduction transfer functions (CTF) and (b) control volume finite difference methods (CVFD). Data-driven reduced-order thermal models (ROMs) for archetype zones, buildings, and system configurations are useful for developing and quantifying energy flexibility strategies in the context of improved building-grid interaction. A low order RC model allows to rapidly assess the energy flexibility of a building. An appropriate and suitable modelling methodology is integral when the target is an in-depth study of the system. A thermal model of a system allows to simulate design conditions (e.g., for new design or retrofit) and to study the thermal response of a building and/or systems.

Conduction Transfer Functions (CTF): CTFs are time series equations for heat transfer through a wall or surface. In the CTF calculation, the current heat transfer rate is a function of previous temperatures on both sides of the wall/surface, going back 24 hours. Obtaining the coefficients for CTF calculations can be challenging, as they depend on the wall construction. However, once the coefficients are determined, it is a powerful and quick method for simulations. CTF calculations are linear and can be found in popular building performance simulation tools, or even implemented in excel, etc.

The control-oriented modelling methodology for buildings and thermal storage devices detailed below is intended to have general applicability and will be demonstrated with case studies, which have been introduced in Chapter 1. Modelling performance results and capabilities are shown in subsequent chapters. Simulation and analysis of thermal and energy fluxes in a building facilitate the choice of the materials, subsystems and control strategies for the local climatic characteristics and building function (Athienitis & O'Brien, 2014). Many thermal processes are relevant in the assessment of building thermal behaviour, such as:

- Heat conduction through exterior walls, roofs, ceilings, floors, and interior partitions.

- Solar radiation through transparent surfaces.
- Latent and sensible heat generated in the space by occupants, lights, and appliances.
- Heat transfer through ventilation and infiltration of outdoor air and other miscellaneous heat gains.

3.2 Lumped parameter finite difference method

The one-dimensional heat transfer process for a wall without heat-generating sources is governed by the following diffusion-type partial differential equation, which is parabolic in time and elliptic in the space coordinates (Patankar, 1980):

$$\rho c_p \frac{\partial T}{\partial t} = \frac{\partial}{\partial x}\left(k\frac{\partial T}{\partial x}\right) \tag{3.1}$$

If k, the thermal conductivity is assumed constant, the equation becomes:

$$\rho c_p \frac{\partial T}{\partial t} = k\frac{\partial^2 T}{\partial x^2} \tag{3.2}$$

The right-hand side of the Equation (3.2) represents all the heat coming or leaving the control volume depending on the temperatures at surrounding control volumes and the left-hand side describes how the temperature of the node changes over time. It is typical for RC models of a building envelope system to be one-dimensional, however, the following studies and methodology carried out here are not necessarily limited to 1-dimensional analysis or model development, and the one-dimensional equation has been introduced above for clarity purposes.

If ρ, k and c_p are constant, the equation is simplified to:

$$\frac{\partial T}{\partial t} = \alpha\frac{\partial^2 T}{\partial x^2}, \quad 0 \le x \le L, \quad t \ge 0 \tag{3.3}$$

where thermal diffusivity $\alpha = k/(\rho c_p)$ m^2/s, k is thermal conductivity (W/(m·K)), ρ is the density (kg/m^3) and c_p is the specific heat capacity (J/K). The domain of the solution is a semi-infinite strip of width L that continues indefinitely in time. In practical computation, the solution is obtained only for a finite time (t_{max}) and a building wall with thickness L. Specified boundary conditions at $x = 0$ and $x = L$, and initial conditions at $t = 0$ are required for the solution to Equation 3.3.

Typical boundary conditions of a wall of thickness L will include convective heat transfer, absorbed solar radiation (heat source) and long-wave radiations exchange with other surfaces. The boundary conditions ($x = 0$ corresponds to exterior surface) are:

(i) At $x = 0$

$$q = -k\frac{\partial T}{\partial x} = G + h_o\left(T_o - T_1\right) = h_o\left(T_{eo} - T_1\right) \tag{3.4}$$

where sol-air temperature $T_{eo} = T_o + \alpha_s G/h_o$.

(ii) At $x = L$ (thickness of the wall, at the interior surface)

$$q = h_i\left(T_2 - T_r\right) \tag{3.5}$$

where q is the heat flux, h is the heat transfer coefficient and G is solar radiation.

Focusing on the formulation as shown in Equation (3.2), and using the explicit finite difference schemes, the explicit finite difference discretization of the right side of Equation 3.2 can be written as:

$$k\frac{\partial^2 T}{\partial x^2} = k \cdot \frac{T_{i+1}^n - T_i^n}{(\Delta x)^2} + \frac{T_{i-1}^n - T_i^n}{(\Delta x)^2} \tag{3.6}$$

Multiplying both sides of Equation (3.2) by the differential of volume and knowing that the thermal capacitance $C = \rho c_p A dx$ [J/K] we get:

$$C \cdot \frac{dT}{dt} = \dot{Q} \tag{3.7}$$

Where $\dot{Q}$ [W] is all the incoming heat into the control volume. The main advantage of explicit finite difference methods is that they are relatively simple and computationally fast. However, the main drawback is that stable solutions are obtained only when:

$$0 < \frac{\alpha \Delta t}{\Delta x^2} < 0.5 \tag{3.8}$$

If this condition is not satisfied, the solution becomes unstable and starts to oscillate (Crank, 1975, Morton & Mayers, 2005). One-dimensional conduction through the walls is generally assumed, as well as uniform irradiation of their surfaces by solar radiation (Athienitis & Santamouris, 2002). However, when thermal bridges are present, such as at corners in rooms and for heat loss through the floor, two-dimensional or three-dimensional analysis could be required.

For a multi-layered wall, an energy balance is applied at each node at regular time intervals to obtain the temperature of the nodes as a function of time. These equations may be solved with the implicit method as a set of simultaneous equations or with the explicit method in which we march forward in time from a set of initial conditions. Wall transient thermal response analysis with finite difference techniques may generally provide a more accurate estimation of temperatures and heat flows owing to the capability to model non-linear effects such as convection and radiation. This method is also suitable if easily adjusting the simulation time step is desired, whereas, in the CTF method, the coefficients must be recalculated for each chosen simulation time step (Delcroix et al., 2013). One disadvantage is that the initial conditions are usually unknown, thus, the simulation must be repeated until a steady periodic response is obtained.

The thermal modelling approach used is the common lumped parameter finite difference method. This approach is based on a space discretization of the material into control volumes. A node is located at the centroid of the control volume. The heat flux between adjacent nodes is described by using resistance analogies: the flux is calculated as proportional to the difference between the temperature of the two nodes. Between control volumes, the conductance U is calculated as kA/L, where k is the thermal conductivity of the material, A the area of the surface of contact and L is the distance between adjacent nodes. If the node has considerable thermal mass, it may be assigned a thermal capacitance, which represents the heat storage capacity of the control volume. By performing a heat balance on the control volume, the differential Equation (3.7) of a node can then be written as (Athienitis & Santamouris, 2002):

$$C_i \frac{dT_i}{dt} = Q_i + \sum_{j=1}^{n} \frac{(T_j - T_i)}{R_{i,j}} \tag{3.9}$$

where Q_i represents the heat generated at a node i or received directly by it from source(s), $R_{i,j}$ represents the thermal resistance between nodes i and j (either conductive or convective terms), T is the temperature at node i or adjacent node j, and C is the thermal capacitance at node i ($C = \rho c_p A dx$). n is the total number of adjacent nodes to node i.

The strategy commonly implemented to determine the transient solution is the application of time discretization (Athienitis & Santamouris, 2002). A fully explicit finite difference approach was used to solve the energy balance equations at each node in the models. The fully explicit approach assumes that the current temperature of a given node depends only on its temperature and the temperature of the surrounding nodes at a previous time step. The term with the time derivative can then be discretized as follows:

$$C_i \frac{dT_i}{dt} \approx C_i \frac{\Delta T_i}{\Delta t} = C_i \frac{T_i^{p+1} - T_i^p}{\Delta t} \tag{3.10}$$

By solving for the temperature at the next time step, the general Equations (3.11) and (3.12) are derived for control volumes with and without capacitance terms, respectively.

$$T_i^{p+1} = T_i^p + \frac{\Delta t}{C_i} \left[Q_i^p + \sum_{j=1}^{n} \frac{(T_j^p - T_i^p)}{R_{i,j}} \right] \tag{3.11}$$

$$T_i^{p+1} = \frac{Q_i^p + \sum_{j=1}^{n} \frac{T_j^p}{Ri,j}}{\sum_{j=1}^{n} \frac{1}{R_{i,j}}} \tag{3.12}$$

An important part of a thermal model of a zone or building (and sometimes a system) is the radiative and convective heat transfer, which are nonlinear processes. However, it is common practice to linearize the heat transfer coefficients to ease solving the system of energy balance equations using linear algebra techniques and represent them with a linear thermal network. When constant average values for radiative and convective heat transfer coefficients do not capture the system dynamics adequately, the following simplified convective and radiative heat transfer coefficient equations were employed (American Society of Heating Refrigerating and Air-Conditioning Engineers", 2009):

$$h_{conv} = 1.26 \cdot |T_{s1} - T_{room}|^{1/3} \tag{3.13}$$

$$h_{rad} = \varepsilon\sigma \cdot \left(T_{s1}^2 + T_{s2}^2\right) \cdot (T_{s1} + T_{s2}) \tag{3.14}$$

where T_{s1} is a surface, T_{s2} is another surface and T_{room} is the room air temperature.

The following three types of approximations are commonly introduced in mathematical models to facilitate representation of the building thermal behaviour (Athienitis & O'Brien, 2014):

1. **Linearization of heat transfer:** Convective and radiative heat transfer are nonlinear processes and the respective heat transfer coefficients are usually linearized so that the system energy balance equations can be solved by direct linear algebra techniques and, if desired, represented by a linear thermal network. Linearization generally introduces less error for long-wave radiant exchanges between surfaces than convection between surfaces and room air. A linear lumped parameter system can be represented by a set of ordinary differential equations and thermal networks. An important subset of linear systems is those with time-varying coefficients - an important case in building energy analysis, where we can often represent thermal conductances such as a known variable level of natural ventilation or time-varying infiltration. It should be noted that when thermal storage undergoes a phase change (e.g., phase change materials (PCM)) a linear approximation may not be possible in most cases and specialized modelling will be required.

2. **Spatial and/or temporal discretization:** Transient heat conduction is described by a parabolic, diffusion-type partial differential equation. Thus, when using finite difference

methods, a conducting medium with significant thermal capacity such as concrete or brick must be discretized into several regions, commonly known as control volumes, which may be modelled by lumped network elements (thermal resistances and capacitances). Also, time-domain discretization is required in which an appropriate time step is employed.

3. **Approximations for the reduction in model complexity - (establishing appropriate model resolution):** These approximations are employed to reduce the number of simultaneous equations to be solved and the required data input or to enable the derivation of closed-form analytical solutions. They are the most important approximations according to Athienitis & O'Brien (2014). Examples include combining radiative and convective heat transfer coefficients, assuming that surfaces are at the same temperature, or considering certain heat exchanges as negligible. These approximations must be carefully selected and applied by considering the expected temperature variations (spatial and temporal) in a zone. As an example, a zone with large windows or floor heating may exhibit large spatial temperature variations, in which case the use of combined film coefficients would result in high errors in room operative temperature or floor heating rate calculations.

The Biot Number, $Bi = hL/k$, is a dimensionless parameter that plays a fundamental role in conduction problems that involve surface convection effects. If $Bi << 1$, the resistance to conduction within the solid is much less than the resistance to convection across the fluid boundary layer, thus an assumption of uniform temperature distribution in the solid is reasonable. Commonly, when $Bi < 0.1$, it is said that the error associated with using the lumped capacitance method is small (less than 5%) (Incropera et al., 2006).

3.3 Development of low-order thermal models

Reduced-order thermal models are often custom-made using general-purpose mathematical programming tools, which offer flexibility compared to commercial simulation tools. MATLAB and Python programming language was used in this work.

3.3.1 Programming tools

MATLAB is a mathematical programming environment that has its own programming language which allows the user to create subroutines (The MathWorks, Inc, 2015). MATLAB is commonly the choice of various engineering disciplines. MATLAB is based on the Ph.D. thesis of Cleve Moler and its initial release was in 1967. It has a GUI designed for controls and simulation of dynamical systems SIMULINK where a control schematic can be built with relative ease. MATLAB includes built-in modules for continuous and discrete transfer functions, different types of signals, a system identification toolbox, a MPC toolbox, and even a fuzzy logic toolbox. MATLAB has an extensive interdisciplinary user-base.

Python is an open-source general-purpose programming language with a design philosophy emphasizing code readability (Python Software Foundation, 2020). Python is the third most popular programming language (behind Java (Arnold et al., 2005) and C (Kernighan & Ritchie, 1988)). The creator Guido van Rossum began working on the programming language in the late 1980s and the first Python 0.2.0 was released in 1991. Libraries such as NumPy (The SciPy community, 2020), SciPy (The SciPy community, 2019) and Matplotlib (The Matplotlib development team, 2020) allow the effective use of Python in scientific computing.

3.3.2 Considerations for control-oriented modelling: order selection, adjustable models, model reset

Adjustable Model Order: The low-order models of the thermal storage device are based on two-dimensional lumped parameter heat conduction and energy conservation equations. These models adopt a grey-box modelling approach, where physically meaningful model parameters are calibrated or identified using measured data from the real building. The developed MATLAB code was written to quickly adjust the order of the model by specifying how many rows and columns of brick nodes will be used and thus changing the number of brick thermal capacitance nodes (i.e., increase or decrease the model order). The model order becomes the number of rows multiplied by the number of columns specified. Each brick node has a capacitance term, C_{bricks}, electric power input, Q_{source}, and convective heat extraction through the air channels, Q_{conv}. The heat transfer from bricks to the airflow of the ETS system was modelled using the general equation for heat exchange through a channel (Lienhard Iv & Lienhard V, 1986), which is introduced in a following sub-section in this chapter.

Model reset: The main goal of these control-oriented models is the accelerated simulation of the ETS device to assess load management strategies and aid in decision-making for system operation. These low-order thermal models, suitable for controls, are intended to be used simultaneously with knowledge of future conditions (such as electricity pricing, occupancy, weather forecasts etc.) to plan the operation strategies within the Building Automation System (BAS) for better performance, which could include the regulation electrical loads or ensuring building energy flexibility. Continuous comparison of the model with actual results from BAS points is expected. Thus, the concept of "model reset" was developed, which could be considered a simple alternative to the Kalman filter technique (Huchuk et al., 2014), which gives satisfactory results (presented in Chapter 5).

These models are designed for short-term control (e.g., 1-2 days) and optimization (e.g., hours) within the control sequences of a BAS, therefore, it is reasonable to conclude that the model can "check" itself against the real available measured values (of brick temperature, outlet air temperature etc.) periodically and update or "calibrate" its variables.

At the specified reset interval (e.g., 6 hours), the model checks the current state of corresponding sensor points and re-initializes the brick temperature model parameter value. The main reason a 6-hour model reset interval was chosen is because that is how often the available weather forecasts are typically updated and released by the national weather service (Canadian Meteorological Service (Environment Canada), 2019).

3.4 Modelling of heat transfer in thermal storage device

For the specific electric thermal storage device used in this study, the focus was on the methodology for control-oriented modelling. The device considered, shown in Figure 3.4, consists of an insulated heat storage tank containing 3,121 kg of magnesite ($MgCO_3$) bricks. Magnesite bricks have mainly been used for high-temperature schemes, where brick temperatures can go up to 871 °C, while water and solutions of water and sodium sulphate have been used for low-temperature (less than 100 °C) energy storage (Lavigne, 2006). Electric wire heating elements are placed between the rows of bricks. The storage device considered is rated for a maximum brick temperature setpoint of 871 °C and the maximum storage capacity of this device is approximately 640 kWh. A fan controls the fraction of total airflow that is driven through the ETS device to retrieve heat from the bricks. The air either passes through the bricks or bypasses the device.

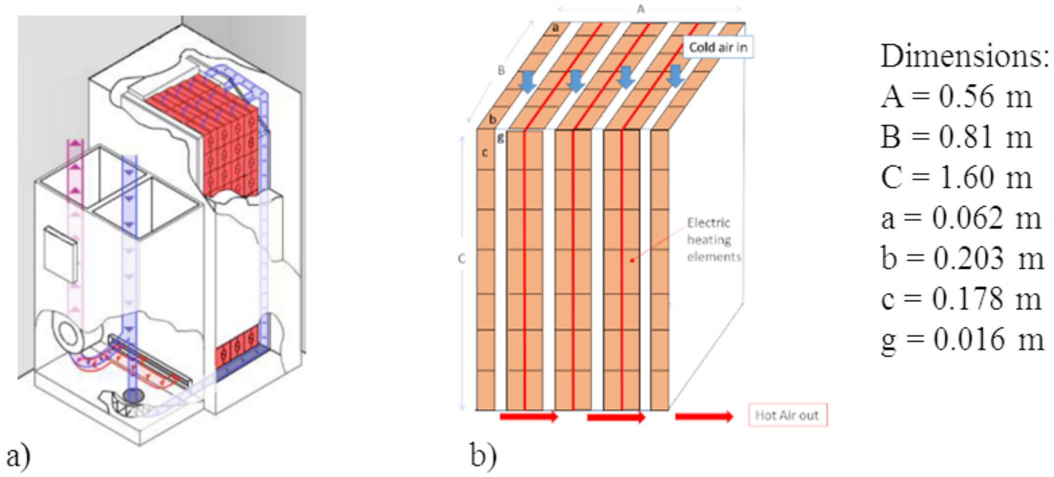

Figure 3.4: (a) Thermal electric storage device, *reprinted with permission from Karine Lavigne* (Lavigne, 2006) and (b) brick charging and discharging schematic

The general equation for heat exchange through a channel (Lienhard Iv & Lienhard V, 1986) was used to model the heat transfer from the storage bricks to the airflow in the brick channels:

$$\frac{T_{b_{out}} - T_{b_{in}}}{T_w - T_{b_{in}}} = 1 - \exp\left(-\frac{hPL}{\dot{m}c_p}\right) \tag{3.15}$$

T_w is the channel wall surface temperature, h is the convective heat transfer coefficient between air and channel surface, P is the perimeter of the channel, L is the length of the channel. Equation (3.15) is also a simplification, as it assumes that the walls of the channel are at a uniform temperature throughout the length, and results in the temperature of airflow following the form of an exponential curve, approaching the wall temperature asymptotically. The above equation can give the variation of air bulk temperature ($T_{b_{out}}$ and $T_{b_{in}}$) along the channel as a function of the distance from the inlet (x) if $T_{b_{out}}$ is replaced by $T_{b(x)}$, L is replaced by $Z(i)$, and

h is adjusted accordingly. Temperatures at each control volume would therefore be calculated as follows:

$$T_{b_{out}}(p,i) = T_w(p) + [T_{b_w}(p,i) - T_w(p)] \cdot e^{\frac{-2 \cdot Z(i)}{a(p)}} \tag{3.16}$$

where $a(p) = \frac{M(p) c_p \rho}{W \bar{h}(p)}$ and the convective heat transfer term can be calculated with this equation, $h = \frac{Nu \cdot k}{DH}$, or estimated/calibrated as often there is not enough information available. Nu is the Nusselt number, k if the conductivity of the air and DH is the hydraulic diameter of the air channel. The energy extracted from the bricks in the air channels (which is subtracted from the brick node energy balance equation) is calculated as follows:

$$Q_{conv}(p) = 4 \cdot M(p) c_p \rho \left[T_{b_{out}}(p,L) - T_{b_{in}}(p,0)\right] \tag{3.17}$$

3.5 Parameter identification and model calibration

Kummert et al. (2006) stated that parameter identification on a detailed building model is a complex problem due to the large number of parameters and to the possibility of achieving the same result through different actions (e.g., increasing the infiltration rate or increasing the thermal conductivity of a low-mass wall or window). The large number of parameters in the building model makes parameter identification a complex problem, and typically the desired level of accuracy is high - where performance differences of less than 10% must be reproduced. For those reasons, among others, a simpler model may be an attractive alternative to complex building simulation tools.

An optimization algorithm can be used to determine unknown parameters, therefore having fewer equations is helpful. Several methods are available to reduce the complexity of a model: merging thermal zones, reducing the discretization of the walls, and merging several walls to combined surfaces. An optimization routine is used to find the parameter values that minimize an objective function. In one of the case studies outlined in Chapter 4, the objective function chosen was the coefficient of variation of the root-mean-square error (CV(RMSE)) between measured power and the prediction at 15-minute intervals, similar to (Lavigne et al., 2014).

Sequential Least Squares Programming (SLSQP) was used for this study using the Python programming language (Python Software Foundation, 2020). The SLSQP algorithm within SciPy (SciPy, 2021) is used here; other algorithms can replace it depending on the user's preference. The objective function CV-RMSE used is shown in Equation (3.18):

$$CV - RMSE(y,\hat{y})[\%] = \frac{1}{y}\sqrt{\frac{1}{n}\sum_{i=1}^{n}(\hat{y}_i - y_i)^2} \tag{3.18}$$

where y is the experimentally measured data (usually energy or power) and $\hat{y}$ is the model predictions. The building was modelled using the fully explicit finite difference method to solve the energy balance equations. Initial values of model parameters are based on the known building material properties and estimates for infiltration, inter-zonal convective transfer, and air capacitance multipliers.

The normalized mean bias error is also a common index when evaluating a model's ability to accurately predict the energy consumption of a building. CV-RMSE and NMBE are usually used for whole-building energy consumption at hourly or monthly time steps, and there are no agreed-upon indices for evaluating sub-hourly data. The common threshold for hourly data assigned by ASHRAE for CV-RMSE is 30%, while NMBE is 10% (Gillespie et al., 2002b).

The performance of the models can be evaluated in terms of several other statistical indices, such as the root-mean-square error (RMSE), Equation (3.19), and the mean absolute error (MAE), Equation (3.20). Also, the infinity norm (i.e., the biggest difference between the model results and measured data) of the absolute error between modelled brick temperature and the measured brick temperature was used to evaluate the accuracy of models with different levels of detail and to give another data point, Equation (3.21)).

$$RMSE\,(y,\hat{y})\,[^{\circ}\mathrm{C}] = \sqrt{\frac{\sum_{i=1}^{n}(\hat{y}_i - y_i)^2}{n}} \tag{3.19}$$

where y is the measured sensor data of the brick temperature, $\hat{y}$ represents model predictions of brick temperature and n is the number of samples.

$$MAE\,(y,\hat{y})\,[^{\circ}\mathrm{C}] = \frac{\sum_{i=1}^{n}|\hat{y}_i - y_i|}{n} \tag{3.20}$$

$$\parallel f \parallel_{\infty}[^{\circ}\mathrm{C}] = \parallel \hat{y}_i - y_i \parallel_{\infty} \tag{3.21}$$

3.5.1 "Effective" brick conductivity:

In the study of control-oriented modelling of an active thermal storage device using bricks as a storage medium, the concept of "effective" brick conductivity was also proposed and investigated to use a model with a relatively low order while still obtaining adequate predictions. This concept consists of the proposition that it is possible to improve the accuracy of a low-order model if it is assumed that it behaves as if the material had a higher conductivity (Date et al., 2016b). It is worth pointing out that this does not reflect any change in the material: it is only a modelling artifice when the objective is to assess the average temperature of the material as an indication of its state of charge.

An optimization routine used for the model identification study of an active thermal storage device had an objective function of the RMSE between measured brick temperature and the prediction at a simulation interval 5 minutes. In this case, the MATLAB function *fmincon* – which finds the minimum of a constrained nonlinear multi-variable function – is used here. The objective function chosen was RMSE and is shown in Equation (3.19).

3.6 Building energy flexibility & contingency quantification

Building load flexibility can be described as a building's potential to adjust its power demand at specific times by postponing or shifting consumption when compared to a reference scenario (or "Business as Usual" (BAU)). The concept of energy flexibility is useful to estimate the amount of energy (or energy flexibility) that a building can provide to the utility grid since the utilization of this flexibility can help lessen the strain on the grid when the demand approaches or exceeds what can be safely supplied. Annex 67, of the International Energy Agency Energy in

Buildings and Communities Programme's (IEA EBC), introduced the concept of "Energy Flexible Building", defined by the Annex as "a building able to manage its demand and generation following local climate conditions, user needs, and grid requirements" (International Energy Agency, 2020).

One important application of energy flexibility is demand response during peak periods. A Building Energy Flexibility Index ($BEFI$) could be used to quantify the potential participation of a customer for such a demand response event, which will be introduced in a subsequent chapter (Athienitis et al., 2020, Date et al., 2020b).

3.6.1 Building Energy Flexibility Index ($BEFI$)

$BEFI$ is a parameter that helps to identify relevant actions that can be undertaken to provide predictable energy flexibility from a building for the utility grid. Optimization algorithms could be used to maximize this index during a user-defined period. The $BEFI$ may also aid in the decision-making process regarding which relevant equipment or systems are to be installed in a building.

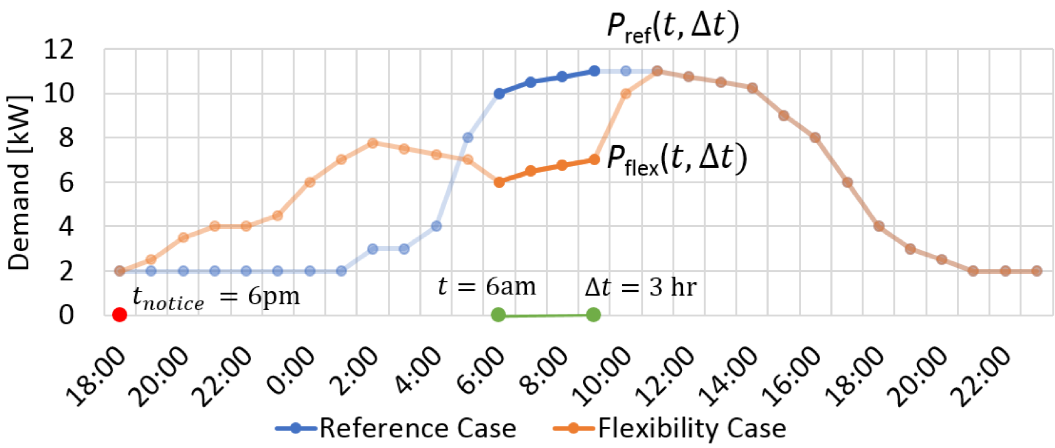

Figure 3.5: Example of Building Energy Flexibility Index ($BEFI$)

A well-designed index would help to quantify the flexibility available from a building, to improve its design, to increase its potential flexibility, to control the building to obtain maximum available flexibility when needed and compare different systems or designs. A visual depiction of a demand response event is shown in Figure 3.5 and a more formal representation of the $BEFI$ is shown in Equation (3.22).

$$BEFI(t, \Delta t, t_{notice}) = \frac{\int_t^{t+\Delta t} P_{ref} dt - \int_t^{t+\Delta t} P_{flex} dt}{\Delta t} \tag{3.22}$$

where $BEFI$ is the Building Energy Flexibility Index, t is the start time of the event, Δt is the duration of the event, t_{notice} is the time of notification for the event, P_{ref} (kW) is the power demand from the reference scenario during an event, and P_{flex} (kW) is the power demand from a flexibility case during an event. The $BEFI$ is the average difference between the power demand of the reference case, P_{ref} (kW), and the power demand of the alternative “flexibility scenario”, P_{flex} (kW), for the given event duration Δt, shown in Equation 3.22. $BEFI$ could also be represented as a percentage by dividing it by the value of P_{ref}.

3.6.2 Contingency reserve:

The contingency reserve is an amount of power that the utility may call from its customers when there is a loss of a generation unit or other unexpected load unbalances. One solution to address this power need is that real-time available thermal load flexibility must be quantified beforehand or continuously calculated during the event and available at short notice (e.g., 10 min) over a period of an hour, up to a few hours. This energy flexibility can be enabled by actions in response to a signal from the grid to the customer.

3.6.3 Prediction uncertainty:

Uncertainty in future predictions from low-order thermal models is an important consideration when evaluating different design or control scenarios. By offering a range of reasonable operating predictions that incorporate uncertainties related to weather forecasting and identified model parameter values, decision-makers can better understand and evaluate the risk associated with the operation options available to them (or rather, the operation options that were considered). Uncertainty in weather forecasts of solar radiation can be as high as 30% (Natural Resources Canada, 2019), and modelling uncertainty can be in that range as well.

3.7 Model predictive control in buildings

Model Predictive Control (MPC) could be described as a "repeated solution" of a finite-time optimal control problem: at each controller time step, a system model and optimization algorithm are used to find the optimal set of values for each control variable at each time step over a prediction horizon. The first time step of the solution is implemented and then the process is repeated at the next controller time step with updated initial state values (which are obtained from the real building) and disturbance forecasts (i.e., weather and occupancy). Variations of this general procedure are also possible, such as implementing two or more time steps of inputs and performing the optimization less often, or having different control and prediction horizon lengths.

Model Predictive Control (MPC) in buildings is a multi-variable control algorithm that involves (repeatably) solving a constrained optimization problem to choose the control action, using a model of the system, forecasts of future disturbances (i.e. weather forecast), future costs, and constraints, and a cost function that is minimized over a moving time horizon (i.e., the period for which future information is available, ranging from a few hours to a few days).

In general, MPC in buildings uses knowledge of forecast weather and anticipated occupancy schedules which can enable better control of the building energy systems, for example, by better managing thermal storage capabilities. Once the optimization algorithm determines the optimal control actions, these actions are applied to a "control horizon", a time period that is often shorter than the prediction horizon. Figure 2.7, first presented in (Blum, 2019), is an informative depiction of the concept of MPC for building operation and Figure 3.6, taken from (Drgoňa et al., 2020), provides a visual example of the characteristic behaviour of MPC for a building.

Setting up a suitable control-oriented thermal building or system model is crucial for MPC. However, the level of modelling effort and knowledge is difficult to estimate as each model is often designed for one specific building. MPC design requires a certain degree of knowledge of building modelling and heat transfer, such as a good understanding of what details are important to include, and which details can be excluded in the control model while still obtaining adequate results. The modelling approach of using a low-order resistance-capacitance (RC) thermal network to represent the building, which has been described previously in this chapter, is a popular modelling method for MPC. These models can be considered "grey-box", and model parameters are often calibrated against real measurement data from the existing building either through manual methods or with an optimization routine. Purely data-driven models are reliable and robust, but they cannot be easily applied in other buildings, and may not be able to properly predict or identify new optimal control strategies that the model was not trained with.

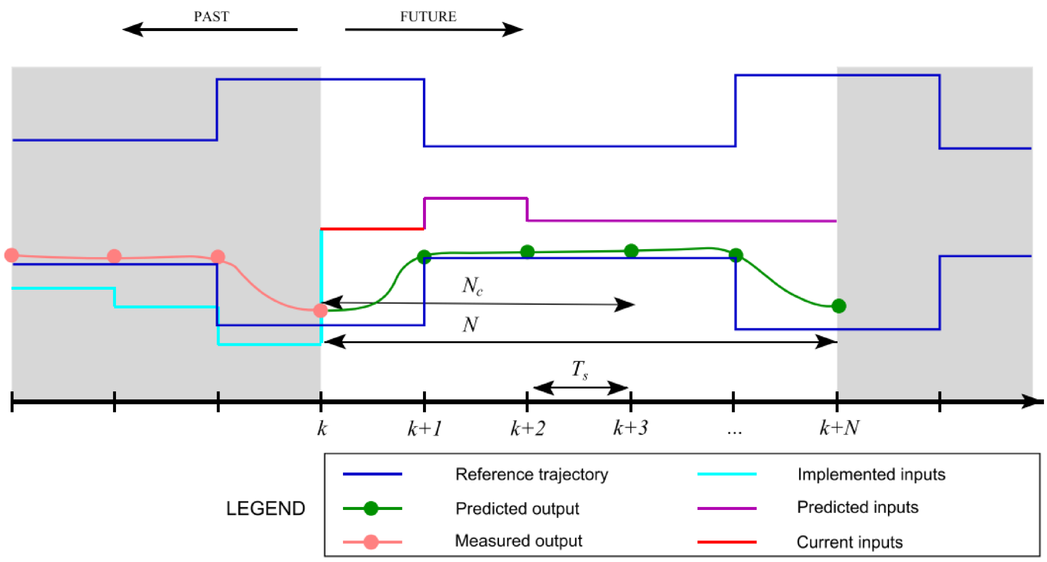

Figure 3.6: Characteristic features and illustrated behavior of MPC for building temperature control, *reprinted with permission from Dr. Jan Drgona* (Drgoňa et al., 2020)

MPC cost functions & constraints: One attractive feature of MPC for buildings is its ability to specify multi-objective cost functions (e.g., energy consumption and thermal comfort) while handling constraints for states and control (actuator or control setpoint) variables systematically.

MPC studies have often focused on the operation of active energy storage (ice banks, chilled water tanks, etc.), mostly for space cooling applications, and under time-of-use rates, however, this research focuses on space heating operation and implements a more unique cost function. Various cost functions have been developed for the case studies in this work, based on 1) a utility rate having both an energy consumption component and an electric demand charge component, 2) newly released "flex" utility rates (Hydro-Québec, 2020b) and 3) the Building Energy Flexibility Index ($BEFI$).

The following are examples of the relevant developed cost functions when the aim is to reduce cost and/or peak demand (which may or may not be during specific times of the day).

1. **Cost function using a utility rate with a fixed energy consumption component and an electric demand charge component**: formulation of this optimization problem is shown in Equation (3.23). As an example, the Hydro-Québec utility rate M, intended for medium-sized commercial buildings, is suitable for this formulation (Hydro-Québec, 2020b).

$$\begin{aligned} \min_{T_{SP}} \quad & J_{PH} = \left(\sum_{i=1}^{N} P_i \Delta t \right) \cdot \left(\text{Cost}_{\text{Energy}} \right) + \max\left(\mathbf{P}\right) \cdot \left(\text{Cost}_{\text{Demand}} \right) \\ \text{subject to} \quad & T_{SP,min} \leq T_{SP} \leq T_{SP,max} \\ & 0 \leq P \leq P_{max} \end{aligned} \tag{3.23}$$

2. **Cost function using a utility rate with a dynamic energy consumption component and an electric demand charge component**: the second optimization problem in consideration is shown in Equation (3.24), which is a special case of Equation (3.23) that has an added dynamic energy cost, specified by the sub-index i.

$$\begin{aligned} \min_{T_{SP}} \quad & J_{PH} = \left(\sum_{i=1}^{N} P_i \Delta t \right) \cdot \left(\text{Cost}_{\text{Energy},i} \right) + \max\left(\mathbf{P}\right) \cdot \left(\text{Cost}_{\text{Demand}} \right) \\ \text{subject to} \quad & T_{SP,min} \leq T_{SP} \leq T_{SP,max} \\ & 0 \leq P \leq P_{max} \end{aligned} \tag{3.24}$$

   Where PH is the prediction horizon (24, 36, 48 hours etc.), N is the number of time steps over the prediction horizon, P_i is the power demand at time i and Δt is the simulation time step. The temperature setpoint is constrained by a lower and upper bound to ensure comfort for the occupants. The objective is to identify a setpoint schedule for the room temperature, T_{SP}. The demand due to space heating P is constrained by the size of the heating equipment P_{max}.

3. **Cost function using Building Energy Flexibility Index ($BEFI$) maximization during a specified time of peak demand**: the last optimization problem example is using $BEFI$ as the cost function.

$$\begin{aligned} \max_{T_{SP}} \quad & J_{PH} = \operatorname{avg}[P_{ref} - P_{flex}]_{,during\ DR\ event} \\ \text{subject to} \quad & T_{SP,min} \leq T_{SP} \leq T_{SP,max} \\ & 0 \leq P \leq P_{max} \end{aligned} \tag{3.25}$$

Equation (6.5) shows a more formal representation of the $BEFI$ (Athienitis et al., 2020).

$$BEFI\,(t, \Delta t, t_{notice}) = \frac{\int_{t}^{t+\Delta t} P_{ref}dt - \int_{t}^{t+\Delta t} P_{flex}dt}{\Delta t} \tag{3.26}$$

where $BEFI$ is the Building Energy Flexibility Index, t is the start time of event, Δt is the duration of event, t_{notice} is time of notification for the event, P_{ref} (kW) is the power demand from the reference scenario during an event, and P_{flex} (kW) is the power demand from a flexibility case during an event. The $BEFI$ is the average difference between the power demand of the reference case, P_{ref} (kW), and the power demand of the alternative “flexibility scenario”, P_{flex} (kW), for the given event duration Δt, shown in Equation (3.26). $BEFI$ could also be represented as a percentage by dividing it by the value of P_{ref}.

Real-time optimizing algorithm: The MATLAB function *fmincon* finds the minimum of a constrained nonlinear multivariable function. The optimization algorithm identifies a setpoint schedule at hourly intervals. These identified values are then fed to the simulation model (“real building”) and linearly interpolated to a specified time interval. Set-point optimization is just one example of how MPC can be employed in buildings and is the only method used in this research.

Prediction and control horizons: Typically, in MPC, the optimal control problem is solved at each defined control step by looking ahead at forecasts such as weather and occupancy schedules over the prediction horizon, PH. The prediction horizon is a time period where we have reasonably reliable information, ranging from a few hours to a couple of days. Using data available from the prediction horizon period, an optimization routine is solved, and an optimal sequence of control moves is identified through the implementation of MPC. The identified schedules and control moves are applied to the building over a “control horizon”, which can be the same length or be shorter than the prediction horizon. Once the current control horizon has ended, the optimization exercise is performed again for the following prediction horizon. This process is repeated until the end of the simulation time (e.g., one day or one year).

Chapter 4

Control-Oriented Modelling of Case Study Buildings with Convective Heating Systems

4.1 Introduction

In this chapter, two simulation-based applications of control-oriented building modelling are presented. The first study is a multi-level control-oriented modelling approach for a detached residential house (Date et al., 2016b) while the second study pertains to MPC model development of a smaller commercial retail building (Date et al., 2017). The application of the detached house presents the development of a multi-level approach to the problem of modelling different thermal zones in a house for control applications. This problem has been treated before by modelling the whole house with a single, all-inclusive RC thermal circuit which may have different levels of resolution. The core feature of the proposed methodology allows the user to switch back and forth between models representing different control levels according to the modelling objectives. The second study determined if the implementation of MPC is useful for lowering electricity bills in small commercial buildings under the typical rates applied in Québec. For an electrically heated building, it was investigated if it is possible to reduce the annual energy bills associated with the combined effect of energy price, demand charges, and a minimum monthly billing charge based on the winter peak. While other MPC studies have used an objective function combining both an energy price and a demand charge (Braun, 1990, Cai et al., 2016a), our goal was to examine how an MPC algorithm with a short-term horizon can offer benefits in the long-term electricity bill.

4.1.1 Control-oriented modelling of thermal zones in a house: a multi-level approach

This section presents the use of a multi-level simplified linear thermal modelling approach based on the electrical analogy for the development of control strategies in conventional detached residential homes equipped with convective electric heating systems[1]. These models are developed with parameter identification techniques of results obtained through comparison with whole building measured data. Although detailed building simulation models can be used directly for testing control strategies, this approach can be quite computationally intense and time-consuming thus simplified models become advantageous. The work presents a methodology to allow a user to switch back and forth between thermal models representing different control levels according to modelling objectives. Different control levels include, but are not limited to, community simulation studies, whole building studies, or zone-level studies. Zone-level models take into account inter-zonal heat transfer. From these simple models, useful information can be extracted without performing any simulation, and this is also explored.

For the development of specific control algorithms for each zone, a house can be treated as a collection of interconnected zonal models, as opposed to a single, large model. This modelling approach has the advantage of maintaining a simple structure for each zone, while also considering the heat transfer between zones; at this control level, issues such as occupancy, thermal comfort or setpoint profiles can be examined in more detail. On the other hand, if a quick estimate of global variables is of interest (e.g., overall thermal load over the next 24-hr) then different zones or entire house may be combined into a single low-order model. In summary, this multi-level approach allows the user to "zoom in and out" so that models at each control level remain manageable, easy to calibrate and easy to physically interpret.

Suitable simplified multi-zone thermal models enable a rapid assessment of control strategies targeting energy reduction, or occupant thermal comfort and advanced control strategies could greatly benefit from adequate, simple models. Model predictions should be meaningful for energy and power results for the whole building level or at the zone level. Zone level detail

[1]This work is based on the published refereed conference papers: (a) Date, J., Candanedo, J., Athienitis, A. K., & Fournier, M. (2016a). Simplified multi-zone thermal modelling of a house for demand reduction & control applications. In Proceedings of CLIMA 2016 Conference Aalborg, Denmark and (b) Date, J., Candanedo, J. A., & Athienitis, A. K. (2016b). Control-oriented modelling of thermal zones in a house: a multi-level approach. In Proceedings of International High Performance Buildings Conference West Lafayette, IN, USA.

allows for even greater potential for advanced controls. Besides energy conservation measures, there is interest in ways to reduce peak power demand (due to space heating or cooling) at critical times and improve building-grid interaction. Simplified thermal models of buildings also offer advantages for district modelling (Baetens et al., 2015, Lauster et al., 2014) and allow for rapid simulation of complex and/or large systems with acceptable accuracy.

Data is used from an existing unoccupied test house, representative of a typical family home in Québec, Canada, as a case study, Figure 4.1. Four zones are considered: basement, main floor, upper floor and attached garage, shown in Figure 4.2. All interior doors were kept closed during experiments and data collection, to minimize horizontal zonal heat transfer. In the most detailed analysis, the zones are modelled with four detailed interconnected zone models; alternative methods of connecting zones are investigated in previous work (Date et al., 2016b). A global low-order whole-house model is used to calculate the thermal load of the house. Results of thermal load predictions are compared, and the resolution of the global whole-house model is investigated.

Figure 4.1: Low-mass residential research-house (EHBE at Laboratoire des technologies de l'énergie (LTE), Hydro-Québec)

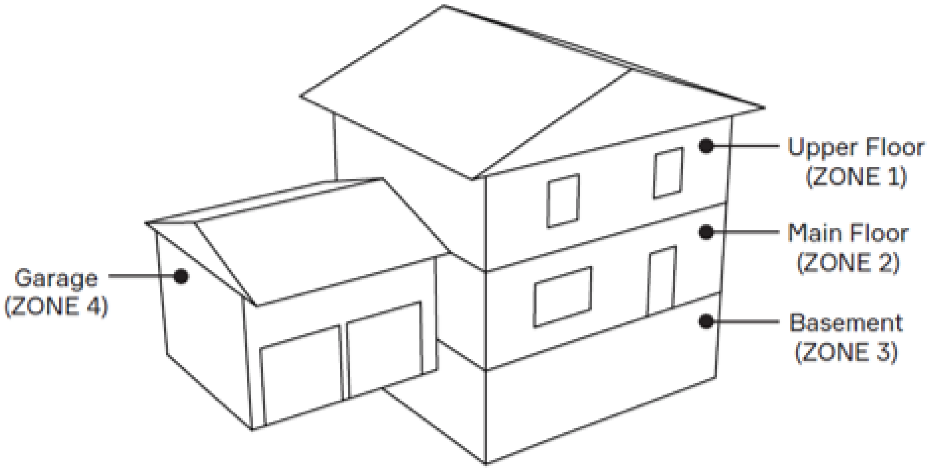

Figure 4.2: Zones of the house

4.1.2 Experimental facility

The Experimental Houses for Building Energetics (EHBE) (Le Bel & Gelinas, 2012), built in 2011, were used for the experiments. The EHBE consists of two 2-storey detached homes with excavated basements, each with a livable area of 120 m^2, excluding the attached garage and basement (Figure 4.1). The homes are of normal construction for Québec with a building envelope consisting of (from exterior to interior) vinyl cladding or brick, air space, air barrier, fibreboard, RSI 3.5 fibreglass, rigid wall insulation panel, air space, drywall, and RSI 5.3 insulation in the roof. The windows are double clear glass with an air gap and no coatings, with a total window area of 19 m^2. The homes are heated with baseboard space heating in each room with no active air mixing and with individual room thermostats.

4.1.3 Methodology

The methodology employed for the identification, inspection, and validation of simplified multi-zone models consists of the following steps:

- Experiments were conducted at unoccupied test homes to obtain measurement data to compare with model predictions.
- A global low-order house model was developed and used to calculate the thermal load of the building.

- A detailed zone-level model was developed to represent the real building and used as a benchmark.
- A Simplified zone-level model was created and the connections between zones are studied.
- Unknown values of parameters of the building models were identified through system identification.
- The simplified thermal model predictions were compared with measured experimental data and the zone-level detailed model predictions.

4.1.4 Building thermal modelling assumptions

Thermal models based on the physics of the system (typically in the form of resistance-capacitance (RC) models) are useful for control studies in buildings. Values of parameters are identified through an optimization technique and should be interpreted as "effective" values rather than "exact" physical parameters (Candanedo et al., 2013). Model details could be added or taken away depending on the needs of the user. For this case, important assumptions used to construct simplified thermal RC networks include:

- The temperature of each surface or cross-section is uniform (e.g., walls, floors, etc).
- The air in each zone is well mixed.
- Radiative and convective heat transfers are combined and constant.
- Air is a non-participating medium with respect to radiation.
- Conduction between each window and window frame is neglected.

An optimization algorithm is used to determine unknown parameters, therefore having fewer equations is helpful. Several methods are available to reduce the complexity of a model: merging thermal zones, reducing the discretization of the walls, and merging several walls to combined surfaces.

4.1.5 Benchmark model (detailed model)

A benchmark detailed model (DM) was developed consisting of 4 zones, with separated walls, windows, doors, resulting in a total of 32 capacitances. A zone represents one storey of the house, shown in Figure 4.3. Figure 4.4 shows one zone (floor) of the detailed model (DM) for floor-level modelling. A zone model such as that in Figure 4.4 represents, for example, the main floor (Zone 2) which is connected to a model depicting the upper floor (Zone 1) and another model representing the basement level (Zone 3) via inter-zonal convection and conduction terms, thus creating a very detailed multi-zone model of the building. Several models can be connected to create a multi-zone model through the "$T_{adjacent}$" terms. The thermal mass of the envelope is modelled as a single layer (i.e., one capacitance). This model is the benchmark model and used as the "real building" in MPC simulation-based studies.

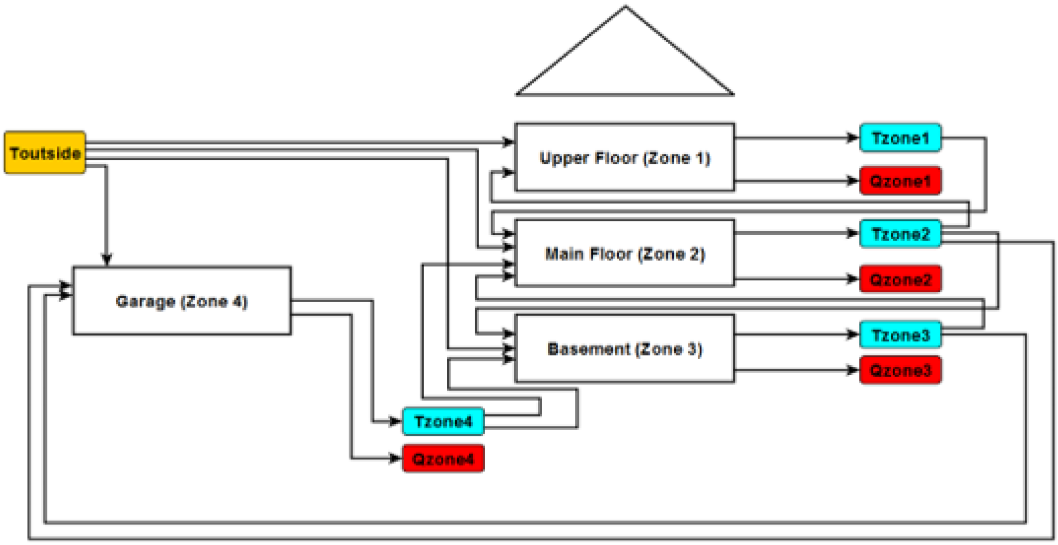

Figure 4.3: Inputs and outputs of all zones

Models of similar detail or structure can represent either the whole building or just a section of the building (floor, room, etc). Here, models are connected via inter-zonal convection and conduction terms to create a multi-zone model at the floor-level with a total of four zones. This section outlines two modelling levels: (i) the floor-level and (ii) the whole building-level. This approach can be expanded in either direction of detail, to zooming out to the community-level, or with further detail at the individual room-level.

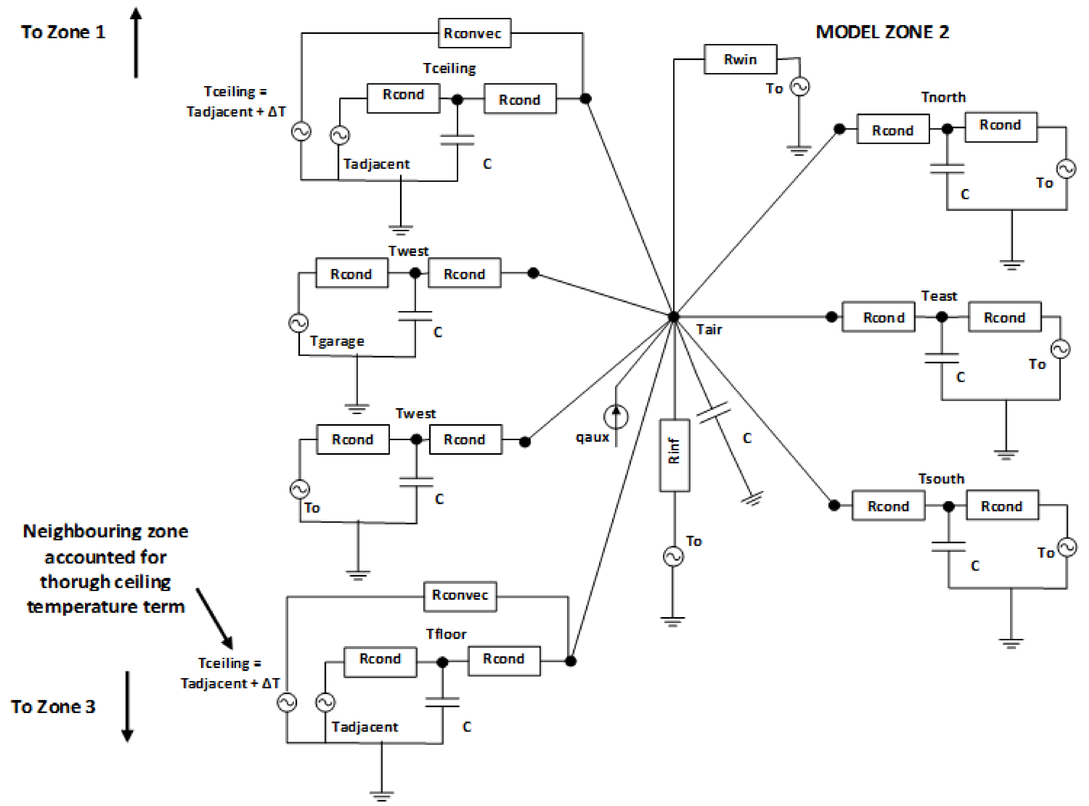

Figure 4.4: Thermal network of detailed model (DM) for one zone

Figure 4.5 depicts the system inputs and outputs for the floor-level model. Each zone (floor) is modelled separately, and these individual zone models are then connected via inter-zonal convective and conductive terms to create a multi-zone model of the whole building. The system outputs of one zone (i.e., zone air temperature) effectively become system inputs to another adjacent zone. For this study, solar radiation as an input was neglected since the experimental setup effectively blocked the influence of solar radiation (Date et al., 2016c).

4.1.6 Multi-level thermal modelling approach

4.1.6.1 Simplified floor-level model

The simple floor-level model combines surfaces into effective areas, creating 14 capacitances for the whole house model, while the benchmark model has 32 capacitances. The thermal mass layer (gypsum board, concrete foundation etc.) of the envelope is modelled as a single capacitance. Figure 4.5 shows an example for the main floor (Zone 2). It was found that a simple floor-level model should include a thermal mass term for the structure between zones (i.e., ceiling/floor material) and the convective and conductive terms should be separated if one is interested in accuracy at the floor level (rather than building level) (Date et al., 2016a).

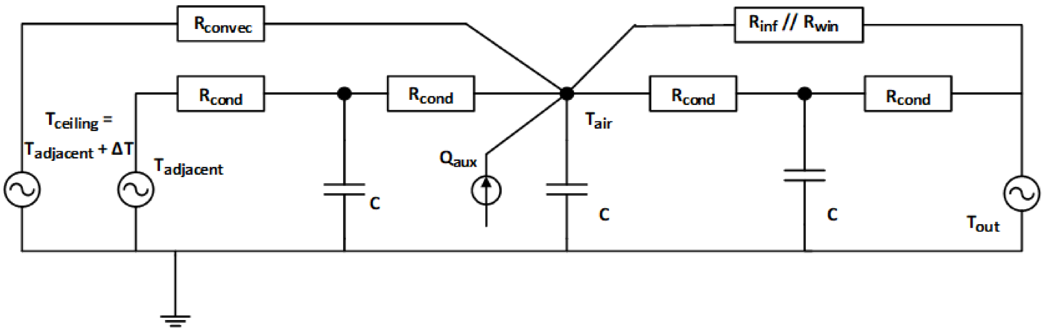

Figure 4.5: Thermal network of floor-level model (one zone)

In all models, experimentally determined data of the zone air temperature stratification was used for the calculation of one-way vertical inter-zonal convective heat transfer (heat transfer driven by a temperature difference) (Date et al., 2016a). In this case, the models use a $T_{ceiling}$ term instead of $T_{adjacent}$ temperature. Therefore, in this study, ΔT represents the average temperature difference between the centre of the room (height = 1220 mm) and the temperature measured near the ceiling (height = 2440 mm) obtained from experimental measurements. This is used for temperature difference convective energy flow from vertically adjacent connected zones (i.e., Zone 1 to Zone 2, or Zone 2 to Zone 3). This approach is an attempt at a simplified method for the convective heat transfer between floors in a multi-story building. Further work on simplified inter-zonal modelling for controls includes taking into consideration the techniques and correlations developed by Riffat (1989).

Figure 4.6 shows the overall thermal network schematic of a whole building of the simple floor-level model structure. It shows the individual zone models (blue rectangles) and how each zone model is connected to adjacent zone models by convection and/or conduction terms. In all models, experimentally determined data of the zone air temperature stratification was used for the calculation of vertical inter-zonal convective heat transfer (heat transfer driven by a temperature difference), depicted by the ΔT source terms. Parameters are identified using an optimization algorithm within Python.

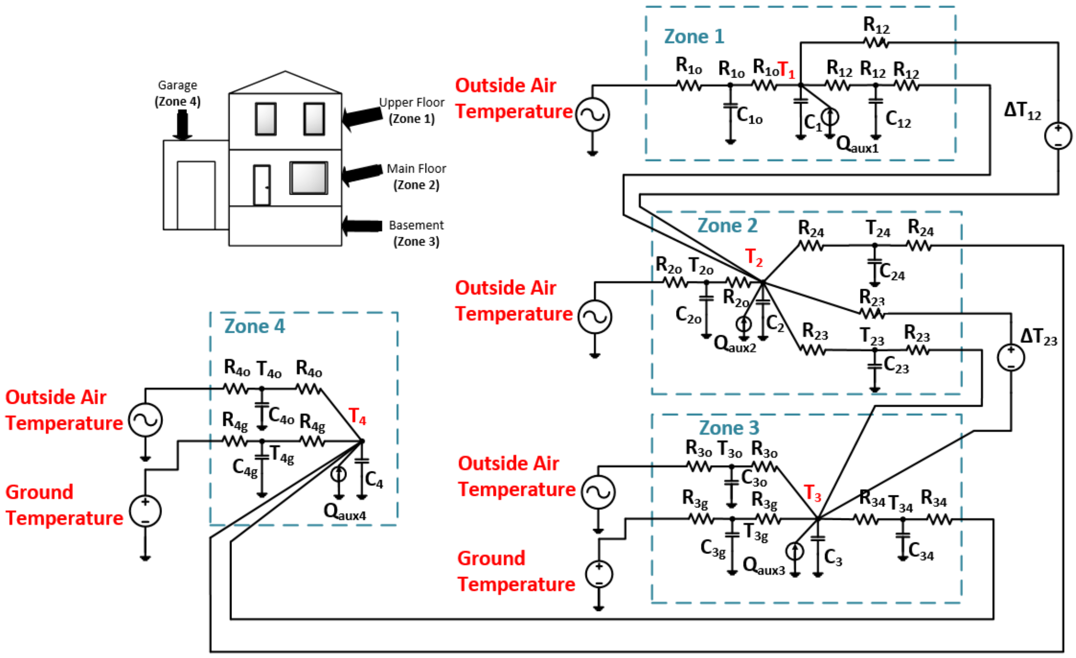

Figure 4.6: Multi-zone thermal network whole building schematic

4.1.6.2 Whole building-level model

At the whole building-level, a first-order (i.e. one capacitance) model is developed and model parameters are identified using the optimization algorithm. Figure 4.7 depicts the system inputs and outputs for the whole building thermal model. Figure 4.8 shows the thermal circuit at the whole building-level, modelled as one equivalent zone with one effective capacitance and one effective resistance, creating a 1R1C model. As the setpoint of each zone within the house may not be the same, an effective whole house setpoint temperature can be defined as:

$$T_{eff,setpoint} = \sum_{j=1}^{n} \left(\frac{T_{setpoint,j} \cdot A_j}{A_{total}} \right) \tag{4.1}$$

Using Equation (4.1) to estimate the effective setpoint for the building (when individual zones are controlled differently), this model structure can be useful to obtain quick estimates of whole building loads and operation or for district/community scale simulation studies.

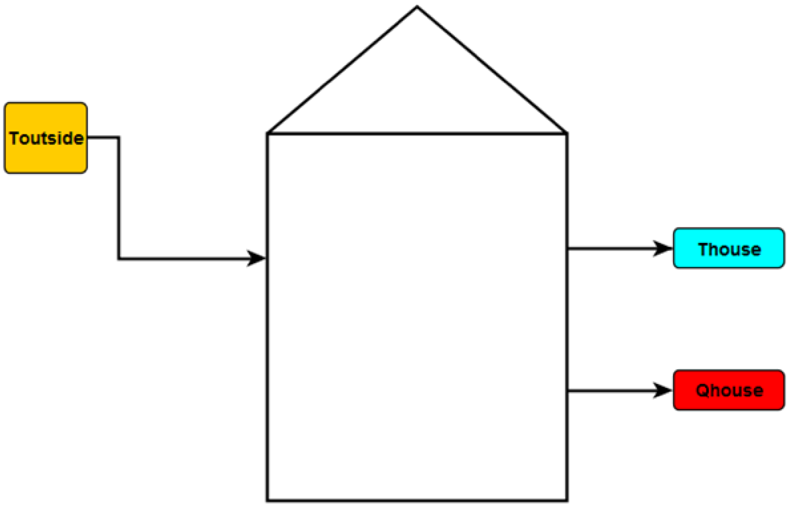

Figure 4.7: Global house model

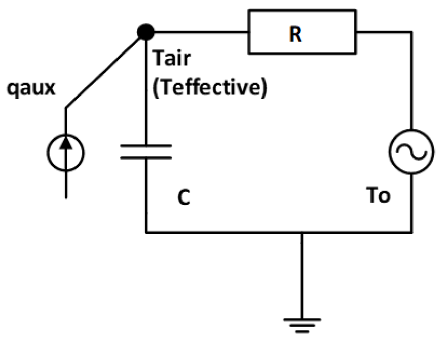

Figure 4.8: 1R1C whole house model, CV-RMSE = 21%

4.1.7 Calibration of models

An optimization routine is used to find the parameter values that minimize an objective function. In this case, the objective function chosen was the coefficient of variation of the root-mean-square error (CV-RMSE) between measured power and the prediction at 15-minute intervals (Lavigne et al., 2014). The training data length was 5.4 days of data. The minimize scalar function of one or more variables using the Sequential Least Squares Programming (SLSQP) method was used for this study using the Python programming language. The SLSQP algorithm is used here; other algorithms can replace it depending on the user's preference. Since the individual results of each zone and whole building power use are of importance, the CV-RMSE of each zone was minimized (for the floor-level models), and then whole building results were investigated. The objective function (CV-RMSE) used is shown in:

$$J(y,\hat{y}) = \frac{1}{\bar{y}}\sqrt{\frac{1}{n}\sum_{i=1}^{n}(\hat{y}_i - y_i)^2} \tag{4.2}$$

where y is the experimentally measured data (thermal power) and $\hat{y}$ represents the model predictions. The building was modelled using the fully explicit finite difference method to solve the energy balance equations. Initial values of model parameters are based on the known building material properties and estimates for infiltration, inter-zonal convective transfer, and air capacitance multipliers. A comparison between the benchmark model, the zone-level control-oriented model and the building-level control-oriented model is shown in Figures 4.9 and 4.10, and a table outlining the modelling error (CV-RMSE) is given in Table 4.1.

4.1.7.1 Calibration of benchmark model and floor-level model

The parameter values of the benchmark (detailed) floor-level model and simplified floor-level model were identified, and the power use predictions were compared. The focus was on the accuracy of power prediction rather than room temperature prediction, as most building simulation models are calibrated against the power or energy consumption of the whole building. Results after calibration using 5.4 days of model training data are found in Table 4.1.

Table 4.1: Calibration of multi-zone models

Multi-zone models	**Detailed Model**	**Floor Level Model**
CV-RMSE - Zone 1 (Top Floor)	23%	26%
CV-RMSE - Zone 2 (Main Floor)	25%	23%
CV-RMSE - Zone 3 (Basement)	19%	26%
CV-RMSE - Zone 4 (Garage)	7%	6%
CV-RMSE - Whole Building	13%	15%

4.1.7.2 Calibration of building-level model

Table 4.2 shows the values for the parameters R and C of the 1R1C thermal model of the whole house. Initial and second guesses were made based on geometry and material properties of the building and then an optimization routine was conducted to identify R and C values which results in the lowest CV-RMSE, when model predictions are compared to experimentally measured data. For the initial guess of the 1R1C model, *R* and *C* were determined by adding the resistances according to the series and parallel circuit laws and capacitances were added together. In the second guess, a capacitance multiplier of 15 was chosen.

Table 4.2: 1R1C global model calibration results

1R1C model	Initial Guess	Second Guess	After Identification
R (Kelvin/kW)	7.1	7.1	6.4
C (MJ/Kelvin)	49.1	57.7	17.2
Effective air capacitance multiplier	1	15	N/A
CV-RMSE	51%	55%	20%
Time Constant (τ = RC)	97 Hours	114 Hours	31 Hours

One noteworthy result from the identification process of the 1R1C model using an optimization routine is the value of the *C* parameter, as it is much smaller (almost 3 times smaller) than what the expected "effective" *C* value based on the geometry and material properties of the building. These results suggest that new, revised methods are needed to estimate effective capacitances of buildings. Figure 4.9 shows the predictions of the floor-level model and experimental heating power data. For visual clarity, only one day of data and predictions is shown here. The predictions of each zone's power demand contribution are shown, and the simple whole house 1R1C power profile is overlaid (dashed line).

The concept of the multi-level thermal modelling approach for different control applications can be summarized as follows. The top benchmark model is the most detailed version of the building thermal model. From there, one can choose to look at optimal control at the zone level by using the simplified zone-level models or at global whole building operation by using the building level model. It is a simple procedure to interchange between the different modelling levels depending on the needs or interests of the model user. The characteristics and results of the three thermal modelling levels are summarized in Table 4.3. A comparison between the benchmark model, the zone-level control-oriented model and the building-level control-oriented model is shown in Figure 4.10.

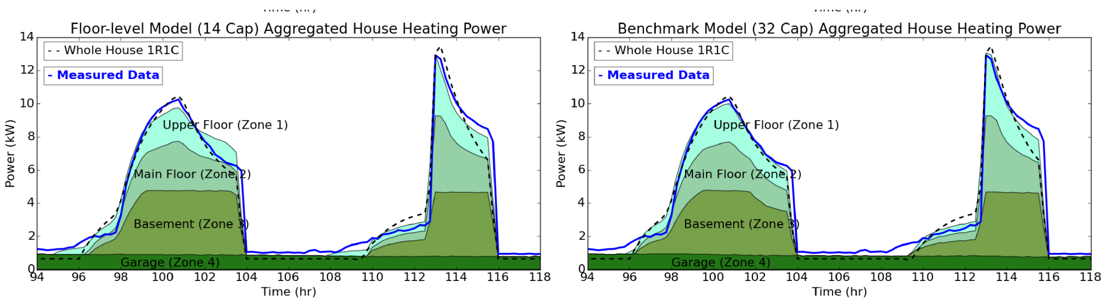

Figure 4.9: Model verification results of left: simplified floor-level model, and right: benchmark detailed model

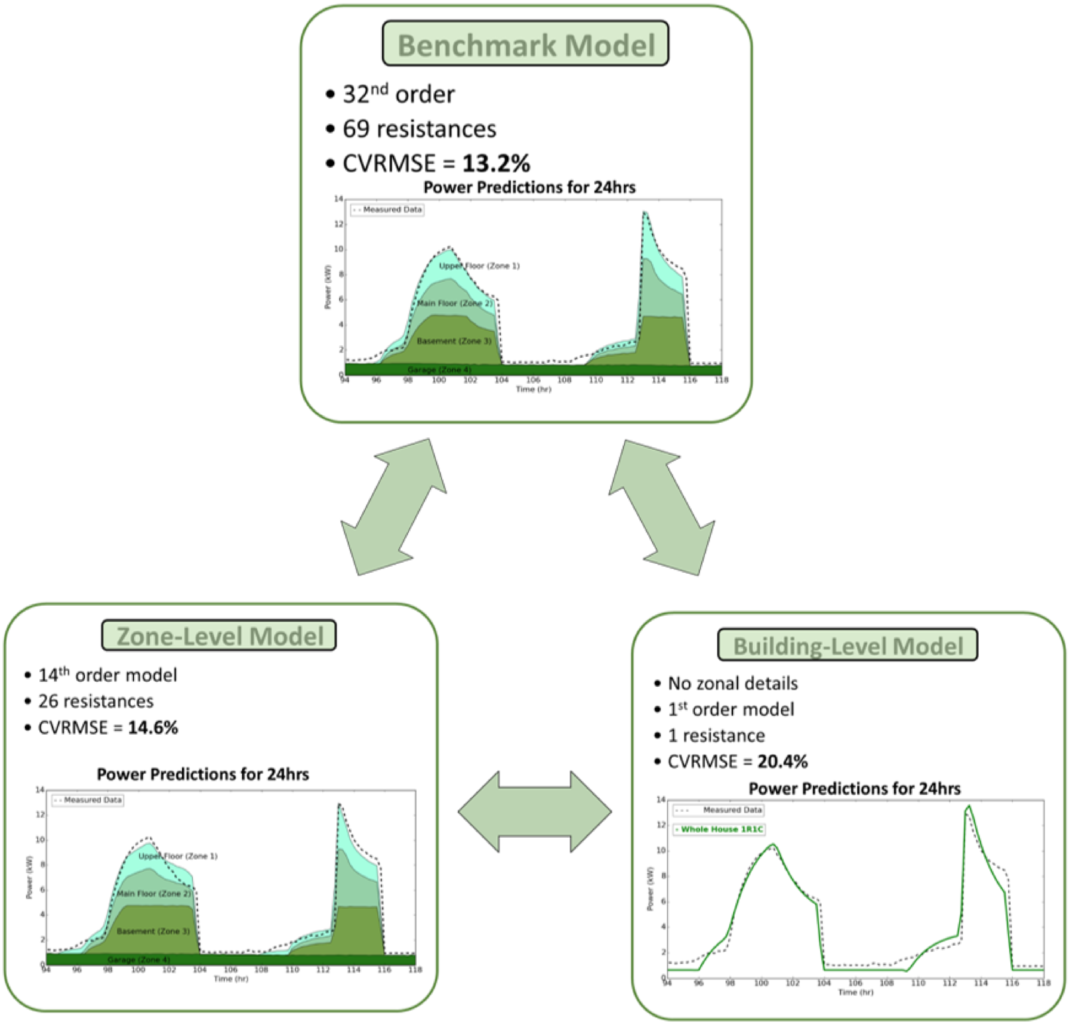

Figure 4.10: Multi-level modelling approach summary

Table 4.3: Summary of three thermal modelling levels

	Benchmark Model	Zone-Level Model	Building-Level Model
Model Order (number of capacitance)	32	14	1
Number of Resistances	69	26	1
Building CV-RMSE	13%	15%	20%

4.1.8 Whole-building model: is 1R1C enough?

From the preceding discussion, it seems apparent that a 1R1C model provides an accurate representation of the heating load of the whole house over a period of several days (and when calibrated with training data of several days). Several questions arise: Is there a need to add more capacitances (e.g., 2 or 3) to the model? Do these models predict the heating load accurately in the short term (say, the next 3 hours)? How does the model training period affect the accuracy of the model? What kind of information can be obtained about the house dynamics from a quick inspection of the models (i.e., without simulation)?

4.1.8.1 Alternative whole house-level models

Three model structures for the whole house load calculation are shown below in Figure 4.8, Figure 4.11, and Figure 4.12. The first model corresponds to the 1R1C presented in the previous section. As more capacitances are introduced, the model is more capable to capture the shorter-term dynamic behaviour of the system outputs based on inputs. CV-RMSE values shown correspond to calibration using 5.4 days of training data and evaluated over a prediction horizon of the same length.

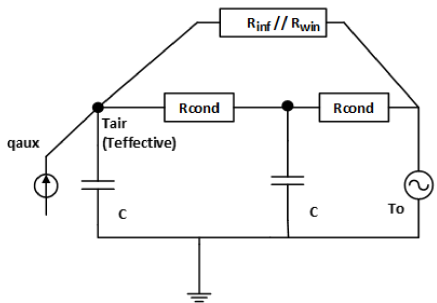

Figure 4.11: 3R2C whole house model, CV-RMSE = 20%

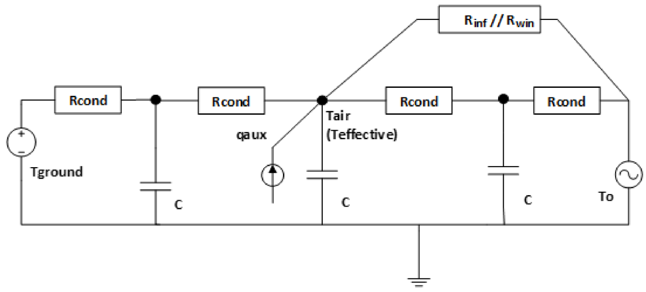

Figure 4.12: 5R3C whole house model, CV-RMSE = 19%

4.1.8.2 Effect of (i) training data period and (ii) length of prediction horizon

The three whole building models were trained with datasets of different lengths: 5.4 days (the entire measurement period), 1 day, 6 hours and 3 hours. Different *R* and *C* parameters are found depending on the training data period. The predictions of the models were then evaluated in terms of their CV-RSME values over different prediction horizons; results are shown in Figures 4.13 to 4.16. Each of the bar graphs corresponds to different training data lengths and the models are then evaluated for different prediction horizon lengths shown in the four tables. However, it should be noted that the specific data that the model was trained on was used for the CV-RSME calculation of that specified time length.

One notable result seen in Figure 4.16 is that with just 3 hours of training data, two of the simple whole building models (3R2C and 5R3C) can predict the total 5.4 days of operation with acceptable accuracy, while the simplest 1R1C performs poorly. In general, long training data periods result in a model that is satisfactory for long time scales, but not necessarily good for short-term predictions (although this is largely dependent on the particular calibration period chosen). In a control application of a real building, simple models could prove useful when short lengths of training data for calibration are available, particularly if the models could be "checked" and systematically re-calibrated at specific times (e.g., once per week or once per day) with the buildings sensor data.

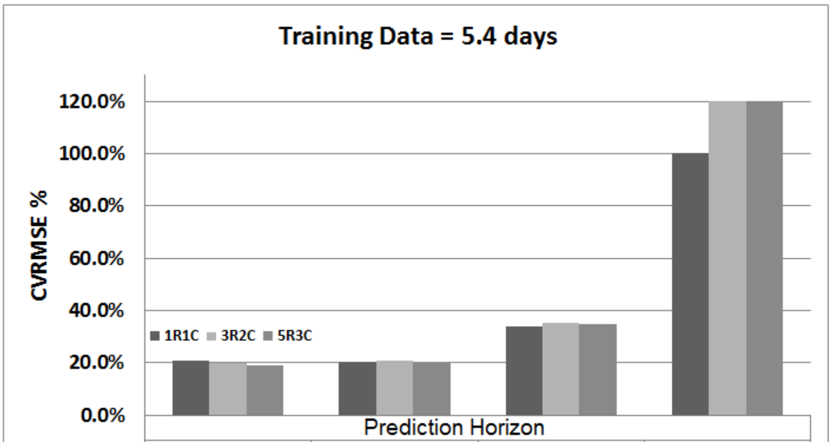

	5.4 days	1 day	6 hours	3 hours
1R1C	20.8%	20.2%	34.0%	100.0%
3R2C	19.8%	20.7%	35.2%	120.0%
5R3C	19.2%	20.4%	34.8%	120.0%

Figure 4.13: Model error (CV-RMSE) for different prediction horizons and training data 5.4 days

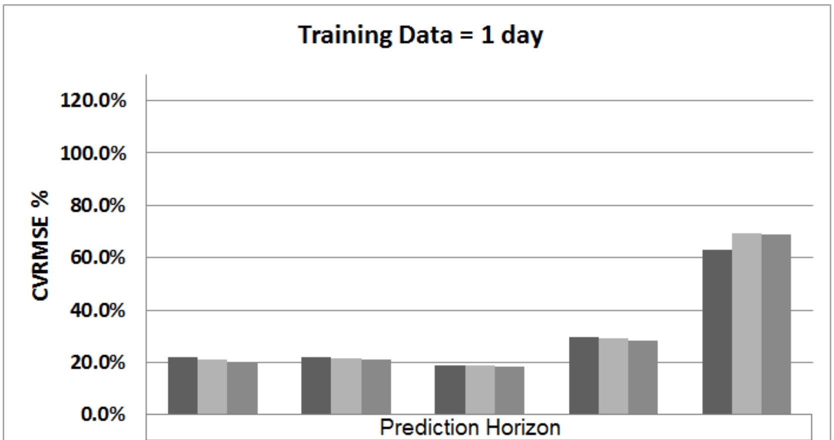

	5.4 days	3 days	1 day	6 hours	3 hours
1R1C	21.8%	21.9%	18.6%	29.5%	62.8%
3R2C	20.9%	21.4%	18.9%	29.0%	69.1%
5R3C	20.3%	20.9%	18.4%	28.1%	68.6%

Figure 4.14: Model error (CV-RMSE) for different prediction horizons and training data 1 day

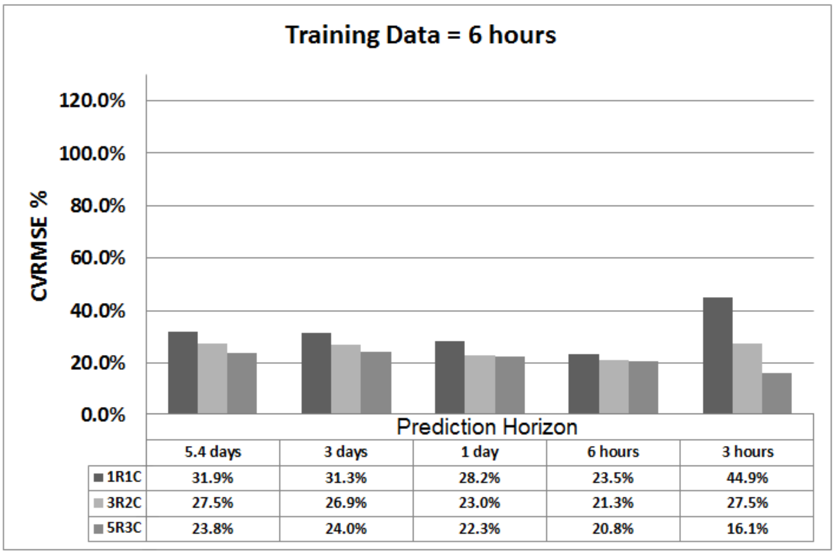

Figure 4.15: Model error (CV-RMSE) for different prediction horizons and training data 6 hours

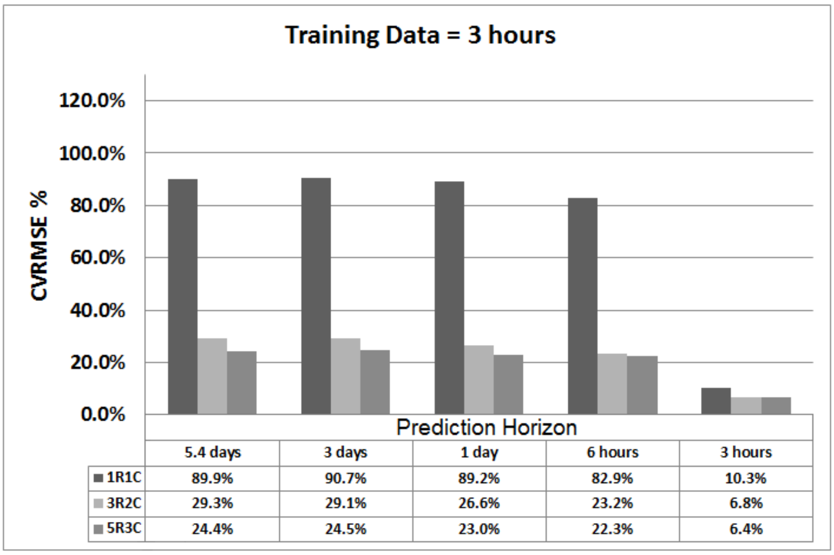

Figure 4.16: Model error (CV-RMSE) for different prediction horizons and training data 3 hours

4.1.9 Frequency domain analysis

Frequency domain analysis of these systems could prove useful in comparatively evaluating a model's accuracy, almost by inspection, without the need for a simulation. After solving for the state-space representation of the three models (refer to (Candanedo et al., 2013) for procedure), the frequency response of the indoor air temperature T_{in} output to the electric heating input

q_{HVAC} for the three whole-house models were plotted and are shown in Figures 4.17, 4.18, 4.19. The magnitude on the left axis refers to °C/Watt.

The following example illustrates how frequency domain analysis enables a quick and simple assessment of a model. The 1R1C model based on 3-hour long training data predicts that, while keeping other inputs at zero, a continuous heating input of 1000 W would result in a steady room air temperature of roughly 16 °C. It is not realistic that such little amount of heating would result in such a high air temperature; this result indicates that 1R1C model trained with 3 hours of data is not accurate enough to represent steady-state or low-frequency phenomena. This meaningful result is found without performing any simulation. For the 1R1C models calibrated with different training periods (Figures 4.17, 4.18, 4.19) there are significant differences in the predicted steady-state values (e.g., 16 °C/kW vs 8 °C/kW); though, the lines nearly overlap for training data periods of 6 hours and longer. For the 3R2C and 5R3C models, there is significant variation in the phase angle results (corresponding to different time delays) between different training data lengths.

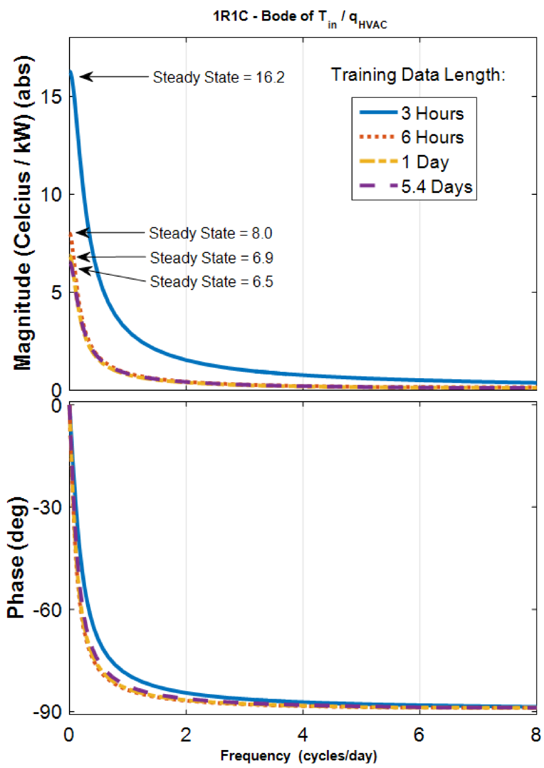

Figure 4.17: Frequency response - indoor air temperature to heating power (1R1C)

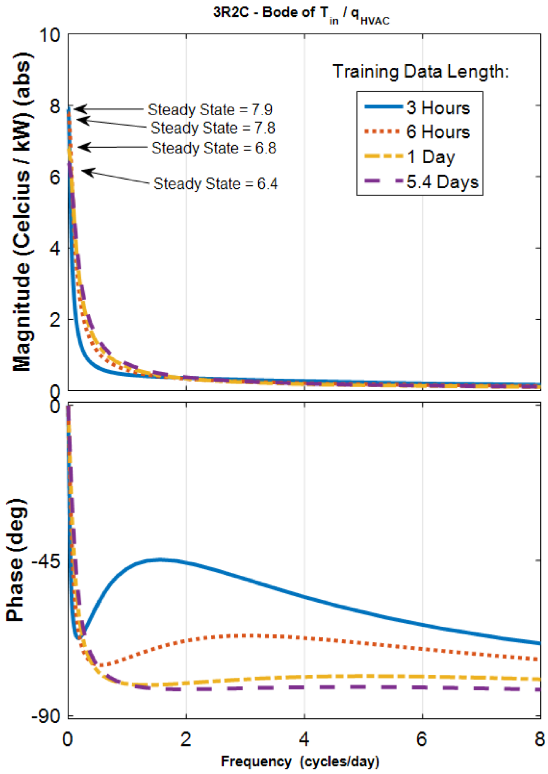

Figure 4.18: Frequency response - indoor air temperature to heating power (3R2C)

4.1.10 Control scenario

The developed control-oriented models facilitate the study of various control strategies for the house. For example, setpoint profiles used in different zones are investigated through simulation and then evaluated according to their impact on peak reduction. It is assumed that occupants wake up at 6am. These simulations were performed for a very cold day where the minimum outdoor air temperature reached -26 °C.

The scenario shown in Figure 4.20 employs different setpoint profiles in the three floors of the house, with preheating in the basement. A space heating peak of 8.8 kW is observed, compared to 12.5 kW for the base case with an occupied basement (30% reduction). The identified scenario consumes 4 kWh more than the base case.

The basement (Zone 3) has a three-hour ramp from 18 °C and is preheated at 23 °C for three hours. The setpoint is then dropped to 19 °C during the peak hours and finally raised back to the 21 °C. From Figure 4.20 it is seen that the proposed setpoint profiles yield a significant reduction in the thermal peak loads in the morning.

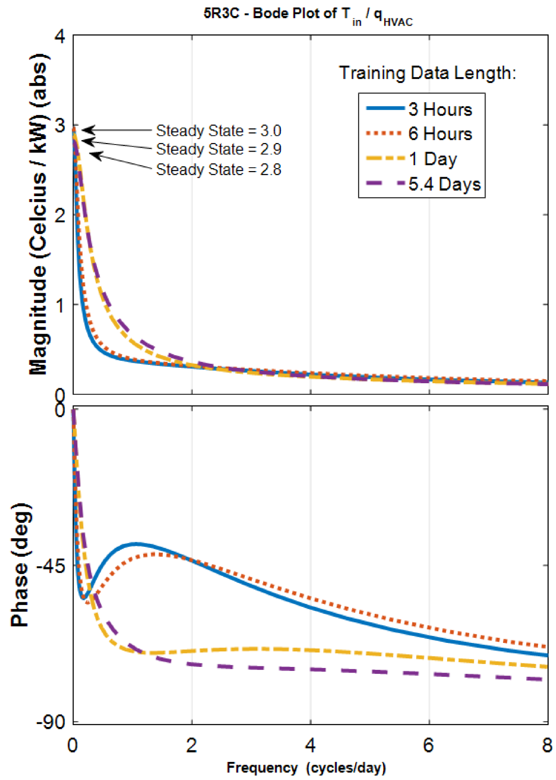

Figure 4.19: Frequency response - indoor air temperature to heating power (5R3C)

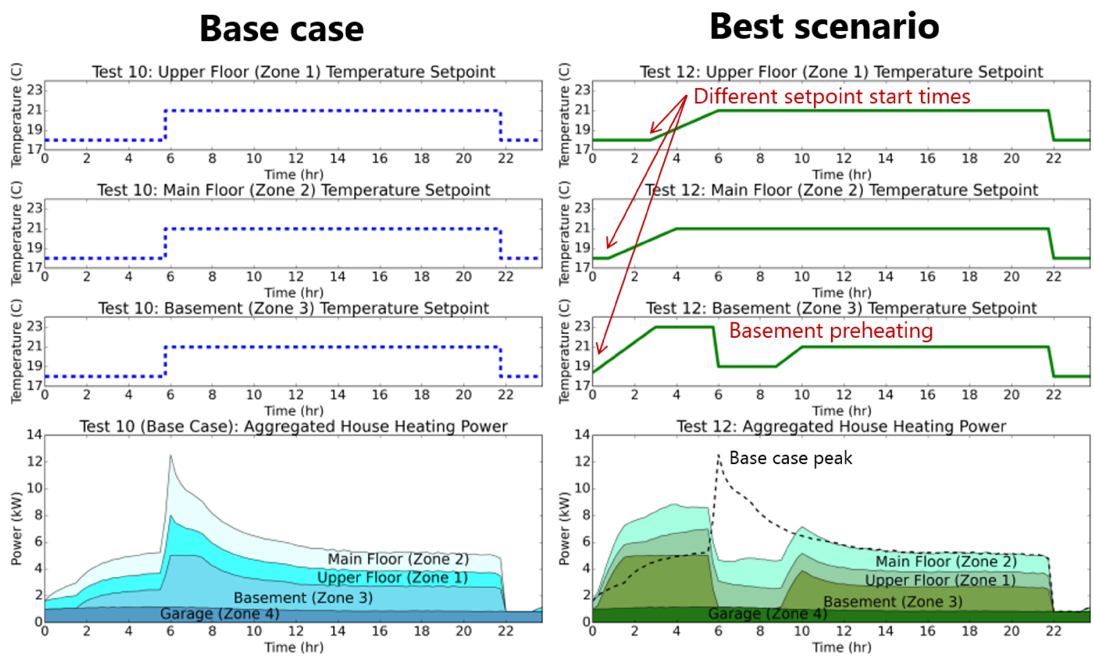

Figure 4.20: Control scenario results

This multi-level approach allows the user to "zoom in and out" so that models at each control level remain manageable, easy to calibrate and easy to physically interpret. A global low-order model (1R1C) is developed and used to rapidly calculate the thermal load of the building, while a very detailed benchmark floor-level model is developed and can be used for verification and MPC-based simulation studies. For the development of specific control algorithms for each zone, an adequate simplified zone-level model must be identified. It was found that if zone-level accuracy is of importance, one must incorporate into the model the thermal mass of the structure between zones. Work remains to be done on how to improve the guidelines for the initial guess of the grey-box model parameters.

4.1.11 Conclusion: multi-level modelling of a house

This study outlined a methodology for multi-level control-oriented modelling for buildings with several zones. This multi-level approach allows the user to "zoom in and out" so that models at each control level remain manageable, easy to calibrate and easy to physically interpret. A global low-order model (1R1C) is developed and used to rapidly calculate the thermal load of the building, while a very detailed benchmark floor-level model is developed and can be used for verification and MPC-based simulation studies. For the development of specific control algorithms for each zone, an adequate simplified zone-level model must be identified. It was found that if zone-level accuracy is of importance, one must incorporate into the model the thermal mass of the structure between zones.

Three building-level models were then evaluated to investigate the effect of incorporating additional capacitance terms. Using these three building-level models, the effects of different lengths of training data periods on the accuracy of different prediction horizons were explored. It was found that a 1R1C whole-house model can perform well for either longer horizon or short ones, but not simultaneously for both. Frequency analysis was used to quickly evaluate the whole building models without the need to perform a simulation. Interesting differences emerged in the phase angle predicted by the different models. Work remains to be done on how to improve the guidelines for the initial guess of the grey-box model parameters.

4.2 Predictive setpoint optimization of a small commercial building subject to a winter demand penalty affecting 12 months of utility bills

This study looked at the implementation of MPC in a small commercial building in a heating dominated climate and developing suitable models for model-based control studies[2]. The goal of this study is to investigate the potential of MPC for lowering electricity bills in commercial buildings under the typical rates applied in Québec, which include a demand charge that heavily penalizes winter peaks. Two slightly different cost functions target the minimization of the utility rate during each prediction horizon while meeting upper and lower indoor temperature constraints. A parametric study indicated that despite minor differences all studied MPC scenarios result in significant reductions in both yearly utility bills and peak power demand.

This study investigated how MPC can be used to lower electricity bills in commercial buildings under the typical rates applied in Québec. The goal was to evaluate the potential of MPC in buildings of common construction, without any high-tech features, technologies, or systems. In Québec, Canada, where greater than 99.8% of the electric power is generated through hydroelectric plants (Hydro-Québec, 2016), it is not unusual to find commercial buildings using electricity as their only energy source.

This is a result of low electricity rates, high fuel prices and limited distribution of gas in certain regions. It is estimated that heating in the commercial and institutional building sector accounts for 9% of the province's winter peak demand (Hydro-Quebec Distribution, 2012). These buildings represent a significant portion of the electric load in the province. During winter, peak loads associated with space heating impose a heavy burden on the grid. Thus, there is increasing interest in demand response strategies, especially on cold winter days.

A particular aspect of commercial customer rates in Québec is that the building's winter peak demand can affect the utility bill for an entire year. The minimum billing demand charged in the electricity bill is set at 65% of the peak power recorded during the winter (Dec 1 – Mar

[2]This work is based on the published refereed conference paper: Date, J., Candanedo, J., Athienitis, A. K., & Lavigne, K. (2017). Predictive Setpoint Optimization of a Commercial Building Subject to a Winter Demand Penalty Affecting 12 Months of Utility Bills. Proceedings of Building Simulation 2017 Conference. San Francisco, California.

31) falling within the previous 12-month period. This rule means that special attention must be given to the control strategies over the winter period. MPC is an established control technique in other engineering fields such as chemical processing and electrical engineering (Qin & Badgwell, 2003) and is a promising strategy for improved controls in buildings. It has received increasing attention in buildings research but has yet to become a mainstream practice. MPC is a multivariable control algorithm that uses an internal dynamic model of the system, a history of past control moves, forecasts of future disturbances (i.e., weather forecast) and an optimization cost function that is minimized over the receding prediction horizon. The basic principle of MPC in buildings is that knowledge of forecast weather and anticipated occupancy enables better control of the building energy systems, for example, by better managing thermal storage capabilities. Because of the number of variables and constraints that must be considered, optimization can become quite complex. Setting up a suitable building control model is crucial for MPC. The degree of modelling effort is difficult to assess in advance as each model is typically tailored for one specific building. MPC design requires expert knowledge on building modelling, such as a good understanding of what details are appropriate to include or exclude in the control model. Several modelling environments are suitable for MPC studies, all with their advantages and disadvantages. This point has been addressed by (Perera et al., 2016) in a paper comparing MATLAB and Modelica. However, one major aspect still incomplete in the field of MPC and building control research is an effective way to visualize the process flows, which hinders the ability to easily convey research results to a wide audience. This is a topic of ongoing research and development.

4.2.1 Objectives

As mentioned above, the goal of this study is to determine if the implementation of MPC can be useful for lowering electricity bills in commercial buildings under the typical rates applied in Québec. This work investigated, for the case of an electrically heated building, the reduction of the annual energy bills associated with the combined effect of energy price, demand charges, and a minimum monthly billing charge based on the winter peak. While other MPC studies have used an objective function combining both an energy price and a demand charge (Braun, 1990, Cai et al., 2016a), our goal was to examine how an MPC algorithm with a short-term horizon can offer benefits in the long-term electricity bill.

The building introduced in this study was previously investigated by Lavigne et al. (2014), who used an offline demand response approach to optimize the operation of the building to reduce the building's total power demand during peak periods while maintaining comfort for occupants.

Simulink, MATLAB's graphical environment, is used in this study to model and visualize the MPC process. Simulink is a graphical programming environment for modelling, simulating, and analyzing multi-domain dynamic systems. Its primary interface is a graphical block diagramming tool and a customizable set of block libraries.

The main objectives of this study include:

- To investigate the performance of an MPC algorithm for the planning of setpoint trajectories in a commercial building under utility rates commonly used in Québec, and in a heating-dominated climate.
- To investigate how a short-term optimization of a few days might impact annual electrical energy bills. For instance, a high peak in winter affects the electricity bill even in the summer months.
- To perform a sensitivity study on how the length of the prediction horizon affects the overall cost.
- To explore the potential of a graphical interface (Simulink) to test predictive control and showcase its performance, for example, the simulation will continuously display the projected monthly bill based on energy use and the maximum power measured since the end of the last billing period.

4.2.2 Building description

This study is based on an existing 427 m^2 (4,600 ft^2) single storey commercial building built in 2009, shown in Figure 4.21. The building is located 150 km north of Montreal in Trois-Rivières, Canada, and is used as a retail bank establishment. The wall insulation is 3 K·m^2/W (R-17), roof insulation is 6 K·m^2/W (R-34) and it is slab on grade construction. The windows are double-glazing with low-e coating and an air gap of 12.7 mm. The building has an average energy consumption of 269 kWh/m^2 and a maximum power demand of about 50 kW. The building is an all-electric building conditioned with convective heating and cooling systems. It is serviced by three rooftop units: two for heating and cooling and the third for cooling only. The third unit is an assembled system recirculating air with a condenser on the roof for cooling and services an unoccupied zone, thus requiring no fresh air. In addition, there are terminal reheat units and baseboard heaters throughout the building.

Figure 4.21: Retail bank building

The building's winter daily load profile follows the typical pattern of buildings in this region. A nighttime setback of the temperature setpoint is initiated during unoccupied times as a method to reduce overall energy consumption and is brought back to levels that are more comfortable just before occupants arrive. While this strategy is aimed at reducing energy use, it results in high peak demand in the morning when the temperature is raised (e.g., from 18 °C at night to 23 °C during the day).

4.2.3 Electric utility rate: effect of winter peak

There are several utility rates available, depending on their overall energy consumption and peak power demand. This study will concentrate on the rate structure labelled Rate M (Table 4.4) by the utility provider (Hydro-Québec, 2020a).

Table 4.4: Structure of utility Rate M

Rate M (Medium Sized Business Customers)	
Demand Charge (Cost$_{Demand}$):	\$14.37 / kW
Price of energy (Cost$_{Energy}$)	
- First 210,000 kWh	4.93¢/ kWh
- Remaining	3.66¢/ kWh

Rate M has a demand charge and two different energy prices: one for the first 210,000 kWh and a second for any remaining consumption. In this rate structure, there is a minimum demand charge of 65% of the winter peak load, where this minimum is set at all times throughout the year. Therefore, control strategies during the winter months can affect the bill during non-winter months, and thus special attention should be given.

4.2.4 Retail bank building - MPC methodology

This study makes use of MATLAB and Simulink (MATLAB'S graphical simulation environment), as a tool to investigate and evaluate MPC strategies.

For this exercise, a simple Resistance-Capacitance (RC) thermal network is used to model the building using the explicit finite difference method and is employed as the "simulation model" (i.e., intended to represent as accurately as possible the building's response). The model is based (calibrated) on real measurement data at 15-min intervals of whole-building power demand.

A second low-order model (a "control-oriented" model) is used to search for a near-optimal temperature setpoint schedule over a prediction horizon of 1-2 days, thus leveraging the thermal mass of the building. A fully explicit finite difference approach was used to solve the energy balance equations at each node in the model. Equations (4.3) and (4.4) were used for nodes with and without a thermal capacitance term, respectively.

$$T_i^{p+1} = T_i^p + \frac{\Delta t}{C_i}\left[Q_i^p + \sum_{j=1}^{n} \frac{(T_j^p - T_i^p)}{R_{i,j}}\right] \tag{4.3}$$

$$T_i^{p+1} = \frac{Q_i^p + \sum_{j=1}^{n} \frac{T_j^p}{Ri,j}}{\sum_{j=1}^{n} \frac{1}{R_{i,j}}} \tag{4.4}$$

4.2.4.1 Bank building simulation model

The building was modelled as a single zone with five effective thermal capacitances (one for the air, one for the exterior walls and roof, one for interior partitions and two for the concrete floor slab). The effect of solar radiation on the behaviour of the building was also incorporated into the model. It is assumed that 50% of solar radiation transmitted through the windows is absorbed by the floor while the other 50% is absorbed by the other five interior surfaces. It is also assumed there is a carpet over the concrete floor slab.

The simulation model plays the role of the "real building" and facilitates rapid simulation studies of MPC strategies. The simulation model (Figure 4.22) was fed the temperature setpoint found by the control model (used for the optimization calculations). The Simulink PID controller block was used to model heating/cooling control.

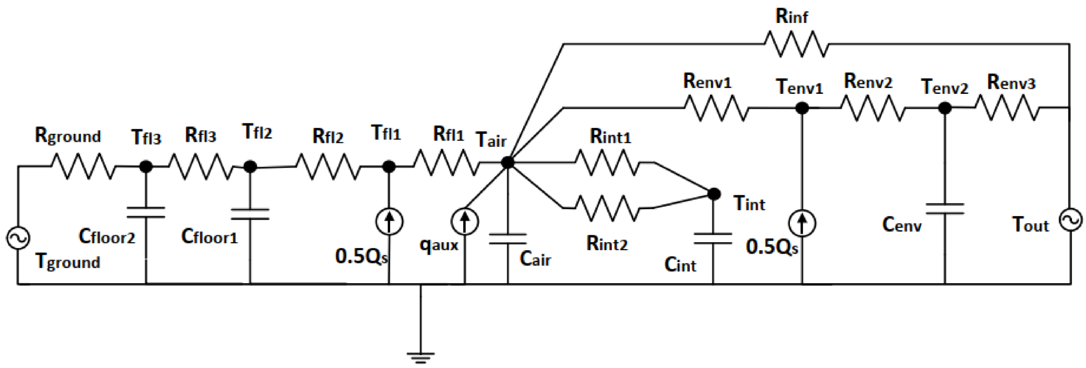

Figure 4.22: Simulation RC model

4.2.4.2 Bank building control model

A second RC thermal network model was developed for the control model (Figure 4.23). This second model was slightly less detailed and consisted of four effective thermal capacitances. Details of the two RC thermal models can be found in Table 4.5. This control model is used to predict, at future times (control horizon), the optimal operation of the building based on the current state of the building and forecasts of disturbances. A cost function is minimized over a prediction horizon to determine optimal control moves (i.e., setpoint schedule) calculated for a control horizon. This identified setpoint schedule is then sent to the "real building" (simulation model) for the time steps corresponding to the next control horizon.

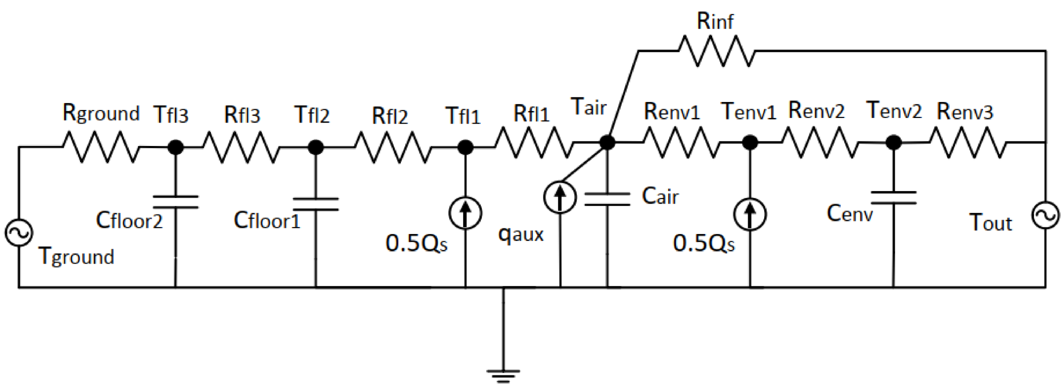

Figure 4.23: Control RC model

The heating control (Equation 4.5) for the controller model was approximated with proportional-integral control. In proportional-integral (PI) control, commonly used in buildings, the auxiliary heating or cooling is equal to the error between the setpoint temperature and the actual zone temperature multiplied by a proportional constant plus the magnitude of the error and the duration of the error multiplied by an integral constant.

$$Q_{aux,i} = K_p \cdot e_i + K_{int} \cdot \sum_{i=1} (e_i \cdot \Delta t) \tag{4.5}$$

where:

K_p = proportional control constant

K_{int} = integral control constant

Δt = control simulation time step

and

$$e_i = T_{sp,i} - T_{air,i} \tag{4.6}$$

where:

$T_{sp,i}$ = air temperature setpoint at time step i

$T_{air,i}$ = actual measured (or calculated/predicted) air temperature at time step i

It is acknowledged that the simulation model and control model are quite similar to one another. Nevertheless, in this investigation, the main objective is to study the building operation

Table 4.5: Details of the two RC thermal models

	Control Model	**Simulation Model**
Order	4	5
Time Step	5 minutes	15 seconds
Controller settings	PI controller coded in MATLAB script	Simulink controller block
CV-RMSE	14.1%	10.4%
NMBE	-2.8%	2.2%

results based on the objective function that incorporates the Rate M electricity cost structure and it suffices to have two slightly different models to illustrate this point. The intention is to analyze whether whole-year utility charges can be reduced when this cost function is implemented into the optimization routine of the control model.

The MPC simulation was "warmed up" for several days before gathering the results for the whole year simulations. This allows enough time for the models to thermally stabilize and give suitable representative results. At the beginning of each control horizon, the current states of the simulation model are fed to the control model as initial conditions. This allows the control model to have knowledge of the current building operation at the start of the new control horizon.

The statistical indices of CV-RMSE and NMBE were used for the model validation process. ASHRAE Guideline 14 (Gillespie et al., 2002a) suggests that a CV-RMSE below 30% and NMBE below 10% on an hourly basis ensures a calibrated model (shown in Table 4.5).

4.2.4.3 System disturbances

Real and predicted disturbances (namely weather data for this investigation) typically differ slightly from one another. To consider the inaccuracies of weather forecast into the prediction control model, noise was added to the real weather data of outdoor air temperature and solar radiation using the *rand()* and *randi()* functions within MATLAB, as shown in Figure 4.24 and Figure 4.25 for four winter days.

4.2.4.4 Cost functions & constraints

MPC studies have often focused on the operation of active energy storage (ice banks, chilled water tanks, etc.), mostly for cooling applications, and under time-of-use rates, but in this study,

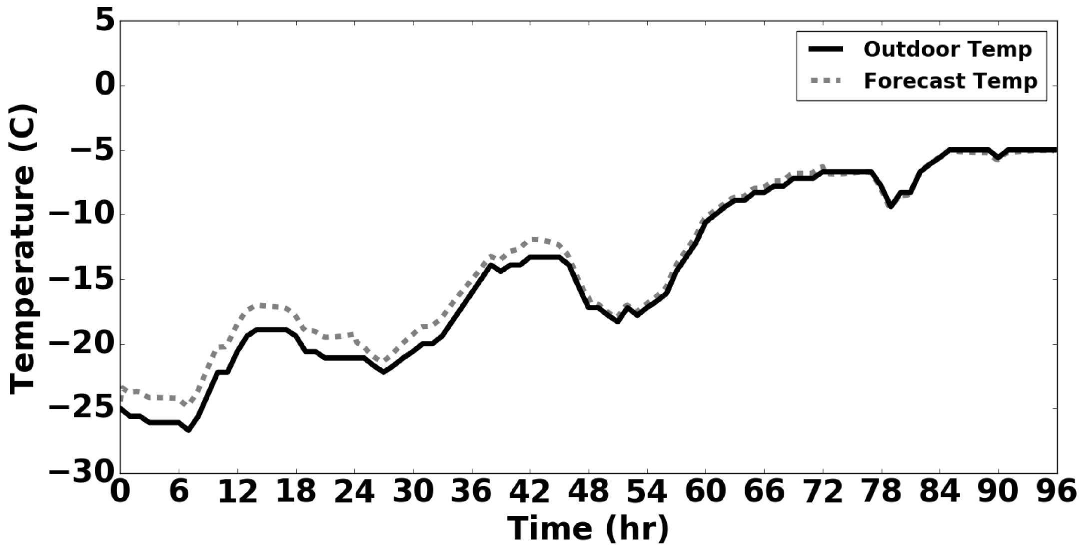

Figure 4.24: Outdoor temperature and forecast temperature for four winter days

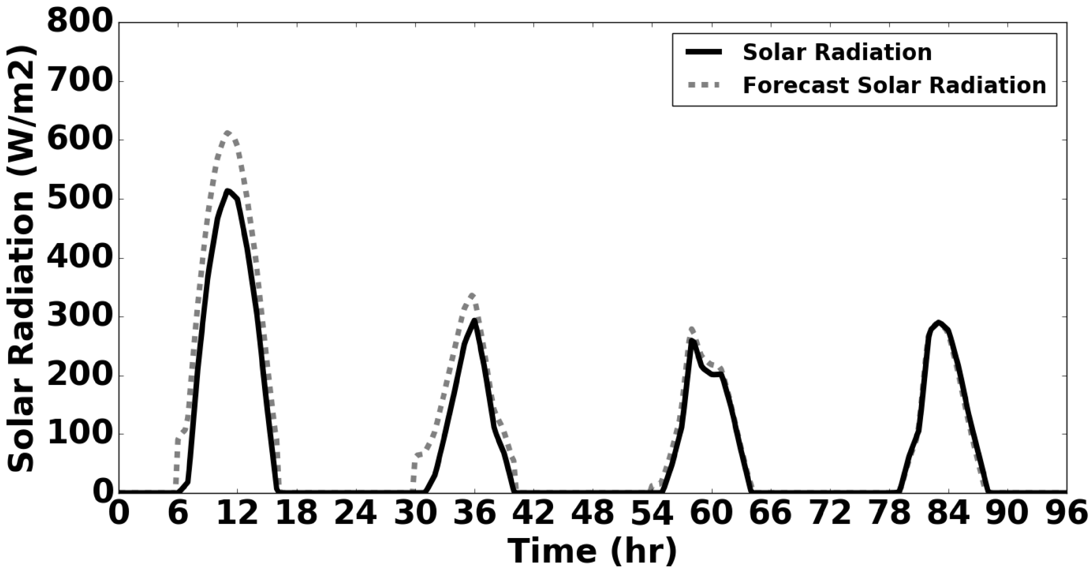

Figure 4.25: Solar radiation and forecast data for four winter days

a more unique cost function was implemented. Two cost functions have been executed and their results compared. The first cost function implemented is shown in Equation (4.7) and is based on the Utility Rate M described in Table 4.4.

$$J_{PH} = \left(\sum_{i=1}^{N} P_i \Delta t \right) \cdot (\text{Cost}_{Energy}) + \max(\mathbf{P}) \cdot (\text{Cost}_{Demand}) \tag{4.7}$$

In winter, the electricity peak demand in Québec occurs on weekday mornings between 6 a.m. and 9 a.m. and weekday evenings between 4 p.m. and 8 p.m. For this study, the morning peak was investigated, as evening peaks largely occur from residential customer demands.

The objective function that incorporates a demand penalty between 6 a.m. and 9 a.m. is shown in (4.8).

$$J_{PH} = \left(\sum_{i=1}^{N} P_i \Delta t\right) \cdot (\mathrm{Cost}_{Energy}) + 0.5 \cdot \max(\mathbf{P})_{\mathrm{PeakHours}} \cdot (\mathrm{Cost}_{Demand}) + 0.5 \cdot \max(\mathbf{P}) \cdot (\mathrm{Cost}_{Demand}) \tag{4.8}$$

An objective function such as the one proposed in Equation (4.8) should be applied with some caution, as it might result in shifting the peak to a different time.

Where PH is the prediction horizon (24, 36, 48 hours etc.), N is the number of time steps over the prediction horizon, P_i is the power demand at time i and Δt is the simulation time step. The setpoint is constrained by a lower and upper bound to ensure comfort for the occupants. An optimized setpoint schedule is identified at 1-hour intervals, from prediction control simulations at 5-minute intervals. This optimization is repeated at periodic intervals (e.g., 6 hr).

4.2.4.5 Real-time optimizing algorithm

The MATLAB function *fmincon* finds the minimum of a constrained nonlinear multivariable function. The optimization algorithm identifies a setpoint schedule at hourly intervals. These identified values are then fed to the simulation model ("real building") and linearly interpolated to a time interval of 15 seconds (the time step used in Simulink).

4.2.4.6 Prediction and control horizons

Periodically, the control problem is solved optimally by incorporating knowledge of expected weather over the "prediction horizon". Then, by solving an optimization algorithm based on the data corresponding to the prediction horizon, the MPC strategy determines an optimal sequence of control moves. These moves are applied to a "control horizon", which is often shorter than the prediction horizon. The simulation proceeds by applying the calculated "moves" over the duration of the control horizon. Next, the optimization routine is executed again for the following prediction horizon. This sequence is repeated until the end of the simulation time (e.g., one day, one year, etc.).

It was assumed that operation of the building during the months from May through September is always the same as the original operation. In other words, the MPC set up for this study was only applied to the winter operation (because of the rate M structure, this also affects the summer energy bill). The topic of enhanced operation during the summer will be studied in future work.

4.2.5 Results and discussion

A parametric analysis has been performed on combinations of the control horizons (update frequency) and prediction horizons. First, different combinations were evaluated with the first cost function in Equation (4.7) under temperature constraints. These scenarios are shown in Table 4.6. Next, the same combinations were evaluated with the cost function in Equation (4.8), shown in Table 4.7.

The yearly utility bill and peak power reduction (in percentage) are outlined in both above tables. In general, all MPC scenarios result in similar significant reductions in both utility bills and peak power demand. For example, it is seen that scenario 2 with a control horizon of 12 hours and a prediction horizon of 24 hours results in a cost savings of 25% and a peak power reduction of 38%, by implementing a new optimized temperature schedule every 12 hours. The cost per square meter would change from \$30.19/m^2 to \$22.57/m^2, or a yearly savings of \$7.62/m^2.

Figure 4.26 shows a comparison between typical operation and MPC scenario 2 of the heating load for four winter days. The weather details of these four days are shown previously in the System Disturbances section.

Figure 4.26 shows the optimized setpoint of scenario 2. The main difference between the typical temperature setpoint schedule and the optimized setpoint schedule is a preheating of the building in the hours prior to the start of occupation and a slightly reduced temperature during occupied times.

Table 4.6: MPC results for varying update frequencies and prediction horizons

Scenario #	**Control Horizon (hr)**	**Prediction Horizon (hr)**	**Yearly Utility Bill ($)**	**Peak Reduction (%)**
REF	**N/A**	**N/A**	**$12,889**	**N/A**
1	6	24	$9,709	36%
2	12	24	$9,647	38%
3	24	24	$9,684	38%
4	6	36	$9,828	35%
5	12	36	$9,695	36%
6	24	36	$9,722	36%
7	36	36	$9,648	37%
8	6	48	$9,783	36%
9	12	48	$9,646	36%
10	24	48	$9,637	36%
11	36	48	$9,649	37%
12	48	48	$9,659	37%

Table 4.7: MPC results for varying update frequencies and prediction horizons (add penalty during peak hours)

Scenario #	**Control Horizon (hr)**	**Prediction Horizon (hr)**	**Yearly Utility Bill ($)**	**Peak Reduction (%)**
REF	**N/A**	**N/A**	**$12,889**	**N/A**
13	6	24	$10,019	36%
14	12	24	$9,825	37%
15	24	24	$9,773	37%
16	6	36	$10,058	36%
17	12	36	$9,916	35%
18	24	36	$10,048	30%
19	36	36	$9,779	35%
20	6	48	$10,037	36%
21	12	48	$10,048	35%
22	24	48	$10,148	30%
23	36	48	$9,789	36%
24	48	48	$9,738	36%

4.2.5.1 Effects of MPC on the monthly utility bill

Shown in Figure 4.26 for MPC scenario 2 is a significant peak reduction during every winter month, and the effect of this on the yearly utility bill is shown in Figure 4.27. By reducing the 12-month winter peak (from 54.5 kW to 33.9 kW), not only are the winter months utility bills reduced, a reduction in the summer month utility bills is also observed (Figure 4.28). Even though the peak demands in the summer months have not been reduced, the summer month bills

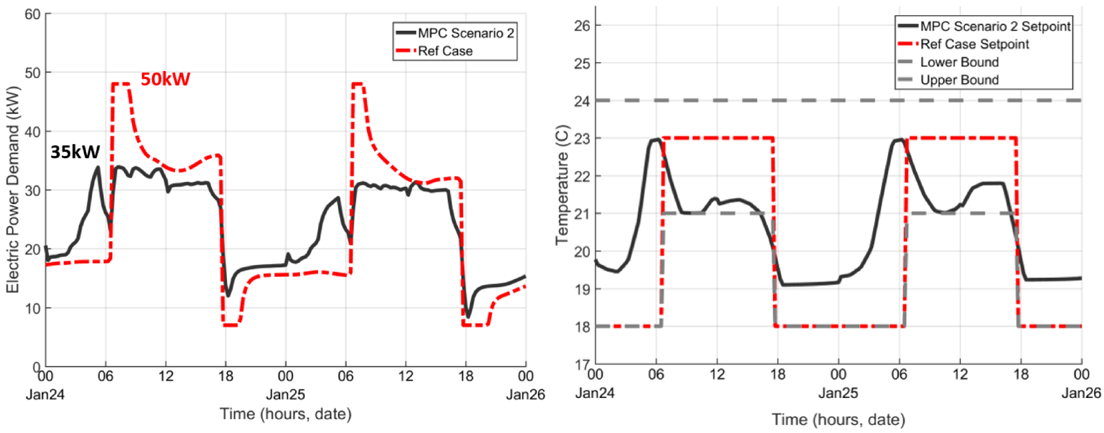

Figure 4.26: Model predictive setpoint optimization

depend on the maximum peak over the previous 12-month period. It is also evident that overall building energy consumption for the 12-month period is slightly decreased (Figure 4.29). By implementing MPC during the winter months, the overall utility bill for the year can be reduced by 25%; the results of each month are shown in Figure 4.27 in Canadian dollars.

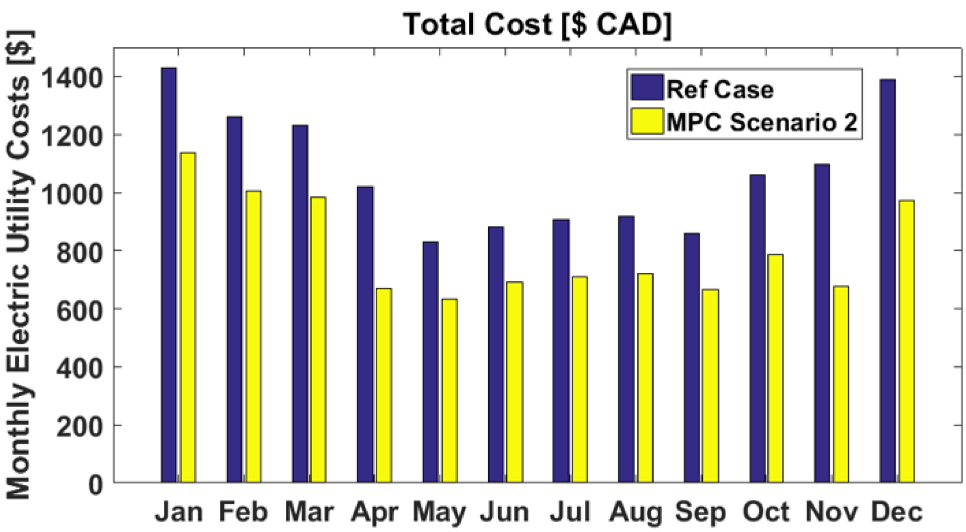

Figure 4.27: Monthly utility bill for MPC scenario 2 (control horizon = 12h, prediction horizon = 24h)

4.2.5.2 Effects of MPC on the yearly utility bill

From the implementation of MPC with the two introduced cost functions, the most significant improvement is the reduction in the peak demand, while only slight improvements to energy consumption are found. The main difference between the typical temperature setpoint schedule and the optimized setpoint schedule is a preheating of the building in the hours prior to the start

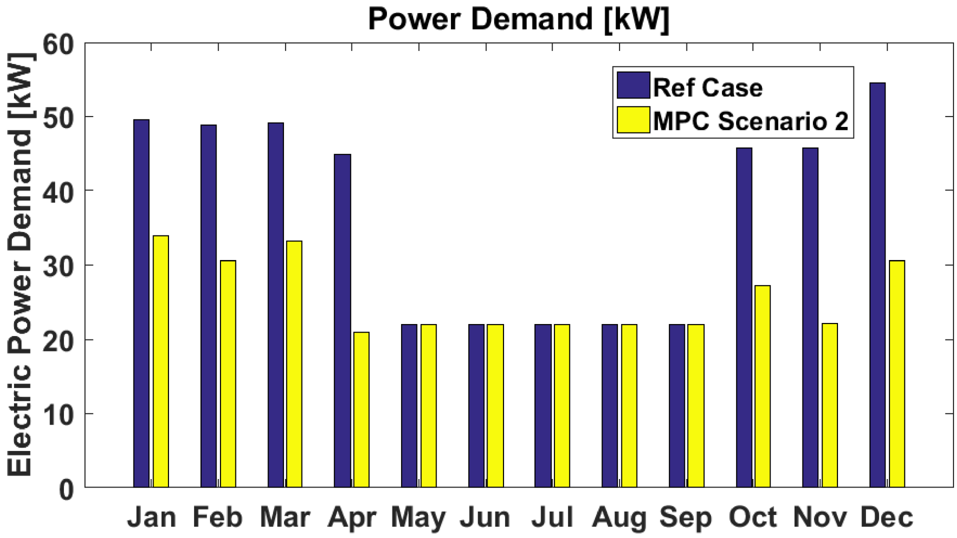

Figure 4.28: Monthly peak demand for MPC scenario 2 (control horizon = 12h, prediction horizon = 24h)

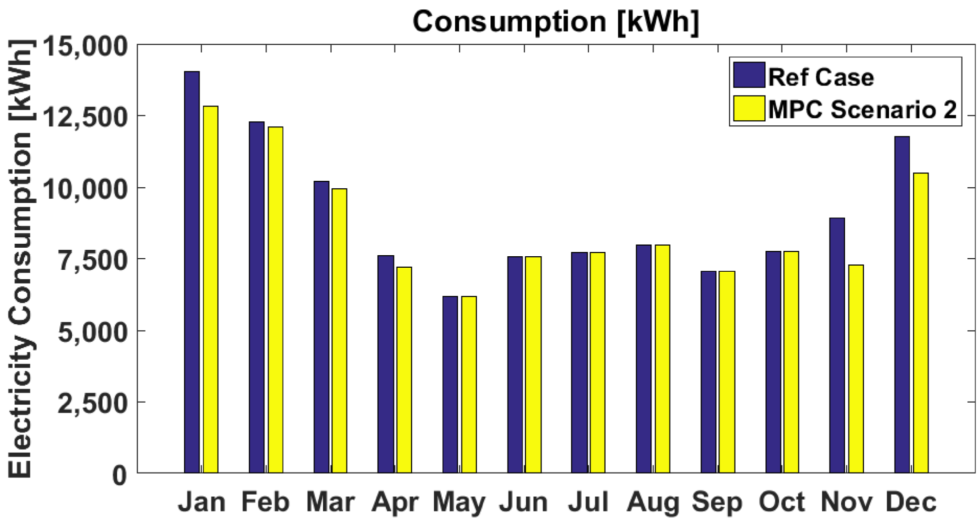

Figure 4.29: Monthly consumption for MPC scenario 2 (control horizon = 12h, prediction horizon = 24h)

of occupation. By leveraging the thermal storage capacity of the building structural materials, preheating allows to smooth out the peak heating in the morning when the building is transitioning from the unoccupied to occupied time of the day. It is also evident that this incorporation of preheating the building for a few hours, with an optimized temperature schedule, does not increase the overall building's energy consumption.

Though in theory, a more frequent control update should produce improved results, it seems that a control horizon of six hours is not the most optimal length, and a longer control horizon should be used. Update frequencies of 12 hours or more show good results for both cost savings over the year and reduction of the peak demand. There are several possible reasons for these results, such as discrepancies between the simulated forecast and the real weather. Another cause could be due to the control model ”initializing” more often when a shorter control horizon is used, resulting in an increase of model warm-up periods (“stabilization”) which occur at the beginning of each prediction horizon.

In addition, it is seen that by incorporating increased future information with longer prediction horizons, there are diminishing improvements. The longer prediction horizons (48-hr vs. 24-hr) may have more significant results in a building with a large thermal mass within the building materials than the building used for this study.

Realistically, a prediction horizon longer than a few days could not be employed due to the limitations of the accuracy of the weather forecast over longer periods of time. A multi-zone control model will be used in a future study to obtain more accuracy and control options.

The reader should keep in mind that the building used in this study is rather small and is a very standard and basic construction. There are no special features, systems, or storage technology, but by simply implementing an optimized setpoint schedule based on weather forecast over a day or two, occupancy schedules and comfort constraints, significant savings and peak power reductions can be achieved. These results could be even more notable in a building ten times larger (e.g., 50,000 ft^2) and could result in tens of thousands of dollars of savings in electric utility charges per year.

If MPC is widely adopted in the building operation sector, several advantages can be envisioned. Firstly, as seen from this study, the utility bill of the customer can be reduced by up to 25%. The occupants of the building can obtain improved comfort, and the stability of the electric grid is improved as large heavy loads are now smoothed out over time. For the utility provider, another advantage is the overall energy consumption of the customer is not necessarily lower, while peaking times can be reduced. This allows the utility provider to consider increasing its customer base by inviting customers from out of province, as the surplus of supply will be available any time of the year. Currently, peaking power days where the demand is greater than supply only occur a few times per year in the winter in Québec.

If this trend continues and peaking days were to increase due to things such as population increase or infrastructure growth, the province may need to buy electricity from out-of-province utility companies (which would likely come from non-renewable sources) or Hydro-Québec may need to invest in infrastructure to increase the grid capacity, such as new hydroelectric dams.

4.2.6 Conclusion: small commercial building MPC study

This study presented an example of implementing MPC in a conventional building (a building of basic construction, systems, and technologies) to reduce the yearly utility bill and avoid the summer peak load penalty given to the customer. Through the software program Simulink, two cost functions were studied with different control and prediction horizons.

The cost function aimed to minimize the utility rate during each prediction horizon while meeting upper and lower indoor temperature constraints. Through a parametric study, it was seen that longer control horizons (greater than six hours), produced better results for this building. A cost savings of 25% on the yearly electric utility bill and a peak power reduction of 38% were achieved, simply by implementing a new optimized temperature schedule for the building every 12 hours. The cost per square meter would change from \$30.19/m^2 to \$22.57/m^2, or a yearly savings of \$7.62/m^2.

The main difference between the typical operation temperature schedule and the optimized setpoint schedule is a preheating of the building the few hours prior to the start of occupation. The development of self-learning control models for both building response and optimization represents an area of research that has yet to be fully explored in relation to buildings. Learning techniques should help overcome system challenges such as building-use hours, or a change in HVAC equipment that alters the building response. Further research should focus on evidence that directly compares the performance of specific optimization algorithms, parameters (timestep, horizon), and climate forecast accuracy for the same scenario. It is suggested that the sensitivity analysis of timestep and horizon, and climate forecast accuracy be further explored to understand the effects they have on performance. This will enable better methods to minimize and deal with these uncertainties in using MPC for building control. The topic of enhanced operation during the summer months will also be studied in future work.

As there is no standard software available to test and develop control strategies in buildings (Candanedo et al., 2013), Simulink, or a similar tool with a graphical interface, may be an option for this problem. In theory, once a flexible and robust structure has been established for the connections between the weather forecast, the control model and the building simulation, Simulink could be used to rapidly test MPC in different buildings (via simulation) by easily swapping out control models and building models within the Simulink file. However, much work is still needed to improve the user-friendliness and flexibility of this approach. For example, considerable care is needed in keeping track of the time scales of the various data. The weather data, control model time step, identified schedule time step, and building simulation time step may all be different and thus proper time synchronization is crucial for obtaining reliable MPC simulation results.

4.3 Conclusion

In this chapter, two control-oriented building modelling applications through simulation studies were presented. The first study investigated a multi-level control-oriented modelling approach for a detached residential house (Date et al., 2016b) while the second study pertains to MPC model development of a smaller commercial retail building (Date et al., 2017). The study on the detached house presented the development of a multi-level approach to the problem of modelling different thermal zones in a house for control applications. The core feature of the proposed methodology allows the user to switch back and forth between models representing different control levels according to the modelling objectives. The goal of the second study was to determine if the implementation of MPC is useful for lowering electricity bills in commercial buildings under the typical rates applied in Québec. For an electrically heated building, it was investigated if it is possible to reduce the annual energy bills associated with the combined effect of energy price, demand charges, and a minimum monthly billing charge based on the winter peak. Work remains to be done on how to improve the guidelines for the initial guess of the grey-box model parameters. There is also no standard software available to test and develop control strategies in buildings, which presents an area of further research and development (Blum et al., 2019).

Chapter 5

Development of a Control-Oriented Model of an Active Thermal Energy Storage Device

5.1 Introduction

One of the major challenges associated with buildings and integration of intermittent distributed renewable energy sources is that the peak consumption periods seldom coincide with the availability of power generation from these renewable sources. This supply-demand mismatch has been illustrated by the concept of the “duck curve” (Denholm et al., 2015): peak consumption periods (morning and evening) do not coincide with the period of maximum solar generation in the middle of the day. Furthermore, the price and the available power supplied by the electric grid are often significantly variable. Building load flexibility – which may be enhanced by the incorporation of energy storage devices (Jensen et al., 2017, Reynders et al., 2018) – coupled with advanced control strategies is a key factor to optimize energy consumption to match the availability of renewable energy. The implementation of advanced control strategies is essential for the optimization of energy consumption while preserving occupant comfort.

Effective control strategies should be able to manage the various systems of a building, including thermal and/or electrical storage devices, and should take advantage of the thermal inertia of the building structure (Junker et al., 2018, Liu & Heiselberg, 2019, Reynders et al., 2018, 2017). The operation of a building is directly affected by the fluctuations in weather and occupancy, which result in large load fluctuations between day and nighttime (which in turn yield large fluctuations in the electricity demand). To deal with these fluctuations, a good understanding of the dynamic behaviour of buildings and a focus on energy management (rather than simply indoor temperature control), is necessary.

The study in this chapter focuses on the development of a control-oriented thermal model for an electrically heated thermal Energy Storage Device (ETS)[1]. This model is intended to be used within an advanced control strategy methodology for energy and load management in typical Canadian commercial and institutional buildings during the heating season. While most research efforts have often focused on improvements to the building envelope and energy efficient HVAC systems, advanced control strategies have a largely unexploited potential for saving energy, improve load regulation and optimize thermal comfort. The control-oriented model presented here is intended to facilitate the development and deployment of predictive control strategies for an ETS. This study focuses on an air-based electrically-heated high temperature thermal storage device.

5.2 Description of thermal energy storage device

ETS systems convert electrical power to heat that is stored during low electricity price periods (or when demand on the grid is low) and can deliver heat to the building during peak demand periods that may have higher electricity prices (Moffet et al., 2012). Total energy consumption is not reduced when this device is deployed, however, it can provide a significant reduction of the electricity bill when there exists a demand charge in the utility pricing structure (Bedouani et al., 2001, Syed, 2011) or operate strategically when dynamic tariffs exist. With a well-designed mix of on-peak and off-peak electric heating, the load can be levelled, and the addition of new generating capacity can be delayed (Cooke et al., 1980). ETS systems use bricks as a medium to store heat from electricity when the electric grid may benefit from a higher consumption (for example during off-peak periods) and release heat from the bricks to the building when the electricity supplies are expensive, such as during peak demand periods.

[1]This work is based on a published refereed conference paper and a peer-reviewed journal article: (a) Date, J. A., Candanedo, J. A., Athienitis, A. K., & Lavigne, K. (2018). Control-oriented modeling of an air-based electric thermal energy storage device. In Proceedings of ASHRAE Winter Conference 2018 Chicago, Illinois and (b) Date, J. A., Candanedo, J. A., Athienitis, A. K., & Lavigne, K. (2020a). Development of reduced order thermal dynamic models for building load flexibility of an electrically-heated high temperature thermal storage device. Science and Technology for the Built Environment.

Thermal energy storage devices suitable for buildings can be categorized into either low-temperature, or high-temperature storage schemes. For low-temperature energy storage (less than 100 °C), water and solutions of water and sodium sulphate have been used. For high-temperature schemes, magnesite bricks have mainly been used, where the brick temperature can safely reach up to 871 °C. A focus on forced-air electric heat storage with bricks as the storage is seen in this thesis, as this storage device is found in different areas in Canada (Québec, Yukon, Prince Edward Island), and the developed model can be modified in the future for the water-based device that contains the same brick storage mechanism with an additional air to water heat exchanger.

The storage device comprises an insulated heat storage tank containing 3,121 kg of magnesite bricks, where electric wire heating elements are placed between rows of bricks. The device is rated for a maximum brick temperature setpoint of 871 °C, however, at the time the data was extracted from the BAS, the maximum brick temperature setpoint was set at 750 °C. The device is rated for a storage capacity of 640 kWh. Air is driven through the ETS device by a controllable fan and extracts heat from the bricks. The air can either pass through the bricks or bypass the device and get delivered to the conditioned zone. Figure 5.1 shows schematics of the device, while specific device specifications are shown in Table 5.1.

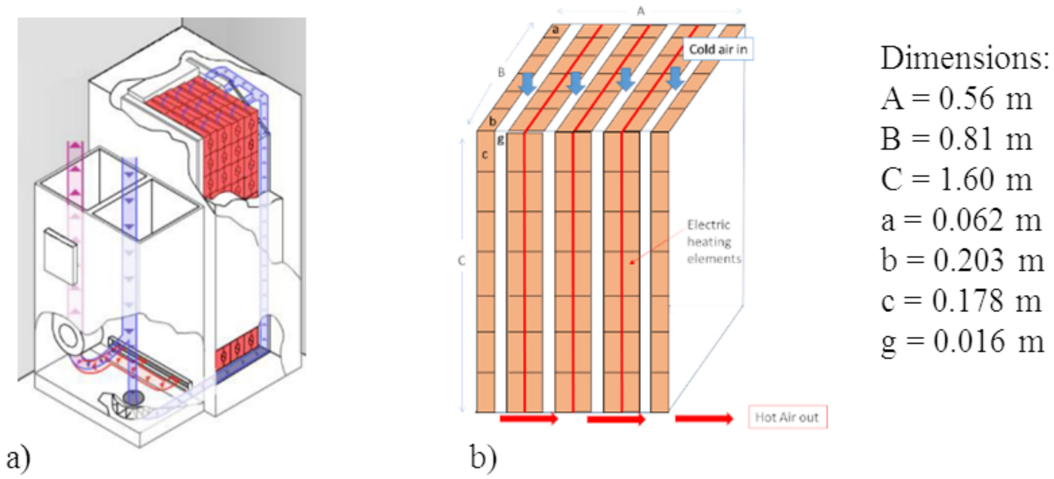

Figure 5.1: Thermal electric storage device, *reprinted with permission from Karine Lavigne* (Lavigne, 2006)

The control of the ETS device requires more detail than those for typical heating systems. The following considerations are needed for adequate control of the ETS: 1) control during the time when the storage medium is being heated/charged, 2) determination and control of the

Table 5.1: Electric Thermal Storage (ETS) device specifications

Electric Thermal Storage (ETS) device specifications	
Parameter	Value
Charging Input	106 kW
Storage Capacity	640 kWh
Storage Material	High-density ceramic brick
Number of Heating Elements	24
Maximum Brick Temperature	750 °C
Weight of Bricks	3,121 kg

maximum allowable brick temperature during brick charging, and 3) control of the total heat to be stored in the storage medium. During the thermal storage discharge cycle (releasing heat from the bricks to the air in the HVAC duct), proper control to maintain consistent outlet air temperature under possible large fluctuations in the brick temperature.

A key goal is to match the amount of stored thermal energy to the predicted energy use requirements during the following discharge cycle. The control strategy should estimate the heat requirements of the building or conditioned zone for the following day and determine how much heat energy to charge and store in the device and at what temperature. Another goal is to reduce the utility cost incurred by the building owner.

The current control of the air-based ETS looks at the outdoor ambient temperature and available power of the building. The outdoor air temperature at a given time the night before is used to set the maximum brick storage temperature, while the maximum allowed delivered power to the ETS for heating the bricks is determined by the available power (which is the difference between the maximum "allowed" power demand of the building minus the actual power demand). The maximum allowed power demand is specified by the building operators, as a measure to reduce electricity bills that are incurred from peak building loads.

The outdoor temperature can fluctuate significantly between nighttime and daytime, especially during shoulder seasons. These devices are often equipped with owner-selectable set point control that facilitates the adjustment of the storage capacity (Cooke et al., 1980). Thermocouples are embedded in the thermal storage material and are used for controlling heat input. During the discharge cycle, air heated from the bricks is mixed with ambient air in a controllable manner.

5.3 Methodology

5.3.1 Adjustable model order

The proposed control-oriented models of the ETS described below are based on two-dimensional lumped parameter equations for heat conduction and energy conservation. These models use a grey-box modelling approach, in which physically meaningful parameters are calibrated with measurement data.

The developed MATLAB code was written to easily modify the order of the model: adjustment of the two-dimensional grid of brick thermal capacitance nodes can be done quickly and easily by defining the number of brick node rows and columns. Multiplying the number of rows by columns gives the resulting number of brick capacitance nodes for the model.

An example of the 1-capacitance model is shown in Figure 5.2. The thermal network is made of one row of resistances and nodes along the x-axis of the bricks, one column along the y-axis and a convective conductance to the room air node. This thermal network structure of rows and columns allows for rapid modification of model order by the user without having to re-write or add any equations to the simulation. When the user specifies a model with 2 rows and 2 columns, the result is a 4-capacitance thermal network model for the device, which is depicted in Figure 5.3. Higher row and column amount and configurations can be readily evaluated. Each brick node has an associated capacitance term, C_{bricks}, electric power input, Q_{source} and convective heat extraction via air channels, Q_{conv}.

Figure 5.4 shows the side view schematic of the bricks in the ETS. The heat transfer from bricks to the airflow of the ETS system was modelled using the general equation for heat exchange through a channel (Lienhard Iv & Lienhard V, 1986).

5.3.2 Measured data used for model development and analysis

Measured data from an air-based ETS device installed in a building located in Sherbrooke, Canada are used for model development and analysis. This two-storey building, built in 1989, has a total floor area of roughly 9,000 m^2. Measurements at 15-min intervals have been collected

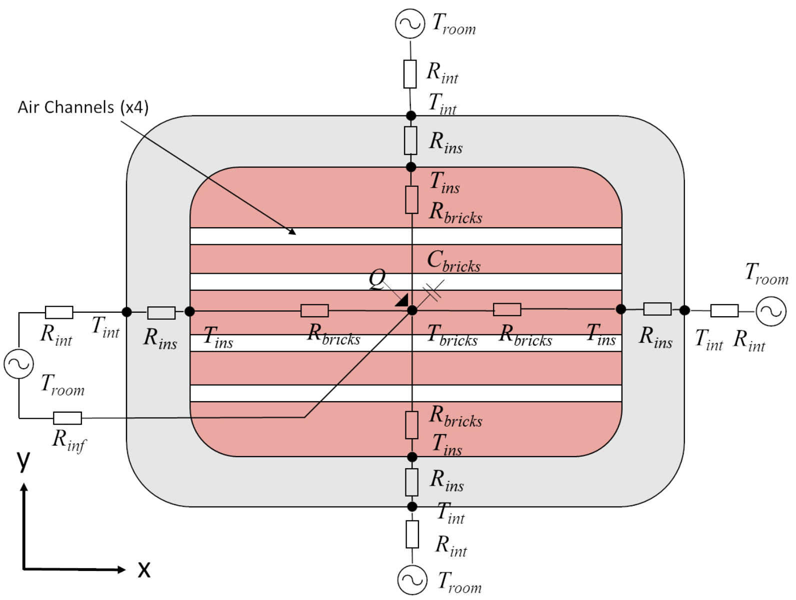

Figure 5.2: Top view example of brick charging thermal network (2-dimensional heat transfer)

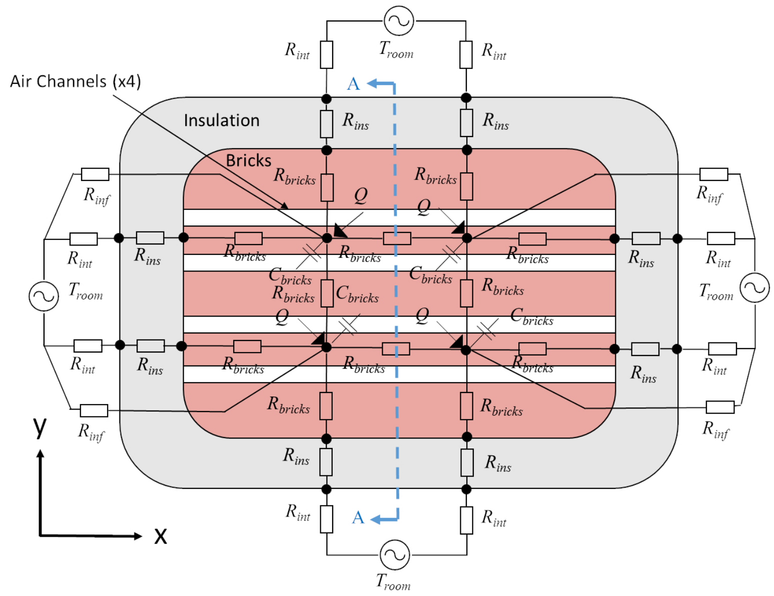

Figure 5.3: Top view example of brick charging thermal network (2-dimensional heat transfer)

at this building since 2014. The building, located in Sherbrooke (QC), Canada, had a peak demand in February 2015 of 600 kW, with a consumption of 166 MWh for that month. The on-site ETS has a heating load capacity of 106 kW and can supply hot air to a warehouse zone within the building.

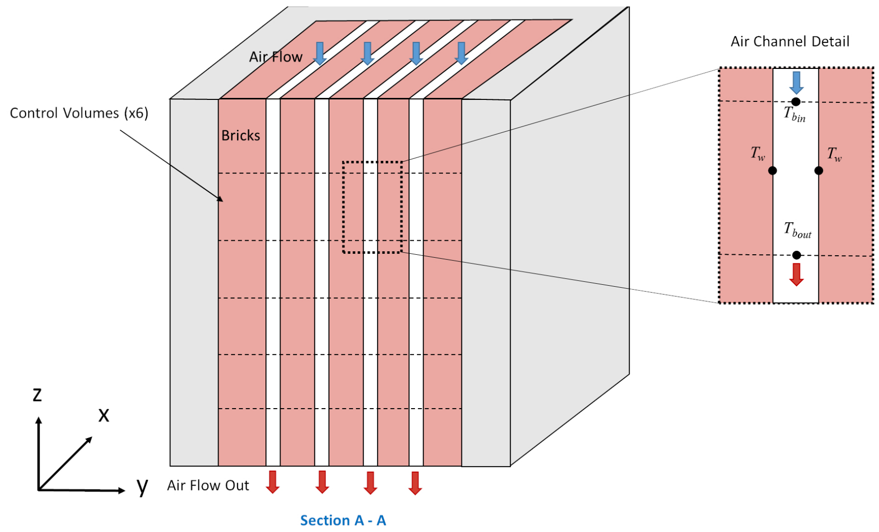

Figure 5.4: Side view example of brick charging thermal network (2-dimensional heat transfer)

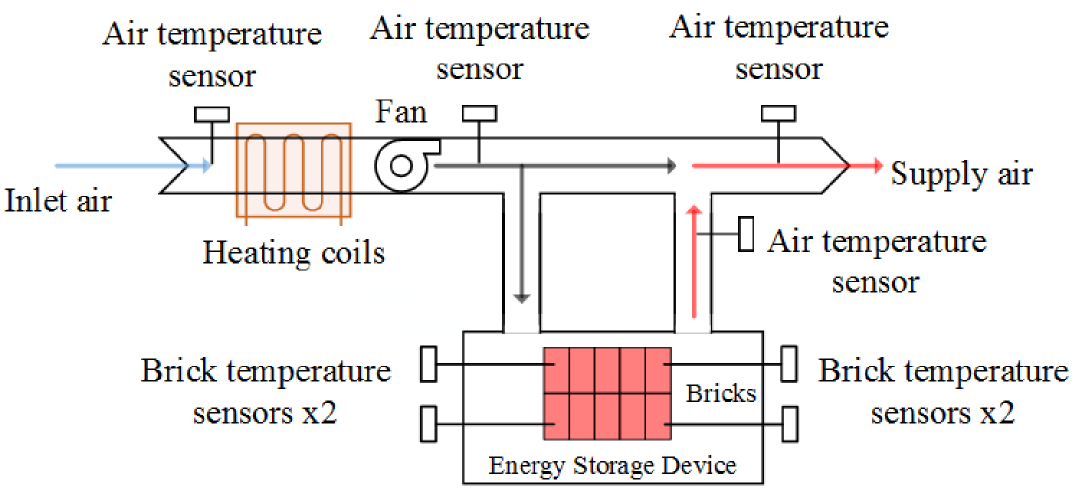

Figure 5.5: HVAC system with ETS and temperature sensor locations

The warehouse zone is conditioned by the air-based system shown in Figure 5.5. Air temperatures are measured throughout the HVAC system and brick temperatures are measured in four locations. When the ETS is in use, part of the air supply is drawn through the device to provide additional heat energy to the zone. The control variable options of the system are depicted in Figure 5.6.

The control variables are:

- the electric power to the ETS, $P_{elec,ETS}$ which provides heat to the bricks;

- the fan operation mode, Fan_{ETS}, indicates whether the fan driving the air through bricks is on/off;
- Q_{coil}, the heat delivered to the inlet air in the duct;
- Q_{aux} which is additional auxiliary heating in the zone.

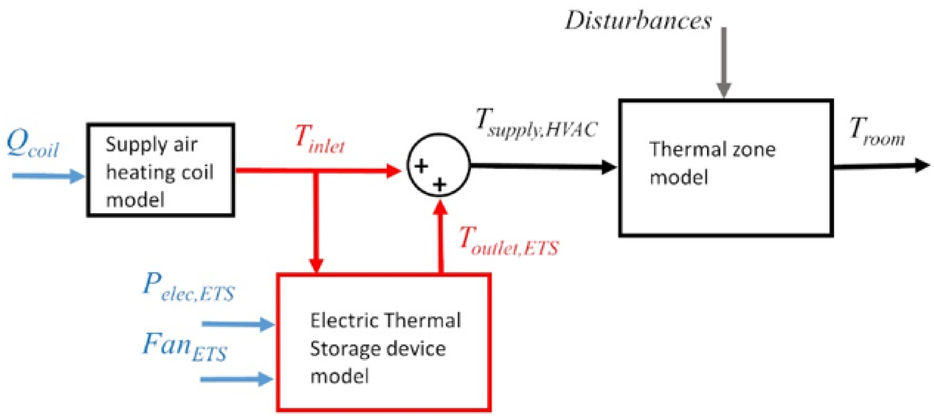

Figure 5.6: System control variables

T_{inlet} is the temperature of the air entering the ETS and bypassing the ETS; $T_{outlet,ETS}$ is the outlet air temperature of the ETS; and $T_{supply,HVAC}$ is the supply air temperature to the zone. T_{room} is the internal air temperature of the zone. Disturbances include outdoor air temperature and solar radiation.

5.3.3 Development of thermal models

Heat transfer in bricks: To charge the ETS device, electricity is passed through the wires embedded in the bricks. The wires heat up the bricks, thus transferring thermal energy to the bricks. The thermal modelling approach used is the common lumped parameter finite difference method. This approach is based on a space discretization of the material into control volumes. A node is located at the centroid of the control volume. The heat flux between adjacent nodes is described by using resistance analogies: the flux is calculated as proportional to the difference between the temperatures of the two nodes. Between control volumes, the conductance is calculated as kA/L, where k is the thermal conductivity of the material, A the area of the surface of contact and L is the distance between adjacent nodes. If the node has considerable thermal mass, it may be assigned a thermal capacitance, which represents the heat storage capacity of the control volume. By performing a heat balance on the control volume, the differential equation of a node can then be written as (Athienitis & Santamouris, 2002):

$$C_i \frac{dT_i}{dt} = Q_i + \sum_{j=1}^{n} \frac{(T_j - T_i)}{R_{i,j}} \tag{5.1}$$

Where Q_i represents the heat generated at a node i or received directly by it from source(s), $R_{i,j}$ represents the thermal resistance between nodes i and j (either conductive or convective terms), T is the temperature at node i or adjacent node j, and C is the thermal capacitance at node i ($C = \rho c_p A dx$). n is the total number of adjacent nodes to node i.

The strategy commonly implemented to determine the transient solution is the application of time discretization (Athienitis & Santamouris, 2002). A fully explicit finite difference approach was used to solve the energy balance equations at each node in the models. The fully explicit approach assumes that the current temperature of a given node depends only on its temperature and the temperature of the surrounding nodes at a previous time step. The term with the time derivative can then be discretized as follows:

$$C_i \frac{dT_i}{dt} \approx C_i \frac{\Delta T_i}{\Delta t} = C_i \frac{T_i^{p+1} - T_i^p}{\Delta t} \tag{5.2}$$

By solving for the temperature at the next time step $p+1$, the general equations (5.3) and (5.4) are derived for control volumes with and without capacitance terms, respectively.

$$T_i^{p+1} = T_i^p + \frac{\Delta t}{C_i} \left[Q_i^p + \sum_{j=1}^{n} \frac{T_j^p - T_i^p}{R_{i,j}} \right] \tag{5.3}$$

$$T_i^{p+1} = \frac{Q_i^p + \sum_{j=1}^{n} \frac{T_j^p}{R_{i,j}}}{\sum_{j=1}^{n} \frac{1}{R_{i,j}}} \tag{5.4}$$

Due to high brick temperatures of 750 °C, non-negligible heat losses from the ETS device to the air of the mechanical room occur. There are both convective and radiative losses from the ETS to the room which are calculated at each time step using simplified convective and radiative heat transfer coefficient Equations (5.5) (ASHRAE: American Society of Heating Refrigerating and Air-Conditioning Engineers, 2009), and (5.6), where $T_{surface}$ is the mean value of the surfaces of the walls in the mechanical room ($T_{surface}$ is assumed to be the same temperature as room air temperature).

$$h_{conv} = 1.26 \cdot |T_{int} - T_{room}|^{1/3} \tag{5.5}$$

$$h_{rad} = \varepsilon\sigma \cdot \left(T_{int}^2 + T_{surface}^2\right) \cdot \left(T_{int} + T_{surface}\right) \tag{5.6}$$

Thermal energy storage device heat transfer from bricks to airflow: The heat transfer from bricks to the airflow of the ETS system was modelled using the general equation for heat exchange through a channel (Lienhard Iv & Lienhard V, 1986) as shown here:

$$\frac{T_{b_{out}} - T_{b_{in}}}{T_w - T_{b_{in}}} = 1 - exp\left(-\frac{hPL}{\dot{m}c_p}\right) \tag{5.7}$$

T_w (temperature of the wall surface of the channel) is taken as the average brick temperature T_brick. h is the convective heat transfer coefficient between channel surface and air in the channel, P is the perimeter of the channel and L is the length of the channel. The above equation can give the variation of air bulk temperature ($T_{b_{out}}$ and $T_{b_{in}}$) along the channel as a function of the distance from the inlet (x) if $T_{b_{out}}$ is replaced by $T_{b(x)}$, L is replaced by $Z(i)$, and h is adjusted accordingly. Control volume temperatures are calculated as follows:

$$T_{b_{out}}(p,i) = T_w(p) + [T_{b_{in}}(p,i) - T_w(p)] \cdot e^{\frac{-2 \cdot Z(i)}{a(p)}} \tag{5.8}$$

where $a(p) = \frac{M(p)c_p\rho}{W\bar{h}(p)}$ and $h = \frac{Nu \cdot k}{DH}$

Nu is the Nusselt number, k if the conductivity of the air and DH is the hydraulic diameter of the air channel. h may be calibrated as not all needed information may be available. The energy extracted from the bricks in the air channels (which is subtracted from the brick node energy balance equation) is calculated as follows:

$$Q_{conv}^{p} = 4 \cdot M(p) c_p \rho \left[T_{b_{out}}(p,L) - T_{b_{in}}(p,0) \right] \tag{5.9}$$

The airstream model for this application has 6 sections lengthwise along the air channel. Uniform temperatures are assumed at the brick surfaces within each section. A section detail of a typical control volume is shown in Figure 5.4. The exit temperature of each channel section, $T_{b_{out}}(p,i)$, is used as the inlet temperature of the next section, $T_{b_{in}}(p,i+1)$. It was found that a model with at least six sections was necessary to follow the measured data and produce accurate outlet air temperature results.

For example, in the case of Figure 5.2 (1-capacitance model) the following Equation (5.10) calculates the temperature at the next time step of the brick node:

$$T_{bricks}^{p+1} = T_{bricks}^{p} + \frac{\Delta t}{C_{bricks}} \left[Q_{source}^{p} - Q_{conv}^{p} + 4 \cdot \frac{1}{R_{bricks}} \left(T_{ins}^{p} - T_{bricks}^{p} \right) + \frac{1}{R_{inf}} \left(T_{room}^{p} - T_{bricks}^{p} \right) \right] \tag{5.10}$$

For the case of the 1-capacitance brick model shown in Figure 5.2, T_{bricks} represents the temperature of the entirety of the bricks in the device, C_{bricks} is the total thermal capacitance of the bricks, Q_{source} is the electrical power input via the electric wires embedded in the bricks, Q_{conv} is the heat extracted to the air from the bricks in the air channel, R_{bricks} is the resistance of the bricks (divided into 4 components), T_{ins} is the surface temperature of the insulation layer, R_{inf} is the infiltration losses to the mechanical room and T_{room} is the air temperature of the mechanical room.

Model reset: The main purpose of these control-oriented models is the quick and easy simulation of the ETS device in order to estimate load management strategies. These models suitable for control are intended to be used, along with information of future conditions (such as electricity pricing, occupancy, weather forecasts etc.), to plan future operation strategies within the BAS to improve electrical loads and associated peaks and to provide building energy flexibility for improved building-grid interaction. Continuous comparison of the model with actual results is expected. Thus, the concept of "model reset" was also developed as part of the overall methodology. These models are suitable for use in short-term control strategies (1-2 days) and optimization (hours) within the BAS, thus one can assume that the model can "reset" itself by periodically looking at the real measured values (of brick temperature, outlet air temperature etc.) and update or "calibrate" important model parameters. A depiction of the reset interval concept is shown in Figure 5.7. At the desired reset interval, the model checks the current state of sensors and re-initializes the brick temperature model parameter value.

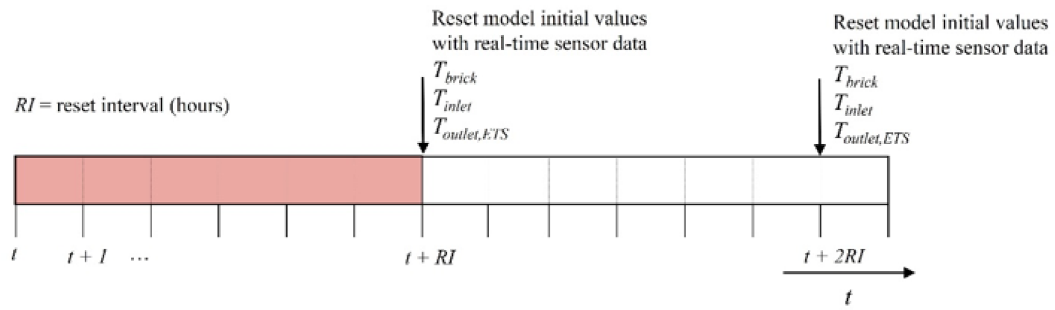

Figure 5.7: Depiction of reset interval. At the chosen reset interval, the model checks the current state of sensors and re-initializes the parameter values with measured data

A performance comparison is done between a model running for an extended period versus the same model with model reset at 6-hour intervals. A 6-hour model reset interval was chosen is because that is usually the frequency with which the available weather forecasts are updated and released by the national weather service (Canadian Meteorological Service (Environment Canada), 2019). While shorter reset intervals provide a closer match between model outputs and measurements, the reset intervals investigated (3 h, 6 h, 24 h) are meant to reflect the prediction horizons that are realistically useful for automated model predictive control.

5.4 Modelling results and discussion

This section presents simulation results. First, the prediction performance of two low-resolution models and one high-resolution model is assessed in terms of (a) heat transfer to bricks and (b) heat transfer from bricks to airflow. Next, varying model reset intervals, from 3 to 24 hours are studied. Finally, the concept of "effective" brick conductivity for model prediction improvement was examined.

5.4.1 Modelling results: heat transfer in bricks

Different orders of thermal model resolutions of the ETS system are studied. The model order of highest resolution model 140 (14 rows and 10 columns). This 140-capacitance node model is compared to measured data from the BAS and two low-resolution models suitable for control. The first low-resolution model consists of four brick capacitances (2 rows and 2 columns); while the second low-resolution model consists of one single capacitance (1 row and 1 column). The time step used in the simulation is far below the critical time step of the models (5 hours for the 140 resistance-capacitance model).

The results of three days of charging are shown in Figure 5.8: The model output of average brick temperatures predicted by the models is compared to the measured data obtained from the BAS. The fan operation (which is at 0% operation during the charging data period) and the power input to the bricks are also taken from measured data from the BAS. While Figure 5.8 shows results for the model running continuously without using feedback to adjust the model predictions, Figure 5.9 incorporates a "reset" of the models at 6-hour intervals. In other words, every 6 hours the model "checks" the real measured brick temperature value and re-initializes the brick temperature in the model at that point in time.

The performance of the models was evaluated in terms of several statistical indices (Table 5.2), such as the root-mean-square error (RMSE) and the mean absolute error (MAE). Also, the infinity norm (i.e., the biggest difference between the model results and measured data) of the absolute error between modelled brick temperature and measured brick temperature is presented.

Table 5.2: Heat transfer in bricks modeling – statistical indices (January 6 to 8. 2017)

Model	**Bricks RMSE [°C (°F)]**	**Bricks MAE [°C (°F)]**	**Bricks $\|\| \bar{T}_{model} - \bar{T}_{measured} \|\|_\infty$ [°C (°F)]**
1-Capacitance	95 (203)	91 (196)	120 (248)
4-Capacitance	85 (185)	81 (178)	108 (226)
140-Capacitance	34 (93)	31 (88)	65 (149)
With Model Reset every 6 Hours			
1-Capacitance	18 (64)	12 (54)	60 (140)
4-Capacitance	17 (63)	11 (52)	57 (135)
140 Capacitance	15 (59)	11 (52)	53 (127)

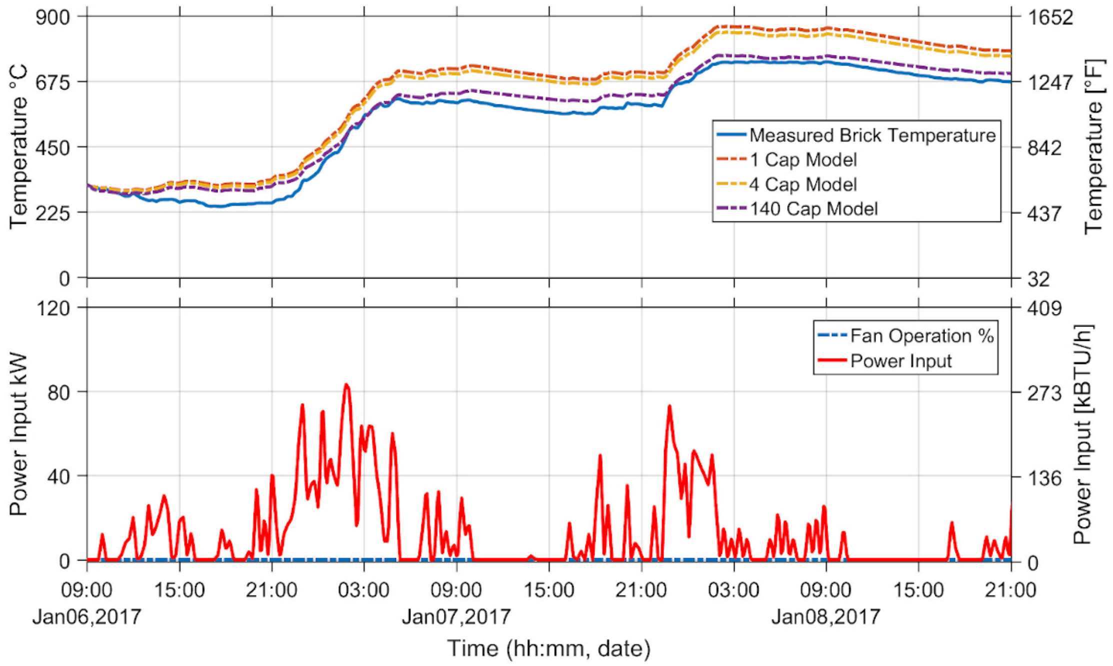

Figure 5.8: Three days of heat transfer in bricks modelling results. Results are shown for 3 models: a 1 brick capacitance model, a 4 brick capacitances model and a detailed 140 brick capacitances model

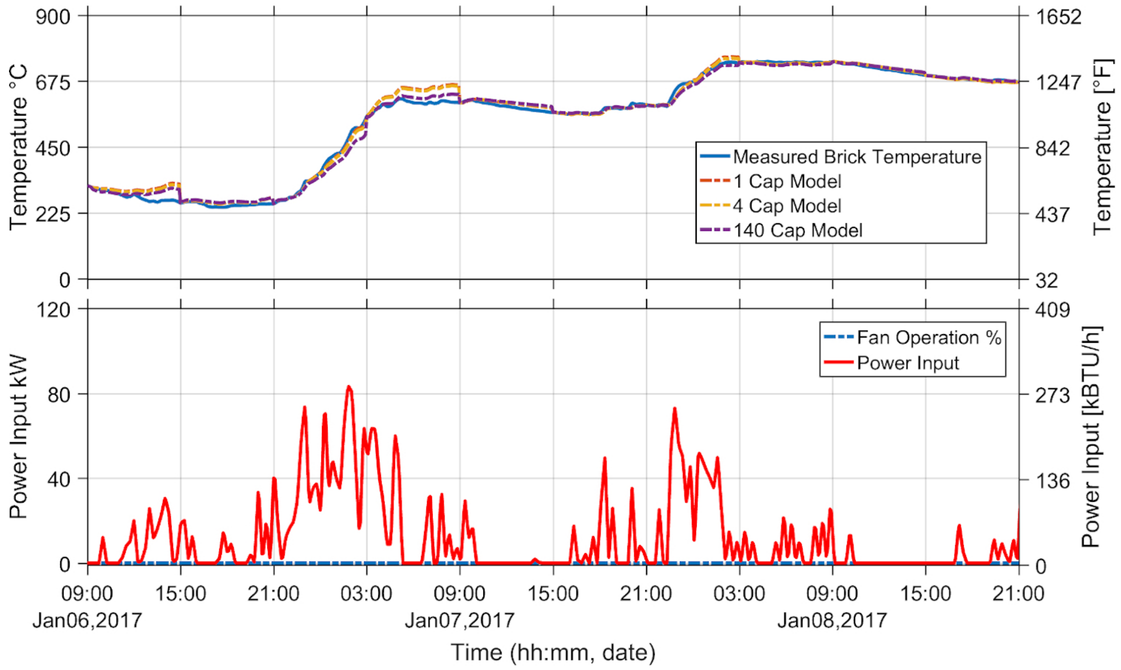

Figure 5.9: Three days of heat transfer in bricks modelling results with model reset at intervals of 6 hours

When no reset is applied, the high-resolution model (140 brick capacitance nodes) performs significantly better than the two low order models, with an RMSE of 34 °C compared to 85 °C for the 4-capacitance model and 95 °C for the 1-capacitance model. However, when a model reset at 6-hour intervals is introduced, all the models perform quite well; the predictions of even the single capacitance model are satisfactory and only slightly less accurate than the higher resolution (RMSE of 18 °C for the 1-capacitance model vs. 15 °C for the detailed 140-capacitance model).

5.4.2 Modeling results: heat transfer from bricks to airflow

Figure 5.10 shows the model results corresponding to the heat transfer from bricks to the airflow over a period of several hours. It is worth mentioning that the available dataset for the heat transfer mode from bricks to airflow is much shorter than the dataset corresponding to the "charging" mode (heating the bricks with the electric coils). A comparison is done between measured data and the model outputs of average brick temperature and outlet air stream temperature. Three data points are taken from the BAS and used for comparison: 1) the fan operation, 2) the power input, and 3) the inlet air stream temperature. Figure 5.10 shows results for the model running continuously for the entire period without reset incorporated; while Figure 5.11 incorporates a 6-hour interval model reset of 6-hour.

Table 5.3 shows the statistical indices for modelling of heat transfer from bricks to airflow without model reset and with reset at 6-hour intervals. The RMSE associated with the airflow through the bricks ranges from 3.5 °C (140-capacitance model with reset) up to 4.1 °C (1-capacitance model without reset). The three introduced models perform well when simulating without model reset but have considerable improvements when model reset is incorporated.

Table 5.3: Statistical indices for modeling heat transfer from bricks to airflow (January 9, 2017)

Model	Bricks RMSE [°C (°F)]	Bricks MAE [°C (°F)]	Bricks [°C (°F)]	Outlet Air RMSE [°C (°F)]	Outlet Air MAE [°C (°F)]
1-Capacitance	54 (129)	46 (115)	80 (176)	4.1 (39.4)	2.8 (37.0)
4-Capacitance	52 (126)	45 (108)	77 (171)	4.0 (39.2)	2.7 (36.9)
140-Capacitance	42 (108)	38 (100)	75 (167)	3.5 (38.3)	2.4 (36.3)
With Model Reset every 6 Hours					
1-Capacitance	36 (97)	25 (77)	70 (158)	3.4 (38.1)	2.2 (36.0)
4-Capacitance	34 (93)	24 (75)	65 (149)	3.4 (38.1)	2.2 (36.0)
140-Capacitance	33 (91)	25 (77)	75 (167)	3.0 (37.4)	2.0 (35.6)

In the next section, modelling of several days, the different model resolutions are tested against data from several days of operation. There is a mix of different operating modes in the

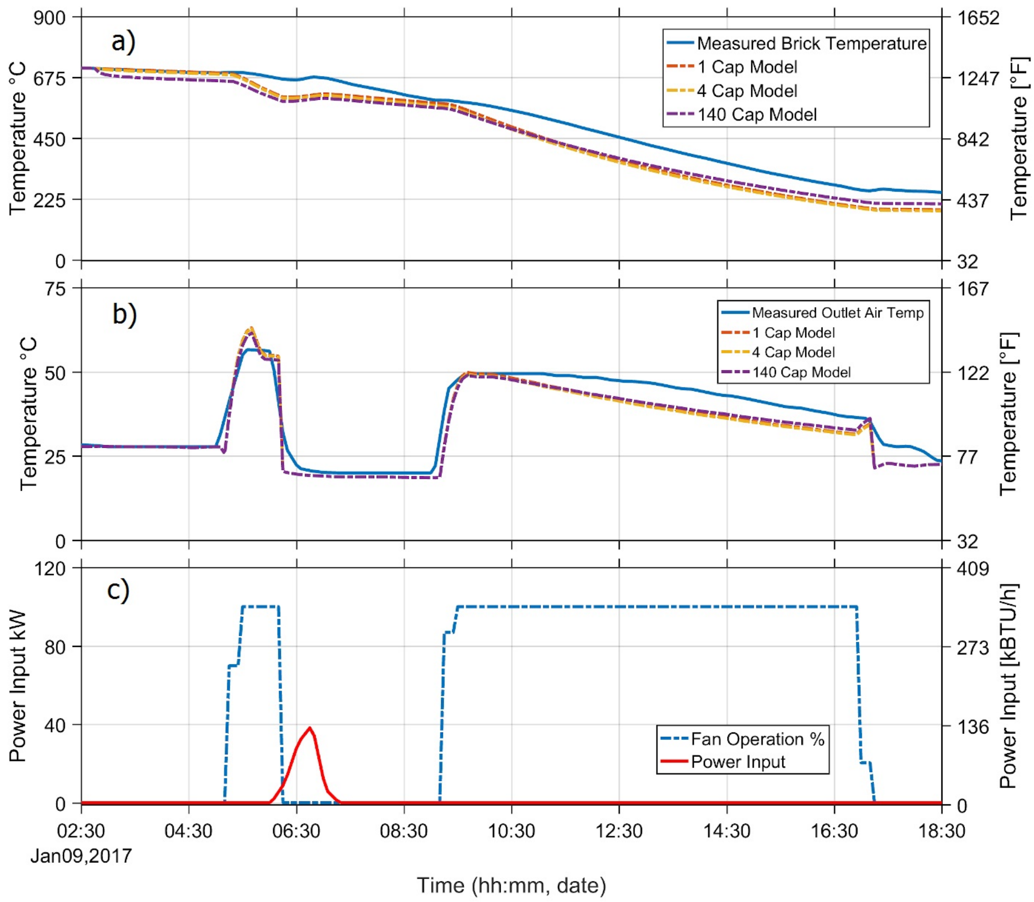

Figure 5.10: Several hours of modelling heat transfer from bricks to airflow, a) Brick temperature, b) outlet air temperature and c) power input and fan operation

data, with periods of only heat transfer in bricks (i.e., no fan operation) and periods of heat transfer from bricks to airflow.

5.4.3 Modelling of several days

Figure 5.12 and Figure 5.13 show modelling results from December 30th, 2016, through January 9th, 2017, with and without model reset. During this period, all modes of operation for the ETS took place (i.e., heat transfer to bricks, free floating and heat transfer from bricks to airflow). Therefore, this dataset provides a good example to test the usefulness of the ETS control-oriented models developed in this study under different dynamic conditions.

The three models predict well the brick temperatures and the outlet air temperatures; the performance of the models improves when model reset is introduced. The concept of resetting the model periodically with available sensor data can be easily implemented during the operation

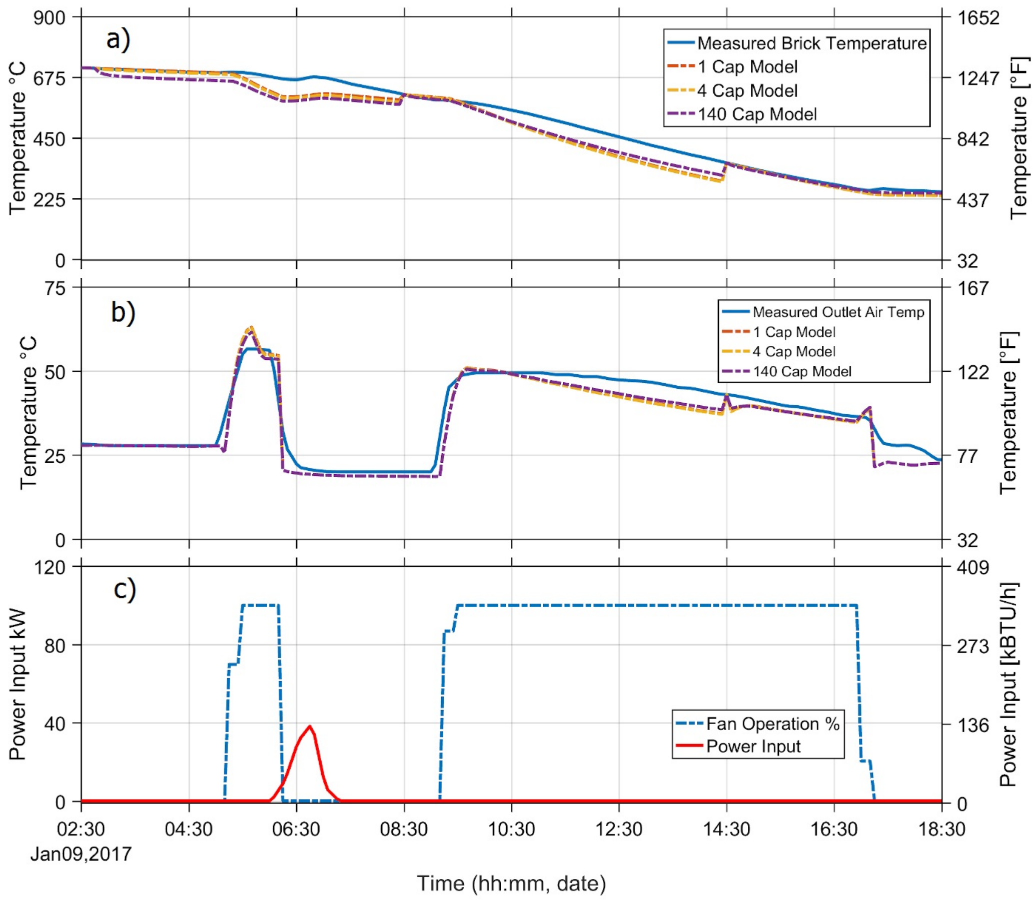

Figure 5.11: Several hours of modelling heat transfer from bricks to airflow with model reset at intervals of 6 hours, a) Brick temperature, b) outlet air temperature and c) power input and fan operation

of the system. Table 5.4 shows the error analysis of the three models with and without model reset at 6 hours intervals.

Table 5.4: Several days of simulation – statistical indices (December 30, 2016 – January 9, 2017)

Model	**Bricks RMSE [°C (°F)]**	**Bricks MAE [°C (°F)]**	**Bricks [°C (°F)]**	**Outlet Air RMSE [°C (°F)]**	**Outlet Air MAE [°C (°F)]**
1-Capacitance	58 (136)	46 (115)	114 (237)	1.2 (34.2)	0.4 (32.7)
4-Capacitance	51 (124)	41 (106)	104 (219)	1.2 (34.2)	0.4 (32.7)
140-Capacitance	27 (81)	22 (72)	70 (158)	1.1 (34.0)	0.4 (32.7)
With Model Reset every 6 Hours					
1-Capacitance	18 (64)	13 (55)	71 (160)	1.2 (34.2)	0.4 (32.7)
4-Capacitance	17 (63)	12 (54)	65 (149)	1.1 (34.0)	0.4 (32.7)
140-Capacitance	16 (61)	11 (52)	60 (140)	1.0 (33.8)	0.3 (32.5)

When there is no reset, the high-resolution model (140 brick node capacitances) has an

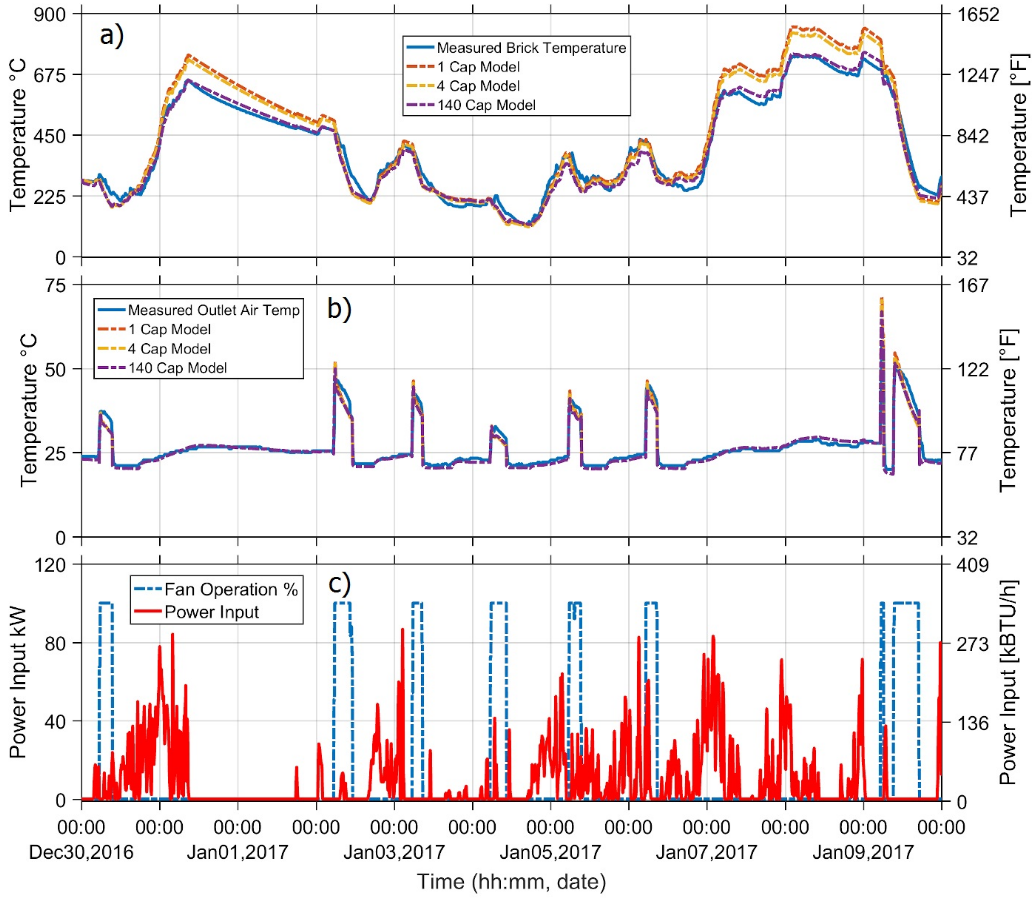

Figure 5.12: Several days of operation of the ETS showing model performances. Results of a model with 1 brick capacitance, a model with 4 brick capacitances and a model with 140 brick capacitances, a) Brick temperature, b) outlet air temperature and c) power input and fan operation

RMSE of 27 °C compared to 51 °C for the 4-capacitance model and 58 °C for the 1-capacitance model. When the models are reset at 6-hour intervals with measured data, all the models perform almost the same and the errors are all reduced. The RMSE is decreased by 40%, MAE by 33% and infinity norm by 43% for the 1-capacitance model, while the RMSE is decreased by 34%, MAE by 29% and infinity norm by 39% for the 4-capacitance model and for the detailed 140-capacitance model the RMSE is decreased by 11%, MAE by 11% and infinity norm by 10%. In the next section, different model reset interval lengths are investigated to determine if a 6-hour interval is adequate or necessary for this purpose.

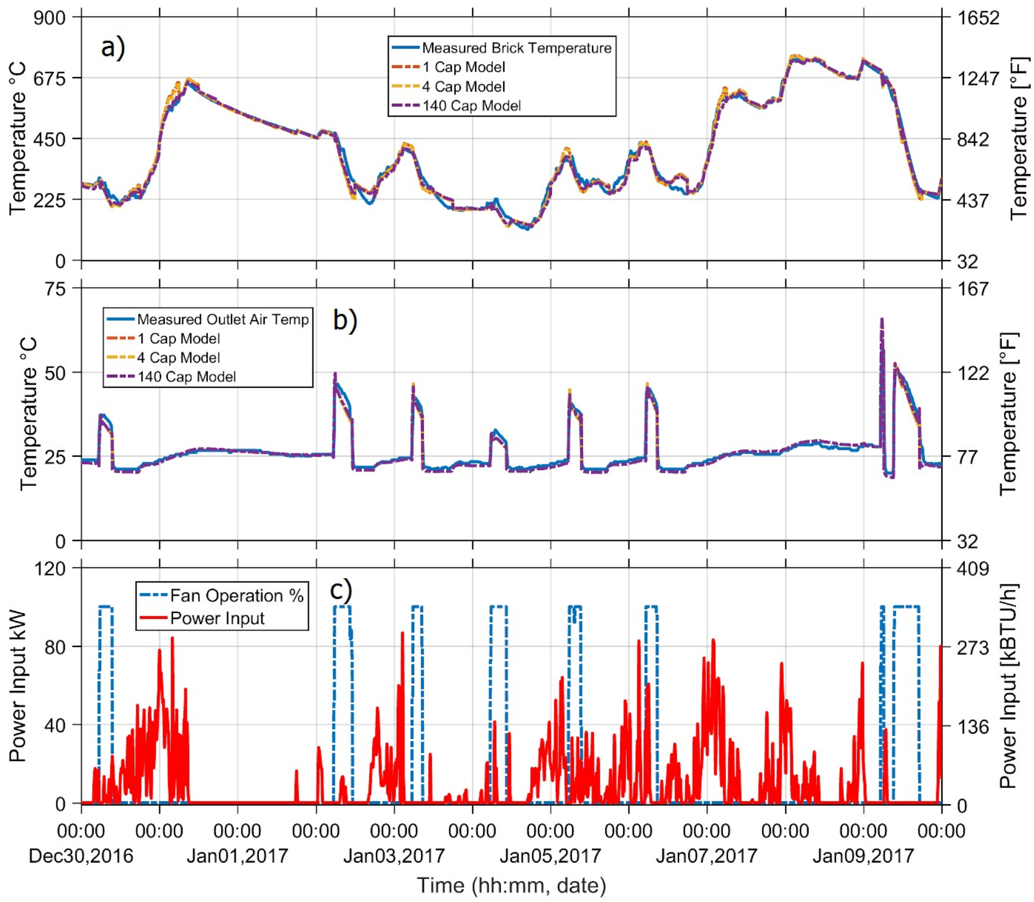

Figure 5.13: Several days of model results with model reset at 6-hour intervals. Results of a model with 1 brick capacitance, a model with 4 brick capacitances and a model with 140 brick capacitances, a) Brick temperature, b) outlet air temperature and c) power input and fan operation

5.4.4 Investigation of model reset interval length

Simulation results corresponding to model reset intervals from 3 hours up to 24 hours were investigated. Figures 5.14, 5.15, and 5.16 show the statistical analysis of several days of simulation for different model resolutions and model reset lengths.

Table 5.5 shows the details for the parametric study of the model reset interval length. Model performance improves when model reset is introduced into the simulation, thus showing that the concept of resetting or calibrating a control model periodically with available sensor data is a useful way to improve the performance of the model while keeping its resolution low and structure simple; it is also a realistic and practical approach when the intent is to apply the model for control purposes and feedback data is collected continuously. Even a model reset with an interval as long as 24 hours can significantly reduce the error observed for the lower

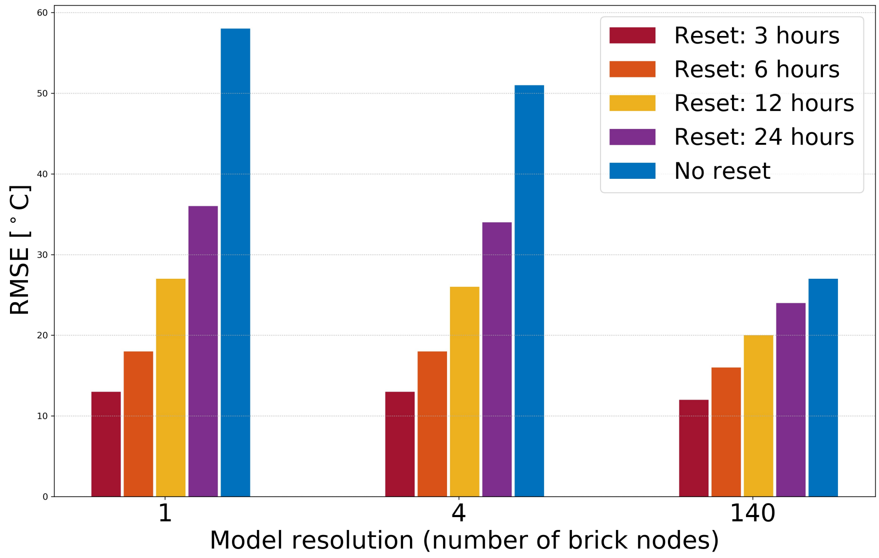

Figure 5.14: Simulation RMSE results of three thermal models with different reset intervals ranging from 3 to 24 hours

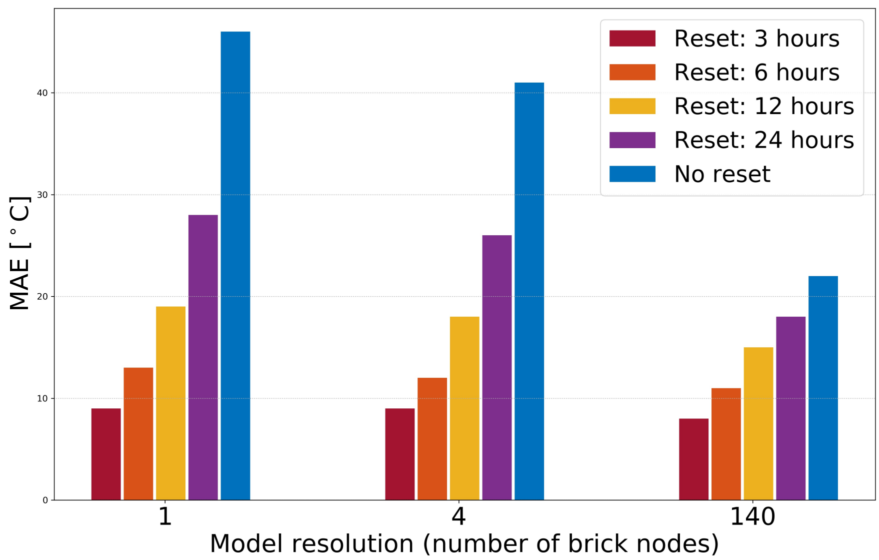

Figure 5.15: Simulation MAE results of three thermal models with different reset intervals ranging from 3 to 24 hours

resolution models: for example, for the 1-capacitance model with a 24-hour reset interval when compared to simulating with no reset, the MAE has a percent difference of 48%, and is reduced from 46 °C to 28 °C. The reset interval does not have a significant impact on the results of the more detailed models.

Next, parameter identification of the brick conductivity was studied to determine whether using an "effective" brick conductivity value would improve the model predictions, just as incorporating a model reset has improved the model results.

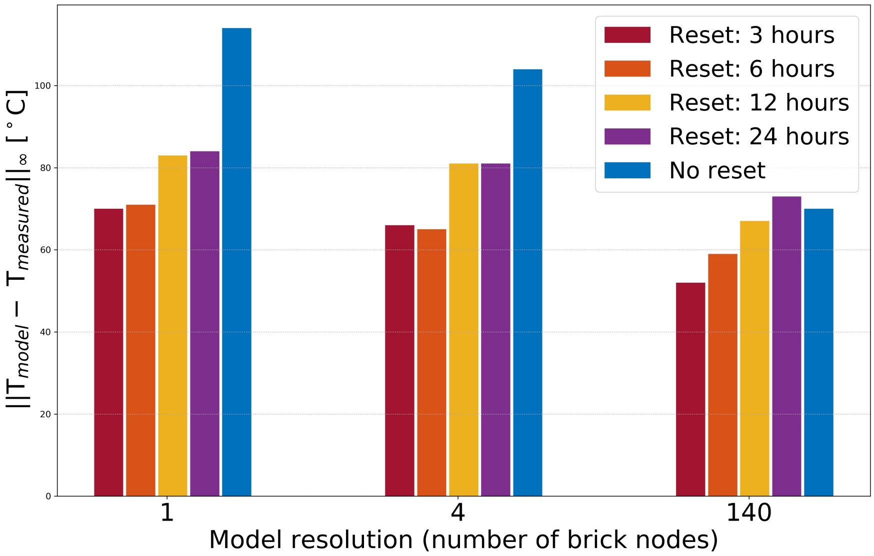

Figure 5.16: Simulation infinity norm results of three thermal models with different reset intervals ranging from 3 to 24 hours

Table 5.5: Results with different model reset intervals from no reset up to 24 hour reset interval (several days of simulation)

Model	**Reset Interval [Hours]**	**Bricks RMSE [°C (°F)]**	**Bricks MAE [°C (°F)]**	**Bricks [°C (°F)]**
1-Capacitance	3	13 (55)	9 (48)	70 (158)
	6	18 (64)	13 (55)	71 (160)
	12	27 (81)	19 (66)	83 (181)
	24	36 (97)	28 (82)	84 (183)
	No Reset	58 (136)	46 (115)	114 (237)
4-Capacitance	3	13 (55)	9 (48)	66 (151)
	6	18 (64)	12 (54)	65 (149)
	12	26 (79)	18 (64)	81 (178)
	24	34 (93)	26 (79)	81 (178)
	No Reset	51 (124)	41 (106)	104 (219)
140-Capacitance	3	12 (54)	8 (46)	52 (126)
	6	16 (61)	11 (52)	59 (138)
	12	20 (68)	15 (59)	67 (153)
	24	24 (75)	18 (64)	73 (163)
	No Reset	27 (81)	22 (72)	70 (158)

5.4.5 Identification of "effective" brick conductivity

The concept of "effective" brick conductivity was also proposed and investigated to use a model with a relatively low order while still obtaining adequate predictions. This concept consists of the proposition that it is possible to improve the accuracy of a low-order model if it is assumed that it behaves as if the material had a higher conductivity (Date et al., 2016b). It is worth pointing out that this does not reflect any change in the material: it is only a modelling artifice when the objective is to assess the average temperature of the material as an indication of its state of charge.

An optimization routine is used to find the brick conductivity values that minimize an objective function. In this case, the objective function chosen was the root-mean-square-error (RMSE) between measured brick temperature and the prediction at a simulation interval of 5 minutes. Model reset was not incorporated into the conductivity identification process. The MATLAB function *fmincon* – which finds the minimum of a constrained nonlinear multivariable function – is used here; other algorithms may replace this function depending on the user's preference. The objective function chosen was RMSE. The optimization problems are described as follows:

$$\begin{aligned} \min_{k_{brick}} \quad & \sqrt{\frac{\sum_{i=1}^{n}(\hat{y}_i - y_i)^2}{n}} \\ \text{subject to} \quad & k_{brick,min} \leq k_{brick} \leq k_{brick,max} \end{aligned} \tag{5.11}$$

Where y is the measured sensor data of the brick temperature, $\hat{y}$ represents model predictions of brick temperature and n is the number of samples. For a given number of capacitances, the conductivity k is adjusted until the RMSE is minimized. The different "effective" brick conductivity values versus the number of brick nodes (i.e., model detail resolution) are plotted in Figure 5.17 for ten (10) different thermal models with different levels of resolution.

Having an effective brick conductivity related to the number of brick nodes in the model, the error can be reduced in the lower resolution models. Figure 5.20 and Table 5.6 show the overall results for the "effective" brick conductivity study. For the case of the 1-capacitance model, the RMSE is reduced by 34% when a brick conductivity of 97.1 W/m·K rather than 4.3 W/m·K is used, while the MAE is decreased by 28%.

If there is no reset and the real brick conductivity value of 4.3 W/m·K is used in the 1-capacitance model, an RMSE of 58 °C, an MAE of 46 °C and an infinity norm of 114 °C is observed. However, by using a 1-capacitance model with 6-hour model reset and incorporating an "effective" value for the brick conductivity, the error values improve, with an RMSE of 16 °C, an MAE of 11 °C and an infinity norm of 59 °C. These results can be compared to that of

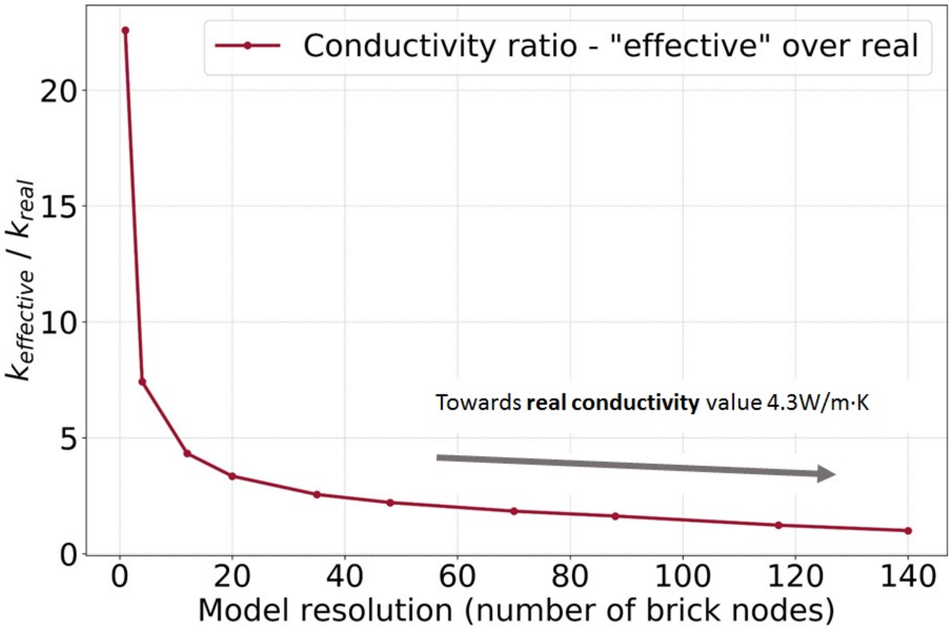

Figure 5.17: Simulation results of models using effective conductivity compared to real conductivity = 4.3W/m·K

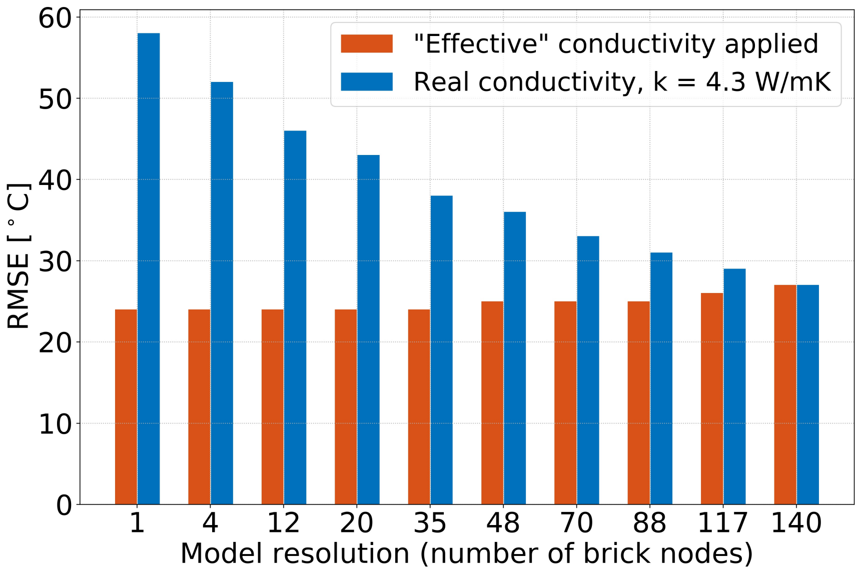

Figure 5.18: Simulation RMSE results of models using effective conductivity compared to real conductivity = 4.3W/m·K

the 140-capacitance model where model reset is not incorporated (RMSE of 27 °C, MAE of 22 °C and an infinity norm of 70 °C), Therefore, this simple model with slight modifications gives satisfactory predictions and thus can aid with control and decision making of the ETS device and operation of the building.

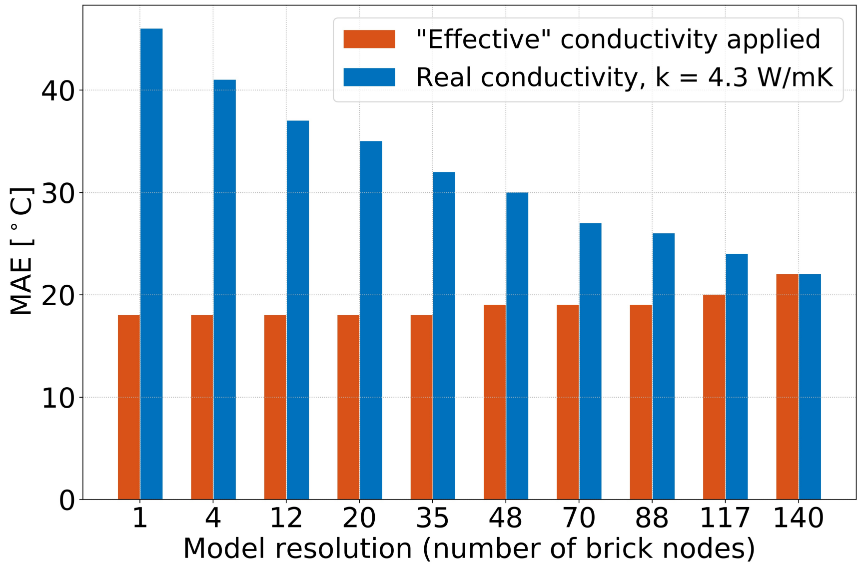

Figure 5.19: Simulation MAE results of models using effective conductivity compared to real conductivity = 4.3W/m·K

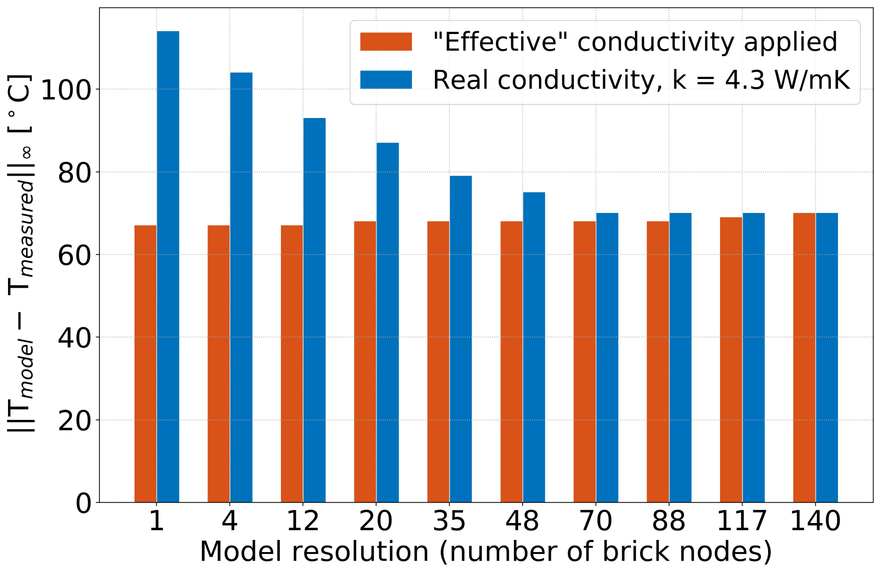

Figure 5.20: Simulation infinity norm results of models using effective conductivity compared to real conductivity = 4.3W/m·K

5.5 Control scenarios of ETS for building load flexibility

This section will focus on the potential of the ETS storage system to enhance the flexibility of the electric load of the building. This example will help in the long-term objective of earning a better understanding of the thermal behaviour of buildings and heating systems under different control

Table 5.6: "Effective" conductivity based on number of brick nodes (several days of simulation)

Model	**Brick conductivity [W/m·K]**	**Brick conductivity [BTU/(hr·ft·°F)]**	**Bricks RMSE [°C (°F)]**	**Bricks MAE [° C (°F)]**	**Bricks [°C (°F)]**
1-capacitance	97.1 ("effective")	56.1 ("effective")	24 (75)	18 (64)	67 (153)
	4.3 (real)	2.5 (real)	58 (136)	46 (115)	114 (237)
4-capacitance	31.9 ("effective")	18.4 ("effective")	24 (75)	18 (64)	67 (153)
	4.3 (real)	2.5 (real)	52 (126)	41 (106)	104 (219)
12-capacitance	18.6 ("effective")	10.7 ("effective")	24 (75)	18 (64)	67 (153)
	4.3 (real)	2.5 (real)	46 (115)	37 (99)	93 (199)
20-capacitance	14.4 ("effective")	8.3 ("effective")	24 (75)	18 (64)	68 (154)
	4.3 (real)	2.5 (real)	43 (109)	35 (95)	87 (189)
35-capacitance	11.0 ("effective")	6.4 ("effective")	24 (75)	18 (64)	68 (199)
	4.3 (real)	2.5 (real)	38 (100)	32 (90)	79 (174)
48-capacitance	9.5 ("effective")	5.5 ("effective")	25 (77)	19 (66)	68 (154)
	4.3 (real)	2.5 (real)	36 (97)	30 (86)	75 (167)
70-capacitance	7.9 ("effective")	4.6 ("effective")	25 (77)	19 (66)	68 (154)
	4.3 (real)	2.5 (real)	33 (91)	27 (81)	70 (158)
88-capacitance	7.0 ("effective")	4.0 ("effective")	25 (77)	19 (66)	68 (154)
	4.3 (real)	2.5 (real)	31 (88)	26 (79)	70 (158)
117-capacitance	5.3 ("effective")	3.1 ("effective")	26 (79)	20 (68)	69 (156)
	4.3 (real)	2.5 (real)	29 (84)	24 (75)	70 (158)
140-capacitance	4.3 ("effective")	2.5 ("effective")	27 (81)	22 (72)	70 (158)
	4.3 (real)	2.5 (real)	27 (81)	22 (72)	70 (158)

scenarios. This study evaluates the amount of heat modulated by the ETS and the duration of the effect on the grid. This characterization will then be used to set simple control strategies to exploit the thermal storage potential, considering both energy consumption and thermal comfort.

In this case, there is a zone in the building that needs to be heated; the controller's objective is to minimize energy/power using simple control scenarios while keeping the zone within thermal comfort boundaries. Other objectives in the future could include minimization of cost under diverse scenarios (demand charge penalty, fluctuations of energy price, utility-triggered cost incentive). Figure 5.21 shows the temperature setpoint profile, occupied hours of the zone, and outdoor air temperature that were used for the control study.

This two-storey building, built in 1989, has a total floor area of roughly 9,000 m^2. The building, located in Sherbrooke (QC), Canada, had a peak demand of 600 kW in February 2015. The on-site ETS can supply heated air to a warehouse zone within the larger building. The warehouse zone serviced by the ETS has dimensions 55 m by 30 m, with a floor area of

$1650m^2$. Three control scenarios are evaluated for the system consisting of an air duct heating coil, ETS and warehouse building zone (refer to Figure 5.5).

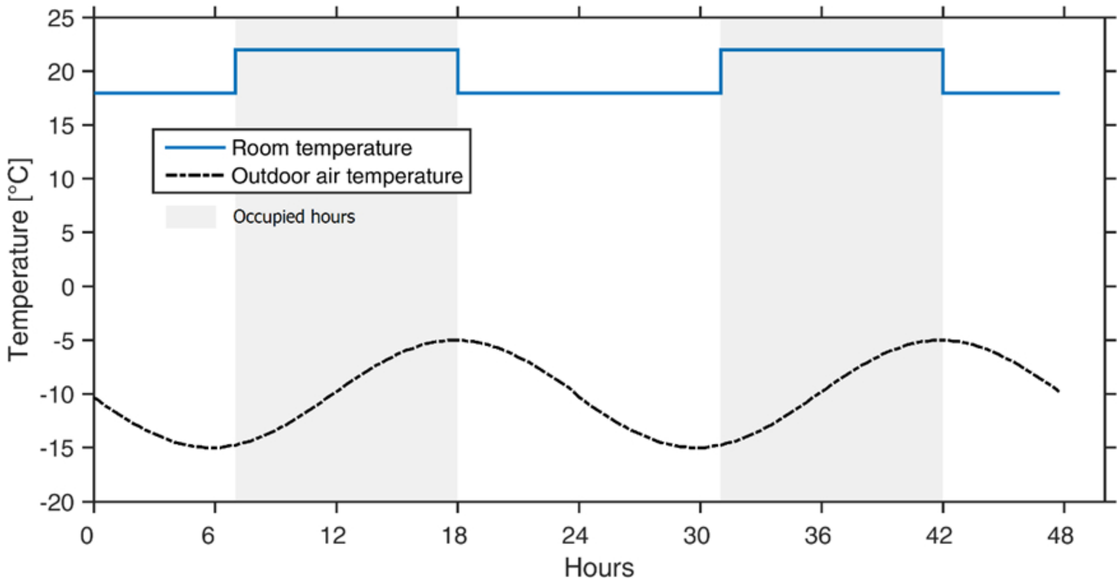

Figure 5.21: Control study on cold day: outdoor air temperature and zone temperature setpoint

5.5.1 Control scenario 1: building zone without active thermal Storage (reference case)

Control scenario 1 (Figure 5.22) is the warehouse zone operating on a cold day without any use of the ETS. All heating for the zone is provided by the standard HVAC heating coil with a heating peak of 67 kW (228 kBTU/hr).

5.5.2 Control scenario 2: building zone with active thermal storage device (typical operation)

The typical operation of the ETS and warehouse zone is shown in Figure 5.23. The ETS is charged in the night during off-peak hours and is then used during morning peak hours of 6a.m.-9a.m. to supplement the HVAC heating of the zone by supplying part of its heating load requirement. The zone temperature setpoint has a nighttime setback of 18 °C; when the setpoint is increased from 18 °C to 22 °C at 7a.m., a heating load peak of 60 kW (205 kBTU/hr) in the mornings occurs. The ETS provides approximately 170 kWh (580 kBTU) of heating, or “energy flexibility”, to the warehouse during this occupied time.

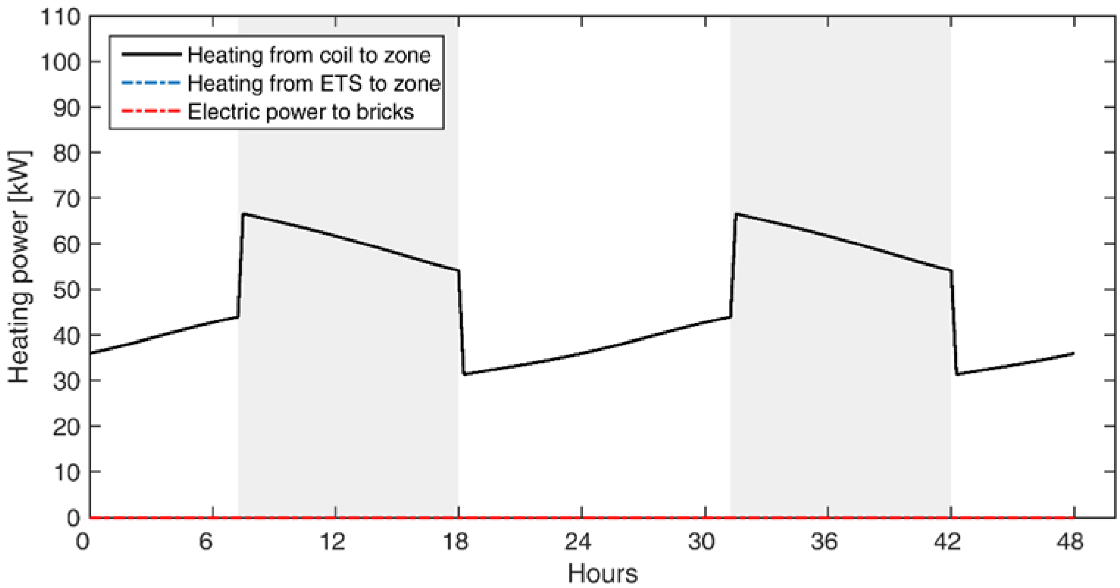

Figure 5.22: Control scenario 1- cold winter day heating without use of ETS

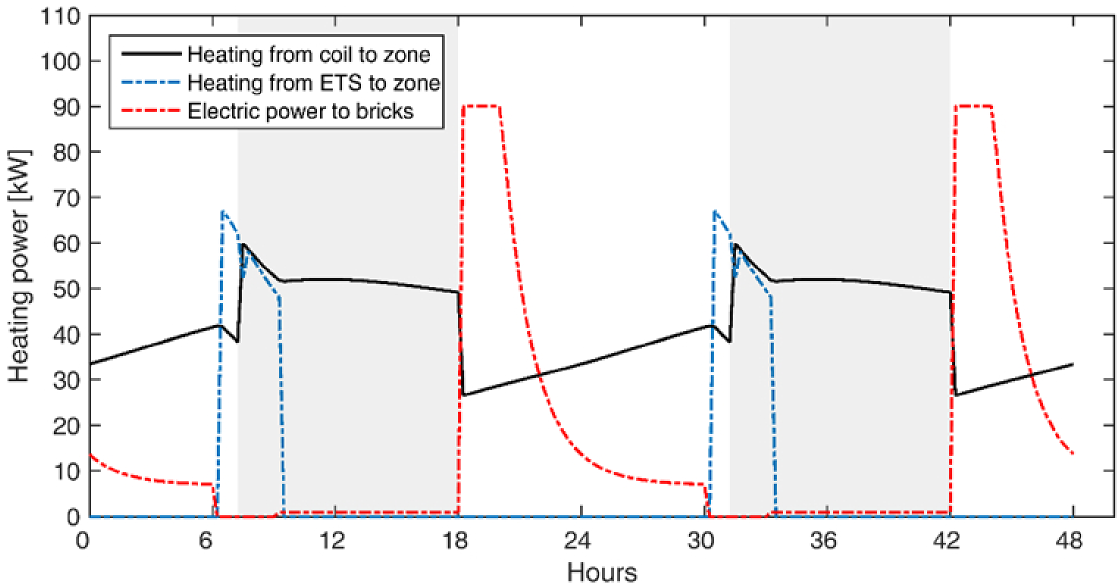

Figure 5.23: Control scenario 2 – cold winter day heating with supplemental heating by ETS during morning peak period 6a.m.-9a.m. (simulation)

5.5.3 Control scenario 3: building zone with active thermal storage device and limiting heating coil)

With an adequate control-oriented model of the ETS and zone, and available day-ahead weather predictions, it is feasible to quickly perform control scenario studies to determine if there is an alternative control strategy that would improve the building operation, energy use, or peak demand. In control scenario 3, the heating output from the heating coil is limited and the ETS is used during the morning peak hours of 6a.m.-9a.m. When the heating coil output is limited, its peak demand is 31 kW (106 kBTU/hr) during peak hours and 58 kW (198 kBTU/hr) later in the day. Again, the ETS provides approximately 170 kWh (580 kBTU) of heating to the warehouse during this occupied time. Results for two days are shown in Figure 5.24, while the results for the three scenarios are shown for comparison in Figure 5.25.

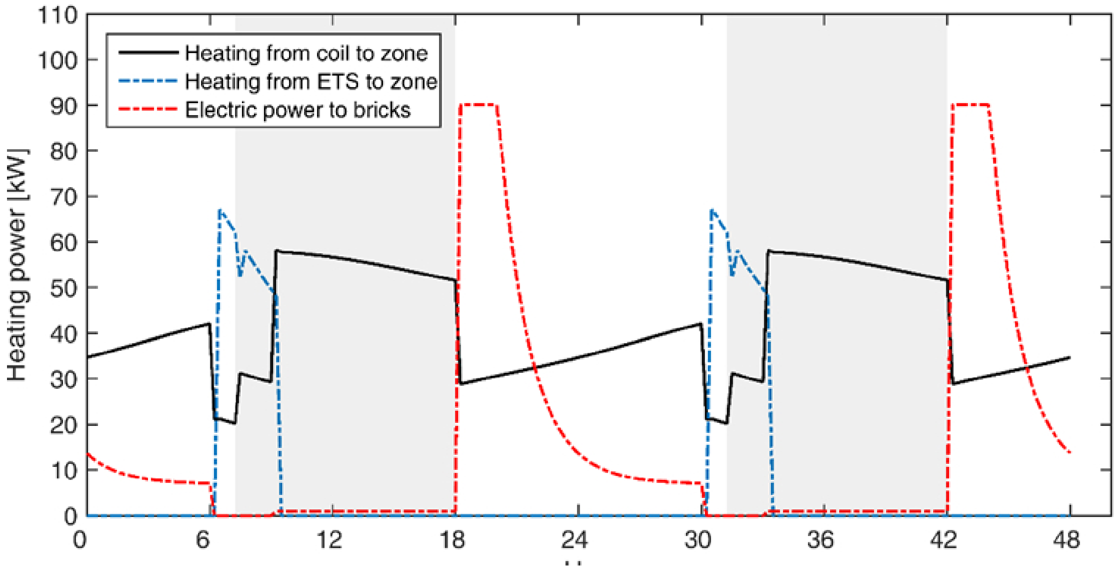

Figure 5.24: Scenario 3 – building zone with thermal storage device and limiting heating coil (simulation)

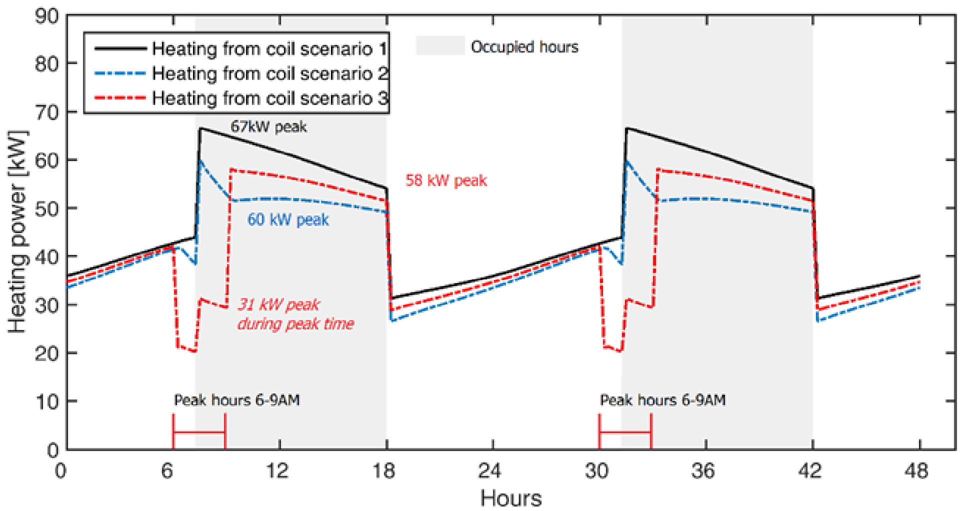

Figure 5.25: Heating from coil for the three control scenarios

It should be noted that the zone serviced by the heating coil and ETS is quite large (1650 m^2) and slow in terms of its thermal response. When the setpoint changes from 18 °C to 22 °C, it takes practically the entire day to reach to 22 °C. Another main advantage of the ETS is aiding

Table 5.7: Heating use of different control scenarios (24 hr period)

	Scenario 1 – without ETS	Scenario 2 – with ETS	Scenario 3 – with ETS & limiting heating coil
Electricity to bricks [kWh (kBTU)]	0	382 (1,200)	382 (1,200)
Heat from bricks [kWh (kBTU)]	0	170 (534)	170 (534)
Heat from coil [kWh (kBTU)]	1145 (3,598)	1016 (3,192)	998 (3,136)
Coil peak [kW (kBTU/hr)]	67 (229)	60 (205)	58 (198) 31 (106) during peak hours
Total kWh (kBTU) in 24 hours	1145 (3,598)	1397 (4,389)	1380 (4,335)
Energy Flexibility [Wh/m^2 (BTU/ft2)]	N/A	103 (33)	103 (33)

in reaching a zone air temperature of 22 °C more rapidly on very cold days, thus improving the thermal comfort for the occupants.

If the ETS was used during peak load hours of 6a.m.-9a.m. and with the anticipation of the rise in zone setpoint temperature from 18 °C to 22 °C, power peak at peak load time is reduced by 7 kW or 11%. While, when the heating coil is limited during peak times, the peak load can be reduced by 36 kW or 73% (Figure 5.25). This is equivalent to 103 Wh/m^2 of flexibility and represents 14% of the total energy consumption due to space heating and ETS charging in the 24-hour period (or 17% of only space heating). Additional results of the control studies are shown in Table 5.7. The potential of peak demand reduction is related to the installed storage system size, so further peak reduction would be possible if storage capacity sizing is chosen as a function of desired peak demand reduction. This is one example of how a control-oriented model could be used to rapidly study and decide on alternative control strategies for the zone and ETS device.

5.6 Conclusion

This thesis section presented a general methodology for the development and analysis of control-oriented models for the enhancement of operation of an electric thermal storage device (ETS) and energy use within a building. The ETS presented is one available size, though other sizes with different storage capacities exist. The developed control-oriented modelling methodology applies to different system sizes of the active storage device. The modelling results for the different operating conditions – the heat transfer to bricks and heat transfer from bricks to airflow – show that even a low-resolution thermal model with 1-capacitance which represents all the brick medium could be adequate for the control to optimize charging and discharging of the ETS device. The 1-capacitance model can predict the temperature of the bricks over several days with an average difference of 58 °C between modelled brick temperature and measured brick temperature, while with the 140-capacitance model an average difference of 27 °C was observed. Incorporating periodic model reset based on measured sensor data values significantly improves the model performance. As an example, the RMSE is reduced from 58 °C to 18 °C for the 1-capacitance model when model reset is integrated into the model methodology for control.

The concept of "effective" brick conductivity was also examined, and the conductivity changes based on the detail level of the ETS model (i.e., the number of brick nodes). By having an "effective" brick conductivity that varies according to the number of brick nodes in the model, the error can be reduced in the low-resolution models. In other words, simpler models can be used if an "effective" conductivity is applied. By using a 1-capacitance model with model reset and applying an "effective" value for the brick conductivity, the RMSE is 24 °C and the MAE is 18 °C, which are comparable to the errors of the 140-capacitance model where model reset is not incorporated (RMSE of 27 °C, MAE of 22 °C and an infinity norm of 70 °C). Combining the two concepts of model reset and "effective" brick conductivity, low-resolution models that are fast and easy to develop are robust contenders for control-oriented applications such as Model Predictive Control.

If the ETS was used and the heating coil is limited during peak of 6a.m.-9a.m. and with the anticipation of the rise in zone setpoint temperature from 18 °C to 22 °C, the peak load can be reduced by 36 kW or 73%.

An energy flexibility amount of up to 103 Wh/m^2 floor area is provided to the building during the critical time for the grid and represents up to 17% of the energy consumption due to space heating for the zone. The control examples shown here illustrate the potential of the ETS storage system to enhance the flexibility of the electric load of the building and helps in the long-term objective of getting a better understanding of the thermal behaviour of buildings and heating systems under different control scenarios.

Chapter 6

Energy Flexible Building: Predictive Load Management of Passive and Active Energy Storage under a Demand Response Program

6.1 Introduction

There is a continuing global focus targeted at decreasing Greenhouse Gas (GHG) emissions, with a strong push for electricity from cleaner sources (rather than coal or gas, for example); however, as an increasing percentage of electricity production comes from renewable and intermittent sources, a greater strain is being put on electric grids. As utility grids have recently been integrating more clean renewable energy generating resources such as photovoltaics (PV) or wind turbines, this increase in intermittent production results in a variable supply, which has created new obstacles for both utilities and their customers.

As more distributed renewable energy sources are being incorporated into existing utility grids, a challenge is created where there is a mismatch between times of high consumption from buildings and times of peak power generation from these intermittent renewable sources. While peak solar generation occurs midday, the typical time where peak consumption from buildings can be morning, evening (for the residential sector), or afternoon (for the commercial sector). The well-known "duck curve" for the California market depicts this mismatch well (Denholm et al., 2015). This supply-demand mismatch is also observed in other regions but for different reasons (for instance in heating-dominated climates). To incentivize electricity customers and building owner/operators to alter their electricity demand to off-peak times, different demand-side management and DR programs are offered by many utilities.

Recently in the research field, the concept of energy flexibility (i.e., the capacity of the building to respond to the needs of the electric grid) has received significant attention. By estimating the amount of energy flexibility a building can provide to the grid, this flexibility can be used to alleviate the burden on the grid when the electricity demand from customers approaches or exceeds what the grid is capable of supplying. International Energy Agency Energy in Buildings and Communities Programme's (IEA EBC) Annex 67 introduced the notion of "Energy Flexible Building", defined by the Annex as *a building able to manage its demand and generation in accordance with local climate conditions, user needs and grid requirements* (International Energy Agency, 2020).

The majority (over 99.8%) of electric power generated in Québec, Canada is by hydroelectric plants, where commercial buildings often use electricity as the main or only heating and energy source. This abundant and stable source of hydroelectricity has fostered low electricity rates in the region while elevating fuel prices due to limited gas distribution infrastructure in some areas. During very cold winter days, a heavy demand on the grid is observed and is partially due to space heating peak loads. The heating of commercial and institutional (C & I) buildings accounts for about 9% of the province's winter peak load, and this amount can be considered a meaningful portion of the electric load in the province (Hydro-Québec Distribution, 2012). Due to these mentioned issues related to peak demand, there is increasing activity in quantifying the energy flexibility of buildings and increasing participation in demand response programs.

The electric energy system includes many aspects spanning from generation units to the final electricity end-uses by customers. It is worthwhile and feasible to consider optimizing this entire electric energy system, and not only restricting this endeavour to the grid. Buildings are part of this system as end-uses and are capable of supply some form of energy flexibility to the electric system. To achieve energy flexibility, building science and advanced system control must be incorporated to the design and operation of flexible buildings. Using the models that were presented in the previous chapter, this chapter evaluates MPC for buildings in cold climate regions with dedicated dispatchable thermal storage and outlines a methodology for identifying and evaluating the efficacy of a control strategy.

A notable feature of some Québec commercial customer rates is that each monthly bill throughout the year can be affected by the building's highest winter demand. The minimum monthly electric billing demand is set at 65% of the peak power reported during the winter months. Thus, appropriate consideration should be given to the demand management strategies of a building during winter since it can affect the bills over the year.

This chapter presents an evaluation of the energy flexibility potential of a zone equipped with a dedicated thermal storage device[1]. One aim is to match stored thermal energy in a dedicated storage device to the zone heating energy demand for the following day. To achieve this, an estimate of the heat requirements of the conditioned zone for the following day is needed and optimal controls through MPC are evaluated. Prediction uncertainties due to model parameter identification and weather forecasts are also considered.

6.2 Concept of Building Energy Flexibility Index ($BEFI$)

Building control can take advantage of thermal mass to shift power consumption from one critical period to another. Different end-uses can be rescheduled before or after a specific period without adverse impacts, such as a reduction of thermal comfort. We can think also of specific systems within HVAC (active thermal storage or batteries) or embedded in the building – like heavy radiant floor – that can be used to shift energy consumption without affecting occupant comfort. When coordinating these different systems, future or expected needs, availabilities and constraints that may depend on occupant activity schedule, weather, grid state, day of the week, etc. must be considered. MPC is an optimal tool to achieve this.

The most relevant application of energy flexibility is demand response during peak periods of the grid. A Building Energy Flexibility Index ($BEFI$) could be used to quantify the potential participation of a customer for such a demand response event. A preliminary introduction and description of the concept of a $BEFI$ with case studies can be found in two previous conference papers on the topic (Athienitis et al., 2020, Date et al., 2020b).

[1]This work is based on a published refereed conference paper and a peer-reviewed journal article: (a) Date, J., Candanedo, J. A., & Athienitis, A. K. (2021). A methodology for the enhancement of the energy flexibility and contingency response of a building through predictive control of passive and active storage. Energies, 14(5) and (b) Date, J. A., Candanedo, J. A., Athienitis, A. K., & Lavigne, K. (2020b). Energy flexible building: predictive load management of passive and active energy storage under a demand response program. In Proceedings of eSIM 2020 Conference Vancouver, BC.

$BEFI$ is an informative indicator that helps determine useful actions to be undertaken that provide predictable energy flexibility from a building. Optimization could be performed to maximize this index for a specific period. $BEFI$ may become a valuable consideration to support decisions regarding applicable equipment or systems for a building.

A well-designed index would aid in a) quantifying the available flexibility from a building for the grid, b) identifying improved design options to increase its potential flexibility, c) controlling the building to get maximum available flexibility when needed, and d) compare different systems or designs. A depiction of a demand response event is shown in Figure 6.1 while Equation (6.1) shows a more formal representation of the $BEFI$ (Athienitis et al., 2020).

$$BEFI(t, \Delta t, t_{notice}) = \frac{\int_t^{t+\Delta t} P_{ref} dt - \int_t^{t+\Delta t} P_{flex} dt}{\Delta t} \tag{6.1}$$

where $BEFI$ is the Building Energy Flexibility Index, t is the start time of the event, Δt is the duration of the event, t_{notice} is time of notification for the event, P_{ref} is power demand of reference scenario during the event, and P_{flex} is power demand of flexibility case during event.

An example is illustrated in Figure 6.1. Suppose a DR event occurs at time t, and this event lasts for a duration of time Δt. The utility provider informs the building operators ahead of time at time t_{notice} that the DR event will occur. The trajectory of the load follows one trajectory, in blue, for the *reference* case and an adjusted trajectory, in orange, for the "*flexibility-adjusted*" curve.

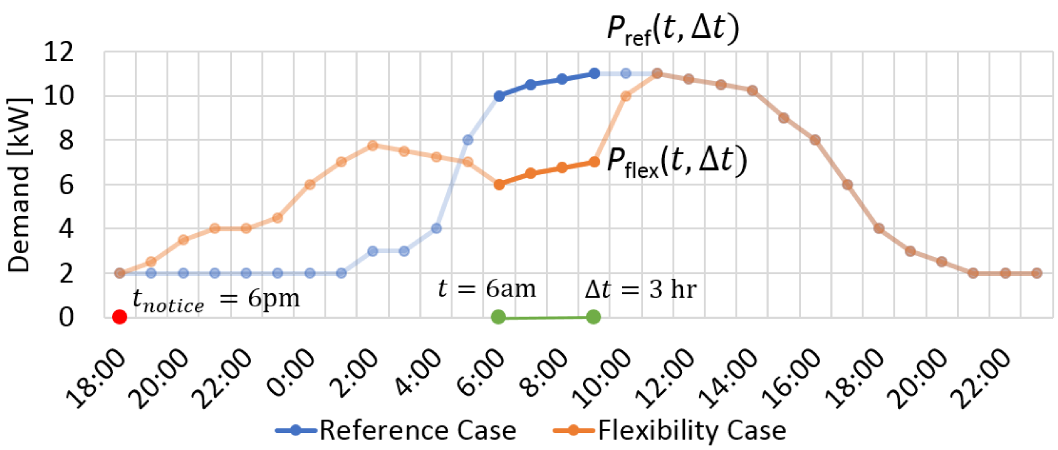

Figure 6.1: Example: Building Energy Flexibility Index ($BEFI$)

The $BEFI$ is the average difference between the power demand of the reference case, P_{ref} and the power demand of the alternative "flexibility scenario", P_{flex}, for the given event duration Δt, shown in Equation 6.1. $BEFI$ could also be represented as a percentage by dividing it by the value of P_{ref}.

6.3 Methodology

Data-driven reduced-order thermal models (ROMs) for different archetype zones and system configurations are useful tools to identify strategies for developing and quantifying energy flexibility in the building-grid interaction. These models, which account for thermal mass and the inherent thermal delay, are typically first- to third-order Resistance-Capacitance (RC) thermal networks and can be calibrated with a smart meter and weather data or more detailed data from building automation systems (BAS) and smart thermostats.

An MPC-based simulation study is presented in this chapter, where estimated heat requirements of the conditioned zone for the following day and optimal control schedules are identified for the thermal storage device and zone temperature setpoint. Several other simulation studies are carried out to assess the versatility of the optimal schedules, and different weather forecasts, control horizons, and cost functions are evaluated. The subsequent MPC studies were carried out in the following steps, as shown in Figure 6.2:

1. **Real building measurement data** was collected from the BAS. Data includes variables such as building power [kW], zone air temperature, weather data, and specific data points for the ETS device. Data is collected at 15-minute intervals.
2. **Numerical thermal building or device control-oriented models** were developed. These models are physics-based ROM grey-box RC thermal networks. These models were calibrated using the collected data from the first step. Critical parameters were identified using the gradient descent-based optimization function *fmincon* in MATLAB. A detailed explanation of the model development process and performance for the ETS device is found in Chapter 5 (Date et al., 2018, 2020a,b).

3. **Predictive control strategies for very cold days** were identified for improved management of peak loads and building energy flexibility. The $BEFI$ was quantified depending on when a notification signal is given to the building owner from the utility. A heuristic approach is compared to optimized MPC. See Chapter 3 for further details on the developed $BEFI$.

4. **Shoulder season MPC studies** were done to improve the operating conditions of the ETS. The aim is to reduce energy consumption by storing the amount of energy needed for a milder shoulder-season day. Current control methods can cause over-charging of the device on milder shoulder-season days, which can result in waste through excess thermal energy generation and storage.

5. **Model prediction uncertainty** associated with the weather forecast and identified model parameters is accounted for by evaluating numerous uncertainty scenarios and visually presenting the uncertainty bounds.

6. **Contingency strategies were assessed** to quantify the available energy flexibility for the grid by the building at specific times. Two strategies were considered: 1) Reducing the zone temperature setpoint for 3 hours and 2) discharging the stored thermal energy from the storage device for 3 hours.

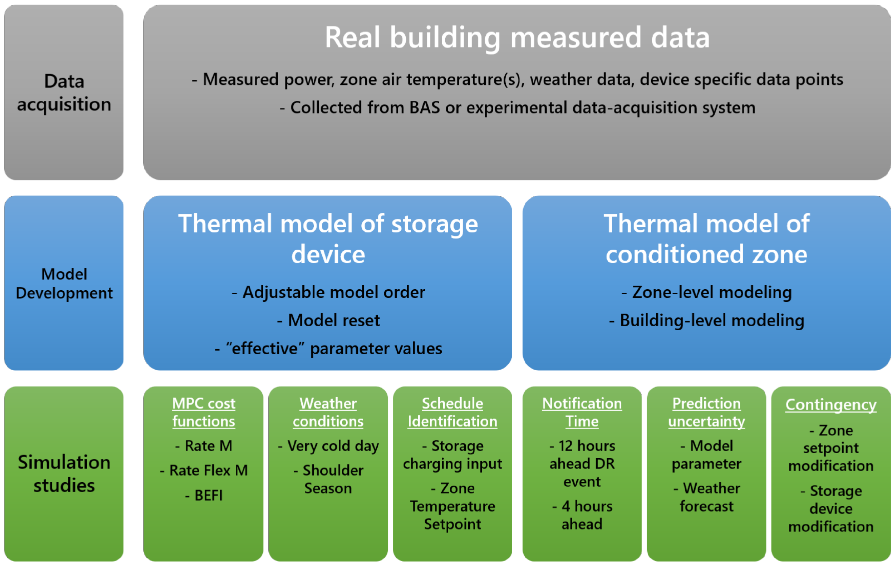

Figure 6.2: Outline of methodology

6.3.1 Québec commercial customer electricity rates

In Québec, Canada, some utility rates carry a charge related to energy consumption and one related to the peak power demand of a building (or group of buildings) owned by the customer. Rate M, which is for the large commercial building sector, has a demand charge and two energy prices (Hydro-Québec, 2020b), as outlined in Table 6.1. At any given month, the minimum demand charge applied is set to 65% of the peak winter load, which is a special feature for this type of rate. Appropriate attention should be given to the building heating and general operation over the winter period when peak demand is experienced due to large space heating loads.

Table 6.1: Pricing structure of utility Rate M and Rate Flex M

Rate M **Large Commercial Building Sector**	
Demand Charge	\$14.58 / kW
First 210,000 kWh energy consumed	5.03¢/ kWh
Remaining energy consumed	3.73¢/ kWh
Rate Flex M **Large Commercial Building Sector**	
Winter Dec. 1-Mar. 31	
Demand Charge	\$14.58 / kW
Price of energy consumed outside peak events	3.17¢/ kWh
Price of energy consumed during peak events	50.00¢/ kWh
Summer Apr. 1-Nov. 30	
Demand Charge	\$14.58 / kW
First 210,000 kWh energy consumed	5.03¢/ kWh
Remaining energy consumed	3.73¢/ kWh

6.3.2 Predictive load management scenarios

The current control for setting the maximum allowable power of charging input to the ETS is based on a linear scale function which relates the current outdoor temperature to this power input, as shown in Table 6.2 and Figure 6.3. The outdoor temperature is read once per day at 6p.m. and used for the next 24 hours of control.

Table 6.2: Control of ETS power input: scale function

T_{ext}	P_{ETS}	**Brick Temperature**
0 °C	0%	93 °C
-18 °C	**100%**	871 °C

Using MPC to incorporate the predictions of occupancy schedules and weather forecasts over the next day or two into the control of the system, a new optimal value for the maximum ETS charging input can be identified at each hour can be identified to minimize electricity costs and energy consumption, while also maintaining the desired space conditioning for the occupied warehouse zone. Concurrently, a zone temperature profile is identified, which minimizes the following cost functions.

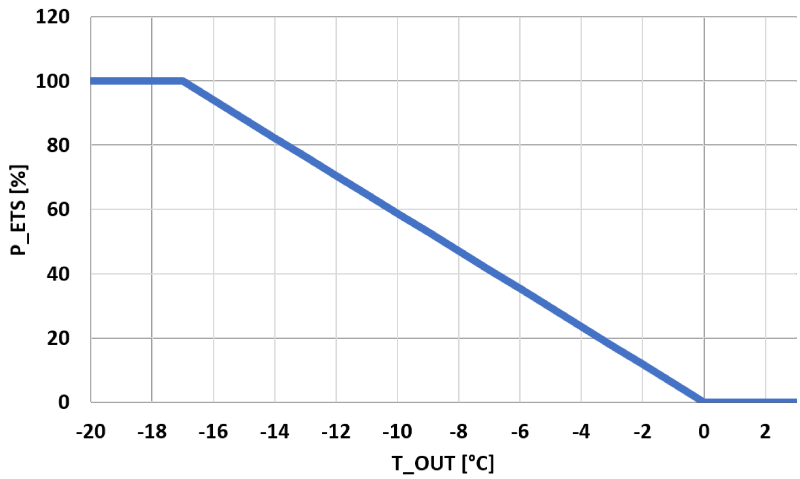

Figure 6.3: Thermal storage power input depending on outdoor temperature

Three cost functions incorporating Rate M, Flex Rate M, and $BEFI$ have been implemented and their associated operation results are compared to the typical manual control.

1. **Cost-function using Rate M.** The formulation of the first optimization problem is shown in equation (6.2). The utility Rate M in Table 6.1 is used for this cost function.

$$
\begin{aligned}
\min_{T_{SP},\, P_{ETS,maxSP}} \quad & J_{PH} = \left(\sum_{i=1}^{N} P_i \Delta t\right) \cdot \left(\text{Cost}_{\text{Energy}}\right) + \max\left(\mathbf{P}\right) \cdot \left(\text{Cost}_{\text{Demand}}\right) \\
\text{subject to} \quad & T_{SP,min} \leq T_{SP} \leq T_{SP,max} \\
& 0 \leq P \leq P_{max} \\
& 0 \leq P_{ETS,maxSP} \leq P_{ETS,max}
\end{aligned}
\tag{6.2}
$$

2. **Cost-function using Rate Flex M.** Equation (6.3) shows the second optimization problem used, where the variable electricity cost shown in Figure 6.4 is minimized. Equation (6.3) is a special case of Equation (6.2); however, it has an added varying energy cost term,

which is indicated with the subindex i, and has a higher cost during peak times (Table 6.1).

$$\begin{aligned} \min_{T_{SP},\, P_{ETS,maxSP}} \quad & J_{PH} = \left(\sum_{i=1}^{N} P_i \Delta t \right) \cdot \left(\text{Cost}_{\text{Energy},i}\right) + \max\left(\mathbf{P}\right) \cdot \left(\text{Cost}_{\text{Demand}}\right) \\ \text{subject to} \quad & T_{SP,min} \leq T_{SP} \leq T_{SP,max} \\ & 0 \leq P \leq P_{max} \\ & 0 \leq P_{ETS,maxSP} \leq P_{ETS,max} \end{aligned} \tag{6.3}$$

N is the number of time steps over the prediction horizon PH (24, 36, 48 hours etc.), P_i is the power demand at time i, and Δt is the time step. The objective is to identify two variables that minimize the cost associated with the utility rate charge: 1) an optimized setpoint schedule for the room temperature T_{SP}, and 2) the maximum charging power input to the ETS, $P_{ETS,maxSP}$. The temperature setpoint is constrained by a lower ($T_{SP,min}$) and upper ($T_{SP,max}$) bound, to maintain a level of thermal comfort for the zone occupants. The demand due to space heating P is constrained by the size of the heating equipment P_{max}. Similarly, the maximum charging power input to the ETS is constrained by the device specifications, $P_{ETS,max}$. MPC simulations are at 5-minute intervals to produce more detailed time granularity while optimized values are identified at 1-hour intervals, so schedule identification can be accomplished quicker.

3. **Cost-function using $BEFI$ Maximization during peak demand.** The third and final optimization problem under consideration was using $BEFI$ as the cost function. The value of $BEFI$ is to be maximized during a demand event corresponding with a peak demand period.

$$\begin{aligned} \max_{T_{SP},\, P_{ETS,maxSP}} \quad & J_{PH} = \text{avg}[P_{ref} - P_{flex}]_{,during\ DR\ event} \\ \text{subject to} \quad & T_{SP,min} \leq T_{SP} \leq T_{SP,max} \\ & 0 \leq P \leq P_{max} \\ & 0 \leq P_{ETS,maxSP} \leq P_{ETS,max} \end{aligned} \tag{6.4}$$

Equation (6.5) shows a more formal representation of the $BEFI$ (Athienitis et al., 2020).

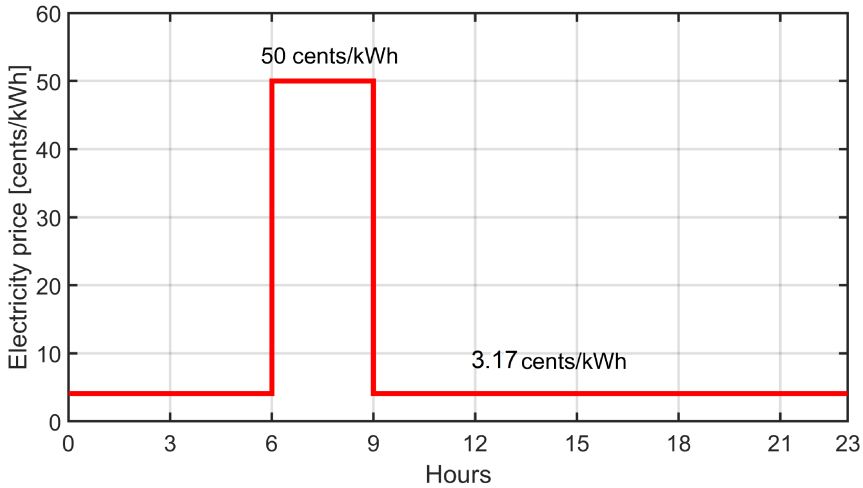

Figure 6.4: Utility rate Flex M over 24 hours

$$BEFI\,(t, \Delta t, t_{notice}) = \frac{\int_t^{t+\Delta t} P_{ref}dt - \int_t^{t+\Delta t} P_{flex}dt}{\Delta t} \tag{6.5}$$

where $BEFI$ is the Building Energy Flexibility Index, t is the start time of the event, Δt is the duration of the event, t_{notice} is time of notification for the event, P_{ref} [is power demand of reference scenario during the event, and P_{flex} [kW] is power demand of flexibility case during event. Essentially, the $BEFI$ is taken as the average difference between the power demand of the reference case, P_{ref} [kW] and the power demand of the alternative “flexibility scenario”, P_{flex} [kW], for the given event duration Δt, shown in equation 6.5. $BEFI$ could also be represented as a percentage by dividing it by the value of P_{ref}.

For the sake of simplicity, in this case the prediction and control horizons are the same length of time and MPC was only initiated with a notification signal: either 30 hours for a 12-hr ahead notification at 6p.m. or 22 hours for a 4-hr ahead notification at 2a.m. (for a DR event at 6a.m.). Further studies could be carried out on the performance related to the control horizon length, however, Date et al. (2017) found that longer control horizons (12 hours or more) were favourable for a similar building in a similar climate.

6.3.3 Weather conditions - cold winter day

MPC simulations were carried out over 10 days with a focus on the last 48-hour period, The outdoor temperature conditions are representative of very cold winter days and are shown in

Figure 6.5, ranging from -20 °C to 3 °C. As a benchmark for comparison, a business as usual (BAU) indoor temperature setpoint profile was created, with a nighttime setpoint of 18 °C and a daytime setpoint of 22 °C and can be seen in the top graph of Figure 6.6 as a dashed black line. The zone temperature setpoint is constrained by a lower bound $T_{SP,min}$ (17 °C at night and 19 °C during the day) and an upper bound $T_{SP,max}$ (24 °C at all times) to maintain a level of occupant thermal comfort. To demonstrate the methodology, typical known occupancy schedules for the warehouse (7a.m.-6p.m.) and weather data were used for this MPC study, however, an existing weather forecast tool such as CanMETEO (Natural Resources Canada, 2019) could (or should) be incorporated into eventual implementation within the BAS.

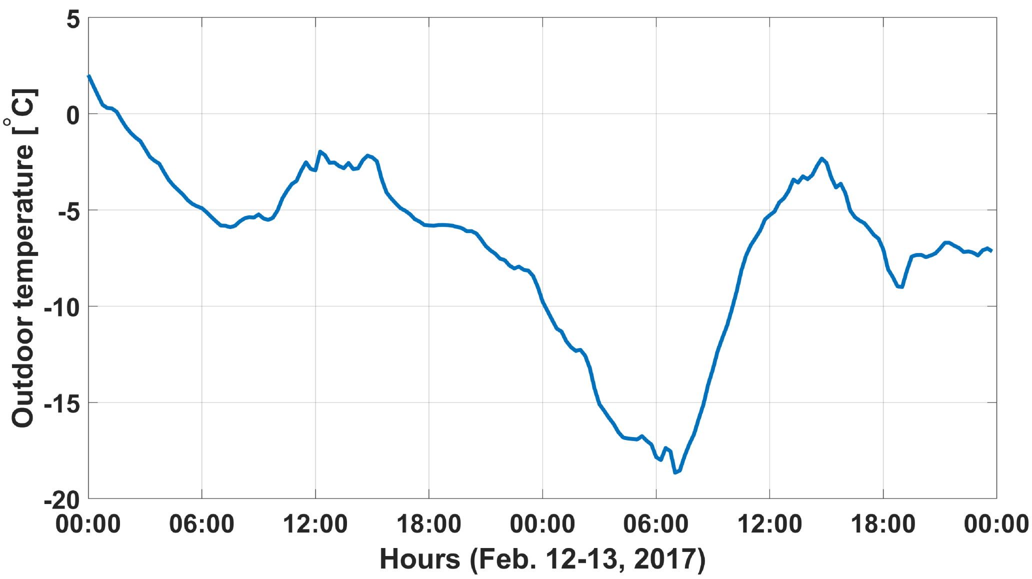

Figure 6.5: Outdoor air temperature February 12 and 13, 2017, control study on cold days

6.4 Demand response results with 12- and 4-hour notifications

Two scenarios were investigated with a notification of demand response event given ahead of time. In the first scenario, the notification is given to the building owner at 6p.m. (12-hours ahead) indicating a DR event at 6a.m. on the following day and ending at 9a.m. (for an event duration of 3 hours). The notification triggers an MPC algorithm that determines two things at each timestep: 1) an optimized zone temperature setpoint profile, and 2) an optimized maximum allowable power input for charging the ETS device. The second scenario has a notification of 4 hours ahead of the DR event, which is sent at 2a.m.

6.4.1 Predictive load management simulation

Table 6.3 shows the results from simulation for the different scenarios. The scenarios 1) BAU with ETS, 2) MPC Rate M, 3) MPC Rate Flex M, and 4) MPC $BEFI$ have been compared to the "Business as Usual (BAU)" case without ETS.

Table 6.3: MPC Simulation Results for improved operation of ETS and zone temperature setpoint on a very cold day

	BAU without thermal storage	**BAU with thermal storage**	**MPC: Rate M**	**MPC: Rate Flex M**	**MPC: $BEFI$**
12 hours ahead notification of DR event (18:00)					
Event Peak [kW] (6a.m.-9a.m.)	73	33	31	0	0
Wh/m^2 in PH	763	1170	905	1034	1321
$BEFI$ [kW] (6a.m.-9a.m.)	–	36	36	65	65
$BEFI$ [%] (6a.m.-9a.m.)	–	55	56	100	100
4 hours ahead notification of DR event (2:00)					
Event Peak [kW] (6a.m.-9a.m.)	73	33	28	25	0
Wh/m^2 in PH	659	844	641	633	945
$BEFI$ [kW] (6a.m.-9a.m.)	–	36	38	48	65
$BEFI$ [%] (6a.m.-9a.m.)	–	55	59	74	100

The first scenario with a 12-hour notification time is shown in Figure 6.6, while Figure 6.7 shows results for the case with 4 hours notification time. By carrying out MPC with active thermal storage, an increase of $BEFI$ is observed during critical peak events, as well as improved energy flexibility available to the grid. Table 6.3 shows that with a notification from the utility to the customer given at 6p.m. (12 hours ahead of a 6a.m. event) a $BEFI$ ranging from 55% to 100% is capable. This correlates to a reduction of peak demand during the critical event hours by an average of 36 kW (63%) to 65 kW (8%) for 3 hours, depending on the utility rate structure. Two identified scenarios saw that no power demand for heating was required during the critical morning hours of 6a.m. to 9a.m., resulting in a $BEFI$ of 100%.

It was found that Rate Flex M is the most advantageous for reducing the peak demand, while a greater reduction of energy consumption on a 24-hour period is seen with Rate M. A longer notification time also results in a higher $BEFI$ during the critical times, as there is more time for the MPC to identify improved operation strategies or implement preheating. When the equation for $BEFI$ is used as the objective function, favourable results for peak reduction are found and are comparable with the scenario of the Rate Flex M; however, one disadvantage is that there is no incentive to reduce energy within the objective function formulation, and thus for

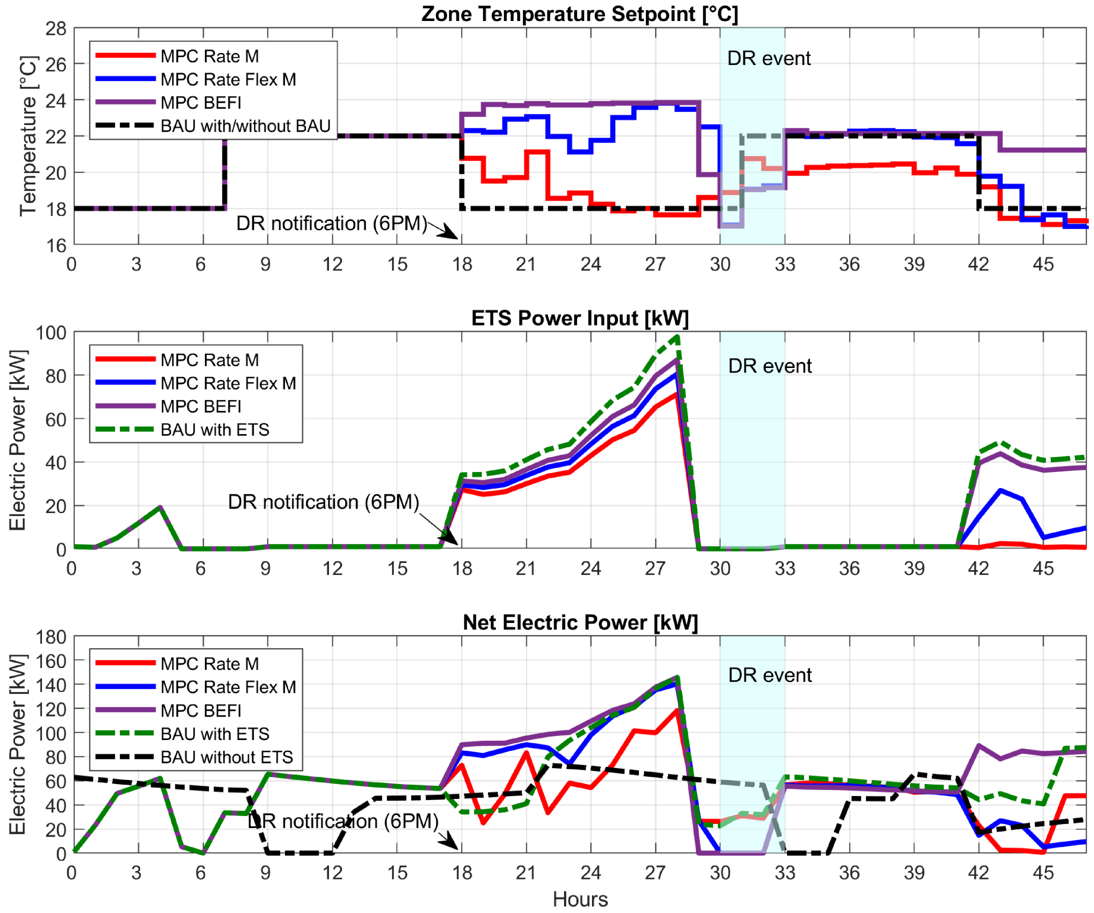

Figure 6.6: MPC utility rate study: identified zone setpoint profiles and electric power use with notification 12 hours ahead, cold winter day

this scenario a high energy consumption is observed (13% more compared to BAU with thermal storage at 1,321 Wh/m^2).

Similarly, with a relatively short notification time of 4-hours (given at 2a.m.) shown in Figure 6.7, implementing MPC can reduce the peak demand during the critical hours and a *BEFI* of up to 48 kW (74%) for 3 hours with Rate Flex M (Table 6.3) is seen. Figures 6.8 to 6.10 comparatively show the peak demand, *BEFI* [kW] and energy consumption for the control options. The results show that implementing MPC with active thermal storage and a well-chosen objective function, an increased *BEFI* and an increase in energy flexibility to the grid during critical peak events are both attainable.

Figures 6.11 and 6.12 show estimated electricity costs for a 30-day period for the warehouse section of the building. These are estimates, as the whole building experiences a peak demand between 500-600 kW on a very cold winter day, while only the warehouse section is

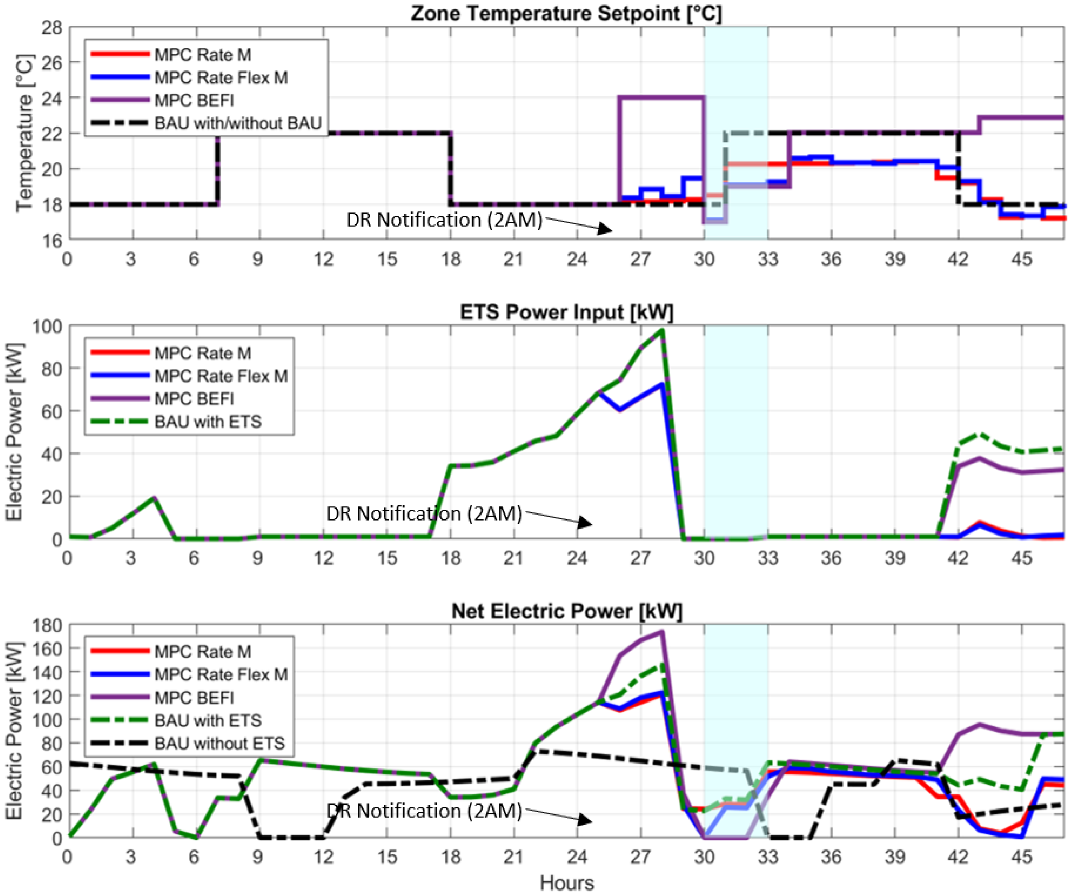

Figure 6.7: MPC utility rate study: identified zone setpoint profiles and electric power use with notification 4 hours ahead, cold winter day

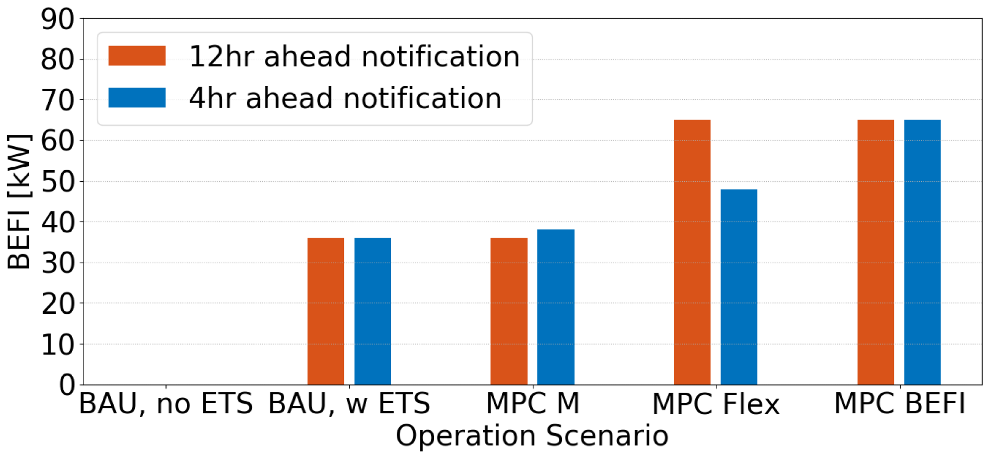

Figure 6.8: MPC study: *BEFI* during DR event, cold winter day

examined here, which experiences a peak demand of 150 kW. The two graphs help to visualize how reducing peak and/or energy consumption during the peak demand event of 6a.m.-9a.m. can affect the electricity costs incurred by the customer for the month. Details of the demand charge and energy charge components for the different utility rates and different scenarios are

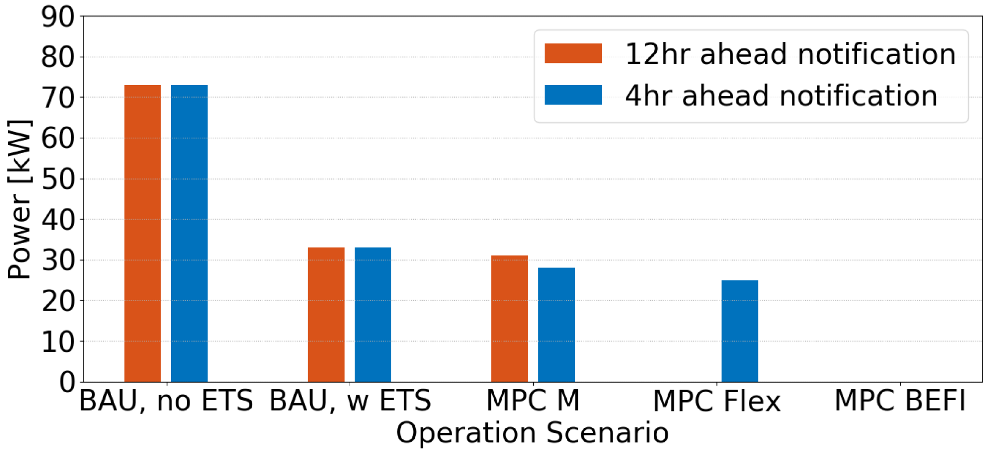

Figure 6.9: MPC study: peak demand during DR event, cold winter day

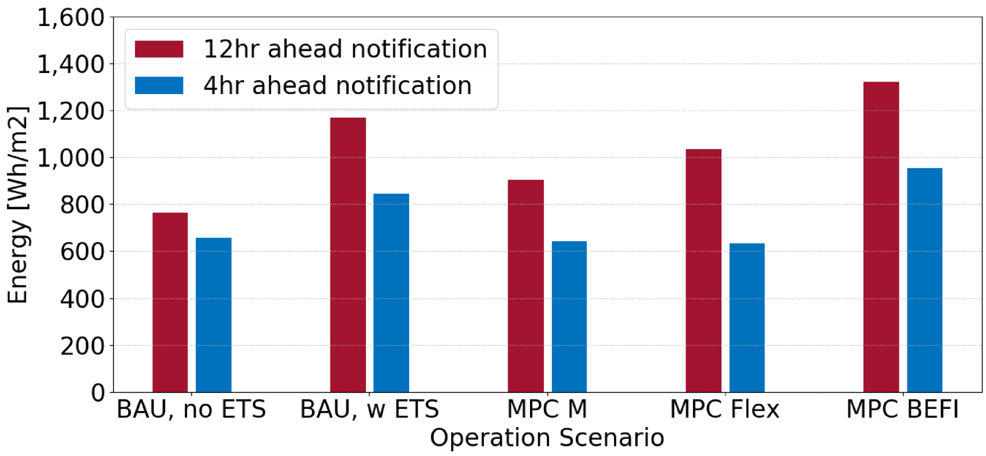

Figure 6.10: MPC study: energy use during DR event, cold winter day

shown in Tables 6.4 and 6.5.

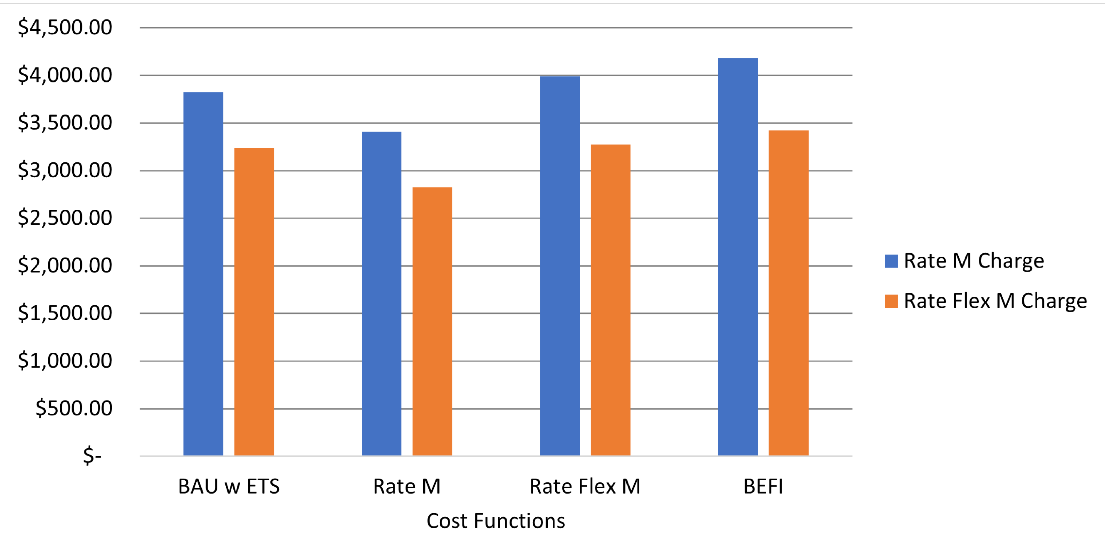

Figure 6.11: MPC study: electricity cost 30 days, 12-hour notification

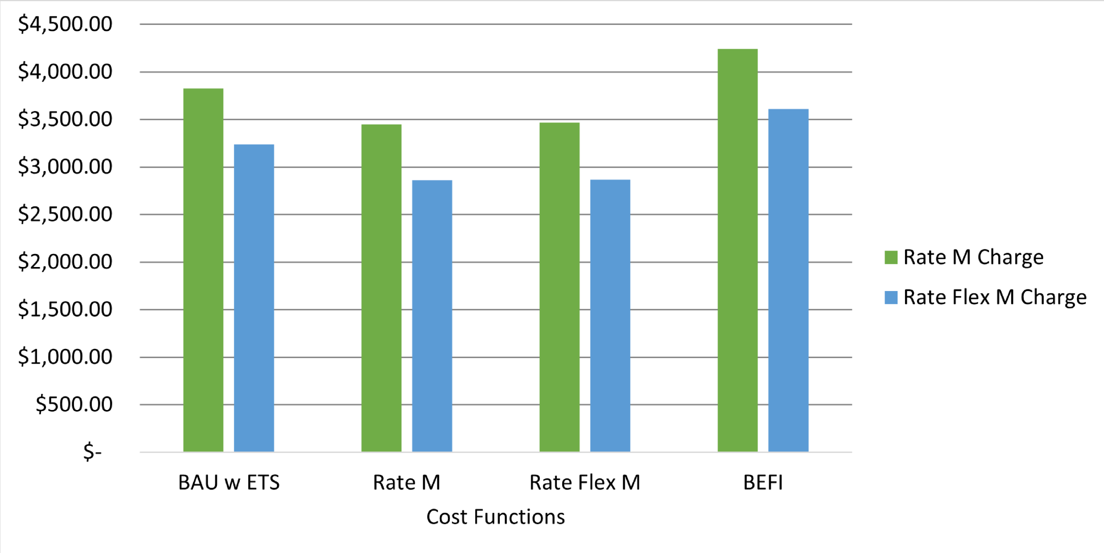

Figure 6.12: MPC study: electricity cost 30 days, 4-hour notification

Table 6.4: MPC study: electricity cost 30 days, 12-hour notification

12-hour ahead notification	**BAU no ETS**	**BAU w ETS**	**Rate M**	**Rate Flex M**	*BEFI*
Rate M Demand Charge	$ 1,064.34	$ 2,125.47	$ 1,723.74	$ 2,046.37	$ 2,123.71
Rate M Energy Charge	$ 1,416.21	$ 1,700.48	$ 1,682.72	$ 1,945.83	$ 2,061.53
Rate M Total	**$ 2,480.55**	**$ 3,825.95**	**$ 3,406.46**	**$ 3,992.20**	**$ 4,185.24**
Rate Flex M Demand Charge	$ 1,064.34	$ 2,125.47	$ 1,723.74	$ 2,046.37	$ 2,123.71
Rate Flex M Energy Charge	$ 983.66	$ 1,112.67	$ 1,100.84	$ 1,226.30	$ 1,299.21
Rate Flex M Total	**$ 2,048.00**	**$ 3,238.14**	**$ 2,824.58**	**$ 3,272.67**	**$ 3,422.92**

Table 6.5: MPC study: electricity cost 30 days, 4-hour notification

4-hour ahead notification	**BAU no ETS**	**BAU w ETS**	**Rate M**	**Rate Flex M**	*BEFI*
Rate M Demand Charge	$ 1,064.34	$ 2,125.47	$ 1,765.31	$ 1,784.29	$ 2,531.29
Rate M Energy Charge	$ 1,416.21	$ 1,700.48	$ 1,683.59	$ 1,682.91	$ 1,709.56
Rate M Total	**$ 2,480.55**	**$ 3,825.95**	**$ 3,448.90**	**$ 3,467.20**	**$ 4,240.85**
Rate Flex M Demand Charge	$ 1,064.34	$ 2,125.47	$ 1,765.31	$ 1,784.29	$ 2,531.29
Rate Flex M Energy Charge	$ 983.66	$ 1,112.67	$ 1,098.73	$ 1,084.46	$ 1,077.39
Rate Flex M Total	**$ 2,048.00**	**$ 3,238.14**	**$ 2,864.04**	**$ 2,868.75**	**$ 3,608.68**

It is observed that the utility cost to the customer can be reduced by 12-30% when compared to the BAU operation with ETS under the Rate M. When comparing BAU with ETS under Rate M to MPC with Flex Rate M as the cost function and utility rate structure, the cost can be reduced and the event peak demand is eliminated, as shown in Figure 6.9. As this problem is multi-faceted with competing objectives such as monthly energy costs, peak demand charges that can affect whole year costs, and specific peak demand event times that are pertinent to the utility, choosing the optimal strategy depends on what the main objective is, thus one strategy and/or utility pricing structure may not result in the best outcome for all the objectives under investigation. From these studies, one can make general recommendations for specific objectives: if the cost to the customer is most important then remaining with Rate M may be the most advantageous, if peak demand reduction during the peak event times is most important, then using a MPC cost function of either Flex Rate M or $BEFI$ would be recommended, but if a best compromise between those objectives is desired, it is seen that use of Flex Rate M as the utility rate and cost function results in the best compromise in (DR event) peak reduction and cost to the customer.

6.5 Shoulder season performance: cold day followed by a warm day

Shoulder season building energy performance is also an important consideration as consuming unnecessary energy on warmer days is easy to do with an inadequate or simple control strategy. When a milder shoulder-season day is on the horizon after a cold day, the thermal storage device often consumes excess energy by charging the bricks and storing more energy than needed for the next day. Currently, the ETS measures the weather once per day at 6p.m. to determine the charging amount needed during the night to store energy that is to be used the next day. When a cold day is followed by a warm day, this determined charging amount may be unnecessary and excess electricity would be used to store thermal energy when the actual required thermal energy for space conditioning for the next day is lower. Energy use could be improved by incorporating weather forecasts into the decision-making process for establishing the charging input amount. An example of a cold day followed by a warm day during the shoulder season is shown in Figure 6.13, where at 6p.m. the outdoor temperature is below 0 °C, while it is seen that the next day is warmer going up to 10 °C.

Results of the shoulder season MPC study are shown in Figure 6.14 and Table 6.6. The studies evaluate the performance using the three previously studied objective functions (Rate M, Rate Flex M and $BEFI$) with notifications at 12-hour and 4-hour ahead of an event. It is seen that even a milder shoulder-season day can benefit from well thought out MPC strategies, where energy consumption can be lowered by up to 43% and a $BEFI$ of up to 100% can be achieved. It is seen that both Rate M and Rate Flex M give improved results, however, an objective function

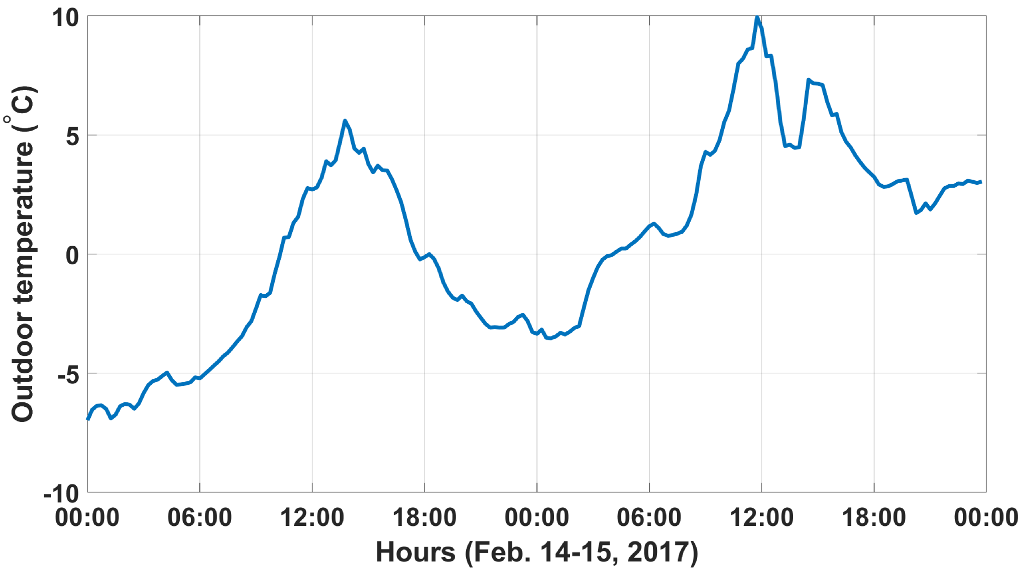

Figure 6.13: Control study on cold day followed by a warm day: outdoor air temperature February 14 and 15, 2017

Table 6.6: MPC Simulation Results for improved operation of ETS and zone temperature setpoint on a warmer shoulder season day

	BAU without thermal storage	**BAU with thermal storage**	**MPC: Rate M**	**MPC: Rate Flex M**	**MPC: *BEFI***
12 hours ahead notification of DR event (18:00)					
Event Peak [kW] (6a.m.-9a.m.)	65	31	25	25	0
Wh/m^2 in *PH*	490	454	389	386	614
BEFI [kW] (6a.m.-9a.m.)	–	25	41	41	57
BEFI [%] (6a.m.-9a.m.)	–	55	68	75	100
4 hours ahead notification of DR event (2:00)					
Event Peak [kW] (6a.m.-9a.m.)	65	31	26	24	0
Wh/m^2 in *PH*	456	443	259	328	395
BEFI [kW] (6a.m.-9a.m.)	–	25	41	41	57
BEFI [%] (6a.m.-9a.m.)	–	55	71	72	100

of $BEFI$ increases energy consumption and is not suitable for this type of day, where the primary objective is to better manage or reduce energy consumption.

6.6 Accounting for prediction uncertainty

To better assess the risk in operation options, it is useful to present to decision-makers the range of reasonable operating predictions that may results when accounting for the uncertainties related to weather forecasting and the identified model parameter values. It has been observed that uncertainty in weather forecasts can be as high as 30% and modelling uncertainty can be in that range as well.

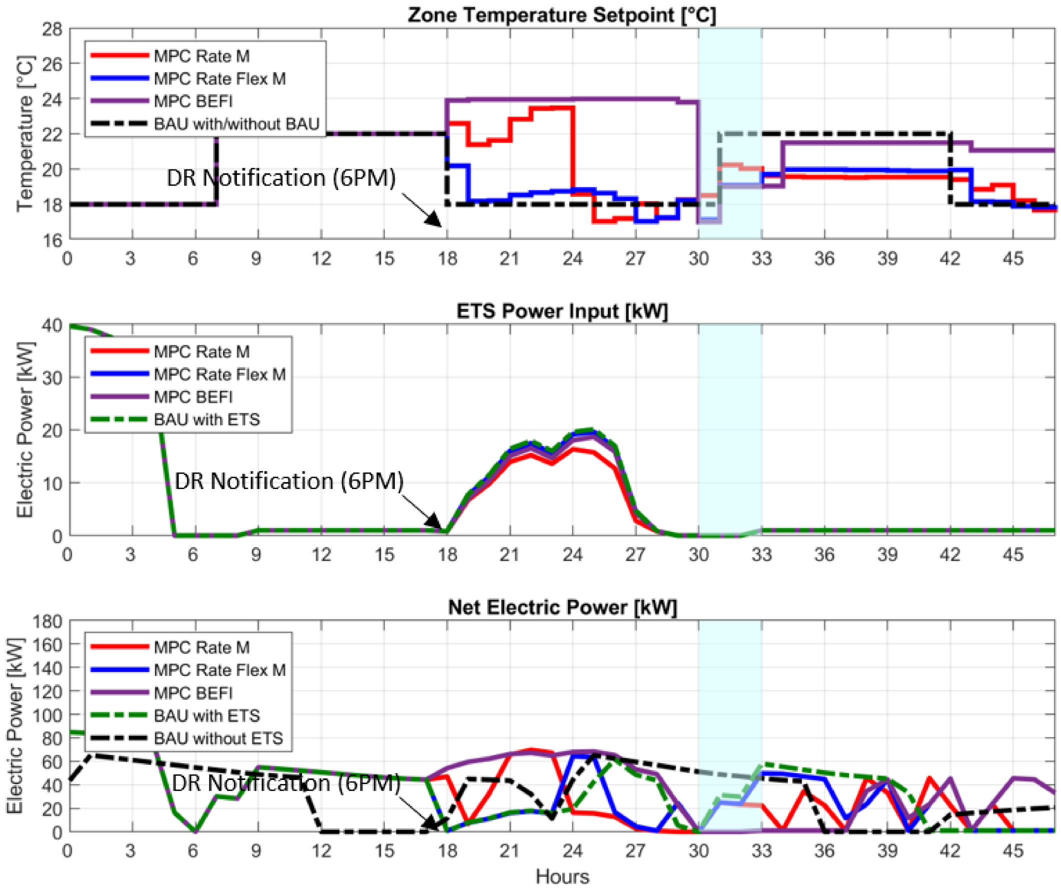

Figure 6.14: MPC utility rate study: identified zone setpoint profiles and electric power use with notification 12 hours ahead, warm shoulder season day

Six scenarios have been evaluated that incorporate combinations of $\pm 10\%$ deviation from the identified brick conductivity and $\pm 3°C$ deviation from the weather forecast (Date et al., 2020a). These six scenarios were carried out for the three different cost functions (Rate M, Rate Flex M and $BEFI$) at the two notification times (12-hour and 4-hour), resulting in a total of 36 cases under evaluation.

Figures 6.16 to 6.20 can aid one to make a more informed decision on whether utilizing a more advanced control strategy (in this case MPC) can be favourable and whether there is an appropriate risk level. Figure 6.20 illustrates the example of varying net electric power depending on the weather forecast and identified model parameter k_{brick} accuracy when an operating schedule has been identified using the objective function Rate Flex M. The grey area on the graph is a set of possible trajectories of the net power curve. Using this type of visualization and evaluation for decision-making by building operators/owners and the utility grid would allow a better understanding of expected variations due to the uncertainties of the scenario. Future work

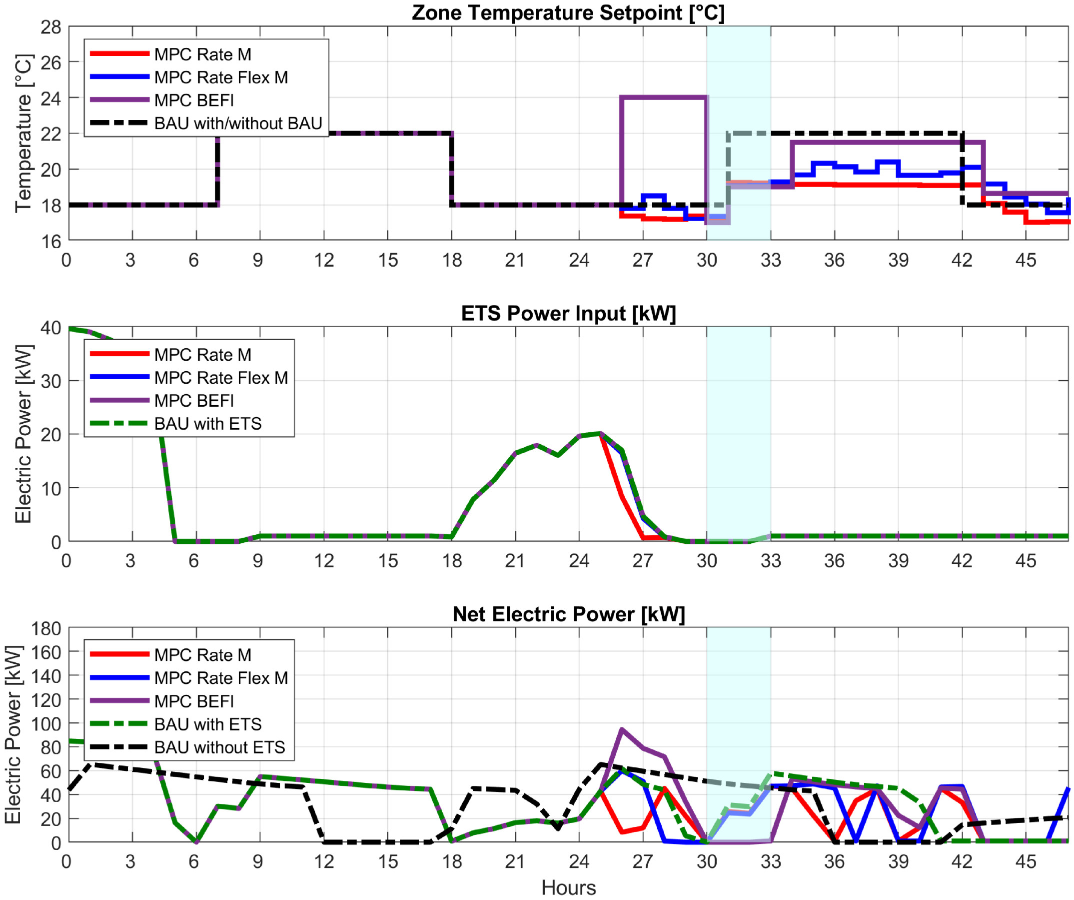

Figure 6.15: MPC utility rate study: identified zone setpoint profiles and electric power use with notification 4 hours ahead, warm shoulder season day

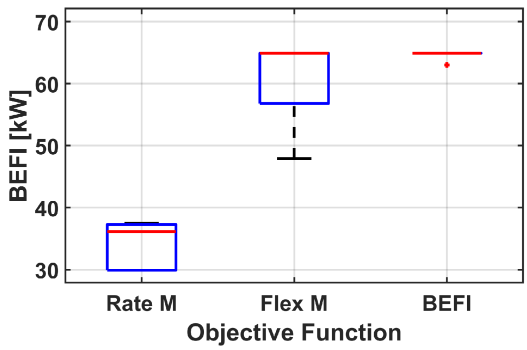

Figure 6.16: Uncertainty of $BEFI$ predictions: 12-hr ahead notification, cold winter day

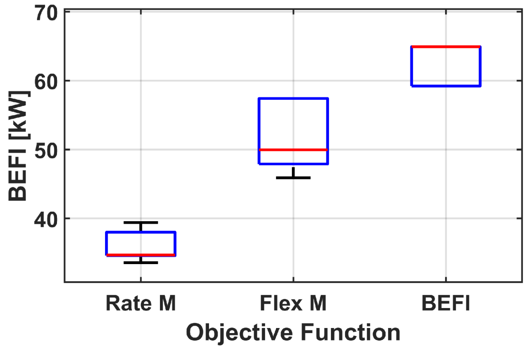

Figure 6.17: Uncertainty of $BEFI$ predictions: 4-hr ahead notification, cold winter day

could include incorporating an existing weather forecasting tool into the methodology, such as CanMETEO (Natural Resources Canada, 2019), to further evaluate the effects of weather uncertainty on MPC performance.

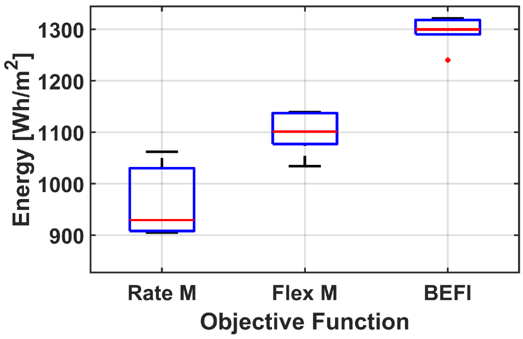

Figure 6.18: Uncertainty of Energy predictions: 12-hr ahead notification, cold winter day

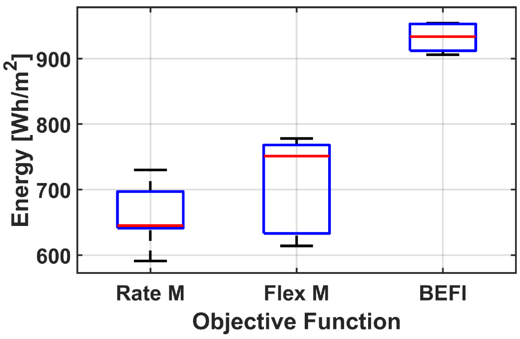

Figure 6.19: Uncertainty of Energy predictions: 4-hr ahead notification, cold winter day

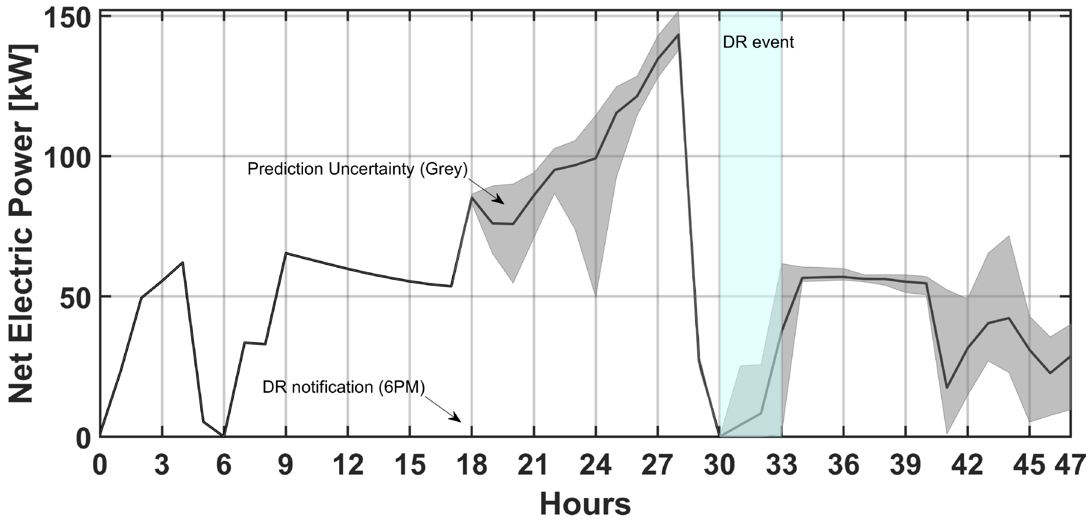

Figure 6.20: Uncertainty of *BEFI* predictions: net electric power prediction for scenario with MPC Rate Flex M, cold winter day

6.7 Contingency event evaluation

The contingency reserve is an amount of power the utility may call from its customers when needed to face the loss of a generation unit or other unexpected load imbalance. Usually this is requested very close to the demand event (15 minutes before), while a flexibility control event could be given more notification time. To address this need from the grid, real-time thermal building load flexibility should be predicted ahead of time or calculated continuously and available at short notice (e.g., 10 minutes) over a time duration of about an hour or a few hours.

This energy flexibility can be unlocked by certain actions in response to a signal from the grid. This section calculates the $BEFI$ (kW and %) to quantify real-time thermal load flexibility of the building. A preliminary contingency study on a school building was introduced in Athienitis et al. (2020), while two strategies suitable for this building equipped with dedicated thermal storage are analyzed here: 1) reducing the zone temperature setpoint for 3 hours, and 2) discharging the thermal storage device for 3 hours.

The developed model is to determine the power demand difference between the reference case (BAU, no ETS) when the two contingency strategies outlined in the previous paragraph are enabled and quantify the energy flexibility potential.

First contingency strategy: lower zone temperature setpoint. The first contingency strategy is shown in Figure 6.22, where the temperature setpoint for the warehouse zone is reduced by 2 °C for 3 hours (Figure 6.21). It was found that the $BEFI$ varies from 0 kW up to 47 kW (or 0% up to 100%). The $BEFI$ in this scenario is dependent on the time of day due to the operation of the reference case which incorporates a nighttime setback in the zone temperature schedule.

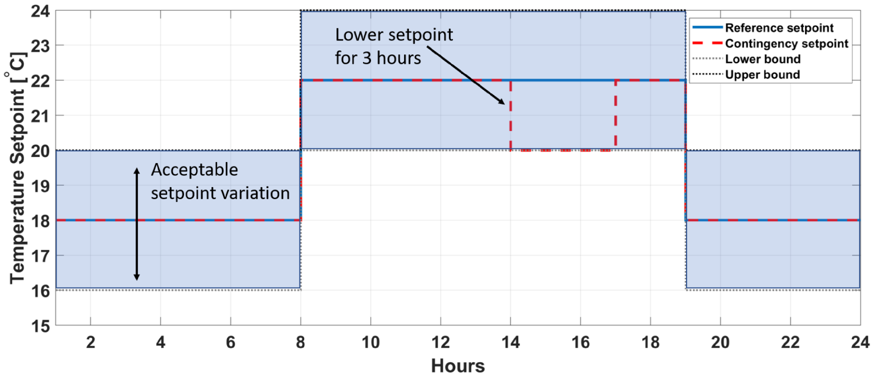

Figure 6.21: Contingency strategy 1) reduce zone temperature setpoint for a duration of 3 hours at each hour - $BEFI$ at hourly intervals

Second contingency strategy: Use thermal storage device. When the second strategy of discharging heat from the thermal storage device for durations of 3 hours is implemented, the $BEFI$ was 0 up to 41 kW (or 0 to 100%), shown in Figure 6.23. Positive results were calculated for both contingency strategies, where a maximum $BEFI$ of 47 kW (97%) can be achieved for a duration of 3 hours. The highest $BEFI$ values are seen at the start of the day when there is the biggest potential to reduce peaks due to the current abrupt setpoint change from night setback to daytime comfort levels. A zero value for $BEFI$ is seen in the evening due to the setpoint change

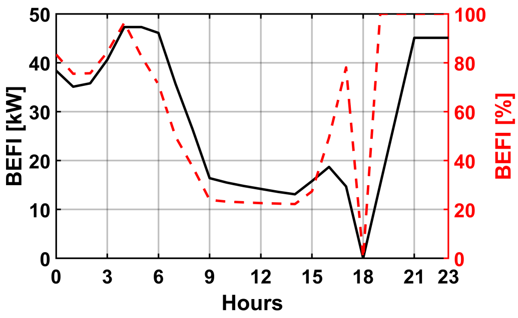

Figure 6.22: Contingency strategy 1) reduce zone temperature setpoint for a duration of 3 hours at each hour - $BEFI$ at hourly intervals

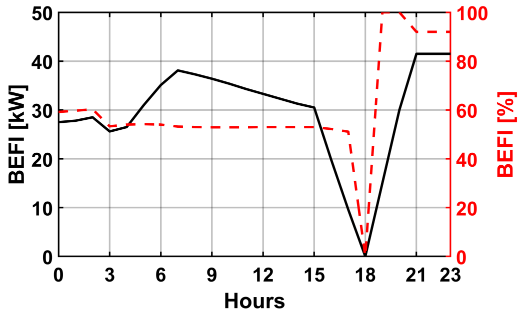

Figure 6.23: Contingency strategy 2) discharge ETS for a duration of 3 hours at each hour - $BEFI$ at hourly intervals

back to the nighttime setback value. There is zero heating demand with current operation, and thus the power cannot be lowered any further as the zone air temperature is free-floating until it reaches the lower nighttime value.

6.8 Conclusion

This chapter presented the developed methodology for implementing MPC strategies for space heating to a warehouse zone equipped with a dedicated active thermal storage device. The goal was to predict and maximize the Building Energy Flexibility the building could provide to the electric grid by evaluating the $BEFI$ for the different strategies. Three MPC cost functions were studied: 1) the minimization of electricity cost subject to a utility rate with peak demand charge (Rate M), 2) the minimization of electricity cost subject to a utility rate with dynamic pricing (Rate Flex M), and 3) the maximization of $BEFI$ during the critical DR event.

The two notification times of four and 12 hours ahead of a DR event with set duration were analyzed, and an MPC routine was implemented at hourly intervals to identify two schedules: 1) an optimized zone temperature setpoint profile and 2) an optimized dynamic maximum allowable power input for charging the ETS. MPC with thermal storage was shown to increase $BEFI$ and provide energy flexibility to the grid during peak times and can perform superior to manual BAU control. As an example, a $BEFI$ of 55% to 100% is achieved when the notification from the utility to the customer is 12 hours ahead of a 6a.m. event. Depending on the objective function, this means that the average demand during the critical times can be reduced by an amount between 36 kW (55%) and 65 kW (100%). It was found that Rate Flex M is more effective in reducing the peak demand, while Rate M achieves a greater reduction of energy consumption on a 24-hour period. When the equation for $BEFI$ is used as the objective function peak reduction is found that are comparable with the scenario of the Rate Flex M, however, one disadvantage is there is no incentive to reduce energy, and thus this scenario consumes the most. Optimizing not only the zone profile is important as well as optimizing (limiting) the maximum allowable power to the thermal storage device aids in reducing both peak demand and energy consumption of the building.

It should be noted that thermal comfort conditions of the zone are different than that of BAU case for the different scenarios are different and that should be weighed when choosing a strategy. Since the zone in this study is a warehouse, it could be argued that there is more room for flexibility in the comfort limits compared with an office or residential building.

It is observed that the utility cost to the customer can be reduced by 12-30% when compared to the BAU operation with ETS under the Rate M. When comparing BAU with ETS under Rate M to MPC with Flex Rate M as the cost function and utility rate structure, the cost can be reduced and the event peak demand is eliminated, as shown in Figure 6.9. As this problem is multi-faceted with competing objectives such as monthly energy costs, peak demand charges that can affect whole year costs, and specific peak demand event times that are pertinent to the utility, choosing the optimal strategy depends on what the main objective is, thus one strategy and/or utility pricing structure may not result in the best outcome for all the objectives under investigation. From these studies, one can make general recommendations for specific objectives: if the cost to the customer is most important then remaining with Rate M may be the most advantageous, if peak demand reduction during the peak event times is most important, then using a MPC cost function of either Flex Rate M or $BEFI$ would be recommended, but if a best compromise between those objectives is desired, it is seen that use of Flex Rate M as the utility rate and cost function results in the best compromise in (DR event) peak reduction and cost to the customer.

Uncertainty of prediction results due to variations in weather forecasts and model parameter uncertainty was also evaluated. Six scenarios of $\pm 10\%$ deviation from the identified brick conductivity and $\pm 3°C$ deviation from the weather forecast were considered for the cost functions of Rate M, Rate Flex M and $BEFI$.

A building equipped with dedicated active thermal storage is a compelling contender for participating in contingency events. The strategies studied for contingency reserve were 1) reducing the zone temperature setpoint temperature by 2 °C for 3 hours, and 2) using the stored thermal energy in the dedicated thermal storage device by discharging the device for 3 hours. Encouraging results were found, where a $BEFI$ of up to 47 kW (97%) is achieved for 3 hours.

Future work could include using this methodology to design optimal utility pricing structures, rather than the design optimal control strategies. This methodology could be used for other similar convectively conditioned buildings and clusters of buildings for participation in community-scale energy aggregator events. A greater focus on occupancy modelling could eventually be incorporated into this methodology. There is still work to be done in terms of implementation of the methodology into real Building Energy Management Systems.

Chapter 7

Conclusion

This thesis explored the development of a methodology for modelling buildings and zones with convective heating systems and a dedicated active high-temperature thermal storage device. The models were also used within studies on model predictive control and building energy flexibility strategies to improve building-grid interaction in the context of Québec winter (heating season) operation of buildings equipped with convective heating systems.

A multi-level thermal building modelling methodology was developed and tested on a residential case study and commercial building case study. Extensive research was done to develop suitable reduced order (and detailed) thermal models for an active thermal storage device (ETS), where different concepts such as "model reset", fast order reduction and evaluation and "effective" model parameters were presented. A methodology suitable for testing and implementation of MPC, including building energy flexibility potential evaluation and uncertainty analysis was presented and outlined in Chapter 6. A new useful index called the Building Energy Flexibility Index ($BEFI$) was developed in collaboration with several colleagues and industry partners and was explained and show-cased in a simulation study.

The "grey-box" resistance-capacitance (RC) thermal network modelling approach was the focus for the developed reduced-order models suitable for control applications. Using the explicit finite difference method and incorporating calibration techniques, a multi-level modelling approach was developed for a detached residential home, and several other models for commercial buildings and an active thermal energy storage device were developed, investigated, and used in simulation-based improved heuristic and predictive control studies. Lastly, the Building Energy Flexibility Index ($BEFI$) was introduced, and different flexibility and contingency studies were evaluated and presented.

The main approach for modelling heat transfer in the enclosure (building or zone) is a low-order lumped parameter explicit finite difference method which can incorporate parameter calibration and/or parameter identification techniques, such as optimization. The control-oriented models for building zones and thermal storage devices are based on one- or two-dimensional lumped parameter equations for heat conduction and energy conservation. These models use a grey-box modelling approach, in which physically meaningful parameters can be calibrated with measured data or identified using optimization techniques. As reduced-order thermal models are often custom-made using general-purpose mathematical programming tools, which offer flexibility compared to commercial simulation tools, the programming languages MATLAB and Python were used in this work.

The developed methodology includes several steps. First, data from a real building should be collected and analyzed. Choosing appropriate typical buildings and sensor points are integral steps of the methodology, for the eventual creation of generalized archetypical models. The building envelope elements of the building (walls, floor, ceiling) are represented as a thermal network of resistances and capacitances. Internal partitions should also be included if they have considerable thermal mass. The level of model complexity of the network will depend on each case. Physics-based models of important HVAC elements (convective systems in this case) were developed. These models are physics-based ROM grey-box RC thermal networks. Calibration of model parameters is carried out either manually or effective parameters are identified using an optimization routine. Calibration of these models was carried out using the collected data from the first step. The gradient descent-based optimization function *fmincon* in MATLAB or SLSQP in Python was used to identify important parameter values. Model-based operational strategies were tested and developed using the developed thermal models for better load management and/or improved occupant comfort. Heuristic approaches were compared to optimized control MPC using *fmincon* in MATLAB for some of the case studies. In the last case study, model prediction uncertainty due to identified model parameters and the weather forecast was accounted for by evaluating various uncertainty scenarios and plotting the uncertainty bounds for the duration of the identified operation schedule. Contingency strategies were evaluated (on one case study) to quantify the energy flexibility available from the building to the grid at specific times.

The study on the residential building outlined a methodology for multi-level control-oriented modelling for buildings with several zones. This multi-level approach allows the user to "zoom in and out" so that models at each control level remain manageable, easy to calibrate and easy to physically interpret. A global low-order model (1R1C) was developed and used to rapidly calculate the thermal load of the building, while a very detailed benchmark floor-level model was developed and can be used for verification and MPC-based simulation studies. For the development of specific control algorithms for each zone, an adequate simplified zone-level model must be identified. It was found that if zone-level accuracy is of importance, one must incorporate into the model the thermal mass of the structure between zones. It was found that a 1R1C whole-house model can perform well for either longer horizon or short ones, but not simultaneously for both. Frequency analysis was used to quickly evaluate the whole building models without the need to perform a simulation. Interesting differences emerged in the phase angle predicted by the different models. Work remains to be done on how to improve the guidelines for the initial guess of the grey-box model parameters.

In another case study, a small commercial bank building, an example of implementing MPC in a conventional building (a building of basic construction, systems, and technologies) to reduce the yearly utility bill and avoid the summer peak load penalty given to the customer was presented. Through the software program Simulink, two cost functions were studied with different control and prediction horizons. The cost function aimed to minimize the utility rate during each prediction horizon while meeting upper and lower indoor temperature constraints. Through a parametric study, it was seen that longer control horizons (greater than six hours), produced better results for this building. A cost savings of 25% on the yearly electric utility bill and a peak power reduction of 38% were achieved, by implementing a new optimized temperature schedule for the building every 12 hours. The main difference between the typical operation temperature schedule and the optimized setpoint schedule is a preheating of the building in the few hours prior to the start of occupation. With the new optimized operation, the cost per square meter for the bank would change from \$30.19/m^2 to \$22.57/m^2, or a yearly savings of \$7.62/m^2.

The last case study that was looked at in this thesis comprises a 1650 m^2 warehouse facility equipped with a dedicated active high-temperature thermal energy storage device. A general methodology was presented for the development and analysis of control-oriented models for the enhancement of operation of an electric thermal storage device (ETS) and energy use within a building. The modelling results for the different operating conditions – the heat transfer to bricks and heat transfer from bricks to airflow – show that even a low-resolution thermal model with 1-capacitance, which represents all the brick medium, could be adequate for the control to optimize charging and discharging of the ETS device. The 1-capacitance model can predict the temperature of the bricks over several days with an average difference of 58 °C between modelled brick temperature and measured brick temperature, while with the 140-capacitance model an average difference of 27 °C was observed. Incorporating periodic model reset, based on measured sensor data values, significantly improves the model performance. As an example, the RMSE is reduced from 58 °C to 18 °C for the 1-capacitance model when the model reset is integrated into the model methodology for control.

The concept of "effective" brick conductivity was also examined, and the conductivity changes based on the detail level of the ETS model (i.e., the number of brick nodes). By having an "effective" brick conductivity that varies according to the number of brick nodes in the model, the error can be reduced in the low-resolution models. In other words, simpler models can be used if an "effective" conductivity is applied. By using a 1-capacitance model with model reset and applying an "effective" value for the brick conductivity, the RMSE is 24 °C and the MAE is 18 °C, which are comparable to the errors of the 140-capacitance model where model reset is not incorporated (RMSE of 27 °C, MAE of 22 °C and an infinity norm of 70 °C). Combining the two concepts of model reset and "effective" brick conductivity, low-resolution models that are fast and easy to develop are robust contenders for control-oriented applications such as Model Predictive Control.

Lastly, the developed methodology for implementing MPC strategies for space heating to a warehouse zone equipped with a dedicated active thermal storage device was presented. The goal was to predict and maximize the Building Energy Flexibility the building could provide to the electric grid by evaluating the $BEFI$ for the different strategies. Three MPC cost functions were studied: 1) the minimization of electricity cost subject to a utility rate with peak demand charge (Rate M), 2) the minimization of electricity cost subject to a utility rate with dynamic pricing (Rate Flex M), and 3) the maximization of $BEFI$ during the critical DR event. The two notification times of four and 12 hours ahead of a DR event with set duration were analyzed, and an MPC routine was implemented at hourly intervals to identify two schedules: 1) an optimized zone temperature setpoint profile and 2) an optimized dynamic maximum allowable power input for charging the ETS. MPC with thermal storage was shown to increase $BEFI$ and provide energy flexibility to the grid during peak times and its performance is superior to manual BAU control. As an example, a $BEFI$ of 55% to 100% is achieved when the notification from the utility to the customer is 12 hours ahead of a 6a.m. event. Depending on the objective function, this means that the average demand during the critical times can be reduced by an amount between 36 kW (55%) and 65 kW (100%). It was found that Rate Flex M is more effective in reducing the peak demand, while Rate M achieves a greater reduction of energy consumption on a 24-hour period. When the equation for $BEFI$ was used as the objective function peak reduction was found that are comparable with the scenario of the Rate Flex M, however, one disadvantage found was that there is no incentive to reduce energy, and thus this scenario consumes the most. Optimizing not only the zone profile is important as well as optimizing (limiting) the maximum allowable power to the thermal storage device aids in reducing both peak demand and energy consumption of the building. A building equipped with dedicated active thermal storage is a compelling contender for participating in contingency events. The strategies studied for contingency reserve were 1) reducing the zone temperature setpoint temperature by 2 °C for 3 hours, and 2) using the stored thermal energy in the dedicated thermal storage device by discharging the device for 3 hours. Encouraging results were found, where a $BEFI$ of up to 47 kW (97%) is achieved for 3 hours.

7.1 Contributions

The major contributions from this thesis are listed below:

- Development of a comprehensive methodology for modelling of typical Québec buildings and zones with convective heating systems and a dedicated active high-temperature thermal storage device during winter operation.

- Development and evaluation of a multi-level simplified linear thermal modelling approach based on the electrical analogy for the development of control strategies in conventional detached residential homes equipped with convective electric heating systems.
- MPC evaluation using Québec utility rates to improve peak demand, lower consumption and lower utility costs for the customer.
- Development of a control-oriented model of an electrically heated thermal energy storage device (ETS).
- Introduction of the concepts of "model reset" and targeted "effective" model parameter values.
- Development of a new index, Building Flexibility Index ($BEFI$), to be used to evaluate potential flexibility control scenarios for improved building-grid interaction. This was a collaborative effort with Hydro-Quebec researchers, my supervisor, and other students in the lab.
- Predictive control strategies for very cold days were identified for improved management of peak loads and building energy flexibility. The $BEFI$ was quantified depending on when a notification signal is given to the building owner from the utility.
- Model prediction uncertainty associated with the weather forecast and identified model parameters is accounted for by evaluating numerous uncertainty scenarios and visually presenting the uncertainty bounds.
- Contingency strategies were assessed to quantify the available energy flexibility for the grid by the building at specific times.

7.1.1 Publications

The published papers from this thesis, as well as the papers that are under development and a contribution to the ASHRAE Applications Handbook, are listed below:

Journal articles:

1. **Date, J.**, Candanedo, J. A., & Athienitis, A. K. (2021). A methodology for the enhancement of the energy flexibility and contingency response of a building through predictive control of passive and active storage. *Energies*, 14(5).

2. **Date, J.**, Candanedo, J. A., Athienitis, A. K. & Lavigne, K. (2020) Development of reduced order thermal dynamic models for building load flexibility of an electrically-heated high temperature thermal storage device, *Science and Technology for the Built Environment*, 26:7, 956-974, DOI: 10.1080/23744731.2020.1735260

3. Candanedo, J.A., Athienitis, A. K., Delcroix, B., Saberi, A., John, C., Morovat, N., **Date, J. A.**, Vallianos, H. C. (*In Progress*). Towards a methodology for the development of grey-box control-oriented models for building operation. *Science and Technology for the Built Environment*.

Refereed conference papers:

1. **Date, J. A.**, Candanedo, J. A., Athienitis, A. K., and Lavigne, K. (2021). Energy flexible building: predictive load management of passive and active energy storage under a demand response program. In *Proceedings of eSIM 2020/2021 Conference*, Vancouver, BC (Virtual).

2. Athienitis, A. K., Dumont, E., Morovat, N., Lavigne, K., and **Date, J.** (2020). Development of a dynamic energy flexibility index for buildings and their interaction with smart grids. In *Proceedings of ACEEE Summer Study 2020 Conference*, Virtual.

3. **Date, J. A.**, Candanedo, J. A., Athienitis, A. K., and Lavigne, K. (2018). Control-Oriented Modeling of an Air-Based Electric Thermal Energy Storage Device. In *Proceedings of ASHRAE Conference 2018*. Chicago, Illinois.

4. **Date, J. A.**, Candanedo, J., and Athienitis, A. K. (2017). Predictive setpoint optimization of a commercial building subject to a winter demand penalty affecting 12 months of utility bills. In *Proceedings of Building Simulation 2017*. San Francisco, California.

5. **Date, J. A.**, Candanedo, J., and Athienitis, A. K. (2016). Control-oriented modelling of thermal zones in a house: a multi-level approach. In *Proceedings of 4th International High-Performance Buildings Conference at Purdue*. West Lafayette, IN.

6. **Date, J. A.**, Candanedo, J., Athienitis, A. K., and Fournier, M. (2016). Simplified multi-zone thermal modelling of a house for demand reduction & control applications. In *Proceedings of CLIMA 2016 Conference*. Aalborg, Denmark.

Chapter Section of ASHRAE Handbook:

1. American Society of Heating Refrigerating and Air-Conditioning Engineers (2019). Section 3.9 Predictive HVAC Control Strategies. In *ASHRAE Handbook—HVAC Applications*, Chapter 43 Supervisory Control Strategies and Optimization, pages 43.39–43.40. Atlanta, Ga.

7.2 Recommendations for future work

Work remains to be done on how to improve the guidelines for the initial guess of the grey-box model parameters. As there is no standard software available to test and develop control strategies in buildings (Candanedo et al., 2013), Simulink, or a similar tool with a graphical interface, may be an option for this problem. In theory, once a flexible and robust structure has been established for the connections between the weather forecast, the control model and the building simulation, Simulink (or another suitable alternative) could be used to rapidly test MPC in different buildings (via simulation) by easily swapping out control models and building models within the Simulink file. However, much work is still needed to improve the user-friendliness and flexibility of this approach. For example, considerable care is needed in keeping track of time scales of the various data. The weather data, control model time step, identified schedule time step, and building simulation time step may all be different and thus proper time synchronization is crucial for obtaining reliable MPC simulation results.

Further development of an ETS model for wider use (TRNSYS, Modelica etc.) and work should be done to expand the model to be suitable for the hydronic version of the ETS device. Within the developed methodology, incorporation of real weather forecast into uncertainty study and visualization (e.g., CanMETEO (Natural Resources Canada, 2019)) aspects should be considered. There is much interest in building cluster studies in terms of building energy flexibility studies, thus the methodology should be expanded and generalized for assessment of $BEFI$ for larger buildings, building clusters, neighbourhood feeders, etc. Further work into automating the model development and continuous calibration of control-oriented grey-box models is a worthy topic for future research. Lastly, this problem set up could be used for evaluating or identifying new electric utility rate structures that would encourage the use of model predictive control by utility customers, and/or further improve demand response performance.

List of References

Aduda, K. O., Labeodan, T., Zeiler, W., Boxem, G., & Zhao, Y. (2016). Demand side flexibility: Potentials and building performance implications. *Sustainable Cities and Society*, 22, 146–163.

Afram, A. & Janabi-Sharifi, F. (2014). Theory and applications of hvac control systems – a review of model predictive control (mpc). *Building and Environment*, 72, 343–355.

Afram, A., Janabi-Sharifi, F., Fung, A. S., & Raahemifar, K. (2017). Artificial neural network (ANN) based model predictive control (MPC) and optimization of HVAC systems: A state of the art review and case study of a residential HVAC system. *Energy and Buildings*, 141, 96 – 113.

Afroz, Z., Shafiullah, G., Urmee, T., & Higgins, G. (2018). Modeling techniques used in building hvac control systems: A review. *Renewable and Sustainable Energy Reviews*, 83, 64–84.

American Society of Heating Refrigerating and Air-Conditioning Engineers" (2009). *Ashrae Handbook: Fundamentals*. Atlanta, Ga: Ashrae.

Arnold, K., Gosling, J., & Holmes, D. (2005). *The Java programming language*. Addison Wesley Professional.

Arroyo, J., Spiessens, F., & Helsen, L. (2020). Identification of multi-zone grey-box building models for use in model predictive control. *Journal of Building Performance Simulation*, 13(4), 472 – 486.

ASHRAE (2020). *Smart Grid Application Guide: Integrating Facilities with the Electric Grid*. ASHRAE.

ASHRAE: American Society of Heating Refrigerating and Air-Conditioning Engineers (2009). *ASHRAE Handbook: Fundamentals*. Atlanta, GA: ASHRAE.

Athienitis, A. & O'Brien, W. (2014). *Modelling, Design, and Optimization of Net-Zero Energy Buildings*. Wiley.

Athienitis, A., Stylianou, M., & Shou, J. (1990a). Methodology for building thermal dynamics studies and control applications. *ASHRAE Transactions*, (pp. 839 – 848).

Athienitis, A., Stylianou, M., & Shou, J. (1990b). A methodology for building thermal dynamics studies and control applications. *ASHRAE Transactions*, 96.

Athienitis, A., Sullivan, H., & Hollands, K. (1986). Analytical model, sensitivity analysis, and algorithm for temperature swings in direct gain rooms. *Solar Energy*, 36(4), 303 – 312.

Athienitis, A., Sullivan, H., & Hollands, K. (1987). Discrete fourier series models for building auxiliary energy loads based on network formulation techniques. *Solar Energy*, 39(3), 203 – 210.

Athienitis, A. K., Dumont, E., Candanedo, J. A., Morovat, N., Lavigne, K., & Date, J. (2020). Development of a dynamic energy flexibility index for buildings and their interaction with smart grids. *Proceedings of ACEEE Summer Study 2020 Conference*.

Athienitis, A. K. & Santamouris, M. (2002). *Thermal Analysis and Design of Passive Solar Buildings*. London, UK: James & James.

Bacher, P. & Madsen, H. (2011). Identifying suitable models for the heat dynamics of buildings. *Energy and Buildings*, 43(7), 1511 – 1522.

Badiei, A., Allinson, D., & Lomas, K. (2019). Automated dynamic thermal simulation of houses and housing stocks using readily available reduced data. *Energy and Buildings*, 203, 109431.

Baetens, R., De Connick, R., Jorissen, F., Picard, D., Helsen, L., & Saelens, D. (2015). OPENIDEAS - an open framework for integrated district energy simulations. In *Proceedings of 14th International Building Simulation Conference* Hyderabad, India.

Bedouani, B. Y., Labrecque, B., Parent, M., & Legault, A. (2001). Central electric thermal storage (ETS) feasibility for residential applications: Part 2. techno-economic study. *International Journal of Energy Research*, 25, 73 – 83.

Bengea, S., Kelman, A., Borrelli, F., Taylor, R., & Narayanan, S. (2014). Implementation of model predictive control for an hvac system in a mid-size commercial building. *HVAC&R RESEARCH*, 20, 121 – 135.

Billings, S. & Chen, S. (1992). Neural networks and system identification. *IEE control engineering series*, 46, 181–205.

Blum, D., Jorissen, F., Huang, S., Chen, Y., Arroyo, J., Benne, K., Li, Y., Gavan, V., Rivalin, L., Helsen, L., Vrabie, D., Wetter, M., Sofos, M., & Leuven, K. U. (2019). Prototyping the BOPTEST framework for simulation-based testing of advanced control strategies in buildings. In *Proceedings of Building Simulation 2019* Rome, Italy.

Blum, D. H. (2019). Development of a software platform and framework for advanced control system testing and benchmarking. Intelligent Building Operations Workshop 2019. Boulder, Colorado.

Blum, D. H. & Wetter, M. (2017). MPCPy: An open-source software platform for model predictive control in buildings. In *Proceedings of Building Simulation 2017* San Francisco, California, USA.

Bonneau, D., Rongere, F., Covalet, D., & Gauthier, B. (1993). Clim2000: modular software for energy simulation in buildings. In *Proceedings of IBPSA 1993* 1993.

Braun, J. E. (1990). Reducing energy costs and peak electrical demand through optimal control of building thermal storage. *ASHRAE Transactions*, 96, 876 – 887.

BuildingIQ (2019). BuildingIQ. Retrieved from `https://buildingiq.com/`.

BuildOpt-VIE (2020). Available at `www.bph.tuwien.ac.at`.

Bursill, J., O'Brien, L., & Beausoleil-Morrison, I. (2020). Multi-zone field study of rule extraction control to simplify implementation of predictive control to reduce building energy use. *Energy and Buildings*, 222, 110056.

Cai, J., Braun, J. E., Kim, D., & Hu, J. (2016a). General approaches for determining the savings potential of optimal control for cooling in commercial buildings having both energy and demand charges. *Science and Technology for the Built Environment*, 22, 733 – 750.

Cai, J., Kim, D., Jaramillo, R., Braun, J. E., & Hu, J. (2016b). A general multi-agent control approach for building energy system optimization. *Energy and Buildings*, 127, 337 – 351.

Canada, N. R. (2012). Survey of commercial and institutional energy use - buildings 2009 - detailed statistical report 2012. Retrieved from `http://oee.nrcan.gc.ca/publications/statistics/scieu/2009/pdf/scieu2009.pdf`.

Canada, S. (2011). Households and the environment: Energy use, (11-526-s), 40.

Canadian Meteorological Service (Environment Canada) (2019). High resolution deterministic prediction system. Retrieved from `https://weather.gc.ca/grib/grib2_HRDPS_HR_e.html`.

Candanedo, J. A., Allard, A., & Athienitis, A. K. (2011). Predictive control of radiant floor heating and transmitted irradiance in a room with high solar gains. *ASHRAE Transactions*, 117(2), 652 – 665.

Candanedo, J. A., Dehkardi, V. R., & Lopez, P. (2013). A control-oriented simplified building modelling strategy. In *Proceedings of 13th Conference of International Building Performance Simulation Association* Chambery, France.

Candanedo, J. A., Dehkordi, V. R., Saberi-Derakhtenjani, A., & Athienitis, A. K. (2015). Near-optimal transition between temperature setpoints for peak load reduction in small buildings. *Energy and Buildings*, 87, 123–133.

Chen, K., Jiao, Y., & Lee, E. S. (2006). Fuzzy adaptive networks in thermal comfort. *Applied Mathematics Letters*, 19(5), 420 – 426.

Chen, T. Y. & Athienitis, A. K. (2003). Investigation of practical issues in building thermal parameter estimation. *Building and Environment*, 38(8), 1027 – 1038.

Chen, Y., Athienitis, A. K., & Galal, K. E. (2013). Frequency domain and finite difference modeling of ventilated concrete slabs and comparison with field measurements: Part 1, modeling methodology. *International Journal of Heat and Mass Transfer*, 66.

Chen, Y., Shi, Y., & Zhang, B. (2019). Optimal control via neural networks: A convex approach.

Cigler, J., Gyalistras, D., Siroky, J., Tiet, V.-N., & Ferkl, L. (2013a). Beyond theory: the challenge of implementing model predictive control in buildings. In *Proceedings of 11th Clima-RHEVA World Congress*.

Cigler, J. & Prívara, S. (2010). Subspace identification and model predictive control for buildings. In *Proceedings of 2010 11th International Conference on Control Automation Robotics Vision* (pp. 750 – 755). Singapore, Singapore.

Cigler, J., Tomáško, P., & Široký, J. (2013b). BuildingLAB: A tool to analyze performance of model predictive controllers for buildings. *Energy and Buildings*, 57, 34 – 41.

Cooke, W. B. H., Hardy, R. H. S., & Sulatisky, M. T. (1980). Thermal energy storage in forced-air electric furnaces. *IEEE Transactions on Industry Applications*, IA-16(1), 127–133.

Crank, J. (1975). *The Mathematics of Diffusion*. Clarendon Press, second edition.

Date, J., Candanedo, J., Athienitis, A. K., & Fournier, M. (2016a). Simplified multi-zone thermal modelling of a house for demand reduction & control applications. In *Proceedings of CLIMA 2016 Conference* Aalborg, Denmark.

Date, J., Candanedo, J., Athienitis, A. K., & Lavigne, K. (2017). Predictive Setpoint Optimization of a Commercial Building Subject to a Winter Demand Penalty Affecting 12 Months of Utility Bills. *Proceedings of Building Simulation 2017 Conference*. San Francisco, California.

Date, J., Candanedo, J. A., & Athienitis, A. K. (2016b). Control-oriented modelling of thermal zones in a house: a multi-level approach. In *Proceedings of International High Performance Buildings Conference* West Lafayette, IN, USA.

Date, J. A., Candanedo, J. A., Athienitis, A. K., & Lavigne, K. (2018). Control-oriented modeling of an air-based electric thermal energy storage device. In *Proceedings of ASHRAE Winter Conference 2018* Chicago, Illinois.

Date, J. A., Candanedo, J. A., Athienitis, A. K., & Lavigne, K. (2020a). Development of reduced order thermal dynamic models for building load flexibility of an electrically-heated high temperature thermal storage device. *Science and Technology for the Built Environment*.

Date, J. A., Candanedo, J. A., Athienitis, A. K., & Lavigne, K. (2020b). Energy flexible building: predictive load management of passive and active energy storage under a demand response program. In *Proceedings of eSIM 2020 Conference* Vancouver, BC.

Date, J. A., Fournier, M., Chen, Y., & Athienitis, A. K. (2016c). Impact of thermal model resolution on peak heating demand calculation under different setpoint profiles. *ASHRAE Transactions*, 122, 1 – 11.

De Coninck, R. & Helsen, L. (2016). Practical implementation and evaluation of model predictive control for an office building in brussels. *Energy and Buildings*, 111, 290 – 298.

Delcroix, B., Kummert, M., Daoud, A., & Hiller, M. (2013). Improved conduction transfer function coefficients generation in trnsys multizone building model. *Proceedings of BS2013, Chambéry, France*, (pp. 2667–2674).

Deng, K., Goyal, S., Barooah, P., & Mehta, P. G. (2014). Structure-preserving model reduction of nonlinear building thermal models. *Automatica*, 50, 1188 – 1195.

Denholm, P., O'Connell, M., Brinkman, G., & Jorgenson, J. (2015). *Overgeneration from Solar Energy in California. A Field Guide to the Duck Chart*. Technical report, NREL.

Di Giorgio, A. & Liberati, F. (2014). Near real time load shifting control for residential electricity prosumers under designed and market indexed pricing models. *Applied Energy*, 128, 119 – 132.

DOE (2013). *EnergyPlus engineering reference - the reference to EnergyPlus calculations (in case you want or need to know)*. Technical report, US Department of Energy.

Donghun, K. & Braun, J. E. (2012). Reduced-order building modeling for application to model-based predictive control. In *Proceedings of Fifth National Conference of IBPSA-USA* Madison, WI, USA.

Drgoňa, J., Arroyo, J., Cupeiro Figueroa, I., Blum, D., Arendt, K., Kim, D., Ollé, E. P., Oravec, J., Wetter, M., Vrabie, D. L., & Helsen, L. (2020). All you need to know about model predictive control for buildings. *Annual Reviews in Control*, 50, 190–232.

Drgoňa, J., Picard, D., Kvasnica, M., & Helsen, L. (2018). Approximate model predictive building control via machine learning. *Applied Energy*, 2018, 199 – 216.

EnergyPlus (2020). U.S. Department of Energy (DOE). Available at /http://www.eere.energy.gov/buildings/energyplus.

ESP-r (2020). Available at http://www.esru.strath.ac.uk/Programs/ESP-r.htm.

Fernandes, F., Morais, H., Vale, Z., & Ramos, C. (2014). Dynamic load management in a smart home to participate in demand response events. *Energy and Buildings*, 82, 592 – 606.

Fischer, D., Härtl, A., & Wille-Haussmann, B. (2015). Model for electric load profiles with high time resolution for german households. *Energy and Buildings*, 92, 170 – 179.

Foteinaki, K., Li, R., Heller, A., & Rode, C. (2018). Heating system energy flexibility of low-energy residential buildings. *Energy and Buildings*, 180, 95 – 108.

Foucquier, A., Robert, S., Suard, F., Stéphan, L., & Jay, A. (2013). State of the art in building modelling and energy performances prediction: A review. *Renewable and Sustainable Energy Reviews*, 23, 272 – 288.

Fournier, M. & Leduc, M.-A. (2014). Study of electrical heating setpoint modulation strategies for residential demand response. In *Proceedings of eSim Conference 2014* Ottawa, Ontario, Canada.

Fux, S. F., Ashouri, A., Benz, M. J., & Guzzella, L. (2014). EKF based self-adaptive thermal model for a passive house. *Energy and Buildings*, 68(Part C), 811 – 817.

Gillespie, K. L., Cowan, J. D., Frazell, C. W., Haberl, J. S., Heinemeier, K. H., Kummer, J. P., Culp, C. H., Watson, T. E., Arnold, C. G., Baxter, V. D., a Evans, R., Hogan, J. F., Kohloss, F. H., & Montgomery, R. D. (2002a). *Measurement of Energy and Demand Savings*. Technical report, ASHRAE.

Gillespie, K. L., Cowan, J. D., Frazell, C. W., Haberl, J. S., Heinemeier, K. H., Kummer, J. P., Culp, C. H., Watson, T. E., Arnold, C. G., Baxter, V. D., Evans, R. a., Hogan, J. F., Kohloss, F. H., & Montgomery, R. D. (2002b). *ASHRAE Guideline 14-2002: Measurement of Energy and Demand Savings*. Technical report.

Goyal, S. & Barooah, P. (2012). A method for model-reduction of non-linear thermal dynamics of multi-zone buildings. *Energy and Buildings*, 47, 332 – 340.

Hagan, M. T., Demuth, H. B., & Beale, M. (1997). *Neural network design*. PWS Publishing Co.

Haghighat, F. & Athienitis, A. (1988). Comparison between time domain and frequency domain computer program for building energy analysis. *Computer-Aided Design*, 20(9), 525 – 532.

Hilliard, T., Kavgic, M., & Swan, L. (2016). Model predictive control for commercial buildings: trends and opportunities. *Advances in Building Energy Research*, 10, 2.

Hilliard, T., Swan, L., & Qin, Z. (2017). Experimental implementation of whole building mpc with zone based thermal comfort adjustments. *Building and Environment*, 125, 326 – 338.

Hou, X., Xiao, Y., Cai, J., & Braun, J. E. (2016). A distributed model predictive control approach for optimal coordination of multiple thermal zones in a large open space. In *Proceedings of High Performance Building Conference* West Lafayette, IN, USA.

Houda, Z., Sylvain, R., Frederic, S., & Ould Rouis, Y. (2015). Benchmark of optimization techniques for identification of buildings thermal parameters. In *Proceedings of 14th International Conference of the International Building Performance Simulation Association* Hyderabad, India.

Hu, J. & Karava, P. (2014). A state-space modeling approach and multi-level optimization algorithm for predictive control of multi-zone buildings with mixed-mode cooling. *Building and Environment*, 80, 259 – 273.

Huang, H., Chen, L., & Hu, E. (2014). Model predictive control for energy-efficient buildings: An airport terminal building study. In *11th IEEE International Conference on Control Automation (ICCA)* (pp. 1025–1030).

Huang, H., Chen, L., & Hu, E. (2016). Reducing energy consumption for buildings under system uncertainty through robust mpc with adaptive bound estimator. In *Proceedings of High Performance Building Conference* West Lafayette, Indiana, USA.

Huchuk, B., Cruickshank, C. A., & Gunay, H. B. (2014). Recursive thermal building model training using ensemble kalman filters. In *Proceedings of the eSim 2014* Ottawa, Canada.

Hurtado, L., Rhodes, J., Nguyen, P., Kamphuis, I., & Webber, M. (2017). Quantifying demand flexibility based on structural thermal storage and comfort management of non-residential buildings: A comparison between hot and cold climate zones. *Applied Energy*, 195, 1047 – 1054.

Huyck, B., Ferreau, H. J., Diehl, M., De Brabanter, J., Van Impe, J. F., De Moor, B., & Logist, F. (2012). Towards online model predictive control on a programmable logic controller: Practical considerations. *Mathematical Problems in Engineering*.

Hydro-Québec (2016). About Hydro-Québec: OUR ENERGY.

Hydro-Québec (2020a). Hydro-Québec - Rate M. Retrieved from `http://www.hydroquebec.com/business/customer-space/rates/rate-m-general-rate-medium-power-customers.html`.

Hydro-Québec (2020b). Hydro-Québec - Rates for Business Customers. Retrieved from `http://www.hydroquebec.com/business/customer-space/rates/`.

Hydro-Quebec Distribution (2012). *État d'avancement 2012 du Plan d'approvisionnement 2011-2020*. Technical report, Hydro-Québec.

Hydro-Québec Distribution (2012). État d'avancement 2012 du plan d'approvisionnement 2011-2020.

IDA (2020). Available at `http://www.equa.se`.

IEA (2018). *2018 Global Status Report - Towards a zero-emission, efficient and resilient buildings and construction sector*. Technical report, International Energy Agency.

Incropera, DeWitt, Bergman, & Lavine (2006). *Fundamentals of heat and mass transfer*. John Wiley and Sons.

Inderfurth, A., Nytsch-Geusen, C., & Ribas Tugores, C. (2015). Parameter identification for low-order building models using optimization strategies. In *Proceedings of 14th International Building Simulation Conference* Hyderabad, India.

International Energy Agency (2020). IEA EBC Annex 67. Retrieved from `http://www.annex67.org/`.

Iria, J. & Soares, F. (2019). A cluster-based optimization approach to support the participation of an aggregator of a larger number of prosumers in the day-ahead energy marke. *Electric Power Systems Research*, 168, 324 – 335.

Široký, J., Oldewurtel, F., Cigler, J., & Prívara, S. (2011). Experimental analysis of model predictive control for an energy efficient building heating system. *Applied Energy*, 88(9), 3079 – 3087.

Jain, A., Behl, M., & Mangharam, R. (2017a). Data predictive control for building energy management. In *2017 American Control Conference (ACC)* (pp. 44–49).

Jain, A., Smarra, F., & Mangharam, R. (2017b). Data predictive control using regression trees and ensemble learning. In *2017 IEEE 56th Annual Conference on Decision and Control (CDC)* (pp. 4446–4451).

Jensen, S. Ø., Marszal-Pomianowska, A., Lollini, R., Pasut, W., Knotzer, A., Engelmann, P., Stafford, A., & Reynders, G. (2017). IEA EBC Annex 67 Energy Flexible Buildings. *Energy and Buildings*, 155, 25 – 34.

Johnson Controls (2015). Johnson controls helps stanford university drastically reduce water and energy use in new central plant. Retrieved from `http://www.johnsoncontrols.com/mediacenter/news/press-releases/2015/06/15/johnsoncontrols-helps-stanford-university-drasticallyreduce-water-and-energy-use-i`

Jorissen, F., Boydens, W., & Helsen, L. (2019). TACO, an automated toolchain for model predictive control of building systems: implementation and verification. *Journal of Building Performance Simulation*, 12, 180–192.

Jorissen, F. & Helsen, L. (2016). Towards an automated toolchain for MPC in multi-zone buildings. In *Proceedings of High Performance Building Conference* West Lafayette, IN, USA.

Junker, R. G., Lindberg, K. B., Reynders, G., Lopes, R. A., Relan, R., Azar, A. G., & Madsen, H. (2018). Characterizing the energy flexibility of buildings and districts. *Applied Energy*, 225, 175 – 182.

Kernighan, B. W. & Ritchie, D. M. (1988). *The C Programming Language*. Prentice Hall Professional Technical Reference.

Kim, D., Bae, Y., Yun, S., & Braun, J. E. (2020). A methodology for generating reduced-order models for large-scale buildings using the krylov subspace method. *Journal of Building Performance Simulation*, 13, 419 – 429.

Kim, D. & Braun, J. E. (2015). A general approach for generating reduced-order models for large multi-zone buildings. *Journal of Building Performance Simulation*, 8, 435 – 448.

Kim, D. & Braun, J. E. (2018). Development, implementation and performance of a model predictive controller for packaged air conditioners in small and medium-sized commercial building applications. *Energy and Buildings*, 178, 49 – 60.

Kircher, K. J. & Zhang, K. M. (2015). On the lumped capacitance approximation accuracy in RC network building models. *Energy and Buildings*, 018, 454 – 462.

Kolokotsa, D. (2016). The role of smart grids in the building sector. *Energy and Buildings*, 116, 703 – 708.

Kotzur, L., Markewitz, P., Robinius, M., Cardoso, G., Stenzel, P., Heleno, M., & Stolten, D. (2020). Bottom-up energy supply optimization of a national building stock. *Energy and Buildings*, 209, 109667.

Kummert, M., André, P., & Argiriou, A. A. (2006). Comparing control strategies using experimental and simulation results: Methodology and application to heating control of passive solar buildings. *HVAC&R Research*, 12, 715 – 737.

Kummert, M., André, P., & Nicolas, J. (2001). Optimal heating control in a passive solar commercial building. *Solar Energy*, 69, 103 – 116.

Lauster, M., Brüntjen, M., Leppmann, H., Fuchs, M., Teichmann, J., Streblow, R., & Müller, D. (2014). Improving a low order building model for urban scale applications. In *Proceedings of Fifth German-Austrian IBPSA Conference* Aachen, Germany.

Lavigne, Daoud, A., Sansregret, S., & Leduc, M.-A. (2014). Demand response strategies in a small all-electric commercial building in quebec. In *Proceedings of eSim Conference 2014* Ottawa, Ontario, Canada.

Lavigne, K. (2006). Etude de mediums de stockage pour un appareil de stockage thermique hybride. Master's thesis, Universite de Sherbrooke.

Le Bel, C. & Gelinas, S. (2012). All-electric experimental twin housss: The ultimate demand mangement testing tool. In *Proceedings of The IASTED International Symposium on Power and Energy (PE 2013)* Marina Del Rey, California.

Le Dréau, J. & Heiselberg, P. (2016). Energy flexibility of residential buildings using short term heat storage in the thermal mass. *Energy*, 111, 991 – 1002.

Le Mounier, A., Delinchant, B., & Ploix, S. (2014). Determination of relevant model structures for self-learning energy management system. In *Proceedings of Building Simulation and Optimization Conference* London, England.

Leduc, M.-A., Daoud, A., & LeBel, C. (2011). Developing winter residential demand response strategies for electric space heating. In *Proceedings of 12th Conference of IBPSA* Sydney, NSW, Australia.

Lienhard Iv, J. H. & Lienhard V, J. H. (1986). *A heat transfer textbook*. Phlogiston Press, fifth edition.

Lin, Y., Middelkoop, T., & Barooah, P. (2012). Issues in identification of control-oriented thermal models of zones in multi-zone buildings. In *Proceedings of 51st IEEE Conference on Decision and Control* Maui, Hawaii.

Liu, M. & Heiselberg, P. (2019). Energy flexibility of a nearly zero-energy building with weather predictive control on a convective building energy system and evaluated with different metrics. *Applied Energy*, 233-234, 764–775.

Liu, S. & Henze, G. P. (2006). Experimental analysis of simulated reinforcement learning control for active and passive building thermal storage inventory: Part 1. theoretical foundation. *Energy and Buildings*, 38(2), 142 – 147.

Loveday, D. L., Virk, G. S., & Cheung, J. M. (1992). Advanced control for BEMS: A model-based predictive approach. *Building Services Engineering Research and Technology*, 13(4), 217 – 223.

Ma, Y., Anderson, G., & Borrelli, F. (2011). A distributed predictive control approach to building temperature regulation. In *Proceedings of the 2011 American Control Conference*.

Ma, Y., Borrelli, F., Hencey, B., Packard, A., & Bortoff, S. (2009). Model predictive control of thermal energy storage in building cooling systems. In *Proceedings of the 48h IEEE Conference on Decision and Control (CDC) held jointly with 2009 28th Chinese Control Conference* Shanghai, China.

Ma, Y., Vichik, S., & Borrelli, F. (2012). Fast stochastic MPC with optimal risk allocation applied to building control systems. In *Proceedings of 2012 IEEE 51st IEEE Conference on Decision and Control (CDC).*

Mammoli, A., Robinson, M., Ayon, V., Martínez-Ramón, M., fei Chen, C., & Abreu, J. M. (2019). A behavior-centered framework for real-time control and load-shedding using aggregated residential energy resources in distribution microgrids. *Energy and Buildings*, 198, 275 – 290.

Mata, ., Kalagasidis], A. S., & Johnsson, F. (2014). Building-stock aggregation through archetype buildings: France, germany, spain and the uk. *Building and Environment*, 81, 270 – 282.

Mathieu, J. L., Callaway, D. S., & Kiliccote, S. (2011). Variability in automated responses of commercial buildings and industrial facilities to dynamic electricity prices. *Energy and Buildings*, 43(12), 3322 – 3330.

May-Ostendorp, P. T., Henze, G. P., Rajagopalan, B., & Corbin, C. D. (2013). Extraction of supervisory building control rules from model predictive control of windows in a mixed mode building. *Journal of Building Performance Simulation*, 6(3), 199 – 219.

Mikkola, J. & Lund, P. D. (2014). Models for generating place and time dependent urban energy demand profiles. *Applied Energy*, 130, 256 – 264.

Missaoui, R., Joumaa, H., Ploix, S., & Bacha, S. (2014). Managing energy smart homes according to energy prices: Analysis of a building energy management system. *Energy and Buildings*, 71, 155 – 167.

Moffet, M. A., Sirois, F., Joos, G., & Moreau, A. (2012). Central electric thermal storage (ETS) heating systems: Impact on customer and distribution system. In *Proceedings of the IEEE Power Engineering Society Transmission and Distribution Conference* Orlando, FL, USA.

Moreau, A. & Steffes, T. (2009). Managing the heating demand in institutional buildings with an innovative thermal storage system. In *Proceedings of Effstock 2009 - Thermal Energy Storage for Energy Efficiency and Sustainability* Stockholm, Sweden.

Moroşan, P.-D., Bourdais, R., Dumur, D., & Buisson, J. (2010). Building temperature regulation using a distributed model predictive control. *Energy and Buildings*, 42, 1445 – 1452.

Morris, F. B., Braun, J. E., & Treado, S. J. (1994). Experimental and simulated performance of optimal control of building thermal storage. *ASHRAE Transactions*, 100(1), 402–414.

Morton, K. W. & Mayers, D. F. (2005). *Numerical Solution of Partial Differential Equations - An Introduction*. Cambridge University Press, second edition.

Natural Resources Canada (2019). CanMETEO. Available at `https://www.nrcan.gc.ca/energy/canmeteo/19908`.

Nguyen-Hong, Q., Le Mounier, A., Dinh, V.-B., Delinchant, B., Ploix, S., & Wurtz, F. (2017). Meta-optimization and scattering parameters analysis for improving on site building model identification for optimal operation. In *Proceedings of Building Simulation 2017* San Francisco, California, USA.

O'Dwyer, E., Tommasi], L. D., Kouramas, K., Cychowski, M., & Lightbody, G. (2017). Prioritised objectives for model predictive control of building heating systems. *Control Engineering Practice*, 63, 57 – 68.

Oldewurtel, F., Parisio, A., Jones, C. N., Gyalistras, D., Gwerder, M., Stauch, V., Lehmann, B., & Morari, M. (2012). Use of model predictive control and weather forecasts for energy efficient building climate control. *Energy and Buildings*, 45, 15 – 27.

OptiControl (2019). OptiControl. Retrieved from `http://www.opticontrol.ethz.ch/`.

Pallonetto, F., Oxizidis, S., Milano, F., & Finn, D. (2016). The effect of time-of-use tariffs on the demand response flexibility of an all-electric smart-grid-ready dwelling. *Energy and Buildings*, 128, 56 – 67.

Patankar, S. V. (1980). *Numerical Heat Transfer and Fluid Flow*. Taylor & Francis, First edition.

Patteeuw, D., Henze, G. P., & Helsen, L. (2016). Comparison of load shifting incentives for low-energy buildings with heat pumps to attain grid flexibility benefits. *Applied Energy*, 167, 80 – 92.

Perera, D. W. U., Winkler, D., & Skeie, N.-O. (2016). Multi-floor building heating models in matlab and modelica environments. *Applied Energy*, 171, 46 – 57.

Perez, K. X., Baldea, M., & Edgar, T. F. (2016). ntegrated hvac management and optimal scheduling of smart appliances for community peak load reduction. *Energy and Buildings*, 123, 34 – 40.

Picard, D., Sourbron, M., & Jorissen, F. (2016). Comparison of model predictive control performance using grey-box and white-box controller models of a multi-zone office building. In *International Compressor Engineering, Refrigeration and Air Conditioning, and High Performance Buildings Conferences* West Lafayette, IN, USA.

Prívara, S., Cigler, J., Váňa, Z., Oldewurtel, F., Sagerschnig, C., & Žáčeková, E. (2013). Building modeling as a crucial part for building predictive control. *Energy and Buildings*, 56, 8–22.

Prívara, S., Široký, J., Ferkl, L., & Cigler, J. (2011). Model predictive control of a building heating system: The first experience. *Energy and Buildings*, 43, 564 – 572.

Python Software Foundation (2020). *Python Language Reference, version 3.8*. Retrieved from `https://docs.python.org/3.8/reference/`.

QCoefficient, Inc (2019). QCoefficient, Inc. Retrieved from `http://qcoefficient.com/`.

Qin, S. J. & Badgwell, T. A. (2003). A survey of industrial model predictive control technology. *Control Engineering Practice*, 11, 733 – 764.

Radecki, P. & Hencey, B. (2012). Online building thermal parameter estimation via unscented kalman filtering. In *Proceedings of 2012 American Control Conference (ACC)* Montreal, Quebec.

Ramallo-González, A. P., Eames, M. E., & Coley, D. A. (2013). Lumped parameter models for building thermal modelling: An analytic approach to simplifying complex multi-layered constructions. *Energy and Buildings*, 60, 174 – 184.

Rehrl, J. & Horn, M. (2011). Temperature control for hvac systems based on exact linearization and model predictive control. In *Proceedings of the IEEE International Conference on Control Applications*.

Reynders, G., Amaral Lopes, R., Marszal-Pomianowska, A., Aelenei, D., Martins, J., & Saelens, D. (2018). Energy flexible buildings: An evaluation of definitions and quantification methodologies applied to thermal storage. *Energy and Buildings*, 166, 372 – 390.

Reynders, G., Diriken, J., & Saelens, D. (2014a). Bottom-up modeling of the belgian residential building stock : influence of model complexity. In *Proceedings of 9th International Conference on System Simulation in Buildings* Liège, Belgium.

Reynders, G., Diriken, J., & Saelens, D. (2014b). Quality of grey-box models and identified parameters as function of the accuracy of input and observation signals. *Energy and Buildings*, 82, 263 – 274.

Reynders, G., Diriken, J., & Saelens, D. (2014c). Quality of grey-box models and identified parameters as function of the accuracy of input and observation signals. *Energy and Buildings*, 82, 263 – 274.

Reynders, G., Diriken, J., & Saelens, D. (2017). Generic characterization method for energy flexibility: Applied to structural thermal storage in residential buildings. *Applied Energy*, 198, 192 – 202.

Riffat, S. B. (1989). Measurement of heat and mass transfer between the lower and upper floors of a house. *International Journal of Energy Research*, 13(2), 231 – 241.

Rockett, P. & Hathway, E. A. (2017). Model-predictive control for non-domestic buildings: a critical review and prospects. *Building Research & Information*, 45(5), 556–571.

Rode, C. & Grau, K. (2011). Whole building hygrothermal simulation model solar house. *ASHRAE Transactions*, 109, 572 – 582.

SciPy (2021). *SciPy, version 1.6.2*. Retrieved from `https://docs.scipy.org/doc/scipy/reference/`.

Shamsi, M. H., Ali, U., & O'Donnell, J. (2019). A generalization approach for reduced order modelling of commercial buildings. *Journal of Building Performance Simulation*, 12(6), 729–744.

Sharma, I., Dong, J., Malikopoulos, A. A., Street, M., Ostrowski, J., Kuruganti, T., & Jackson, R. (2016). A modeling framework for optimal energy management of a residential building. *Energy and Buildings*, 130, 55 – 63.

Shen, L., Li, Z., & Sun, Y. (2016). Performance evaluation of conventional demand response at building-group-level under different electricity pricings. *Energy and Buildings*, 128, 143 – 154.

Shou, J. (1991). *A computer technique for heating control analysis and application to radiant heating*. PhD thesis, Concordia University.

Siegelmann, H. & Sontag, E. (1995). On the computational power of neural nets. *Journal of Computer and System Sciences*, 50(1), 132–150.

Smarra, F., Jain, A., de Rubeis, T., Ambrosini, D., D'Innocenzo, A., & Mangharam, R. (2018). Data-driven model predictive control using random forests for building energy optimization and climate control. *Applied Energy*, 226, 1252–1272.

Sánchez Ramos, J., Pavón Moreno, M., Guerrero Delgado, M., Álvarez Domínguez, S., & F. Cabeza, L. (2019). Potential of energy flexible buildings: Evaluation of dsm strategies using building thermal mass. *Energy and Buildings*, 203, 109442.

Sperber, E., Frey, U., & Bertsch, V. (2020). Reduced-order models for assessing demand response with heat pumps – insights from the german energy system. *Energy and Buildings*, 223, 110144.

Srivastava, C., Yang, Z., & Jain, R. K. (2019). Understanding the adoption and usage of data analytics and simulation among building energy management professionals: A nationwide survey. *Building and Environment*, 157, 139 – 164.

Steffes Corporation (2010). *ThermElect Owner's and Installer's Manual, version 3*. Dickinson, North Dakota, United States.

Sturzenegger, D., Gyalistras, D., Morari, M., & Smith, R. S. (2016). Model predictive climate control of a swiss office building. In *Proceedings of Clima-RHEVA World Congress* Aalborg, Denmark.

Syed, A. M. (2011). Electric thermal storage option for nova scotia power customers: A case study of a typical electrically heated nova scotia house. *Energy Engineering*, 108, 69 – 79.

Talebi, B., Haghighat, F., & Mirzaei, P. A. (2017). Simplified model to predict the thermal demand profile of districts. *Energy and Buildings*, 145, 213 – 225.

The MathWorks, Inc (2015). *MATLAB R2015b*. Natick, Massachusetts, United States.

The Matplotlib development team (2020). *Matplotlib User's Guide, version 3.2.1*. Retrieved from `https://matplotlib.org/3.2.1/users/index.html`.

The SciPy community (2019). *SciPy v1.4.1 Reference Guide*. Retrieved from `https://docs.scipy.org/doc/scipy/reference/`.

The SciPy community (2020). *NumPy v1.18 Manual*. Retrieved from `https://numpy.org/doc/stable/`.

Touretzky, C. R. & Baldea, M. (2014). Nonlinear model reduction and model predictive control of residential buildings with energy recovery. *Journal of Process Control*, 24, 723 – 739.

TRNSYS (2020). Available at `http://www.trnsys.com/`.

Váňa, Z., Cigler, J., Široký, J., Žáčeková, E., & Ferkl, L. (2014). Model-based energy efficient control applied to an office building. *Journal of Process Control*, 24(6), 790 – 797.

Vande Cavey, M., Bonvini, M., & Helsen, L. (2015). Comparison and application of different state estimation techniques for control in buildings. In *Proceedings of 14th International Conference of the International Building Performance Simulation Association* Hyderabad, India.

Vigna, I., Pernetti, R., Pasut, W., & Lollini, R. (2018). New domain for promoting energy efficiency: Energy flexible building cluster. *Sustainable Cities and Society*, 38, 526 – 533.

Wang, S. & Xu, X. (2006). Simplified building model for transient thermal performance estimation using ga-based parameter identification. *International Journal of Thermal Sciences*, 45, 419 – 432.

Wang, Z. & Hong, T. (2020). Reinforcement learning for building controls: The opportunities and challenges. *Applied Energy*, 269, 115036.

Weiß, T., Fulterer, A. M., & Knotzer, A. (2019). Energy flexibility of domestic thermal loads–a building typology approach of the residential building stock in austria. *Advances in Building Energy Research*, 13(1), 122 – 137.

West, S. R., Ward, J. K., & Wall, J. (2014). Trial results from a model predictive control and optimisation system for commercial building hvac. *Energy and Buildings*, 72, 271 – 279.

Whitmore, J. & Pineau, P.-O. (2021). *État de l'énergie au Québec 2021, Chaire de gestion du secteur de l'énergie*. Technical report, HEC Montréal, prepared for Quebec Ministry of Energy and Natural Resources.

Wong, S., Gaudet, G., & Proulx, L.-P. (2017). Capturing wind with thermal energy storage – summerside's smart grid approach. *IEEE Power and Energy Technology Systems Journal*, 4(4), 115 – 124.

Wong, S. & Pinard, J. P. (2017). Opportunities for smart electric thermal storage on electric grids with renewable energy. *IEEE Transactions on Smart Grid*, 8, 1014 – 1022.

Xu, X. & Wang, S. (2008). A simplified dynamic model for existing buildings using ctf and thermal network models. *International Journal of Thermal Sciences*, 47(9), 1249 – 1262.

Yalcintas, M., Hagen, W. T., & Kaya, A. (2015). An analysis of load reduction and load shifting techniques in commercial and industrial buildings under dynamic electricity pricing schedules. *Energy and Buildings*, 88, 15 – 24.

Ye, Y., Lou, Y., Strong, M., Upadhyaya, S., Zuo, W., & Wang, G. (2020). Development of new baseline models for u.s. medium office buildings based on commercial buildings energy consumption survey data. *Science and Technology for the Built Environment*, 0(0), 1–16.

Yoon, J. H., Bladick, R., & Novoselac, A. (2014). Demand response for residential buildings based on dynamic price of electricity. *Energy and Buildings*, 80, 531 – 541.

Zepter, J. M., Lüth, A., Crespo del Granado, P., & Egging, R. (2019). Prosumer integration in wholesale electricity markets: Synergies of peer-to-peer trade and residential storage. *Energy and Buildings*, 184, 163 – 176.

Zhang, Y., O'Neill, Z., Dong, B., & Augenbroe, G. (2015). Comparisons of inverse modeling approaches for predicting building energy performance. *Building and Environment*, 86, 177–190.

Zhao, J., Lam, K. P., & Ydstie, B. E. (2013). EnergyPlus model based predictive control (EPMPC) by using Matlab/Simulink and MLE+. In *Proceedings of 13th Conference of International Building Performance Simulation Association* Chambéry, France.

Zhu, J., Vaghefi, S. A., Jafari, M. A., Lu, Y., & Ghofrani, A. (2016). Managing demand uncertainty with cost-for-deviation retail pricing. *Energy and Buildings*, 118, 46 – 56.

Appendix A: Experimental Houses for Building Energetics (Twin Houses)

Building Details & Description

The homes used for the experiments are the Experimental Houses for Building Energetics (EHBE) (Fournier & Leduc, 2014, Le Bel & Gelinas, 2012). The test bench consists of two 2-storey detached homes with excavated basements, each with a 60m^2 footprint, excluding the single detached garage. Floor plans are shown in Figures A1, A2 and A3. The houses are 25 ft x 26 ft, three bedrooms, one and a half bathroom cottages with a full basement and a 15 ft x 24 ft attached garage. The wall assemblies of the building were chosen to represent a typical light-weight wood framed house in Québec. The total fenestration area is 19m^2, consisting of vinyl framed windows with double glass and air gap. The construction of the homes was completed in February 2011.

The homes are located in Shawinigan, Québec (46°34'N 72°45'W) and are oriented 35° west of south. The homes are heated with baseboard space heating in each room with individual electronic room thermostats. There is also electric radiant floor heating in the kitchen and bathroom.

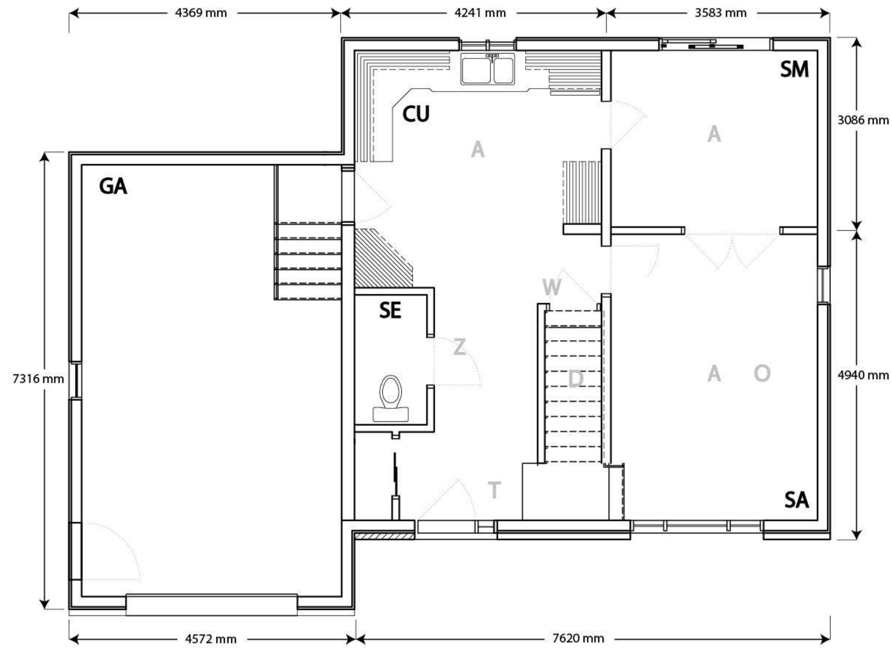

Figure A1: Main Floor - Twin Houses

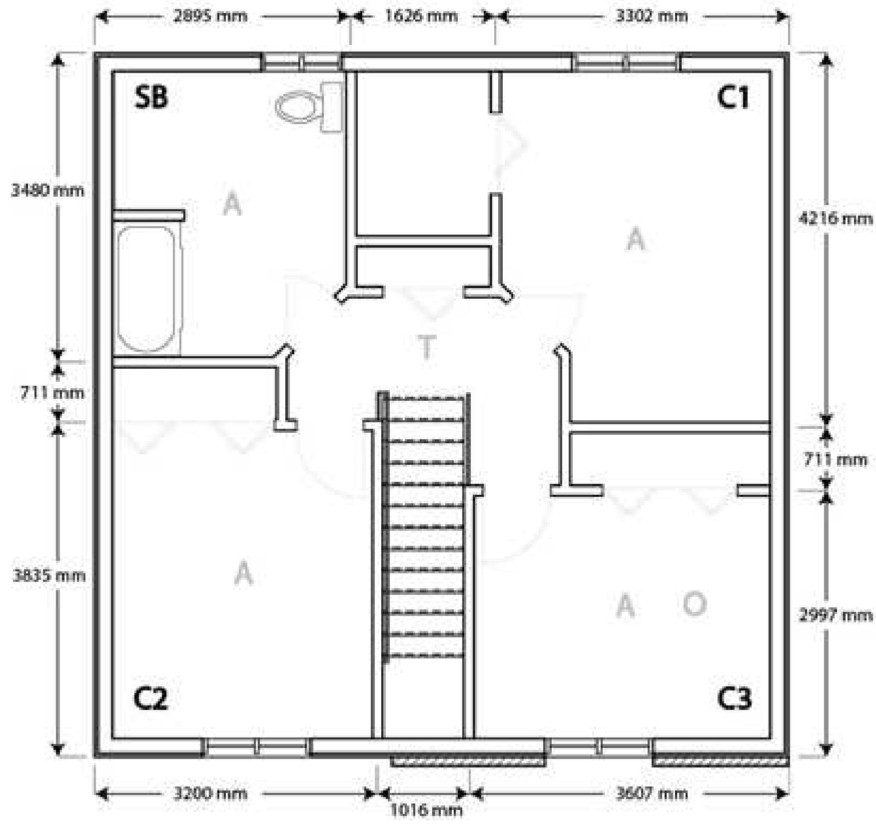

Figure A2: Second Floor - Twin Houses

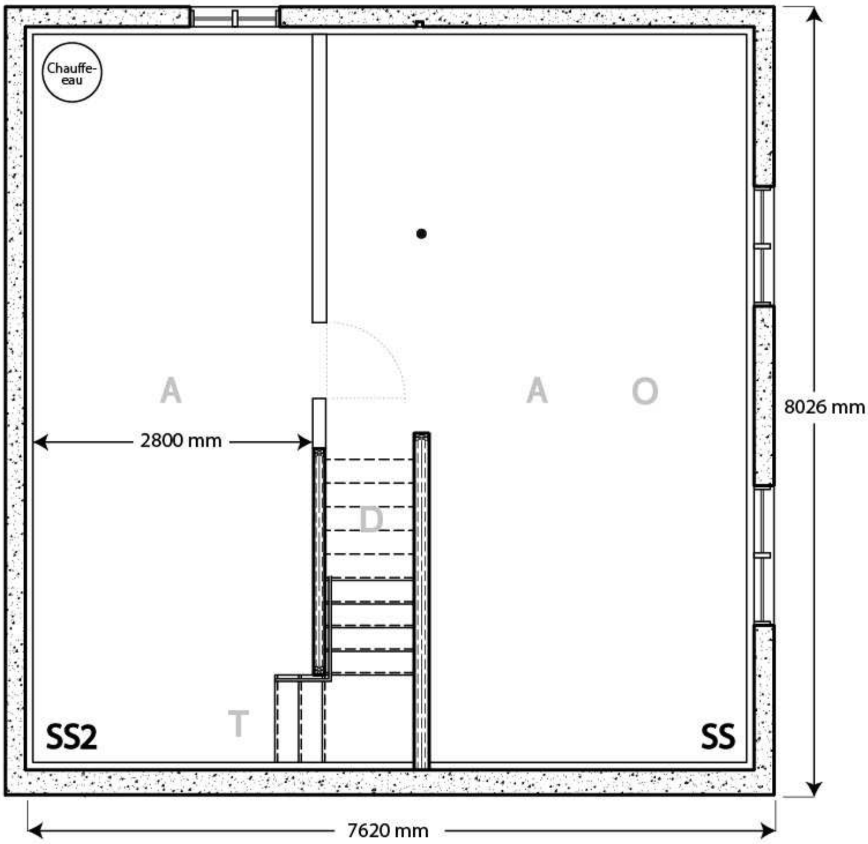

Figure A3: Basement - Twin Houses

The homes are of normal construction for Québec with a building envelope consisting of (from exterior to interior) vinyl cladding or brick, air-space, air barrier, fibreboard, R-20 glass-fiber, Enermax, air-space, drywall and R-30 insulation in the roof instead of R-20. The windows are of double clear glass with an air gap and no coatings, with a total window area of 208 square feet for each house. The interior of the houses is finished with drywall and wood floors except for the kitchen and bathrooms which have ceramic tile floor.

The baseboard heater in each room is controlled by a line-voltage (204 V) electronic thermostat with pulse width modulation at 15 second cycles. The heating capacity in the basement is 4000 W, 4750 W each for the main and second floor, and 2000 W in the garage. The bedrooms each have a rated capacity of 1250 watts. The houses have been fitted with all the air ducts necessary for a central heating/cooling system, though the system is not yet installed. In addition, the kitchen and second storey bathroom are equipped with electric radiant floor heating.

There are approximately 500 sensors in each house with recordings every 15 minutes. The thermocouples instrumented in the homes are special T type and the data acquisition equipment and computers are located in the garage of each house. The sensors measure the following:

- Weather (temperature, solar etc.)
- Room by room electric baseboard heating (in Wh)
- Plug and lighting loads
- Air temperature, relative humidity, air velocity, globe temperature
- Surface temperatures of structure (walls, floors, ceiling layers etc.)
- Temperatures and water content of surrounding soils in several locations

Sample Python Code of Detailed Twin House Model

```
"""
@author: Jennifer
4 zone model of the twin homes
Zone 1: upper floor
Zone 2: main floor
Zone 3: basement
Zone 4: garage

All walls and windows modelled separately
"""

"""
NumPy adds efficient vectors and matrices to Python that support vectorized
operations
"""
import numpy as np
from scipy.interpolate import interp1d

"""
Matplotlib adds Matlab-style graphics to Python and is well-integrated with
the IPython notebook
"""
from matplotlib import pyplot as plt
import matplotlib.patches as mpatches
import math

import time
start_time = time.time()

deltaT     = 15.

# Number of days
No          = 1.;
NT          = No*86400./deltaT # number of time steps in a day

p           = np.arange(0,NT)
p1          = np.arange(0,NT-1)
t           = p*deltaT



"""
Import Data for:
1. Year OAT at 15 minute intervals
2. Temperature set point profile at 15 minute intervals

linearlize to time step interval (15 second intervals)
"""

Nfinal      = int(NT*12) # )
p2          = np.arange(0,Nfinal-1)
dT          = 1. # Temperature
u           = 0.
j           = 1.

qaux1       = np.zeros(Nfinal)
```

```
qaux2       = np.zeros(Nfinal)
qaux3       = np.zeros(Nfinal)
qaux4       = np.zeros(Nfinal)

qmax1       = 3792.
qmax2       = 4596.
qmax3       = 3868.
qmax4       = 1344.

#Height of building
Hh          = 2.489
#Length of building
Lh          = 7.823
#Width of building
Wh          = 7.224

# Exterior Surfaces:
#    Surface 1 = South Wall (Interior) 0
#    Surface 2 = East Wall (Exterior) 1
#    Surface 3 = North Wall (Exterior) 2
#    Surface 4 = West Wall (Interior) 3
#    Surface 5 = Ceiling (Exterior) 4
#    Surface 6 = Floor (Interior) 5
#Internal Height
Hi       = 2.4*2.

# Garage
Hg       = 2.489
Lg       = 7316./1000
Wg       = 4572./1000

# window areas

Wkit     = (915./1000.)*(1015./1000.) #kitchen window
Wdin     = (1830./1000.)*(2080./1000.) # dining room glass door
Wlivside = (610./1000.)*(1420./1000.) # living room side window
Wlivfr   = (2135./1000.)*(1420./1000.) # living room front window
Wbath    = (915./1000.)*(1420./1000.) # upstair bathroom window
Wbed1    = (1220./1000.)*(1420./1000.) # bedroom1 window
Wbed3    = (915./1000.)*(1420./1000.) # bedroom 3 window
Wbed2    = (915./1000.)*(1420./1000.) # bedroom 2 window
Wbase    = (915./1000.)*(610./1000.) # basement back
Wbase2   = ((1220./1000.)*(610./1000.))+((1400./1000.)*(610./1000.)) # basement side
Wgar     = (610./1000.)*(1220./1000.)

# Window Areas ZONE 1(m^2)
Aw1    = np.array([Wbed2 + Wbed3,0.0,Wbath + Wbed1,0.0])
 # Net Wall Areas (m)
A1      = np.array([Lh*Hh-Aw1[0], Wh*Hh-Aw1[1], Lh*Hh-Aw1[2], Wh*Hh-Aw1[3],
                    Wh*Lh, Wh*Lh])

# Window Areas  ZONE 2(m^2)
Aw2    = np.array([Wlivfr, Wlivside, Wkit + Wdin,0.0])
 # Net Wall Areas (m)
A2      = np.array([Lh*Hh-Aw2[0], Wh*Hh-Aw2[1], Lh*Hh-Aw2[2], Wh*Hh-Aw2[3],
                    Wh*Lh, Wh*Lh])
```

```python
# Window Areas ZONE 3(m^2)
Aw3    = np.array([0.0, Wbase2, Wbase, 0.0])
 # Net Wall Areas (m)
A3      = np.array([Lh*Hh-Aw3[0], Wh*Hh-Aw3[1], Lh*Hh-Aw3[2], Wh*Hh-Aw3[3],
                    Wh*Lh, Wh*Lh])

# Window Areas ZONE 4(m^2)
Aw4    = np.array([0.0,0.0,0,Wgar])
 # Net Wall Areas (m)
A4      = np.array([Lg*Hg-Aw4[0], Wg*Hg-Aw4[1], Lg*Hg-Aw4[2], Wg*Hg-Aw4[3],
                    Wg*Lg, Wg*Lg])

#Zone volume
Vol1 = Hh*Lh*Wh
Vol2 = Hh*Lh*Wh
Vol3 = Hh*Lh*Wh
Vol4 = Hg*Lg*Wg

#Window Resistance (U=3)
Rw   = 0.35 #m^2*degC/watt

#interior film coefficient of surfaces walls
h        = 6.1 #watt/(m^2*degC)


#zone air changes
ach1  = 0.019/3
ach2  = 0.019*2
ach3  = 0.019*22
ach4  = 0.019*37
ach12 = 6
ach23 = 5

#specific heat of air
cp = 1000. #joule/(kg*degC)
#density of air
rho = 1.2 # kg/m^3

# infiltration
Uinf1    = ach1*Vol1*cp*rho/3600.
Uinf2    = ach2*Vol2*cp*rho/3600.
Uinf3    = ach3*Vol3*cp*rho/3600.
Uinf4    = ach4*Vol4*cp*rho/3600.
Uinf12   = ach12*Vol1*cp*rho/3600.
Uinf23   = ach23*Vol3*cp*rho/3600.

#For Air flow calculations
beta_air = 0.00343 #coefficient of thermal expansion 1/K
mu_air   = 0.00001827 # dynamic viscosity kg/m s
Pr_air   = 0.71 #Prandtl number
k_air    = 0.0251 #conductivity of air kW/m K
g        = 9.807 #acceleration due to gravity m/s2

"""
THERMAL RESISTANCE OF WALLS (incl air films)
"""
```

```
#vertical exterior walls
#gypsum board layer
Lgyp    = 0.0127 #m
rhogyp  = 640. #kg/m^3
kgyp    = 0.16 # watt/(m*degC)
cgyp    = 1150. # joule/(kg*degC)
#Airgap and enermax
Rener   = 0.708 # (m^2*degC)/watt
#Insulation layer
Rins    = 3.89 #(m^2*degC)/watt
#Air gap, Fiberboard, plywood, vinyl
Rsid    = 0.48 #(m^2*degC)/watt
#Exterior film
ho      = 22.  #watt/(m^2*degC)
#15% framing area
ff      = 0.25 #percentage
#Wood stud
Rf      = 1.1667 #(m^2*degC)/watt

#Exterior wall resistance
Rext    = 1./(((1.-ff)/((Lgyp/kgyp)+Rener+Rins+Rsid+(1./ho)+(1./h)))+
              (((ff)/((Lgyp/kgyp)+Rener+Rf+Rsid+(1./ho)+(1./h))))) #(m^2*degC)/watt

#Ceiling
Rinsc = 5.28 #(m^2*degC)/watt
#attic air film
ha      = 12. #watt/(m^2*degC)
#Ceiling resistance
Rc      = 1./(((1.-ff)/((Lgyp/kgyp)+Rener+Rinsc+(1./ha)+(1./h)))+
              (((ff)/((Lgyp/kgyp)+Rener+Rf+(1/ha)+(1/h))))) #(m^2*degC)/watt

#Roof
#shingle backer board
Rb     = 0.14 #(m^2*degC)/watt
#Wood shingles
Rsh    = 0.078 #(m^2*degC)/watt
#Roof resistance
Rr     = 1./(((1.-ff)/(Rb+Rsh+(1./ho)+(1./ha)))
             +(((ff)/(Rb+Rf+Rsh+(1./ha)+(1./ho))))) #(m^2*degC)/watt

#Assume 30 degree roof slope, calculate ceiling-roff combined resistance
#per unit ceiling area (Assuming no attic ventilation)

#ZONE 1
Ar1    = A1[4]/math.cos(30*3.14/180) #m^2
#Combined Celining-roof resistance ZONE 1
Rroof1  = ((Rc/A1[4])+(Rr/Ar1))*A1[4] #(m^2*degC)/watt

#ZONE 4
Ar4    = A4[4]/math.cos(30*3.14/180) #m^2
#Combined Celining-roof resistance ZONE 1
Rroof4  = ((Rc/A4[4])+(Rr/Ar4))*A4[4] #(m^2*degC)/watt

# Interior floors
# insulation and plywood and truss
rhoply   = 650.
cply     = 2200.
```

```
Lply     = 0.0347
Rfl      = 0.34 #(m^2*degC)/watt
Rjoi     = 2.5
kply     = 0.12

Rair     = 0.18
Rflo     = 1./(((1.-ff)/((Lply/kply)+Rair+(1./h)+(1./h)))
              +(((ff)/((Lply/kply)+Rjoi+(1./h)+(1./h))))) #(m^2*degC)

# Interior walls
Rintw    = 1./(((1.-ff)/((2.*Lgyp/kgyp)+Rair+(2./h)))
              +(((ff)/((2.*Lgyp/kgyp)+Rf+(2./h)))))

#concrete floor
rhocon   = 2240. #kg/m^3
cconf     = 0.75*1000 #joule/kgK
Lconf     = 100./1000.
kcon     = 0.8 #W/mK conductivity

Ragr     = 0.2 #m^2K/W

Rflc     = (Lconf/kcon)+0.2 #(m^2*degC)/watt
cconc    = rhocon*cconf*Lconf


#basement walls
Lgypb    = 0.0127
Lextrinb = 0.050
Lconb    = 0.200
kextrinb = 0.022

cconcw   = rhocon*cconf*Lconb + rhogyp*cgyp*Lgypb

Rwb     = (Lgypb/kgyp)+(Lconb/kcon)#(m^2*degC)/watt

#WALL CAPACITANCES
c        = rhogyp*cgyp*Lgyp #%Joule/m^2 GYPSUM
cply     = cply*rhoply*Lply;
#C        = [c*A(1); c*A(2); c*A(3); c*A(4); c*A(5); cply*A(6)]; %Joule


#Zone 1 resistances

R1inf   =  1./Uinf1       #Infiltration to zone 1
R15     =  1./(A1[2]*h) + 1./(kgyp*A1[2]*2/Lgyp)      #North Wall resistance to half way ir
R5o     =  1./(kgyp*A1[2]*2/Lgyp)+(1/((A1[2])/Rext)) #North Wall resistance
Rw1oN   =  1/(((Aw1[2]/Rw)))                          #North window resistance
R16     =  1./(A1[0]*h) + 1./(kgyp*A1[0]*2/Lgyp)      #South Wall resistance
R6o     =  1./(kgyp*A1[0]*2/Lgyp)+(1/((A1[0])/Rext))  #South Wall resistance
Rw1oS   =  1/(((Aw1[0]/Rw)))                          #South window resistance
R17     =  1./(A1[1]*h) + 1./(kgyp*A1[1]*2/Lgyp)      #East Wall resistance
R7o     =  1./(kgyp*A1[1]*2/Lgyp)+(1/((A1[1])/Rext))  #East Wall resistance
R18     =  1./(A1[3]*h) + 1./(kgyp*A1[3]*2/Lgyp)      #West Wall resistance
R8o     =  1./(kgyp*A1[3]*2/Lgyp)+(1/((A1[3])/Rext))  #West Wall resistance
R19     =  1./(A1[5]*h) + 1./((kply*A1[5]*2/Lply))    #resistance between zones 1 & 2
R29     =  1./(kply*A1[5]*2/Lply)+(1/((A1[5])/(Rflc)))    #resistance between zones 1 & 2
R127    =  1./(A1[4]*h) + 1./(kgyp*A1[4]*2/Lgyp)    #resistance between zone 1 and attic (c
```

```
R27o    =  (Rroof1)/A1[4]    #resistance between ceiling and outside
R12inf  =  1./Uinf12  #Infiltration to zone 1 from zone 2

#Zone 2 resistances

R2inf   =  1./Uinf2 #Infiltration to zone 2
R210    =  1./(A2[2]*h) + 1./(kgyp*A2[2]*2/Lgyp)     #North Wall resistance
R10o    =  1./(kgyp*A2[2]*2/Lgyp)+(1/((A2[2])/Rext)) #North Wall resistance
Rw2oN   =  1/(((Aw2[2]/Rw)))                         #North window resistance
R211    =  1./(A2[0]*h) + 1./(kgyp*A2[0]*2/Lgyp)     #South Wall resistance
R11o    =  1./(kgyp*A2[0]*2/Lgyp)+(1/((A2[0])/Rext)) #South Wall resistance
Rw2oS   =  1/(((Aw2[0]/Rw)))                         #South window resistance
R212    =  1./(A2[1]*h) + 1./(kgyp*A2[1]*2/Lgyp)     #East Wall resistance
R12o    =  1./(kgyp*A2[1]*2/Lgyp)+(1/((A2[1])/Rext)) #East Wall resistance
R213    =  1./(A2[3]*h) + 1./(kgyp*0.25*A2[3]*2/Lgyp)     #West Wall resistance
R13o    =  1./(kgyp*A2[3]*2/Lgyp)+(1/((0.25*A2[3])/Rext)) #West Wall resistance
R214    =  1./(A2[5]*h) + 1./((kply*A2[5]*2/Lply)) #Convective transfer between zones 2 & 3
R314    =  1./(kply*A1[5]*2/Lply)+(1/((A1[5])/Rflo)) #Convective transfer between zones 2 &
R226    =  1./(0.75*A2[3]*h) + 1./(kgyp*0.75*A2[3]*2/Lgyp)#Convective transfer between zone
R426    =  1./(kgyp*0.75*A2[3]*2/Lgyp)+(1/((0.75*A2[3])/Rintw))#Convective transfer between
R23inf  =  1./Uinf23 #Infiltration to zone 2 from zone 3

#Zone 3 resistances

R3inf   =  1./Uinf3 #Infiltration to zone 3
R315    =  1./(0.25*A3[2]*h) + 1./(kgyp*0.25*A3[2]/Lgyp)
+1./(kextrinb*0.25*A3[2]/Lextrinb)+1./(kcon*0.25*A3[2]*2/Lconb) #North Wall resistance
R15o    =  1./(kcon*0.25*A3[2]*2/Lconb)+ 1./(0.25*A3[2]*ho)#North Wall resistance
R315g    =  1./(0.75*A3[2]*h) + 1./(kgyp*0.75*A3[2]/Lgyp)
+1./(kextrinb*0.75*A3[2]/Lextrinb)+1./(kcon*0.75*A3[2]*2/Lconb) #North Wall resistance
R15g    =  1./(kcon*0.75*A3[2]*2/Lconb)+1./(0.75*A3[2]*ho)
Rw3oN   =  1/(((Aw3[2]/Rw)))#North window resistance
R316    =  1./(0.25*A3[0]*h) + 1./(kgyp*0.25*A3[0]/Lgyp)
+1./(kextrinb*0.25*A3[0]/Lextrinb)+1./(kcon*0.25*A3[0]*2/Lconb)#South Wall resistance
R16o    =  1./(kcon*0.25*A3[0]*2/Lconb)+ 1./(0.25*A3[0]*ho)#South Wall resistance
R316g    =  1./(0.75*A3[0]*h) + 1./(kgyp*0.75*A3[0]/Lgyp)
+1./(kextrinb*0.75*A3[0]/Lextrinb)+1./(kcon*0.75*A3[0]*2/Lconb)#South Wall resistance
R16g    =  1./(kcon*0.75*A3[0]*2/Lconb)+1./(0.75*A3[0]*ho)
R317    =  1./(0.25*A3[1]*h) + 1./(kgyp*0.25*A3[1]/Lgyp)
+1./(kextrinb*0.25*A3[1]/Lextrinb)+1./(kcon*0.25*A3[1]*2/Lconb)#East Wall resistance
R17o    =  1./(kcon*0.25*A3[1]*2/Lconb)+ 1./(0.25*A3[1]*ho)#East Wall resistance
R317g    =  1./(0.75*A3[1]*h) + 1./(kgyp*0.75*A3[1]/Lgyp)
+1./(kextrinb*0.75*A3[1]/Lextrinb)+1./(kcon*0.75*A3[1]*2/Lconb)#East Wall resistance
R17g    =  1./(kcon*0.75*A3[1]*2/Lconb)+1./(0.75*A3[1]*ho)
Rw3oE   =  1/(((Aw3[1]/Rw)))#East window resistance
R318    =  1./(0.1*A3[3]*h) + 1./(kgyp*0.1*A3[3]/Lgyp)
+1./(kextrinb*0.1*A3[3]/Lextrinb)+1./(kcon*0.1*A3[3]*2/Lconb)#West Wall resistance
R18o    =  1./(kcon*0.1*A3[3]*2/Lconb)+ 1./(0.1*A3[3]*ho)#West Wall resistance
R318g    =  1./(0.75*A3[3]*h) + 1./(kgyp*0.75*A3[3]/Lgyp)
+1./(kextrinb*0.75*A3[3]/Lextrinb)+1./(kcon*0.75*A3[3]*2/Lconb)#West Wall resistance
R18g    =  1./(kcon*0.75*A3[3]*2/Lconb)+1./(0.75*A3[3]*ho)
R319    =  1./(0.15*A3[3]*h) + 1./((kgyp*0.15*A3[3]*2/Lgyp))#Convective transfer between zc
R419    =  1./(kgyp*0.15*A3[3]*2/Lgyp)+(1/((0.15*A3[3])/Rintw))#Convective transfer betweer
R325    =  1./(A3[5]*h) + 1./((kcon*A3[5]*2/Lconf))#ground resistance to zone 3
R25g    =  1./(kcon*A3[5]*2/Lconf)+(1/((A3[5])/Rflc))#ground resistance to zone 3

#Zone 4 resistances
```

```
R4inf   =  1./Uinf4 #Infiltration to zone 4
R420    =  1./(A4[2]*h) + 1./(kgyp*A4[2]*2/Lgyp)#North Wall resistance
R20o    =  1./(kgyp*A4[2]*2/Lgyp)+(1/((A4[2])/Rext))#North Wall resistance
R421    =  1./(A4[0]*h) + 1./(kgyp*A4[0]*2/Lgyp)#South Wall resistance
R21o    =  1./(kgyp*A4[0]*2/Lgyp)+(1/((A4[0])/Rext))#South Wall resistance
R422    =  1./(A4[1]*h) + 1./(kgyp*A4[1]*2/Lgyp)#East Wall resistance
R22o    =  1./(kgyp*A4[1]*2/Lgyp)+(1/((A4[1])/Rext))#East Wall resistance
R423    =  1./(A4[3]*h) + 1./(kgyp*A4[3]*2/Lgyp)#West Wall resistance
R23o    =  1./(kgyp*A4[3]*2/Lgyp)+(1/((A4[3])/Rext))#West Wall resistance
Rw4oW   =  1/(((Aw4[3]/Rw)))#West window resistance
R424    =  1./(A4[5]*h) + 1./((kcon*A4[5]*2/Lconf))#ground resistance to zone 4
R24g    =  1./(kcon*A4[5]*2/Lconf)+(1/((A4[5])/Rflc))#ground resistance to zone 4
R428    =  1./(A4[4]*h) + 1./(kgyp*A4[4]*2/Lgyp)    #resistance between zone 1 and attic (c
R28o    =  (Rroof4)/A4[4]    #resistance between ceiling and outside

#ADD SOUTH GARAGE DOOR EVENTUALLY

#Temperatures

T1      = np.zeros(Nfinal)# Zone 1 air temperature
T2      = np.zeros(Nfinal)# Zone 2 air temperature
T3      = np.zeros(Nfinal)# Zone 3 air temperature
T4      = np.zeros(Nfinal)# Zone 4 air temperature
T5      = np.zeros(Nfinal)# Zone 1 NORTH wall
T6      = np.zeros(Nfinal)# Zone 1 SOUTH wall
T7      = np.zeros(Nfinal)# Zone 1 EAST wall
T8      = np.zeros(Nfinal)# Zone 1 WEST wall
T9      = np.zeros(Nfinal)# Zone 1 FLOOR (connection to zone 2)
T10     = np.zeros(Nfinal)# Zone 2 NORTH wall
T11     = np.zeros(Nfinal)# Zone 2 SOUTH wall
T12     = np.zeros(Nfinal)# Zone 2 EAST wall
T13     = np.zeros(Nfinal)# Zone 2 WEST wall
T14     = np.zeros(Nfinal)# Zone 2 FLOOR (connection to zone 3)
T15     = np.zeros(Nfinal)# Zone 3 NORTH wall
T15g    = np.zeros(Nfinal)# Zone 3 NORTH wall in contact with ground
T16     = np.zeros(Nfinal)# Zone 3 SOUTH wall
T16g    = np.zeros(Nfinal)# Zone 3 SOUTH wall in contact with ground
T17     = np.zeros(Nfinal)# Zone 3 EAST wall
T17g    = np.zeros(Nfinal)# Zone 3 EAST wall in contact with ground
T18     = np.zeros(Nfinal)# Zone 3 WEST wall
T18g    = np.zeros(Nfinal)# Zone 3 WEST wall in contact with ground
T19     = np.zeros(Nfinal)# Zone 3 wall connection to zone 4
T20     = np.zeros(Nfinal)# Zone 4 NORTH wall
T21     = np.zeros(Nfinal)# Zone 4 SOUTH wall
T22     = np.zeros(Nfinal)# Zone 4 EAST wall
T23     = np.zeros(Nfinal)# Zone 4 WEST wall
T24     = np.zeros(Nfinal)# Zone 4 connection to ground
T25     = np.zeros(Nfinal)# Zone 3 ground connection
T26     = np.zeros(Nfinal)# Zone 2 connection to zone 4
T27     = np.zeros(Nfinal)# ZONE 1 Ceiling (connection to outside through roof)
T28     = np.zeros(Nfinal)# ZONE 4 Ceiling (connection to outside through roof)
Tg      = np.ones(Nfinal)*20.# Ground temperature
To      = np.zeros(Nfinal)# Outdoor Air temperature
T1[0]    = 20.5
T2[0]    = 20.5
T3[0]    = 20.5
```

```
T4[0]    = 20.5
T5[0]    = 20.5
T6[0]    = 20.5
T7[0]    = 20.5
T8[0]    = 20.5
T9[0]    = 20.5
T10[0]   = 20.5
T11[0]   = 20.5
T12[0]   = 20.5
T13[0]   = 20.5
T14[0]   = 20.5
T15[0]   = 20.5
T15g[0]  = 20.5
T16[0]   = 20.5
T16g[0]  = 20.5
T17[0]   = 20.5
T17g[0]  = 20.5
T18[0]   = 20.5
T18g[0]  = 20.5
T19[0]   = 20.5
T20[0]   = 20.5
T21[0]   = 20.5
T22[0]   = 20.5
T23[0]   = 20.5
T24[0]   = 20.5
T25[0]   = 20.5
T26[0]   = 20.5
T27[0]   = 20.5
T28[0]   = 20.5

# Capacitances of air

#C1       = 11*cp*rho*Vol1 #Joule
#C2       = 9.*cp*rho*Vol2 #Joule
#C3       = 7.*cp*rho*Vol3 #Joule
#C4       = 5.*cp*rho*Vol4 #Joule

C1       = 1.*cp*rho*Vol1 #Joule
C2       = 15*cp*rho*Vol2 #Joule
C3       = 36.*cp*rho*Vol3 #Joule
C4       = 5.*cp*rho*Vol4 #Joule

# Thermal mass capacitance
#Zone 1
C15      = c*A1[2] # North wall
C16      = c*A1[0] # South wall
C17      = c*A1[1] # East wall
C18      = c*A1[3] # West wall
C19      = cply*A1[5] # floor
C127     = c*A1[4] # ceiling
#Zone 2
C210     = c*A2[2] # North wall
C211     = c*A2[0] # South wall
C212     = c*A2[1] # East wall
C213     = c*0.25*A2[3] # West wall
C214     = cply*A2[5] # floor
C226     = c*0.75*A2[3] # connection to zone 4
```

```
#Zone 3
C315    = cconcw*0.25*A3[2] # North wall
C315g   = cconcw*0.75*A3[2] # North wall connected to ground
C316    = cconcw*0.25*A3[0] # South wall
C316g   = cconcw*0.75*A3[0] # South wall connected to ground
C317    = cconcw*0.25*A3[1] # East wall
C317g   = cconcw*0.75*A3[1] # East wall connected to ground
C318    = cconcw*0.1*A3[3]  # West wall
C318g   = cconcw*0.75*A3[3]  # West wall connected to ground
C319    = cconcw*0.15*A3[3] # connection to zone 4
C325    = cconc*A3[5] # connection to ground
#Zone 4
C420    = c*A4[2] # North wall
C421    = c*A4[0] # South wall
C422    = c*A4[1] # East wall
C423    = c*A4[3] # West wall
C424    = cconc*A4[5] # connection to ground
C428    = c*A4[4] # ceiling

## WHOLE YEAR SIMULATION
#data        = np.genfromtxt("OATyear.txt", unpack=True) # To outdoor air temperature at 1
#t_new       = np.linspace(1,len(data),240*len(data), endpoint=True)
#To_set      = interp1d(np.arange(1,len(data)+1),data)
#To          = To_set(t_new) # To at 15 second intervals
#
#days = 365
#
#data1       = np.genfromtxt("Tsp1found.txt", unpack=True) # Set point temperature at 15 mi
#t_new1      = np.linspace(1,len(data1),240/4*len(data1), endpoint=True)
#Tsp_set     = interp1d(np.arange(1,len(data1)+1),data1)
#Tsp1        = Tsp_set(t_new1) # Tsp at 15 second intervals
#Tsp1         = np.tile(Tsp1,days)
#
#data2       = np.genfromtxt("Tsp2found.txt", unpack=True) # Set point temperature at 15 mi
#t_new2      = np.linspace(1,len(data2),240/4*len(data2), endpoint=True)
#Tsp_set     = interp1d(np.arange(1,len(data2)+1),data2)
#Tsp2        = Tsp_set(t_new2) # Tsp at 15 second intervals
#Tsp2         = np.tile(Tsp2,days)
#
#data3       = np.genfromtxt("Tsp3found.txt", unpack=True) # Set point temperature at 15 mi
#t_new3      = np.linspace(1,len(data3),240/4*len(data3), endpoint=True)
#Tsp_set     = interp1d(np.arange(1,len(data3)+1),data3)
#Tsp3        = Tsp_set(t_new3) # Tsp at 15 second intervals
#Tsp3         = np.tile(Tsp3,days)
#
#data4       = np.genfromtxt("ss.txt", unpack=True) # Set point temperature at 15 minutes i
#t_new4      = np.linspace(1,len(data4),240/4*len(data4), endpoint=True)
#Tsp_set     = interp1d(np.arange(1,len(data4)+1),data4)
#Tsp4        = Tsp_set(t_new4) # Tsp at 15 second intervals
#Tsp4         = np.tile(Tsp4,days)


### SIMULATION FOR EXPERIMENT 2
## Outdoor air temperature
data3       = np.genfromtxt("To2014-2.txt", unpack=True) # experiment 2
data3       = data3.astype(float)
t_new3      = np.linspace(1,len(data3),240/4*len(data3), endpoint=True)
```

```
Tout_15sec  = interp1d(np.arange(1, len(data3)+1), data3)
To          = Tout_15sec(t_new3)

#Solar radiation on South facade
data5       = np.genfromtxt("SR2014-2.txt", unpack=True) # experiment 2 in Wh/m2
data5       = data5/0.25 # in W/m2
xxx         = np.arange(0,len(data5)-1)

data5       = data5.astype(float)

for kkk in xxx:
    if data5[kkk] < 0:
        data5[kkk] = 0
    else:
        data5[kkk] = data5[kkk]

t_new5      = np.linspace(1,len(data5),240/4*len(data5), endpoint=True)
SR_15sec  = interp1d(np.arange(1, len(data5)+1), data5)
SR          = SR_15sec(t_new5)

days        = 12


#Zone 1 Tsp2014-2.txt
data9       = np.genfromtxt("Tsp2014-2.txt") # experiment 2
t_new9      = np.linspace(1,len(data9),240/4*len(data9), endpoint=True)
Tsp_set9    = interp1d(np.arange(1,len(data9)+1),data9)
Tsp9        = Tsp_set9(t_new9) # Tsp at 15 second intervals
Tspp9       = np.tile(Tsp9,days)

#Zone 1 qaux measured
data10       = np.genfromtxt("qaux1-2014-2.txt") # experiment 2
t_new10      = np.linspace(1,len(data10),240/4*len(data10), endpoint=True)
q_aux10    = interp1d(np.arange(1,len(data10)+1),data10)
qaux10        = q_aux10(t_new10) # Tsp at 15 second intervals

#Zone 2
data6       = np.genfromtxt("Tsp2014-2.txt") # experiment 2
t_new6      = np.linspace(1,len(data6),240/4*len(data6), endpoint=True)
Tsp_set6    = interp1d(np.arange(1,len(data6)+1),data6)
Tsp6        = Tsp_set6(t_new6) # Tsp at 15 second intervals
Tspp6       = np.tile(Tsp6,days)

#Zone 2 qaux measured
data11       = np.genfromtxt("qaux2-2014-2.txt") # experiment 2
t_new11      = np.linspace(1,len(data11),240/4*len(data11), endpoint=True)
q_aux11      = interp1d(np.arange(1,len(data11)+1),data11)
qaux11       = q_aux11(t_new11) # Tsp at 15 second intervals

#Zone 3
data7       = np.genfromtxt("Tsp2014-2.txt") # experiment 2
t_new7      = np.linspace(1,len(data7),240/4*len(data7), endpoint=True)
Tsp_set7    = interp1d(np.arange(1,len(data7)+1),data7)
Tsp7        = Tsp_set7(t_new7) # Tsp at 15 second intervals
Tspp7       = np.tile(Tsp7,days)

#Zone 3 qaux measured
```

```
data12       = np.genfromtxt("qaux3-2014-2.txt") # experiment 2
t_new12      = np.linspace(1,len(data12),240/4*len(data12), endpoint=True)
q_aux12      = interp1d(np.arange(1,len(data12)+1),data12)
qaux12       = q_aux12(t_new12) # Tsp at 15 second intervals

#Zone 4 Tsp2014-2_ZONE4.txt
data8       = np.genfromtxt("Tsp2014-2_ZONE4.txt") # experiment 2
t_new8      = np.linspace(1,len(data8),240/4*len(data8), endpoint=True)
Tsp_set8    = interp1d(np.arange(1,len(data8)+1),data8)
Tsp8        = Tsp_set8(t_new8) # Tsp at 15 second intervals
Tspp8       = np.tile(Tsp8,days)

#Zone 4 qaux measured
data13       = np.genfromtxt("qaux4-2014-2.txt") # experiment 2
t_new13      = np.linspace(1,len(data13),240/4*len(data13), endpoint=True)
q_aux13      = interp1d(np.arange(1,len(data13)+1),data13)
qaux13       = q_aux13(t_new13) # Tsp at 15 second intervals

qaux_all = data10 + data11 + data12 + data13

Tsp1        = Tsp9
Tsp2        = Tsp6
Tsp3        = Tsp7
Tsp4        = Tsp8

#Solar radiation incident on the south windows
SR_south1   = Aw1[0]*SR*0.1 #in W
SR_south2   = Aw2[0]*SR*0.1
SR_south3   = Aw3[0]*SR*0.1
SR_south4   = Aw4[0]*SR*0.1

Teq1        = To + SR*1/ho
Teq2        = To + SR*1/ho
Teq3        = To + SR*1/ho
Teq4        = To + SR*1/ho

Teq1 = To
Teq2 = To
Teq3 = To
Teq4 = To

# Controller parameters

Prop1        = np.zeros(Nfinal)
Int1         = np.zeros(Nfinal)
I1           = np.zeros(Nfinal)
PID1         = np.zeros(Nfinal)
Error1       = np.zeros(Nfinal)
Tsperr1      = np.zeros(Nfinal)

Prop2        = np.zeros(Nfinal)
Int2         = np.zeros(Nfinal)
I2           = np.zeros(Nfinal)
PID2         = np.zeros(Nfinal)
Error2       = np.zeros(Nfinal)
Tsperr2      = np.zeros(Nfinal)
```

```
Prop3        = np.zeros(Nfinal)
Int3         = np.zeros(Nfinal)
I3           = np.zeros(Nfinal)
PID3         = np.zeros(Nfinal)
Error3       = np.zeros(Nfinal)
Tsperr3      = np.zeros(Nfinal)

Prop4        = np.zeros(Nfinal)
Int4         = np.zeros(Nfinal)
I4           = np.zeros(Nfinal)
PID4         = np.zeros(Nfinal)
Error4       = np.zeros(Nfinal)
Tsperr4      = np.zeros(Nfinal)

q15          = np.zeros(Nfinal)
q16          = np.zeros(Nfinal)
q24          = np.zeros(Nfinal)
q34          = np.zeros(Nfinal)
q20          = np.zeros(Nfinal)
q21          = np.zeros(Nfinal)
q22          = np.zeros(Nfinal)
q23          = np.zeros(Nfinal)
q24          = np.zeros(Nfinal)
q28          = np.zeros(Nfinal)
q12          = np.zeros(Nfinal)
q12_2        = np.zeros(Nfinal)
q23_2        = np.zeros(Nfinal)
Rzn12        = np.zeros(Nfinal)
Rzn23        = np.zeros(Nfinal)
test         = np.zeros(Nfinal)
test2         = np.ones(Nfinal)*1.
test3         = np.ones(Nfinal)*1.

Q21         = np.zeros(Nfinal)
Q32         = np.zeros(Nfinal)

# grashof number
L12  = 0.001*Hh
L23  = 0.001*Hh
A12  = A1[4]*0.001
A23  = A2[4]*0.001
Gr12      = np.zeros(Nfinal)
Gr12[0]   = g*beta_air*L12**3/(mu_air**2)
Gr23      = np.zeros(Nfinal)
Gr23[0]   = g*beta_air*L23**3/(mu_air**2)
#inter-zonal convection
Uzn12     = np.zeros(Nfinal)
Uzn12[0]  = (0.3*(Gr12[0]**0.5)*Pr_air*k_air*A12)/L12
Uzn23     = np.zeros(Nfinal)
Uzn23[0]  = (0.3*(Gr23[0]**0.5)*Pr_air*k_air*A23)/L23
Rzn12[0]  =1./Uzn12[0]
Rzn23[0]  =1./Uzn23[0]

dd           = 1.
ddd          = 1.

Kp           = 1400. # watt/degC
```

```
Kp1          = 2000.
Kp2          = 1900.
Kp3          = 2000.
Kp4          = 1600.
Ki           = 0.1
i            = 1.

############################################################
#==========================================================#
############################################################
#CVRMSE - Nelder-Mead OPTIMIZED

##Step C
R4inf = 0.05000652
#
##Step D

##Step E
C2 =     2576625.54
R2inf =   0.67219284
R23inf =     0.00210612
#
##Step F
C1 =    704023.9937
R1inf =   4.77769937
R12inf =  0.00195504487

############################################################
#==========================================================#
############################################################

# Energy balance equations at air nodes using explicit finite difference method
#def cv(parm, qaux_all, p2):
#    C1 = parm
#    Int1       = np.zeros(Nfinal)
#    I1       = np.zeros(Nfinal)
#    Int2       = np.zeros(Nfinal)
#    I2       = np.zeros(Nfinal)
#    Int3       = np.zeros(Nfinal)
#    I3       = np.zeros(Nfinal)
#    Int4       = np.zeros(Nfinal)
#    I4       = np.zeros(Nfinal)
for j in p2:
    if j > 1:
        if abs(Tsp1[j]- Tsp1[j-1]) > 0.01:
            # check to see when setpoint is changed
            Tsperr1[j] = abs(Tsp1[j] - Tsp1[j-1])
            Int1       = np.zeros(Nfinal)
            I1         = np.zeros(Nfinal)
        else:
            pass
    else:
        pass
    if Tsp1[j] > T1[j]:
        # set Error parameter to temperature error
        Error1[j+1]    = Tsp1[j] - T1[j]
    else:
```

```
        Error1[j+1]    = 0
    Prop1[j+1]         = Error1[j+1] # set Prop parameter to Error
    Int1[j+1]          = (Error1[j+1]+Error1[j])*deltaT/2. # set Int parameter to average e
    I1[j+1]            = np.sum(Int1) # sum of Int terms
    PID1[j+1]          = Kp1*Prop1[j]+Ki*I1[j+1] # value of actuator (auxiliary heater)
    # threshold of 0.1 degree C
    if PID1[j+1] > qmax1 and Error1[j+1] > 0.1:
        qaux1[j+1]     = qmax1
    elif Error1[j+1] > 0.1:
        qaux1[j+1]     = PID1[j+1]
    else:
        qaux1[j+1]     = 0
################################
    if j > 1:
        if abs(Tsp2[j]- Tsp2[j-1]) > 0.01:
            # check to see when setpoint is changed
            Tsperr2[j] = abs(Tsp2[j] - Tsp2[j-1])
            Int2       = np.zeros(Nfinal)
            I2         = np.zeros(Nfinal)
        else:
            pass
    else:
        pass
    if Tsp2[j] > T2[j]:
        # set Error parameter to temperature error
        Error2[j+1]    = Tsp2[j] - T2[j]
    else:
        Error2[j+1]    = 0
    Prop2[j+1]         = Error2[j+1] # set Prop parameter to Error
    Int2[j+1]          = (Error2[j+1]+Error2[j])*deltaT/2. # set Int parameter to average e
    I2[j+1]            = np.sum(Int2) # sum of Int terms
    PID2[j+1]          = Kp2*Prop2[j]+Ki*I2[j+1] # value of actuator (auxiliary heater)
    # threshold of 0.1 degree C
    if PID2[j+1] > qmax2 and Error2[j+1] > 0.1:
        qaux2[j+1]     = qmax2
    elif Error2[j+1] >0.1:
        qaux2[j+1]     = PID2[j+1]
    else:
        qaux2[j+1]     = 0
################################
    if j > 1:
        if abs(Tsp3[j]- Tsp3[j-1]) > 0.01:
            # check to see when setpoint is changed
            Tsperr3[j] = abs(Tsp3[j] - Tsp3[j-1])
            Int3       = np.zeros(Nfinal)
            I3         = np.zeros(Nfinal)
        else:
            pass
    else:
        pass
    if Tsp3[j] > T3[j]:
        # set Error parameter to temperature error
        Error3[j+1]    = Tsp3[j] - T3[j]
    else:
        Error3[j+1]    = 0
    Prop3[j+1]         = Error3[j+1] # set Prop parameter to Error
    Int3[j+1]          = (Error3[j+1]+Error3[j])*deltaT/2. # set Int parameter to average e
```

```
    I3[j+1]             = np.sum(Int3) # sum of Int terms
    PID3[j+1]           = Kp3*Prop3[j]+Ki*I3[j+1] # value of actuator (auxiliary heater)
    # threshold of 0.1 degree C
    if PID3[j+1] > qmax3 and Error3[j+1] > 0.1:
        qaux3[j+1]      = qmax3
    elif Error3[j+1] > 0.1:
        qaux3[j+1]      = PID3[j+1]
    else:
        qaux3[j+1]      = 0
################################
    if j > 1:
        if abs(Tsp4[j]- Tsp4[j-1]) > 0.01:
            # check to see when setpoint is changed
            Tsperr4[j] = abs(Tsp4[j] - Tsp4[j-1])
            Int4       = np.zeros(Nfinal)
            I4         = np.zeros(Nfinal)
        else:
            pass
    else:
        pass
    if Tsp4[j] > T4[j]:
        # set Error parameter to temperature error
        Error4[j+1]     = Tsp4[j] - T4[j]
    else:
        Error4[j+1]     = 0
    Prop4[j+1]          = Error4[j+1] # set Prop parameter to Error
    Int4[j+1]           = (Error4[j+1]+Error4[j])*deltaT/2. # set Int parameter to average e
    I4[j+1]             = np.sum(Int4) # sum of Int terms
    PID4[j+1]           = Kp4*Prop4[j]+Ki*I4[j+1] # value of actuator (auxiliary heater)
    # threshold of 0.1 degree C
    if PID4[j+1] > qmax4 and Error4[j+1] > 0.1:
        qaux4[j+1]      = qmax4
    elif Error4[j+1] > 0.1:
        qaux4[j+1]      = PID4[j+1]
    else:
        qaux4[j+1]      = 0
    if Tsp2[j] < Tsp1[j] and T2[j] < T1[j] :
        Q21[j] = 0
    else:
        Q21[j] = ((T2[j]+0.6-T1[j])/R12inf)
    if Tsp3[j] < Tsp2[j] and T3[j] < T2[j]:
        Q32[j] = 0
    else:
        Q32[j] = ((T3[j]+1.-T2[j])/R23inf)
    T1[j+1]      = (deltaT/C1)*(qaux1[j]+((((To[j]-T1[j])/R1inf)+Q21[j]
                    +((T5[j]-T1[j])/R15)+((To[j]-T1[j])/Rw1oN)
                    +((T6[j]-T1[j])/R16)+((Teq1[j]-T1[j])/Rw1oS)
                    +((T7[j]-T1[j])/R17)+((T8[j]-T1[j])/R18)
                    +((T9[j]-T1[j])/R19))+((T27[j]-T1[j])/R127)))+T1[j]
    T2[j+1]      = (deltaT/C2)*(qaux2[j]+((((To[j]-T2[j])/R2inf)-Q21[j]
                    +Q32[j]+((T10[j]-T2[j])/R210)+((To[j]-T2[j])/Rw2oN)
                    +((T11[j]-T2[j])/R211)+((Teq2[j]-T2[j])/Rw2oS)
                    +((T12[j]-T2[j])/R212)+((T13[j]-T2[j])/R213)
                    +((T14[j]-T2[j])/R214))+((T26[j]-T2[j])/R226)))+T2[j]
    T3[j+1]      = (deltaT/C3)*(qaux3[j]+((((To[j]-T3[j])/R3inf)-Q32[j]
                    +((T15[j]-T3[j])/R315)+((T15g[j]-T3[j])/R315g)
                    +((To[j]-T3[j])/Rw3oN)+((T16[j]-T3[j])/R316)
```

```
                 +((T16g[j]-T3[j])/R316g)+((T17[j]-T3[j])/R317)
                 +((T17g[j]-T3[j])/R317g)+((To[j]-T3[j])/Rw3oE)
                 +((T18[j]-T3[j])/R318)+((T18g[j]-T3[j])/R318g)
                 +((T19[j]-T3[j])/R319))+((T25[j]-T3[j])/R325)))+T3[j]
T4[j+1]       = (deltaT/C4)*(qaux4[j]+((((To[j]-T4[j])/R4inf)
                 +((T20[j]-T4[j])/R420)+((T21[j]-T4[j])/R421)
                 +((T22[j]-T4[j])/R422)+((T23[j]-T4[j])/R423)
                 +((To[j]-T4[j])/Rw4oW)+(((T19[j]-T4[j])/R419))
                 +(((T26[j]-T4[j])/R426))+((T24[j]-T4[j])/R424))))+T4[j]
T5[j+1]       = (deltaT/C15)*(((T1[j]-T5[j])/R15)+((To[j]-T5[j])/R5o))+T5[j]
T6[j+1]       = (deltaT/C16)*(((T1[j]-T6[j])/R16)+((Teq1[j]-T6[j])/R6o))+T6[j]
T7[j+1]       = (deltaT/C17)*(((T1[j]-T7[j])/R17)+((To[j]-T7[j])/R7o))+T7[j]
T8[j+1]       = (deltaT/C18)*(((T1[j]-T8[j])/R18)+((To[j]-T8[j])/R8o))+T8[j]
T9[j+1]       = (deltaT/C19)*(((T1[j]-T9[j])/R19)+((T2[j]-T9[j])/R29))+T9[j]
T10[j+1]      = (deltaT/C210)*(((T2[j]-T10[j])/R210)+((To[j]-T10[j])/R10o))
                 +T10[j]
T11[j+1]      = (deltaT/C211)*(((T2[j]-T11[j])/R211)+((Teq2[j]-T11[j])/R11o))
                 +T11[j]
T12[j+1]      = (deltaT/C212)*(((T2[j]-T12[j])/R212)+((To[j]-T12[j])/R12o))
                 +T12[j]
T13[j+1]      = (deltaT/C213)*(((T2[j]-T13[j])/R213)+((To[j]-T13[j])/R13o))
                 +T13[j]
T14[j+1]      = (deltaT/C214)*(((T2[j]-T14[j])/R214)+((T3[j]-T14[j])/R314))
                 +T14[j]
T15[j+1]      = (deltaT/C315)*(((T3[j]-T15[j])/R315)+((To[j]-T15[j])/R15o))
                 +T15[j]
T15g[j+1]     = (deltaT/C315g)*(((T3[j]-T15g[j])/R315g)
                               +((Tg[j]-T15g[j])/R15g))+T15g[j]
T16[j+1]      = (deltaT/C316)*(((T3[j]-T16[j])/R316)+((Teq3[j]-T16[j])/R16o))
                 +T16[j]
T16g[j+1]     = (deltaT/C316g)*(((T3[j]-T16g[j])/R316g)
                               +((Tg[j]-T16g[j])/R16g))+T16g[j]
T17[j+1]      = (deltaT/C317)*(((T3[j]-T17[j])/R317)+((To[j]-T17[j])/R17o))
                 +T17[j]
T17g[j+1]     = (deltaT/C317g)*(((T3[j]-T17g[j])/R317g)
                               +((Tg[j]-T17g[j])/R17g))+T17g[j]
T18[j+1]      = (deltaT/C318)*(((T3[j]-T18[j])/R318)+((To[j]-T18[j])/R18o))
                 +T18[j]
T18g[j+1]     = (deltaT/C318g)*(((T3[j]-T18g[j])/R318g)
                               +((Tg[j]-T18g[j])/R18g))+T18g[j]
T19[j+1]      = (deltaT/C319)*(((T3[j]-T19[j])/R319)+((T4[j]-T19[j])/R419))
                 +T19[j]
T20[j+1]      = (deltaT/C420)*(((T4[j]-T20[j])/R420)+((To[j]-T20[j])/R20o))
                 +T20[j]
T21[j+1]      = (deltaT/C421)*(((T4[j]-T21[j])/R421)+((Teq4[j]-T21[j])/R21o))
                 +T21[j]
T22[j+1]      = (deltaT/C422)*(((T4[j]-T22[j])/R422)+((To[j]-T22[j])/R22o))
                 +T22[j]
T23[j+1]      = (deltaT/C423)*(((T4[j]-T23[j])/R423)+((To[j]-T23[j])/R23o))
                 +T23[j]
T24[j+1]      = (deltaT/C424)*(((T4[j]-T24[j])/R424)+((Tg[j]-T24[j])/R24g))
                 +T24[j]
T25[j+1]      = (deltaT/C325)*(((T3[j]-T25[j])/R325)+((Tg[j]-T25[j])/R25g))
                 +T25[j]
T26[j+1]      = (deltaT/C226)*(((T2[j]-T26[j])/R226)+((T4[j]-T26[j])/R426))
                 +T26[j]
T27[j+1]      = (deltaT/C127)*(((T1[j]-T27[j])/R127)+((To[j]-T27[j])/R27o))
```

```
                    +T27[j]
    T28[j+1]     = (deltaT/C428)*(((T4[j]-T28[j])/R428)+((To[j]-T28[j])/R28o))
                    +T28[j]
    q15[j+1]     = (T5[j]-To[j])/(R5o)
    q16[j+1]     = (T6[j]-To[j])/(R6o)
    q24[j+1]     = (T4[j]-T2[j])/(R426+R226)
    q34[j+1]     = (T4[j]-T3[j])/(R419)
    q20[j+1]     = (T4[j]-To[j])/(R20o)
    q21[j+1]     = (T4[j]-To[j])/(R21o)
    q22[j+1]     = (T4[j]-To[j])/(R22o)
    q24[j+1]     = (T4[j]-Tg[j])/(R24g)
    q28[j+1]     = (T4[j]-To[j])/(R28o)
    Gr12[j+1]    = ((T2[j]+1-T1[j])*g*beta_air*(L12**3))/(mu_air**2)
    Gr23[j+1]    = ((T3[j]+2-T2[j])*g*beta_air*(L23**3))/(mu_air**2)
    Uzn12[j+1]   = (0.3*(Gr12[j]**0.5)*Pr_air*k_air*A12)/L12
    Uzn23[j+1]   = (0.3*(Gr23[j]**0.5)*Pr_air*k_air*A23)/L23
    q12[j+1]     = (abs(T2[j]+1-T1[j]))*Uzn12[j]
    q23[j+1]     = (abs(T3[j]+2-T2[j]))*Uzn23[j]
    q12_2[j+1]   = (abs(T2[j]+1-T1[j]))/R12inf
    q23_2[j+1]   = (abs(T3[j]+2-T2[j]))/R23inf
    Rzn12[j+1]   = 1./Uzn12[j]
    Rzn23[j+1]   = 1./Uzn23[j]
    if Rzn23[j+1] > R23inf:
        Rzn23[j+1] = R23inf
    else:
        pass
    test[j+1] = 0.*((abs(T3[j]+2-T2[j]))/Rzn23[j])
    test2[j+1] =abs(T2[j]+1-T1[j])
    test3[j+1]= abs(T3[j]+1-T2[j])

TT1 = np.mean(T1.reshape(-1, 60), axis=1)
TT2 = np.mean(T2.reshape(-1, 60), axis=1)
TT3 = np.mean(T3.reshape(-1, 60), axis=1)
TT4 = np.mean(T4.reshape(-1, 60), axis=1)

TTavg = ((TT1*(A1[5]))/(A1[5]+A2[5]+A3[5]+A4[5])) +
        ((TT2*(A2[5]))/(A1[5]+A2[5]+A3[5]+A4[5]))+
        ((TT3*(A3[5]))/(A1[5]+A2[5]+A3[5]+A4[5]))+
        ((TT4*(A4[5]))/(A1[5]+A2[5]+A3[5]+A4[5]))

qqaux1 = np.mean(qaux1.reshape(-1, 60), axis=1)
qqaux2 = np.mean(qaux2.reshape(-1, 60), axis=1)
qqaux3 = np.mean(qaux3.reshape(-1, 60), axis=1)
qqaux4 = np.mean(qaux4.reshape(-1, 60), axis=1)
qqauxall = qqaux1 + qqaux2 + qqaux3 + qqaux4
N1 = len(data10[625:1151])-1
N2 = len(data11[625:1151])-1
N3 = len(data12[625:1151])-1
N4 = len(data13[625:1151])-1
Nall = len(qaux_all[625:1151])-1
meas_mean1 =np.mean(data10[625:1151])
meas_mean2 =np.mean(data11[625:1151])
meas_mean3 =np.mean(data12[625:1151])
meas_mean4 =np.mean(data13[625:1151])
meas_meanall =np.mean(qaux_all[625:1151])
CVRMSE1 = np.sqrt(np.sum((data10[625:1151]-qqaux1[625:1151])**2)/N1)/meas_mean1
CVRMSE2 = np.sqrt(np.sum((data11[625:1151]-qqaux2[625:1151])**2)/N2)/meas_mean2
```

```
CVRMSE3 = np.sqrt(np.sum((data12[625:1151]-qqaux3[625:1151])**2)/N3)/meas_mean3
CVRMSE4 = np.sqrt(np.sum((data13[625:1151]-qqaux4[625:1151])**2)/N4)/meas_mean4
CVRMSEall = np.sqrt(np.sum((qaux_all[625:1151]-qqauxall[625:1151])**2)/Nall)/meas_meanall
#CVRMSE = CVRMSE1
#    #        return CVRMSE
#
#np.savetxt('qqaux1-DM.txt',qqaux1,delimiter=',')
#np.savetxt('qqaux2-DM.txt',qqaux2,delimiter=',')
#np.savetxt('qqaux3-DM.txt',qqaux3,delimiter=',')
#np.savetxt('qqaux4-DM.txt',qqaux4,delimiter=',')
#np.savetxt('qqauxall-DM.txt',qqauxall,delimiter=',')


#ONE DAY CVRMSEall

qaux_all1 = qaux_all[625+96*3:625+96*4]
qqauxall1 = qqauxall[625+96*3:625+96*4]
Nall1 = len(qaux_all[625+96*3:625+96*4])-1
meas_meanall1 = np.mean(qaux_all[625+96*3:625+96*4])
CVRMSEall1 = np.sqrt(np.sum((qaux_all[625+96*3:625+96*4]-
                             qqauxall[625+96*3:625+96*4])**2)/Nall1)/meas_meanall1

#6 Hours CVRMSEall

qaux_all6 = qaux_all[625+96*3:(625+96*3)+(6*4)]
qqauxall6 = qqauxall[625+96*3:(625+96*3)+(6*4)]
Nall6 = len(qaux_all[625+96*3:(625+96*3)+(6*4)])-1
meas_meanall6 = np.mean(qaux_all[625+96*3:(625+96*3)+(6*4)])
CVRMSEall6 = np.sqrt(np.sum((qaux_all[625+96*3:(625+96*3)+(6*4)]-
                             qqauxall[625+96*3:(625+96*3)+(6*4)])**2)/Nall6)/meas_meanall6


#3 Hours CVRMSEall

qaux_all3 = qaux_all[625+96*3:(625+96*3)+(3*4)]
qqauxall3 = qqauxall[625+96*3:(625+96*3)+(3*4)]
Nall3 = len(qaux_all[625+96*3:(625+96*3)+(3*4)])-1
meas_meanall3 = np.mean(qaux_all[625+96*3:(625+96*3)+(3*4)])
CVRMSEall3 = np.sqrt(np.sum((qaux_all[625+96*3:(625+96*3)+(3*4)]-
                             qqauxall[625+96*3:(625+96*3)+(3*4)])**2)/Nall3)/meas_meanall3


np.savetxt('qqauxall_detailed.txt',qqauxall[625:1151],delimiter = ',')
np.savetxt('qqauxall_measured.txt',qaux_all[625:1151],delimiter = ',')
#np.savetxt('TTavg_detailed.txt',TTavg[625:1151],delimiter = ',')


####################  optimization  ###################

#p0 = [C11]
#
#from scipy.optimize import minimize
#res = minimize(cv, p0, args=(qaux_all, p2), method='nelder-mead', options={'xtol': 0.3, 'c
#print (np.array(p0))
#print (res.x)

#################### ^^ optimization ^^ ###################
```

```
p2               = np.arange(0.,No*60.*24./deltaT)

TT1              = np.mean(T1.reshape(-1, 60), axis=1) # Averages every 60 values to get 15
TT2              = np.mean(T2.reshape(-1, 60), axis=1) # Averages every 60 values to get 15
TT3              = np.mean(T3.reshape(-1, 60), axis=1) # Averages every 60 values to get 15
TT4              = np.mean(T4.reshape(-1, 60), axis=1) # Averages every 60 values to get 15

qqaux1           = np.mean(qaux1.reshape(-1, 60), axis=1)
qqaux2           = np.mean(qaux2.reshape(-1, 60), axis=1)
qqaux3           = np.mean(qaux3.reshape(-1, 60), axis=1)
qqaux4           = np.mean(qaux4.reshape(-1, 60), axis=1)

Q1               = qqaux1*0.25
Q2               = qqaux2*0.25
Q3               = qqaux3*0.25
Q4               = qqaux4*0.25

Tssp1            = np.mean(Tsp1.reshape(-1, 60), axis=1)
Too              = np.mean(To.reshape(-1, 60), axis=1)
peak1            = max(qqaux1)
peak2            = max(qqaux2)
peak3            = max(qqaux3)
peak4            = max(qqaux4)

TotalE1          = np.sum(Q1)
TotalE2          = np.sum(Q2)
TotalE3          = np.sum(Q3)
TotalE4          = np.sum(Q4)

TotalQ           = Q1 + Q2 + Q3 + Q4
TotalP           = qqaux1 + qqaux2 + qqaux3 + qqaux4

#plt.plot(qqaux4)
p1 = plt.plot(q23,'blue')
p2 = plt.plot(q23_2,'green')
q_23 = mpatches.Patch(color='blue', label='q23')
q_23_2 = mpatches.Patch(color='green', label='q23_2')
plt.legend(handles=[q_23,q_23_2])
plt.show()
np.savetxt('TT1.txt',TT1,delimiter=',')
np.savetxt('TT2.txt',TT2,delimiter=',')
np.savetxt('TT3.txt',TT3,delimiter=',')
np.savetxt('TT4.txt',TT4,delimiter=',')

if days > 12:
    day              = 57
    v                = 0+24*(day-1)
    b                = 24+24*(day-1)
    d                = 0+96*(day-1)
    e                = 96+96*(day-1)
    peakdayE         = np.sum(TotalQ[d:e])/1000;

    Tairpeak1=TT1[d:e]
    Tairpeak2=TT2[d:e]
    Tairpeak3=TT3[d:e]
    Tairpeak4=TT4[d:e]
```

```
    qauxpeak1=qqaux1[d:e]
    qauxpeak2=qqaux2[d:e]
    qauxpeak3=qqaux3[d:e]
    qauxpeak4=qqaux4[d:e]
    qauxpeak=TotalP[d:e]

    Topeak=Too[d:e]
    Tsppeak1=Tssp1[d:e]


print("--- %s seconds ---" % (time.time() - start_time))
```

Identifying Parameters: An Example

A pseudocode for implementation within Python environment and *SciPy* is shown below in Algorithm 1. The R and Ca values are identified for a 1R1C thermal network model with inputs of 1) heating power ($P_{measured}$) and 2) outdoor air temperature (T_{out}) and model output of indoor air temperature T_{zone}.

Algorithm 1: R, C Parameter Identification

Data: $T_{measured}$: Indoor air temperature vector of length l
$P_{measured}$: Input heating power vector of length l
T_{out}: Outdoor air temperature vector of length l
Result: R and C values of model

Initialization: $x_0 = [R_0; C_0]$: Initial parameter vector;
Initialization: $T_{zone}[1]$: Initial indoor air temperature value;
Function `cv(`x_0, $T_{measured}$, $P_{measured}$, T_{out}`)`**:**
    $R, C = x_0$;
    for $i = 1$ **to** l **do**
        $T_{zone}[i+1] = \frac{\Delta t}{C} \times \left(P_{measured}[i] + \frac{T_{out}[i] - T_{zone}[i]}{R}\right) + T_{zone}[i]$;
    end
    $J = \sqrt{\frac{\sum_{i=1}^{n}(T_{zone}[i] - T_{measured}[i])^2}{n}}$;
    `/* The objective function to minimize is RMSE of indoor air temp */`
    return J;
End Function;
res = `minimize(cv,` x_0, *args=(*$T_{measured}$, $P_{measured}$, T_{out}*)*`);`
`/* ‘minimize’ is a SciPy function */`
`/* The output of ’res’ is the identified R and C values */`

These control-oriented models are intended to be used, along with knowledge of future conditions (such as electricity pricing, occupancy, weather forecasts etc.) to plan the operation strategies within the BAS to achieve such goals as demand reduction, energy reduction, improved occupancy comfort or enhanced energy flexibility of the building, to name a few.

Appendix B: MATLAB Code - Sample of Bank Building MPC Model

The building used in the year long model predictive control study is a 427 square meter (4,600sqft) single storey commercial building used as a bank. A 3D rendering of the building can be seen in Figure B1. A rendering of an energy plus model was created of the building with 21 thermal zones, shown in Figure B2. The location of the building is in Trois Riviere, Québec. The wall insulation is 3 RSI, while the roof insulation is 3.45 RSI. The windows are assumed as double glazing low-e type with 12.7mm air gap.

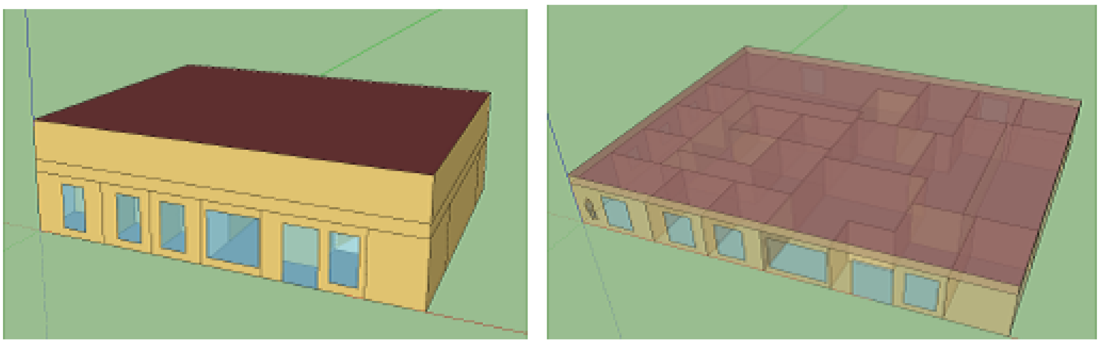

Figure B1: Rendering of the building showing thermal zones (Lavigne et al., 2014)

Figure B2: Thermal zones of the building (Lavigne et al., 2014)

This study makes use of MATLAB and Simulink (MATLAB'S graphical simulation environment), as a tool to investigate and evaluate MPC strategies. The developed simulink model interface prototype is shown in Figure B3 and the MPC code is shown below.

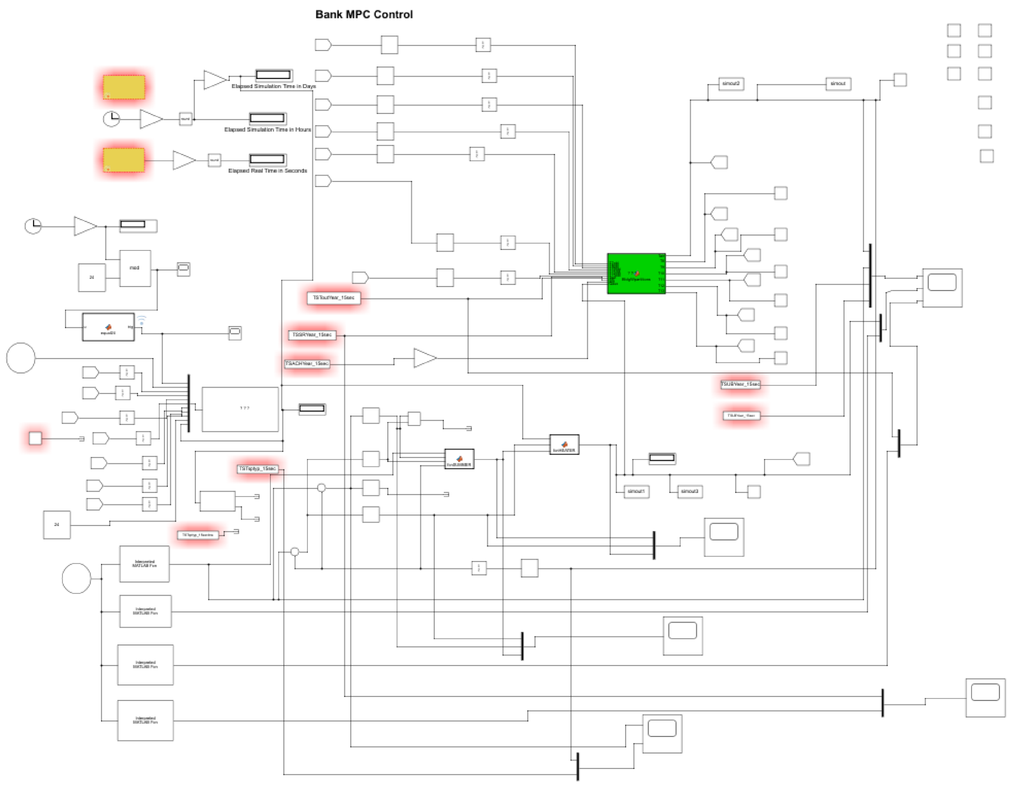

Figure B3: Simulink Model Interface

Sample of MATLAB Bank Building MPC Code

```
function
 bank5minTEST_allinoneYR(trigger,time,T7R,T8R,T9R,T10R,T11R,T12R,qauxR,Phorz2)

    global index
    global index2
    global index3
    global dt
    global Tspid
    global Tout
    global a
    global Tsp
    global ACH
    global SRWIN
    global SR_global
    global Tspid1
    global UB2
    global LB2
    global simout
    global simout1
    global troom
    global troom1
    global troom2
    global qauxx
    global qauxxx
    global Tspidfound
    global ACHYear_15min
    global LBYear_15min
    global ToutYear_15min
    global UBYear_15min
    global SRYear_15min

    global ACHYear_15sec
    global ACHYear_5min
    global LBYear_15sec
    global LBYear_5min
    global ToutYear_15sec
    global ToutYear_5min
    global UBYear_15sec
    global UBYear_5min
    global SRYear_15sec
    global SRYear_5min
    global TspYR
    global Phorz
    global qaux
    global qauxid
    global ToNoise
    global XNoiseold
    global noise
    global SRNoise
    global y2
    global Tspid3
```

```
global EcostYear_15sec

Phorz = Phorz2;

 index = floor(time/15)+1;

 day = floor(time/3600/24)+1;

function [Pmax] = Bank_5min1(Tsp2)

    Hh=3.05; %m
    Lh=18.5; %m       %Length of room (South/North Wall)
    Wh=23; %m %Width of room (West/East Wall)
    Hi=3.05; %m
    Aw=[4.209;0;14.03;3.39]; %m^2 %Window Areas (N/E/S/W)
    A=[Lh*Hh-Aw(1); Wh*Hh-Aw(2); Lh*Hh-Aw(3); Wh*Hh-Aw(4); Wh*Lh;
Wh*Lh]; %m^2 %Net Wall areas
    Vol=A(5)*Hi; %m^3 %room volume
    Rw=0.33; %m^2*degC/watt %Window Resistance (U=3)
    h=8.3; %watt/(m^2*degC) %interior film coefficient of surfaces
walls
    hc=[h; h; h; h; 9; 9.3];%watt/(m^2*degC) %interior film
coeffients
    ach=0.5; % air change per hour for infiltration/exfiltration
    cp=1000; %joule/(kg*degC) %specific heat of air
    rho=1.2; %kg/m^3 %density of air
    Uinf=ach*Vol*cp*rho/3600; %watt/degC %U of infiltration
exterior

    %%%%%%%%%%%%%%%%%%%%%%%%%%%%%%%%%%%%%%%%%%%%%%%%
    %THERMAL RESISTANCES OF WALLS (incl air films)
    %%%%%%%%%%%%%%%%%%%%%%%%%%%%%%%%%%%%%%%%%%%%%%%%
    %Vertical Exterior Walls
    Lgyp=0.013; %m %Gypsum board layer
    rhogyp=640; %kg/m^3
    kgyp=0.16; %watt/(m*degC)
    cgyp=1150; %joule/(kg*degC)
    Rener=0;
    Rins=3; %(m^2*degC)/watt %Insulation layer
    Rsid=0.48; %(m^2*degC)/watt %Air gap, Fiberboard, plywood,
vinyl
    ho=32; %watt/(m^2*degC) %Exterior film
    ff=0.25; %percentage %15% framing area
    Rf=1.1667; %(m^2*degC)/watt %Wood stud
    R(2)=1/(((1-ff)/((Lgyp/kgyp)+Rener+Rins+Rsid+(1/ho)+(1/
h)))+(((ff)/((Lgyp/kgyp)+Rener+Rf+Rsid+(1/ho)+(1/h))))); %(m^2*degC)/
watt %Exterior wall resistance
    R(3)=R(2); %(m^2*degC)/watt
    R(1)=R(2);
    R(4)=R(2);
```

```
        Rinsc=4.67;%(m^2*degC)/watt %Ceiling
        ha=12; %watt/(m^2*degC) %attic air film
        Rc=1/(((1-ff)/((Lgyp/kgyp)+Rener+Rinsc+(1/
ha)+(1/hc(5))))+(((ff)/((Lgyp/kgyp)+Rener+Rf+(1/ha)+(1/
hc(5))))));%(m^2*degC)/watt %Ceiling resistance

        Rb=0.14;%(m^2*degC)/watt %Roof %shingle backer board
        Rsh=0.078;%(m^2*degC)/watt %Wood shingles
        Rr=1/(((1-ff)/(Rb+Rsh+(1/ho)+(1/ha)))+(((ff)/(Rb+Rf+Rsh+(1/
ha)+(1/ho)))));%(m^2*degC)/watt %Roof resistance

        Ar=A(5)/cos(30*3.14/180); %m^2
        R(5)=((Rc/A(5))+(Rr/Ar))*A(5); %(m^2*degC)/watt %Combined
 Celining-roof resistance

        Lcar=0.02;%m %FLOOR        %Concrete slab with carpet
 %carpet and underpad
        kcar=0.06;%watt/mdegC
        rhocar=800;%kg/m3
        Lcon=0.2; %m
        kcon=1.9; %watt/mdegC
        rhocon=2200; %kg/m3
        cins=800;
        Rair=0.18;
        ccon=800;

        R(6)=(Lcon/kcon)+(Lcar/kcar)+(1/ho)+(1/hc(6));%(m^2*degC)
 %Floor resistance
        Rcon=Lcon/kcon;

        c=rhogyp*cgyp*Lgyp; %Joule/m^2 GYPSUM %WALL CAPACITANCES
        c6=ccon*rhocon*Lcon;
        C=[c*A(1); c*A(2); c*A(3); c*A(4); c*A(5); c6*A(6)]; %Joule
        Cair=7*cp*rho*Vol; %Joule

        Aint = 360.25; %m % Interior wall area - sum of all areas
        Cint = rhogyp*cgyp*2*Lgyp*Aint;

        C9=C(1)+C(2)+C(3)+C(4)+C(5); %C9 in Mathcad %Joule/degC
    %Thermal Network %thermal capacitance of interior layer of the
 exterior walls
        C11=C(6)/2; %C11 in Mathcad %Joule %Thermal capacitance of
 interior layer of floor
        C12=C11;
        R78=1/
((A(1)*hc(1))+(A(4)*hc(4))+(A(2)*hc(2))+(A(3)*hc(3))+(A(5)*hc(5))); %degC/
watt %Convective thermal resistance form air node to exterior wall
 surfaces
        R710=1/(kcar*A(6)/Lcar)+1/((A(6)*hc(6)));%degC/watt %Convectiv
 thermal resistance from air node to floor surface
        R7o=1/(Uinf+(sum(Aw)/Rw));%degC/watt %Infiltration and window
 thermal resistance
```

```
        R89= 1/((kgyp*A(1)*2/Lgyp)+(kgyp*A(4)*2/Lgyp)+(kgyp*A(2)*2/
Lgyp)+(kgyp*A(3)*2/Lgyp)+(kgyp*A(5)*2/Lgyp));%degC/watt %resistance
 from inside wall surface to half way into gypsum board
        R9o=(1/((A(1)/R(1))+(A(4)/R(4))+(A(2)/R(2))+(A(3)/R(3))+(A(5)/
R(5))))-R89-R78;%degC/watt %resistace from half way into gypsum board
 to outside
        R1011=0.25*Lcon/(kcon*A(6));%degC/watt %resistance to 1/4 into
 concrete
        R1112=0.5*Rcon/A(6);%degC/watt
        R12g = R1011;

        TS=[(C9/((1/R89)+(1/R9o)));  (C11/((1/R1011)+(1/R1112))); C12/
((1/R1112)+(1/R12g))]; %seconds
        detlaTcrit=min(TS); %seconds

        deltaT = 300; %seconds

        T_low=21; %step down night time temperature USER INPUT
        T_high=23; %step up day time temperature USER INPUT
        T_out=-23;


        No=1; %Number of days
        NT=No*86400/deltaT; %number of time steps in a day
        p=1:1:NT;
        t=p.*deltaT;
        if day <=178
            qmax=55000; %watt
        elseif day >=363
            qmax=55000; %watt
        else
            qmax = 22000;
        end
        qmin = -21000;
        Kp=50000/5.5; %watt/degC %proportional control constand of
 baseboard heater
        Ki=0.8;
        Ki=0.05;
        i=1;

        %          SR = importdata('SR_5min.mat');
        %          To = importdata('To_5min.mat');
        %          ach = importdata('ach_5min.mat');

        if Phorz >24 && Phorz < 48
            H = 1.5;
        else
            H = floor(Phorz/24);
        end



        To = ToNoise(index:index+(H*5760-1));
        ach = ACHYear_15sec(index:index+(H*5760-1));
```

```
        SR = SRNoise(index:index+(H*5760-1));

        z=300/15;
        xx=reshape(To,z,[]);
        To=sum(xx,1)./size(xx,1);

        z=300/15;
        xx=reshape(ach,z,[]);
        ach=sum(xx,1)./size(xx,1);

        z=300/15;
        xx=reshape(SR,z,[]);
        SR=sum(xx,1)./size(xx,1);

        t_new3=linspace(1,numel(Tsp2),12*numel(Tsp2));
        Tsp_5min = interp1(Tsp2, t_new3);
        Tsp3 = Tsp_5min;

        Uinf=ach*Vol*cp*rho/3600;

        R7o=0.9*(1./(Uinf+(sum(Aw)/Rw)));

        %effective transmittance-absorptance of windows
        ta=0.4;
        Teq_15sec = To+0*SR*ta/ho;
        Teq=Teq_15sec;

        days = Phorz/24;

        %Solar radiation incident on the window
        SRwin=Aw(3)*SR; %watts



        Nfinal=NT*days; %second
        dT=1; %second
        u=0;
        j=1;
        qaux=zeros(Nfinal,1)+4000;
        T7=zeros(Nfinal,1);
        T8=zeros(Nfinal,1);
        T9=zeros(Nfinal,1);
        T10=zeros(Nfinal,1);
        T11=zeros(Nfinal,1);
        T12=zeros(Nfinal,1);
        Tg=ones(Nfinal,1)*20; %13 ground temp from ecoterra
measurements. ref: Xiang Chen. 20 from Michael Fournier from HQ
        qaux(1)=4000; %watt

        if time > 0
            %troom1 = troom2(index3-1);
            T7(1)=T7R; %degC
            T8(1)=T8R; %degC
            T9(1)=T9R; %degC
```

```
            T10(1)=T10R; %degC
            T11(1)=T11R; %degC
            T12(1)=T12R;
%             qauxx = squeeze(simout1.Data);
%             qauxxx = qauxx(index3-1);
            qaux(1) = qauxR;
        else
            T7(1)=T_low; %degC
            T8(1)=T_low; %degC
            T9(1)=T_low; %degC
            T10(1)=T_low; %degC
            T11(1)=T_low; %degC
            T12(1)=T_low;
        end


        %Controller parameters
        Prop=zeros(Nfinal,1);
        Int=zeros(Nfinal,1);
        I=zeros(Nfinal,1);
        PID=zeros(Nfinal,1);
        Error=zeros(Nfinal,1);
        Tsperr=zeros(Nfinal,1);

        %Cair = ones(Nfinal,1)*7*cp*rho*Vol;
        dd=1;
        ddd=1;
        u=0;

        dd=1;
        ddd=1;
        Int=zeros(Nfinal,1);
        I=zeros(Nfinal,1);
        u=0;
        aaa=1;
        for aaa = 1:4
        for j=1:Nfinal-1
            if j>1
                if abs(Tsp3(j)- Tsp3(j-1)) > 0.5
                    Tsperr(j) = abs(Tsp3(j)- Tsp3(j-1));
                    Int=zeros(Nfinal,1);
                    ddd=ddd+1;
                else
                    dd=dd+1;
                end
            end
            Error(j+1)=Tsp3(j)-T7(j);
            Prop(j+1)=Error(j+1);
            if Error(j+1) > 0
                Int(j+1)=(Error(j+1)+Error(j))*deltaT/2;
            elseif Error(j+1) > 0
                Int(j+1)=(Error(j+1)+Error(j))*deltaT/2;
            else
                Int(j+1)=0;
```

```
            end
            I(j+1)=sum(Int);
            PID(j+1)=Kp*Prop(j)+Ki*I(j+1);
            if T7(j)> 24 || any(To>20)
                if PID(j+1)<qmin
                    qaux(j+1)=qmin;%watt
                else
                    qaux(j+1) = PID(j+1);
                end
            elseif PID(j+1)>qmax && Error(j+1)>0.1
                qaux(j+1)=qmax;%watt
            elseif PID(j+1)<qmin && Error(j+1)<0.1
                qaux(j+1)=qmin;%watt
            elseif PID(j+1) < 4000 && PID(j+1) > 0
                qaux(j+1) = 4000;
            elseif Error(j+1)>0.1
                qaux(j+1)=PID(j+1);%watt
            else
                qaux(j+1)=4000;%watt
            end
            if time > 0
                if j>1 && j < 10
                    if qaux(j) <= 5000
                        qaux(j) = qaux(j-1);
                    end
                end
            end
            T7(j+1)=(deltaT/Cair)*(qaux(j+1)+((((T8(j)-T7(j))/
R78)+((Teq(j)-T7(j))./R7o(j))+((T10(j)-T7(j))/R710))))+T7(j);

            T8(j+1)=((T7(j)/R78)+0.5*SRwin(j)+(T9(j)/R89))/((1/
R78)+(1/R89));%degC
            T9(j+1)=(deltaT/C9)*(((T8(j)-T9(j))/R89)+((Teq(j)-T9(j))/
R9o))+T9(j);%degC
            T10(j+1)=((T7(j)/R710)+0.5*SRwin(j)+(T11(j)/R1011))/((1/
R710)+(1/R1011));%degC
            T11(j+1)=(deltaT/C11)*(((T12(j)-T11(j))/R1112)+((T10(j)-
T11(j))/R1011))+T11(j);%degC
            T12(j+1)=(deltaT/C12)*(((T11(j)-T12(j))/R1112)+((Tg(j)-
T12(j))/R12g))+T12(j);%degC
            j=j+1;
        end
        dT=abs(T7(Nfinal)-T7(1));

        u=u+1;

        one = 1;
        two = one/3;
        three = 0;
        if aaa<4
        T7(1)=T7(Nfinal-1);
        T8(1)=T8(Nfinal-1);
        T9(1)=T9(Nfinal-1);
        T10(1)=T10(Nfinal-1);
```

```
        T11(1)=T11(Nfinal-1);
        T12(1)=T12(Nfinal-1);
        end
        end

        absqaux = abs(qaux);

        if index > 1
            isit = rem(index-1,5760);
            if rem(index-1,5760) == 0
                Pmax = 0.5*max(absqaux(72:108))*14.37/1000 +
0.5*max(absqaux)*14.37/1000 + (sum(absqaux)/1000)*(300/3600)*0.0493;
            else
                if day > 1
                    test = floor((index-1-5760)/(day-1));
                    instance = floor(288-288*(test)/5760);
                else
                    test = floor((index-1)/(day));
                    instance = floor(288*(test)/5760);
                end
                if instance > 72
                    instance2 = 288-(instance-72);
                elseif instance == 72
                    instance2 = 1;
                else
                    instance2 = 72-instance;
                end
                if instance2 + 36 > 288
                    instance3 = 288;
                else
                    instance3 = instance2+36;
                end
                Pmax =
0.5*max(absqaux(instance2:instance3))*14.37/1000 +
0.5*max(absqaux)*14.37/1000 + (sum(absqaux)/1000)*(300/3600)*0.0493;
            end
        else
            Pmax = 0.75*max(absqaux(72:108))*14.37/1000 +
0.25*max(absqaux)*14.37/1000 + (sum(absqaux)/1000)*(300/3600)*0.0493;
        end



        Ecost = EcostYear_15sec(index:index+(H*5760-1));
        z = 300/15;
        xx=reshape(Ecost,z,[]);
        Ecost3=sum(xx,1)./size(xx,1);
%
         Pmax = 0.5*max(absqaux)*14.37/1000 +
0.5*(sum(absqaux)/1000)*(300/3600)*0.0493;

         Pmax = sum(Ecost3(1:Nfinal)*absqaux)/1000;
```

```
    end

    if trigger == 1
        %wait = waitbar(time/(3600*24*4),'Running
 Optimization...','Position', [1.0928e+03, 367.5000, 270, 56.2500]);
        %qaux = transpose(zeros(length(Tsp(index:index
+((1440*4)-1))),1));
        Pmax = 0;

        if Phorz >24 && Phorz < 48
            H = 1.5;
        else
            H = floor(Phorz/24);
        end

        Tsp1 = TspYR(index:index+(H*5760-1))-5;
        z = 3600/15;
        xx=reshape(Tsp1,z,[]);
        Tsp2=sum(xx,1)./size(xx,1);

        UB1 = UBYear_15sec(index:index+(H*5760-1));
        z = 3600/15;
        xx=reshape(UB1,z,[]);
        UB3=sum(xx,1)./size(xx,1);
        UB3 = zeros(length(UB3),1)+24;

        LB1 = LBYear_15sec(index:index+(H*5760-1));
        z = 3600/15;
        xx=reshape(LB1,z,[]);
        LB3=sum(xx,1)./size(xx,1);

        noise = 10*rand()*(rand()-1/2);
        noise = 0.75*noise + 0.25*XNoiseold;


        aa = randi([0,15]);
        b = randi([0,15]);

        while aa == b
             b = randi([0,15]);
        end

        r = (b-aa).*rand(10,1)+aa;
        r1 = (rand()-1/2)*r;

        t_new5=linspace(1,numel(r),576*numel(r));

        r3 = interp1(r1,t_new5,'spline');
        y2 = 0.25*r3+0.75*XNoiseold;

        options = optimset('MaxFunEvals',100000,'TolFun',
 1.e-4, 'TolX',1.e-4 );
```

```
        Tspid1 = fmincon(@Bank_5min1, Tsp2, [],[],[],[], LB3, UB3, [],
 options);

        if day >2

            while abs(Tspid1(1) - Tspid(index-1))>0.25
                Tspid1(1) = (Tspid(index-1)+Tspid1(1))/2;
                Tspid1(2) = (Tspid1(1)+Tspid1(2))/2;
                Tspid1(3) = (Tspid1(2)+Tspid1(3))/2;

            end

        end

        t_new5=linspace(1,numel(Tspid1),240*numel(Tspid1));
        Tspid2 = interp1(Tspid1, t_new5);
        Tspid(index:index+(H*5760-1)) = Tspid2;
        t_new11=linspace(1,numel(qaux),20*numel(qaux));
        qaux2=interp1(qaux, t_new11);
        qauxid(index:index+(H*5760-1))=qaux2;
        XNoiseold = mean(y2);
        a = a + 1;
        if qauxid == 4000
            g=1;
        end


    end

end
```

Not enough input arguments.

Error in bank5minTEST_allinoneYR_forprint (line 55)
Phorz = Phorz2;

Published with MATLAB® R2018a

Appendix C: Thermelect & Warehouse Details

The specific high temperature thermal energy storage device introduced in this study – the Thermelect – was developed by Hydro-Quebec and Steffes Corporation Steffes Corporation (2010). Specific details can be found in the Owner's and Installer's Installation manual or other available documentation made available by the Steffes Corporation, and some details of the device are shown in Figures C1, C2, and C3. Figure C4 shows the overall HVAC configuration from the BAS dashboard, including the location of the thermelect.

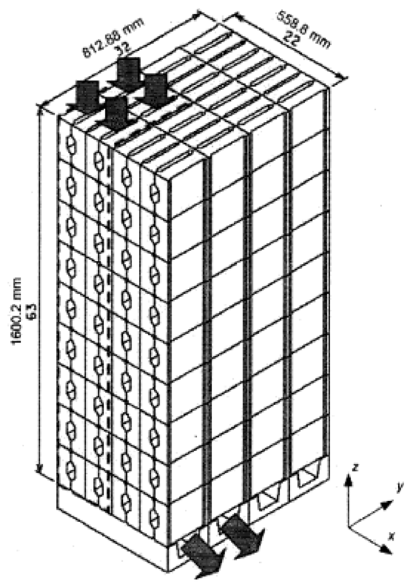

Figure C1: Detail of thermelect brick core (Lavigne, 2006)

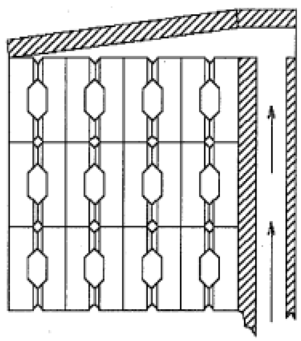

Figure C2: Detail of thermelect brick core air channel (Lavigne, 2006)

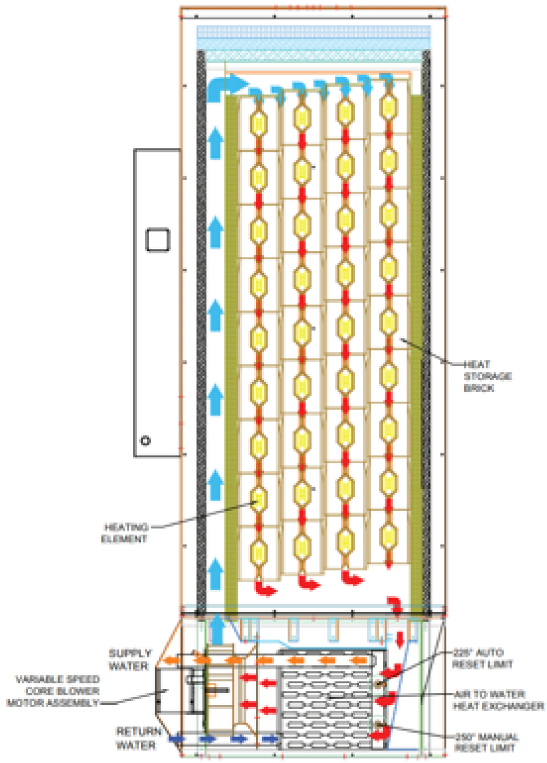

Figure C3: Detail of thermelect (hydronic)

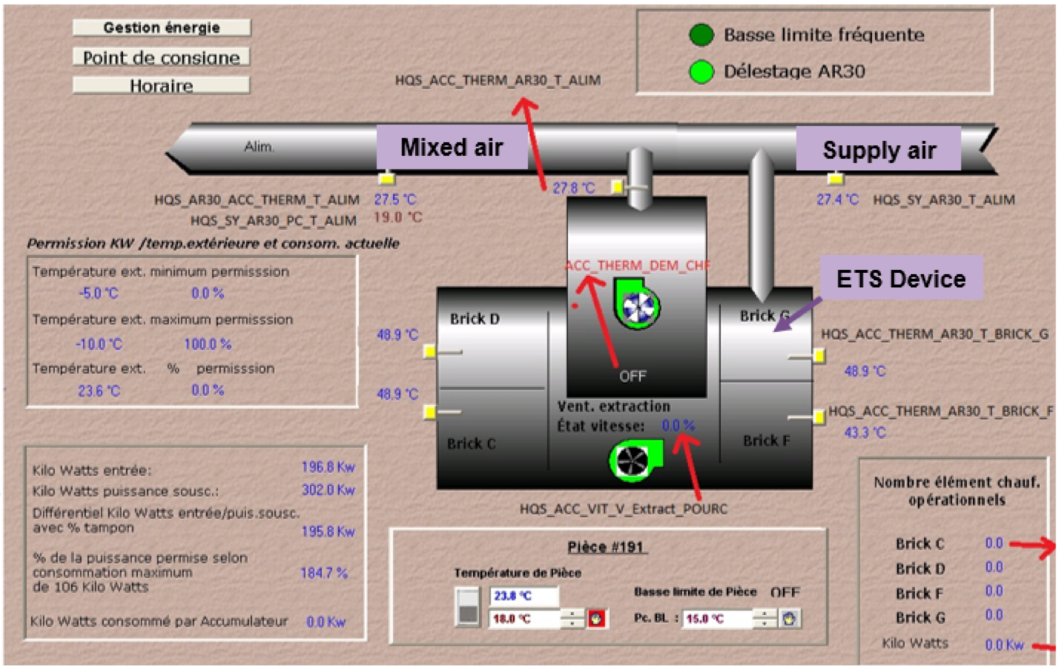

Figure C4: Thermelect BAS system overview